

Mitochondrial calcium uptake pathways as a potential therapeutic target.

Julia Marie Hill

A thesis submitted for the degree of Doctor of Philosophy

Department of Cell and Developmental Biology

University College London

January 2016

I dedicate this thesis to Neil and Jill Hill,
who have always encouraged me to strive, and have always had confidence in me.

Declaration

I, Julia Marie Hill, confirm that the work presented in this thesis is my own. Where information has been derived from other sources, I confirm that this has been indicated in the thesis.

January, 2016

Julia Marie Hill

Acknowledgements

I would like to thank Professor Michael Duchen and Professor Gyorgy Szabadkai for their supervision and guidance throughout my studies and research. Thank you especially to Gyuri for his extensive practical as well as theoretical knowledge, for doing experiments alongside me when necessary, and encouraging me when I was disheartened.

I would also like to thank Eisai for funding my PhD. Without funding I would certainly not have been able to undertake a PhD.

A big thank you is owed to all members of the Duchen and Szabadkai labs, past and present. Drs Zhi Yao, Will Kotiadis, Goncalo Pereira, Nicoletta Plotegher, Tom Briston, Laura Osellame and Jose Vicencio for teaching me many of the techniques I have used in the lab, in addition to their good advice and friendship. Thanks especially to Zhi, Will and Goncalo for your enduring patience and assistance. Many, many thanks also go to Bobby Bentham, Stephanie Sundier, Jenny Sharpe, Gauri Bhosale, Pedro Guedes Dias, Greg Keen and Neta Amior for making my time here not only bearable but enjoyable, it wouldn't have been anywhere near as fun without you. Thank you to Sam Ranasinghe, for keeping the confocals working, and coming to the rescue whenever they weren't.

I extend my thanks also to Dr Gareth Pryce and Professor David Baker of the Blizard Institute at Queen Mary's, and to Professor David Selwood of the Wolfson Institute for Biomedical Research for their collaboration, and for putting me in touch with their fascinating research. Thanks especially to Gareth for all those days spent together mashing up livers, and for not giving up when it wasn't working.

Thank you also to Dr Sean Davidson and Dr Dan Bromage for supplying me with CypD^{-/-} mice from their colony at no cost and no inconvenience. I would also like to express my gratitude to UCL's Biological Services and Biosciences Stores for their underappreciated hard work and consistent cheerfulness.

On a personal note, I want to thank my friends and family who have supported me throughout the PhD. These are too numerous to name, but special thanks go to Ernestas Sirka, my fabulous flatmate of the last three years, for putting up with me all this time, and being there through it all.

Abstract

It has been known since the 1960's that mitochondria have a huge capacity to take up and accumulate calcium from the cytosol, regulating energy production, autophagy, and mitochondrial morphology. Dysfunctional mitochondrial calcium homeostasis is also involved in the pathology of many disease states. Therefore, mitochondrial calcium handling represents an interesting therapeutic target. In this thesis I aimed to investigate related therapeutic avenues and further understand the role of mitochondrial calcium handling machinery.

When mitochondrial calcium uptake exceeds the calcium buffering capacity of the mitochondrial matrix, the mitochondrial permeability transition pore (mPTP) opens in the inner mitochondrial membrane. Pore opening causes mitochondrial depolarisation, energetic collapse, swelling, rupture, and cell death. Using isolated mitochondria, I screened a range of novel mitochondrial targeted derivatives of the canonical mPTP inhibitor, cyclosporin A (CsA), to assess their efficacy as mPTP inhibitors, and as potential therapeutics for neurological disease. Two compounds were found to be more effective than CsA at low concentrations, and one was selected for further study. The compound's target was investigated and found to be Cyclophilin D, and its effect on various mitochondrial parameters was assessed, and it was found to be non-toxic *ex vivo* and *in vitro*.

The molecular identity of the mitochondrial calcium uniporter (MCU) was only recently discovered, followed by discovery of several associated proteins – MCUB, MICU1, MICU2, MICU3, EMRE, and MCUR1. I developed a screen using the bioluminescent protein aequorin to identify mitochondrial specific inhibitors of the MCU, and I developed a stable cell line in which the MCU protein was knocked down, in order to further examine the role of MCU and investigate the effect of reduced mitochondrial calcium uptake on mitochondrial and cellular properties. While mitochondrial calcium uptake was significantly reduced upon stimulation in these cells, cytosolic calcium, oxygen consumption, cell growth and mitochondrial morphology were not affected. I also investigated the protein expression level of the components of the MCU complex in the rat brain throughout development.

Publications

Some of the figures and ideas presented in this thesis have been published in the following reports:

1. Hill J.M., De Stefani D., Jones A.W., Ruiz A., Rizzuto R., & Szabadkai G., (2014) Measuring baseline Ca^{2+} levels in subcellular compartments using genetically engineered fluorescent indicators. *Methods Enzymol*, 543, 47-72. Doi: 10.1016/B978-0-12-801329-8.00003-9.
2. Warne J, Pryce G, Hill JM, Shi X, Lennerås F, Puentes F, *et al.* Selective Inhibition of the Mitochondrial Permeability Transition Pore Protects against Neurodegeneration in Experimental Multiple Sclerosis. *J Biol Chem* 2016; 291(9): 4356-73.
3. Hill J. M., Kriston-Vizi J., Kettler R., Szabadkai G. Developing a screening strategy for mitochondrial specific inhibitors. *In preparation.*

Contents

Contents	Page
Declaration.....	3
Acknowledgements.....	4
Abstract.....	5
Publications.....	6
Contents.....	7
List of Figures.....	10
List of Tables.....	13
Abbreviations.....	14
Materials.....	19
Chapter 1: Introduction	23
Mitochondria.....	23
Mitochondria and Ca ²⁺ handling.....	27
Physiological roles of mitochondrial Ca ²⁺ homeostasis.....	28
Mitochondrial Ca ²⁺ in apoptosis and necrosis.....	30
The Mitochondrial Ca ²⁺ uptake complex.....	32
MCU.....	32
MCUb.....	36
MICU1.....	37
MICU2 and MICU3.....	40
EMRE.....	42
MCUR1.....	43
Solute Carrier 25A23.....	45
Involvement of other proteins in mitochondrial Ca ²⁺ uptake.....	46
The mitochondrial permeability transition pore.....	48
Mechanism of mPTP opening.....	48
mPTP and cell fate.....	50
Molecular identity of mPTP.....	51

Cyclophilin D.....	51
A multiprotein complex: VDAC, ANT and TSPO.....	52
The phosphate carrier.....	53
ATP synthase.....	53
Spastic paraplegia 7.....	56
Mitochondrial Ca ²⁺ as a therapeutic target.....	57
Roles of mitochondrial Ca ²⁺ overload in neurodegenerative disease.....	57
Role of mPTP in neurodegenerative disease.....	59
Aims.....	61
Chapter 2: Targeting the Mitochondrial Permeability Transition Pore.....	62
Introduction.....	62
Existing inhibitors of mPTP.....	62
Methods.....	67
Results.....	73
Initial assessment of compounds.....	73
Investigation of JW47 efficacy and target.....	75
Investigation of the effect of JW47 on mitochondrial parameters.....	77
Investigation of second generation compounds.....	79
Summary.....	80
Discussion.....	82
Chapter 3: Developing an Aequorin-based Screening Approach to Identify	
Inhibitors of MCU	89
Introduction.....	89
Mitochondria as drug targets.....	89
Existing MCU-targeting compounds.....	90
Aequorin.....	91
Designing an aequorin based screening approach.....	93
Methods.....	95
Results.....	100
Initial Screening of the NINDs-2 compound library.....	100
Reconfirming screening results.....	105
Investigating the effect of compounds on other mitochondrial parameters....	108

Summary.....	110
Discussion.....	111
Chapter 4: Investigating the role of the MCU <i>in vitro</i>	115
Introduction.....	115
The mitochondrial calcium uniporter complex (MCU).....	115
Transfection.....	116
Methods of transfection.....	118
Transfecting primary cultures.....	119
Methods.....	121
Results.....	130
Transient transfections with MCU targeted shRNA.....	130
Creating and characterizing a stable MCU knockdown cell line.....	131
Summary.....	139
Transfecting primary neurons.....	140
Discussion.....	143
Chapter 5: Investigating expression levels of the MCU complex during development	149
Introduction.....	149
Methods.....	153
Results.....	154
Summary.....	160
Discussion.....	162
Chapter 6: Conclusions and Future Work	165
References.....	
Appendix.....	193
1: Fluorescein-tagged quinolinium co-localized with mitochondria labelled with TMRM in DIV10 rat cortical neurons.....	193
2: <i>In vivo</i> effect of JW47 in a mouse model of EAE.....	194
3: The NINDS-2 compound library.....	195
4: Delayed calcium deregulation is characterised by an initial small Ca ²⁺ rise in response to glutamate, followed up to two hours after initial glutamate exposure by a secondary, larger Ca ²⁺ rise, simultaneous to a collapse of ΔΨ _m	238

List of Figures

Figure	Title	Page
1.1	Basic mitochondrial structure.....	24
1.2	Oxidative phosphorylation.	26
1.3	Components of ion transport through the IMM.....	28
1.4	Mitochondrial Ca ²⁺ in apoptosis and necrosis.....	32
1.5	MICU1 acts as a gatekeeper, ensuring the sigmoidal response of mitochondria to cytosolic [Ca ²⁺] by undergoing a conformational change on Ca ²⁺ binding.....	39
1.6	Irreversible opening of the mPTP leads to cell death.....	50
1.7	ATP synthase may form mPTP.....	55
1.8	Ca ²⁺ overload leads to neuronal cell death.....	58
2.1	Cyclosporin A indirectly binds calcineurin and directly binds Cyclophilin D, resulting in its two effects of immunosuppression and reduced Ca ²⁺ sensitivity of mPTP.....	63
2.2	CsA was modified to produce new compounds.....	65
2.3	Novel compound JW47 was an effective inhibitor of mPTP opening.....	74
2.4	At 40nM JW47 was a significantly more potent inhibitor of mPTP opening than CsA.....	75
2.5	JW47 inhibits mPTP opening by binding CypD and reducing Ca ²⁺ sensitivity of the pore.	76
2.6	At low concentrations, JW47 has no effect on mitochondrial membrane potential, oxygen consumption, or ATP production in isolated mitochondria.....	78
2.7	At low concentrations, JW47 has no effect on mitochondrial membrane potential, oxygen consumption, or ATP production in rat	

	cortical neurons.	79
2.8	Three derivatives of JW47 were effective inhibitors of mPTP opening.	80
2.9	A flowchart of the presumed mechanism of action for JW47.....	85
3.1	An explanation of aequorin calibration, from measurements made using wild type aequorin reconstituted with wild type coelenterazine, measured at 37°C.....	92
3.2	A haemocytometer.....	96
3.3	The timecourse of each well was reduced to enable high throughput screening.....	100
3.4	An example of how the ratio values were calculated for the 18 second time course.....	101
3.5	Aequorin based screening of the NINDS-2 drug library.....	104
3.6	Three compounds were identified as specific inhibitors of mitochondrial Ca ²⁺ uptake.	105
3.7	Reconfirming the results of the initial screen.....	107
3.8	Drugs A and D act independently of mitochondrial membrane potential, and do not affect oxygen consumption.....	109
4.0	A simplified mechanism of 4mtGCaMP6m fluorescence.....	125
4.1	HEK293T cells transiently transfected with MCU knockdown constructs do not show different MCU protein levels, or altered mitochondrial or cytosolic Ca ²⁺ levels.....	131
4.2	MCU protein levels in HEK293T cells can be significantly reduced by stable transfection.....	132
4.3	HEK293T cells stably transfected with MCU knockdown constructs show significantly reduced mitochondrial, but not cytosolic agonist-induced Ca ²⁺ concentration in comparison to controls.....	133
4.4	Mitochondrial membrane potential and morphology were not affected.	134
4.5	Basal mitochondrial and cytosolic [Ca ²⁺].....	135
4.6	MCU knockdown does not affect the rate of respiration, or the	

	protein level of electron transport chain protein complexes I-V.....	136
4.7	Rates of cell growth SCR and MCU knockdown cells.....	138
4.8	An MCU independent Ca^{2+} increase causes Ca^{2+} induced cell death....	139
4.9	92.6% of cells were neurons.....	140
4.10	Assessment of efficiency and toxicity of different transfection techniques.	141
5.0	The cell cycle.....	150
5.1	Monitoring expression of developmental and mitochondrial markers.....	154
5.2	Level of MCU protein expression at different developmental stages..	156
5.3	Level of MCUB protein expression at different developmental stages.	157
5.4	Level of MICU1 protein expression at different developmental stages.....	158
5.5	Level of MCUR1 protein expression at different developmental stages.	159
5.6	Comparing relative protein levels of MCU, MCUB, MICU1, MCUR1 and GRP75.	160
A1	Fluorescein-tagged quinolinium co-localized with mitochondria labelled with TMRM in DIV10 rat cortical neurons.....	193
A2	In an EAE mouse model, JW47 significantly prevented deterioration of motor skills and improved neurological clinical score.....	194
A3	Delayed calcium deregulation is characterised by an initial small Ca^{2+} rise in response to glutamate, followed up to two hours after initial glutamate exposure by a secondary, larger Ca^{2+} rise, simultaneous to a collapse of $\Delta\Psi_m$	238

List of Tables

Table	Title	Page
1	List of materials and sources.....	19
2	The method used to calculate percentage (%) inhibition for each condition of a calcium retention capacity (CRC) assay.....	68
3	A summary of the primary advantages and disadvantages of a range of transfection techniques.....	118
4	Identities, sequences and details of the shRNA constructs used to create transient knockdown of MCU.....	121
A1	The NINDS-2 compound library.....	195

Abbreviations

AD	Alzheimer's disease
ADP	Adenosine diphosphate
AIF	Apoptosis inducing factor
AMP-PNP	Adenylyl imidodiphosphate
AMPA	α -amino-3-hydroxy-5-methyl-4-isoxazolepropionic acid
AMPK	Adenosine monophosphate activated protein kinase
ANOVA	Analysis of variance
ANT	Adenine nucleotide transport
AraC	Cytarabine
ATCC	American Type Culture Collection
ATP	Adenosine triphosphate
BAD	Bcl2-associated death promoter
BBB	Blood brain barrier
BCA	Bicinchoninic acid
Bcl-2	B-cell lymphoma 2
BKA	Bongkrekic acid
Bmt	Butenyl-methyl-threonine side chain
BSA	Bovine serum albumin
Bz-423	Benzodiazepine 423
CAT	Carboxyatractyloside
cDNA	Complementary DNA
CL	Cardiolipin
CNS	Central nervous system
COX	Cytochrome c oxidase
CRC	Calcium retention capacity
CsA	Cyclosporin A
CypA	Cyclophilin A

CypD	Cyclophilin D
DAPI	4',6-diamino-2-phenylindole
DCD	Delayed calcium deregulation
DHE	Dihydroethidium
DIV	Day in vitro
DMEM	Dulbecco's modified eagles medium
DMSO	Dimethyl sulfoxide
DNA	Deoxyribonucleic acid
dsRNA	Double stranded RNA
E12.5/17	Embryonic day 12.5/17
EAE	Experimental autoimmune encephalomyelitis
EAE	Experimental autoimmune encephalomyelitis
EF hands	Calcium sensing helix-loop-helix structural domain
EGTA	Ethylene glycol tetraacetic acid
EMRE	Essential MCU regulator
ER	Endoplasmic reticulum
ETC	Electron transport chain
ETS	Maximum capacity of the uncoupled electron transport system
FACS	Fluorescence activated cell sorting
FBS	Fetal bovine serum
FCCP	Carbonylcyanide-p-(trifluoromethoxy)-phenylhydrazone
Fmax	Maximum fluorescence emitted
FRET	Forster resonance energy transfer
G1	Gap 1
G2	Gap 2
GFP	Green fluorescent protein
GM	Genetic modification
GRP75	Mitochondrial heat shock protein
GTPase	Guanosine triphosphate hydrolase
HBSS	Hank's buffered salt solution
HCX	Proton-calcium exchanger

HEK 293T	Human embryonic kidney 293T
HEPES	4-(2-hydroxyethyl)-1-piperazineethanesulfonic acid
Htt	Huntintin
IMM	Inner mitochondrial membrane
IP ₃	Inositol triphosphate
KD	Dissociation constant
KD	Knockdown
KO	Knock out
Letm1	Leucine zipper EF hand containing transmembrane protein 1
Lmax	Maximum light emitted
M	Mitosis
MAP2	Microtubule associated protein 2
MCU	Mitochondrial calcium uniporter
MCUb	Mitochondrial calcium uniporter b
MCUR1	Mitochondrial calcium uniporter regulator 1
MICU1	Mitochondrial calcium uptake 1
MICU2	Mitochondrial calcium uptake 2
MICU3	Mitochondrial calcium uptake 3
Miro 1/2	Mitochondrial Rho-GTPase 1/2
MMC	Mitochondrial mega channel
mPTP	Mitochondrial permeability transition pore
mRNA	Messenger RNA
MS	Multiple sclerosis
mtDNA	Mitochondrial DNA
NAD	Nicotinamide adenine dinucleotide
NADH	Reduced nicotinamide adenine dinucleotide
NADPH	Nicotinamide adenine dinucleotidephosphate
NCLX	Sodium/calcium exchanger
NFAT	Nuclear factor of activated T-cells
NHX	Sodium/hydrogen exchanger
NMDA	N-methyl-D-aspartate

nNOS	Neuronal nitric oxide synthase
NO	Nitric oxide
NOS	Nitric oxide synthase
OMM	Outer mitochondrial membrane
OSCP	Oligomycin sensitivity conferring subunit
P0/2/10/21	Day after birth 0/2/10/21
PBS	Phosphate buffered saline
PC	Phosphatidylcholine
PCNA	Proliferating cell nuclear antigen
PD	Parkinson's disease
PE	Phosphatidylethanolamine
PFA	Paraformaldehyde
PI	Propidium iodide
PIC	Phosphate carrier
Ppif	Peptidyl prolyl isomerase F
PT	Permeability transition
qPCR	Quantitative polymerase chain reaction
RFP	Red fluorescent protein
RNA	Ribonucleic acid
RNAi	RNA interference
ROI	Region of interest
ROS	Reactive oxygen species
rRNA	Ribosomal RNA
Ru360	Ruthenium 360
RuR	Ruthenium red
Ry-R	Ryanodine receptors
S phase	DNA synthesis
Sar	Sarcosine side chain of CsA
SCR	Scrambled
SEM	Standard error of the mean
SERCA	Sarco/endoplasmic reticulum Ca ²⁺ -ATPase

shRNA	Short hairpin RNA
SILAC	Stable isotope labelling by amino acids in cell culture
siRNA	Small interfering RNA
SLC25	Solute carrier 25
SmBzCsA	sarcosine-3(4-methylbenzoate)]-CsA
SNP	Single nucleotide polymorphism
SOCE	Store operated calcium entry
SPG7	Spastic paraplegia 7
SR	Sarcoplasmic reticulum
TFAM	Mitochondrial transcription factor A
TG	Thapsigargin
TMRM	Tetramethylrhodamine methyl ester
TPP	Triphenylphosphonium
tRNA	Transfer RNA
TSPO	Peripheral benzodiazepine receptor
UCP	Uncoupling protein
UV	Ultraviolet
VDAC	Voltage dependent anion channel
VDAC	Voltage dependent anion channel
WT	Wild type
$\Delta\Psi_m$	Mitochondrial membrane potential
ΔpH_m	Proton gradient

Materials

Table 1: List of materials and sources

Material	Source	Other information
Tissue culture		
B27	Gibco 17504-044	50X
DMEM	Gibco 31966-021	
DNase	Roche 10104159001	
Fetal bovine serum	Gibco 10500-064	
Glutamax	Gibco 35050-038	100X
Neurobasal	Gibco 21103-049	
Papain	Roche 10108014001	100mg/10ml
Penicillin/streptomycin	Gibco 15070-063	5000 units/ml
Poly-l-lysine	Sigma P4707	
Trypan blue	Gibco 15250-061	
Trypsin	Gibco 25200-056	0.25% (w/v)
Fluorescent Dyes		
Fluo4-AM	Invitrogen Molecular Probes F14201	
Fluo5-N	Invitrogen Molecular Probes F14203	
Hoechst	Invitrogen Molecular Probes H3570	
Propidium iodide	Invitrogen Molecular Probes P1304MP	
Rhodamine 123	Invitrogen Molecular Probes R302	
Sytox green	Invitrogen Molecular Probes S7020	
TMRM	Invitrogen Molecular Probes T668	
Antibodies		
β -actin	Sigma A2228	1:10000
GRP75	Santa Cruz sc-1058	1:2000
Horseradish peroxidase- conjugated secondary antibodies	Thermofisher scientific, various antibodies	All 1:4000
MAP-2	Abcam ab11267	1:2000
MCU	Sigma HPA016480	1:1000
MCUb	Abcam ab17075	1:250
MCUR1	Abcam ab36335	1:1000
MICU1	Sigma HPA03743	1:300
Oxphos cocktail	Novex 458199	1:1000

PCNA	Abcam ab29	1:1000
488-donkey anti mouse	Life technologies A21202	1:4000
Western blots		
B-mercaptoethanol	Sigma M3148	1:50
Blotting pads	Invitrogen LC2010	
ECL	GE Healthcare PRN2106	
Ladder	BioRad 161-0375	
MES running buffer	Novex NP0002	20X
NuPAGE 10% gels	Novex NP0301BOX	1mmx10wells
NuPAGE LDS Sample buffer	Novex NP0007	4X
Ponceau S	Sigma P7170	
PVDF membranes	Immobilin P IPVH00010	
Transfer buffer	Novex NP0006	20X
Tween	Sigma P1379	
Transfection Reagents		
Aequorin adenovirus	Rosario Rizzuto, University of Padova	
Endoport	Gene Tools	
Fugene	Promega E269A	
Lipofectamine LTX	Invitrogen 15338-100	
Morpholino	Gene Tools	
Optimem	Gibco 31985-047	
Viafect	Promega E4983	
Animals		
C57BL/6J mice	Envigo	
CypD -/- mice	Sean Davidson, Hatter Institute, UCL	
<i>Rattus norvegicus</i>	UCL Biological Services	Sprague Dawley
Kits		
BCA protein quantification kit	ThermoScientific 23225	
Cell Titer Glo	Promega G755A	
Rat Neuron Nucleofection Kit	Lonza VAPG-1003	
Chemicals		
A23187	Sigma C7522	
Adenosine diphosphate (ADP)	Sigma 01905	
Antimycin A	Sigma A8674	
Adenosine triphosphate (ATP)	Sigma A2383	
Bovine serum albumin (BSA)	Sigma A7030	
CaCl ₂	Fluka 21114	
Carbonyl cyanide-4-(trifluoromethoxy) phenylhydrazone (FCCP)	Sigma C2920	
Coelenterazine	Invitrogen Molecular Probes	

	C2944
Cyclosporin A (CsA)	Tocris 1101
Digitonin	Sigma D141
DMEM powder	Sigma D5030
Ethylene glycol tetraacetic acid (EGTA)	Sigma E4378
Galactose	Sigma D5388
Glucose	Sigma G8270
Glutamate	Sigma G1626
HEPES	Sigma H3375
Histamine	Sigma H7125
Iodoacetic acid (IAA)	
Ionomycin	Sigma 10634
JW compounds	Selwood laboratory, UCL
KCl	Sigma P9541
KH ₂ PO ₄	Sigma P9791
K-lactobionate	Sigma 153516
L-glutamine	Sigma G3126
L-Malate	Sigma M100
Mannitol	Sigma M4125
MgCl ₂ .6H ₂ O	VWR 25108
MgSO ₄	Sigma M7506
NaCl	Sigma S9625
NaHCO ₃	Sigma S6297
Na ₂ HPO ₄	Sigma S5011
Na ₃ PO ₄	Sigma 342483
Oligomycin	Sigma 75351
Paraformaldehyde (PFA)	Sigma F8775
Phenylmethylsulfonyl fluoride (PMSF)	Sigma 93482
Phosphate buffered saline (PBS)	Gibco 14190-094
Pluronic acid	Invitrogen Molecular Probes F127
Probenecid	Sigma P8761
Puromycin	Sigma P8833
Rotenone	Sigma R8875
Sodium deoxycholic acid	Sigma D6750
Sodium dodecyl sulphate	Sigma L4390
Sodium pyruvate	Sigma P8574
Succinate	Sigma 224731
Sucrose	Sigma S0389
Taurine	Sigma T0625
Thapsigargin	Sigma T9033
Tris-Base	Sigma T1503
Tris-HCl	Sigma T5941
Triton-X100	Sigma T8787

Other

Coverslips (22mm)	VWR 631-0158
Seahorse calibration media	Seahorse Bioscience 100840-000
shRNA (MCU knockdown)	OpenBioSystems

Chapter 1: Introduction

Mitochondria

Mitochondria are cellular organelles responsible for the generation of adenosine triphosphate (ATP), which is used as an energy source in the cell, through the process of oxidative phosphorylation. It is thought that mitochondria were originally independent organisms: a type of α -proteobacteria whose closest living relatives are the typhus bacterium *Rickettsia prowazekii* (Yang *et al.*, 1985; Andersson *et al.*, 1998). These organisms formed an endosymbiotic relationship with early cells around 2 billion years ago in response to increasing oxygen concentration in the earth's atmosphere (Andersson and Kurland, 1998). This relationship conferred on the cells the ability to use oxygen to produce energy, and provided protection and substrates for the *Rickettsia*. Over time, the *Rickettsia* evolved into modern mitochondria, becoming more reliant on the host cell as genetic information was donated to the cell nucleus and the mitochondrial genome shrunk. Mitochondria still contain their own DNA (mtDNA), although it consists of only 16600 base pairs, in comparison to the nuclear genomes of ~3 billion base pairs, and is circular rather than chromosomal. Human mtDNA encodes 37 genes, 22 encode transfer RNAs (tRNA), 13 encode polypeptides, and 2 encode ribosomal RNA (rRNA). The polypeptides encoded in the mtDNA are all subunits of the complexes of the electron transport chain, which produces ATP for the cell through oxidative phosphorylation (Anderson *et al.*, 1981; Macreadie *et al.*, 1983; Chomyn *et al.*, 1985; Chomyn *et al.*, 1986). The small number of polypeptide encoding genes in the mtDNA mean that mitochondria are now heavily reliant on genes encoded in the nuclear DNA. There are many copies of mtDNA within each mitochondrion, bound within complexes called nucleoids, of around 100nm length. Nucleoids also contain the mitochondrial transcription factor A (TFAM), which constitute the main protein content of the nucleoid: often a nucleoid contains only one copy of mtDNA (Kukat *et al.*, 2011).

MtDNA is contained in the mitochondrial matrix, the space in the centre of the mitochondria surrounded by the inner mitochondrial membrane. Mitochondria have two membranes, the inner and outer mitochondrial membranes, separated by the intermembrane space.

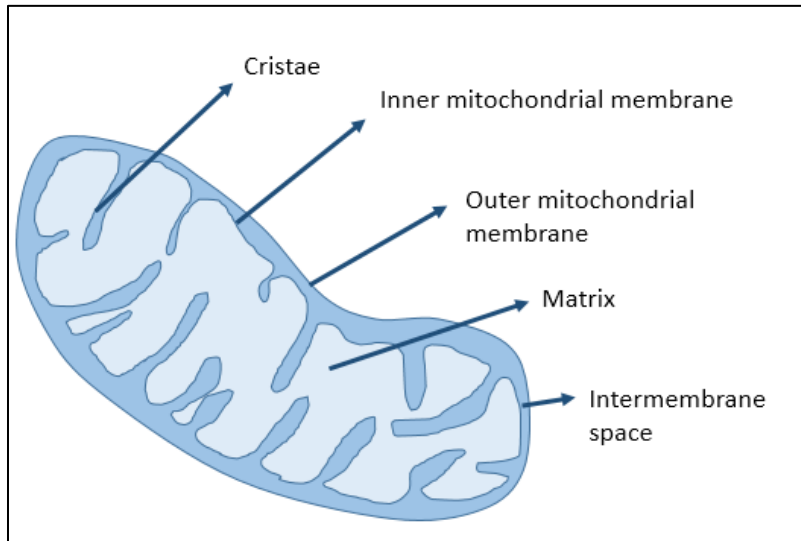


Figure 1.1: Basic mitochondrial structure. Left: the matrix is surrounded by the inner mitochondrial membrane, which forms multiple infoldings called cristae. The inner membrane is surrounded by the outer membrane. Between the two membranes is a distinct compartment, the intermembrane space.

The two membranes are distinct in their composition; the outer mitochondrial membrane (OMM) is a relatively simple phospholipid bilayer, whereas the inner mitochondrial membrane (IMM) is more complex. The IMM consists of a mixture of proteins and phospholipids, including phospholipids of all the major classes; it is much more complex than the OMM and is permeable only to oxygen, CO₂ and H₂O (for overview see (Lemasters, 2007)). Some of the phospholipids of the IMM - phosphatidylethanolamine (PE), phosphatidylcholine (PC) - are common components of cellular membranes, whereas others – cardiolipin (CL) – are mitochondria-specific (Zinser *et al.*, 1991). These phospholipids have important roles in mitochondrial structure, the activity of the respiratory protein complexes, which require an impermeable membrane to create the proton gradient necessary for oxidative phosphorylation, and protein transport into the mitochondria. The IMM also has an unusually high proportion of membrane bound proteins, with a protein:lipid ratio potentially as high as 3:1 (Shaikh and Brown, 2013). The IMM is highly folded, and the infoldings of the membrane are called cristae, see Figure 1.1. These increase the surface area of the IMM, increasing the capacity of the mitochondria to produce ATP from the IMM-

embedded electron transport chain (Mannella, 2006). Mitochondrial morphology is dynamic, and can change between a fragmented or a fused structure in response to cellular and environmental stresses. Mitochondrial dynamics are important to cell health: they have roles in embryonic development (Chen *et al.*, 2003), bioenergetics (Chen *et al.*, 2005), cell signalling (Li *et al.*, 2004; Verstreken *et al.*, 2005), and are involved in the pathogenesis of hereditary optic neuropathies (Rouzier *et al.*, 2012).

ATP is generated by the electron transport chain, a chain of five complexes in the inner mitochondrial membrane (see Figure 1.2). Complex I receives electrons transferred by NADH from the citric acid cycle, which it donates to complex III, moving protons across the IMM as it does so; complex II also donates electrons to complex III, via the reduction of FAD to FADH₂, and the passage of electrons from FADH₂ to ubiquinone. Complex III passes electrons onto complex IV, moving more protons across the IMM. Complex IV combines the electrons with oxygen to produce water, and moves more protons across the IMM. The proton gradient across the IMM then drives ATP production by complex V. Oxidative phosphorylation is a more efficient method of producing ATP than glycolysis, the alternative method in which ATP is produced during the conversion of glucose to pyruvate in the cytosol: it is typically stated that for every molecule of glucose, glycolysis produces 8 molecules of ATP, whereas oxidative phosphorylation produces 30, although these are unlikely to be exact values, due to the energetic cost of substrate transport, and the fact that the mitochondria will not always be in optimal condition (Rich, 2003).

This system, first demonstrated by Peter Mitchell is known as the chemiosmotic mechanism of oxidative phosphorylation and can be summarised as: hydrogen ions are pumped across the mitochondrial inner membrane from the matrix to the intermembrane space by the complexes of the respiratory chain, and thereby generate an electrochemical concentration gradient which is used to drive the production of ATP (Mitchell and Moyle, 1967). This electrochemical gradient defines a membrane potential, ($\Delta\Psi_m$) and a pH gradient (ΔpH_m) across the inner mitochondrial membrane. The proton driving force is usually around -180-220mV, of which 150-180mV is contributed by $\Delta\Psi_m$, and 30-60mV by ΔpH_m (Perry *et al.*, 2011). Therefore $\Delta\Psi_m$ is considered an important parameter to indicate cell health or injury, as it directly relates to the cell's capacity for ATP generation, and is essential for calcium uptake and protein import (Geissler *et al.*, 2000).

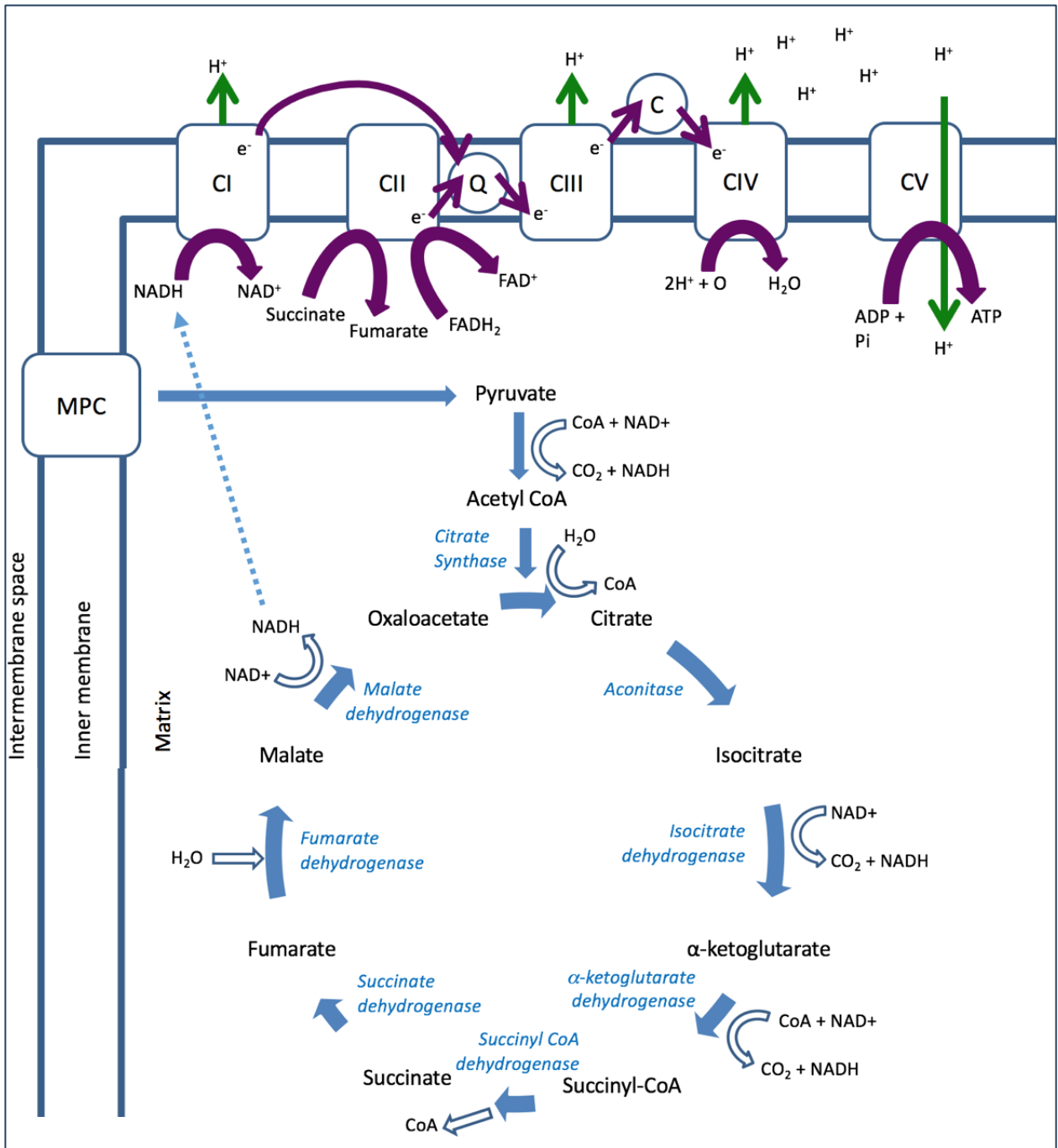


Figure 1.2: Oxidative phosphorylation. The citric acid cycle converts pyruvate (which is imported into the matrix by the mitochondrial pyruvate carrier, MPC) to oxaloacetate in a 9 step cycle. This produces NADH which donates an electron to complex I of the electron transport chain in the inner mitochondrial membrane. Electrons are passed along the electron transport chain and generate a proton gradient, which is used to drive the production of ATP by complex V, the ATP synthase. Movement of protons is represented by green arrows, and movement of electrons by purple arrows.

Mitochondria and Ca²⁺ Handling

The intracellular environment is closely monitored and maintained, and mitochondria have crucial roles in this; in addition to ATP production they are highly involved in cellular Ca²⁺ homeostasis. Ca²⁺ ions were first identified as having control over physiological events in 1883 (Ringer, 1883), and they are ubiquitous second messenger molecules in eukaryotic cells. Our understanding of their vital role has continued to increase since then, with the advent of techniques such as genetically encoded Ca²⁺ indicators, the bioluminescent protein aequorin, and fluorescent Ca²⁺ indicators. Ca²⁺ signals can utilize their localization, frequency or magnitude as a means of conveying information, therefore in order for Ca²⁺ ions to perform their many complex and highly specific functions, the existence of Ca²⁺ pumps, channels and buffers is essential. An excess of free Ca²⁺ in the cell would be damaging to the finely regulated processes which are triggered by specific Ca²⁺ signals. Mitochondria, along with the Golgi apparatus and endoplasmic reticulum (ER), function as cellular Ca²⁺ stores: upon cytosolic Ca²⁺ increase, Ca²⁺ is sequestered by Ca²⁺ binding proteins, the ER and mitochondria. Mitochondria take up Ca²⁺ from the cytoplasm, buffer it in the mitochondrial matrix, and extrude it back into the cytoplasm according to various cellular events and signals. They were the first intracellular organelle to be demonstrated to accumulate Ca²⁺ in 1961 (DELUCA and ENGSTROM, 1961). Basal mitochondrial and cytosolic Ca²⁺ levels are maintained at ~100nM, however upon agonist-induced cytosolic Ca²⁺ increase, mitochondria can accumulate up to 100µM Ca²⁺, although this is cell type dependent and is more typically in the lower micromolar range (Rizzuto and Pozzan, 2006). Ca²⁺ has to cross two membranes in order to reach the matrix and have biochemical effects; the outer mitochondrial membrane (OMM) is broadly permeable to small solutes and ions (<5kDa) due to the non-specific voltage dependent anion channel (VDAC), however the inner mitochondrial membrane (IMM) is impermeable – an essential feature of the chemiosmotic theory - and ion specific transporters are required for uptake into the matrix. Ca²⁺ crosses the ion impermeable IMM through the specific mitochondrial calcium uniporter (MCU). Mitochondrial Ca²⁺ uptake through the MCU depends on the mitochondrial membrane potential gradient generated by respiration, and on the electrochemical Ca²⁺ gradient between the mitochondrial matrix and the cytosol. When oxidative

phosphorylation is uncoupled, and membrane potential and therefore the electrical gradient dissipated, mitochondrial Ca^{2+} uptake ceases (Szabadkai and Duchen, 2008). Extrusion of Ca^{2+} from the mitochondria occurs through the $\text{Na}^+/\text{Ca}^{2+}$ exchanger (in excitable tissue), the $\text{H}^+/\text{Ca}^{2+}$ exchanger (in non excitable tissue) (Marchi and Pinton, 2014) – see Figure 1.3 - both of which have a relatively slow kinetic rate. The mitochondrial permeability transition pore (mPTP) also releases Ca^{2+} , the release of which is sudden and absolute.

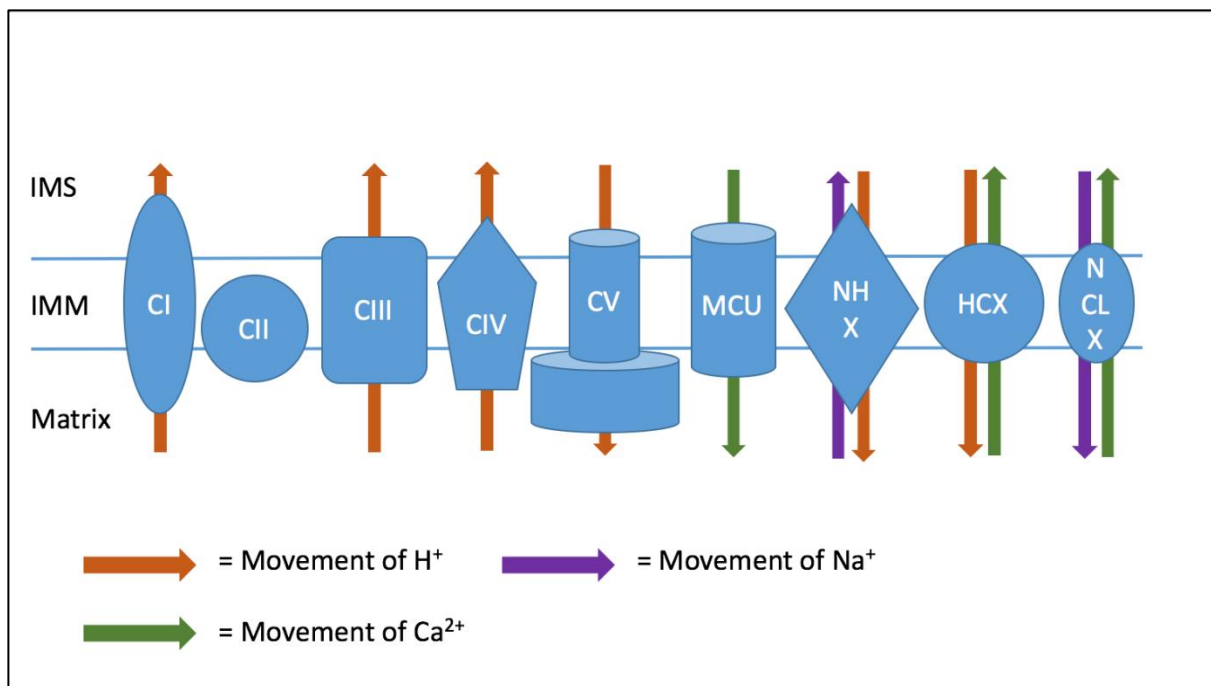


Figure 1.3: Components of ion transport through the IMM. The electron transport chain (complexes I-V) builds up the mitochondrial membrane potential ($\Delta\Psi$) - the electrical driving force for uptake of Ca^{2+} through the MCU - through the export of H^+ ions from the matrix. mPTP, HCX and NCLX extrude Ca^{2+} from the matrix, and the NHX extrudes Na^+ . Together these consist the essential molecular components of mitochondrial Ca^{2+} homeostasis. Adapted from Patron et. al. 2013.

Physiological Roles of Mitochondrial Ca^{2+} Homeostasis

Mitochondrial Ca^{2+} homeostasis is proposed to have a crucial role in regulating energy production and cell survival in normal cell physiology, and is frequently disrupted in disease states (Szabadkai and Duchen, 2008).

The first role of mitochondrial Ca^{2+} homeostasis to be discovered was its role in aerobic metabolism: there are three Ca^{2+} dependent dehydrogenases in the citric acid cycle, which consist of a rate limiting step in substrate supply for ATP synthesis (Denton *et al.*, 1972;

Denton *et al.*, 1978; Lawlis and Roche, 1980). Of the three dehydrogenases, pyruvate dehydrogenase is activated through a Ca^{2+} dependent dephosphorylation step, and isocitrate dehydrogenase and α -ketoglutarate dehydrogenase are activated through the direct allosteric consequence of binding of Ca^{2+} to the enzyme. Ca^{2+} binding increases the V_{max} of these enzymes, and results in increased reduction of the NADH pool (Duchen, 1992), resulting in increased membrane potential, and thus ATP production: ATP demand and ATP supply are simply and directly coupled by Ca^{2+} signalling. Increased mitochondrial Ca^{2+} uptake also results in increased reduction of the flavoprotein pool (Jouaville *et al.*, 1999; Dumollard *et al.*, 2003), and in addition, the Ca^{2+} regulated aspartate/glutamate carriers citrin and aralar – which are involved in transporting NADH into the mitochondria, thereby providing reducing power for oxidative phosphorylation - have been shown to increase ATP production, providing another avenue for the coupling of Ca^{2+} regulation and oxidative phosphorylation (Lasorsa *et al.*, 2003). It has also been suggested that mitochondrial Ca^{2+} has a role in regulating the F_1F_0 -ATPase (Balaban, 2009; Cárdenas *et al.*, 2010), and the Ca^{2+} sensing protein S100A1 has been reported to interact with mitochondrial F_1 -ATPase and result in increased ATP output in cardiomyocytes (Boerries *et al.*, 2007).

Mitochondrial Ca^{2+} is also important in the regulation of autophagy, a lysosomal degradation pathway which activates in response to metabolic stress, nutrient deprivation or growth factor deficiency (Cárdenas and Foskett, 2012). Autophagy can be suppressed or activated through altered mitochondrial ATP production, which indirectly inhibits AMP-activated protein kinase activity (Cardenas 2010). Activation of AMP-activated protein kinase additionally requires the upstream activation of the calcium/calmodulin kinase kinase B (Høyer-Hansen *et al.*, 2007).

Mitochondrial morphology is also influenced by mitochondrial and cytosolic Ca^{2+} levels: after cytosolic Ca^{2+} rise, the GTPase dynamin-like protein 1 (Drp1) which drives mitochondrial fission relocates to the OMM (Breckenridge *et al.*, 2003), and mitochondrial distribution within the cell is governed by the Rho GTPases Miro1 and Miro2 which are Ca^{2+} sensitive (Fransson *et al.*, 2006). Annexin A6, a Ca^{2+} binding protein family which modulates cellular Ca^{2+} signals, also plays a role: in cells lacking Annexin A6, mitochondria are fragmented, mitochondrial membrane potential reduced, and respiration impaired (Chlystun *et al.*, 2013). Mitophagy, the selective autophagy of mitochondria, is also

dependent on mitochondrial morphology, and therefore on Ca^{2+} : it requires the fragmentation of the mitochondrial network in order to segment the areas which are to be removed (Twig *et al.*, 2008).

Mitochondria can act as Ca^{2+} sensors: it has been demonstrated that there are close interactions between the mitochondria and the ER, and so the mitochondria are able to “sense” microdomains of high Ca^{2+} released by the ER, by means of the EF hand domains of Miro1 and Miro2 (Macaskill *et al.*, 2009), which can then shuttle mitochondria to these areas, in order to selectively accumulate Ca^{2+} in these areas and combat the sigmoidal Ca^{2+} uptake curve (Saotome *et al.*, 2008). Strategically placed mitochondria can spatially restrict Ca^{2+} waves to a specific area by constructing a barrier of mitochondrial buffers, and can control the microenvironment of Ca^{2+} channels near which they are localized, providing positive or negative Ca^{2+} feedback and thus regulating further transport (Hoth *et al.*, 1997; Boitier *et al.*, 1999; Tinel *et al.*, 1999).

Ca^{2+} also has pathophysiological roles: Ca^{2+} ions at critical levels lead to cell injury or death by activating various enzymes. These enzymes include calpains (a 15 member family of Ca^{2+} activated cysteine proteases which regulate apoptosis and necrosis), calcineurin (a Ca^{2+} and calmodulin dependent serine/threonine protein phosphatase which induces apoptosis through dephosphorylation of BAD, a Bcl-2 family protein), and nitric oxide synthase (NOS, responsible for synthesis of nitric oxide, an activator of apoptosis), among others (Pinton *et al.*, 2008). Crucially, mitochondrial Ca^{2+} homeostasis has a role in the control of cell death through both necrosis and apoptosis.

Mitochondrial Ca^{2+} in Apoptosis and Necrosis

It has long been known that cellular Ca^{2+} overload leads to necrotic cell death, however its role in apoptosis was only more recently determined, and the specific role of mitochondrial Ca^{2+} uptake has been hard to establish. Although the MCU has low Ca^{2+} affinity, mitochondrial Ca^{2+} overload can occur during cellular stress conditions due to the mitochondria's close proximity to the ER.

Apoptosis is a highly regulated form of cell death necessary in development and normal tissue homeostasis which occurs in a specific sequence of morphological events, whereas necrosis is an uncontrolled form of cell death that usually occurs as a stress response and

presents as uncontrolled cell swelling due to loss of membrane integrity, until cell death occurs (for review, see (Orrenius *et al.*, 2003)). Whether a cell undergoes apoptosis or necrosis also depends on the bioenergetic status of the cell, and the level of mitochondrial function (Leist *et al.*, 1997). Broadly, apoptosis tends to protect from the consequences of injury and tends not to be damaging unless activated inadvertently; it is failure of appropriate apoptosis that causes damage, whereas necrosis is a response to severe injury and inherently damaging.

In necrosis, excessive mitochondrial Ca^{2+} uptake leads to matrix Ca^{2+} overload; this and the accumulation of reactive oxygen species (ROS) leads to the sustained irreversible opening of the mitochondrial permeability transition pore (mPTP). This opening causes a bioenergetic crisis - in which $\Delta\Psi$ collapses, ATP is depleted, and pyridine nucleotides and cytochrome c are lost - leading to necrotic cell death (Vandenabeele *et al.*, 2010). mPTP opening has been shown to be an essential component of necrosis – opening is activated by a high matrix Ca^{2+} concentration, oxidative stress, and low membrane potential, and initial oscillatory opening and closing is followed by persistent opening which leads to cell death (Orrenius *et al.*, 2003).

In reaction to apoptotic stimuli, the pro-apoptotic members of the bcl-2 oncogene family translocate to the mitochondria (where some, such as Bad are indirectly activated by Ca^{2+})(Orrenius *et al.*, 2003). Ca^{2+} then regulates a secondary mechanism in which the OMM permeabilises, and releases pro-apoptotic mitochondrial proteins (e.g. Diablo, cytochrome c), which activate a cascade of caspases, proteolytic enzymes which begin the disintegration of the structural components of the cell (Szalai *et al.*, 1999). Cell death by apoptosis ends in the fragmentation of the cell into apoptotic bodies, which are then engulfed by macrophages (Kerr *et al.*, 1972). Necrosis does not share this clean up mechanism and results in inflammation in the surrounding tissue - such as in ischaemic reperfusion injury – and can therefore be more damaging than apoptosis (Vandenabeele *et al.*, 2010).

In both modes of cell death, mitochondrial Ca^{2+} uptake is a key checkpoint of cell death: up to the maximum Ca^{2+} capacity of the matrix, mitochondria will buffer and extrude Ca^{2+} , whereas beyond the capacity of the matrix, the mitochondria will become overloaded and enter an irreversible cascade toward cell death through necrosis or apoptosis (Figure 1.4).

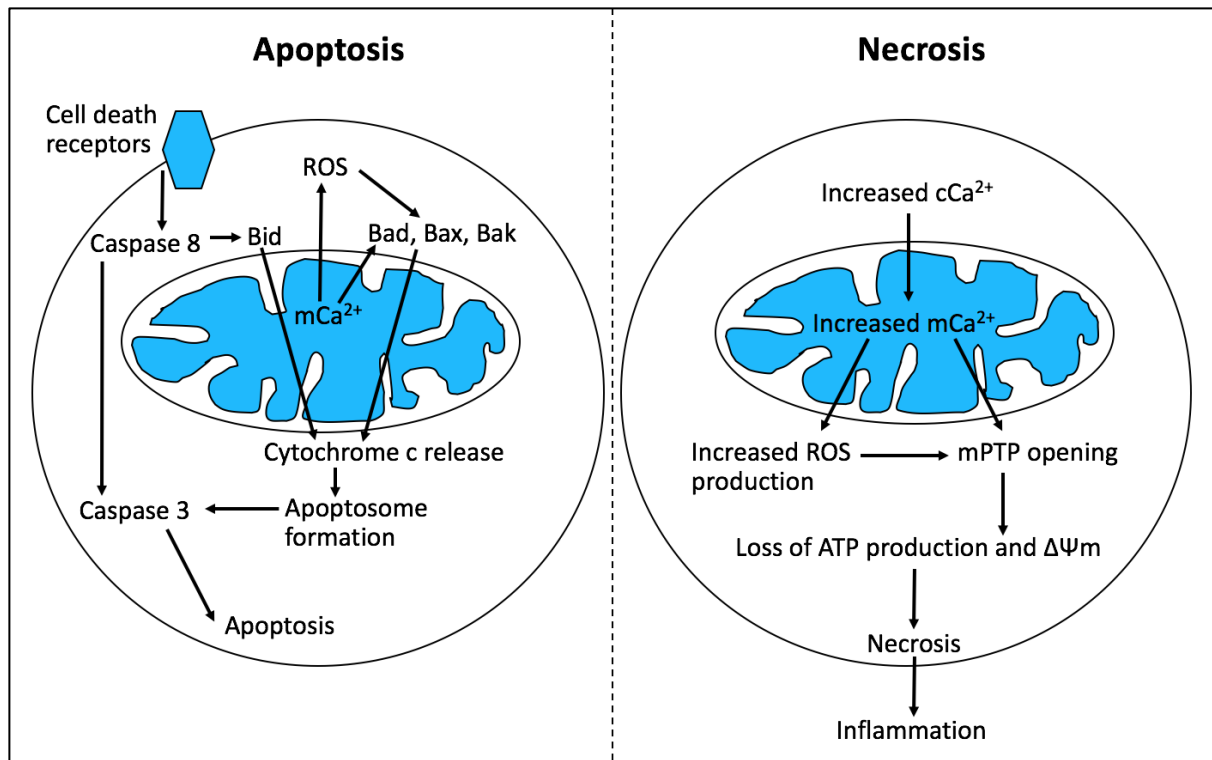


Figure 1.4: Mitochondrial Ca²⁺ in apoptosis and necrosis. In apoptosis, there is an extrinsic pathway mediated by cell death receptors, and an intrinsic pathway mediated by mitochondria. Cell death receptors activate caspase 8, which activates caspase 3, and causes cleavage of Bid. Mitochondrial ROS production, Ca²⁺ and other stimuli activate Bad, Bax, and Bak, which (together with Bid) increase OMM permeability and cause the release of cytochrome c, which causes the formation of the apoptosome. The apoptosome activates caspase 3, beginning the fragmentation of the cell into apoptotic bodies. In necrosis, raised cytosolic [Ca²⁺] (e.g. due to activation of glutamate receptors) leads to raised mitochondrial [Ca²⁺]. This causes increased mitochondrial ROS production through stimulation of oxidative phosphorylation, which contributes to mPTP opening caused by mitochondrial Ca²⁺ overload. mPTP opening results in loss of mitochondrial membrane potential and ATP production, and therefore cell death through necrosis.

The mitochondrial Ca²⁺ uptake complex

Ca²⁺ uptake into mitochondria is mediated by the mitochondrial Ca²⁺ uniporter (MCU). The biochemical properties of the mitochondrial Ca²⁺ uniporter have previously been extensively characterized (for review see (Gunter *et al.*, 2000)), but its molecular identity was only recently discovered. This has sparked a surge of advances in our knowledge of the mitochondrial Ca²⁺ transport system and its components, as described below. The recent discovery of these proteins provides many potential new targets for regulation of mitochondrial Ca²⁺ uptake and its role in bioenergetics, cell survival and cell death.

MCU

In 2011, a protein was simultaneously identified by two groups, and named the mitochondrial Ca²⁺ uniporter (MCU) (Baughman *et al.*, 2011; De Stefani *et al.*, 2011). It was

demonstrated to have all of the previously identified characteristics of the MCU, and to be essential and sufficient for channel activity.

The uniporter had been previously described as a rapid electrogenic transporter which takes up Ca^{2+} into the matrix driven by an electrochemical potential gradient for Ca^{2+} , which includes the mitochondrial membrane potential ($\Delta\Psi$) generated by the respiratory chain (Kirichok *et al.*, 2004). It had been demonstrated that MCU mediated Ca^{2+} uptake occurs almost immediately after a rise in cytosolic $[\text{Ca}^{2+}]$ and that mitochondria could rapidly accumulate Ca^{2+} concentrations of over $100\mu\text{M}$ (Montero *et al.*, 2000). The previously disputed low affinity of the MCU (KD 20-30 μM) had been explained by the discovery that mitochondria lie in close proximity to the Ca^{2+} channels of the endoplasmic reticulum (ER), sarcoplasmic reticulum (SR), and plasma membrane, and act by sensing microdomains of high Ca^{2+} (David *et al.*, 1998; Glitsch *et al.*, 2002), thus revealing that mitochondria respond to a rapid and transient event.

The identification of the MCU gene was made possible by the generation of MitoCarta, a mitochondrial gene data set detailing gene products with known mitochondrial localization (Pagliarini *et al.*, 2008). Both groups used an *in silico* search - although with different criteria: the Mootha group searched for genes closely related to MICU1, which the same group had previously described as essential for mitochondrial Ca^{2+} uptake (see below), whereas the Rizzuto group searched using also using the expected properties of the uniporter - to identify the gene *ccdc109a*. The gene is located on chromosome 10, and produces a 40kDa protein, with a 35kDa mature form after cleavage of its mitochondrial targeting sequence, which was found to interact with MICU1 (Baughman *et al.*, 2011). The gene is ubiquitously expressed in mammalian tissues, but absent in *S. cerevisiae* which are known to lack a mitochondrial Ca^{2+} transporter (De Stefani *et al.*, 2011). Both groups also determined (in HEK293T and HeLa cells) that MCU is essential for mitochondrial Ca^{2+} uptake: MCU silencing almost completely eliminates mitochondrial Ca^{2+} uptake in intact and permeabilised cells, and that MCU overexpression increases uptake (Baughman *et al.*, 2011; De Stefani *et al.*, 2011). The identity of the MCU was further confirmed by measuring the electrophysiological properties of the purified protein expressed in a planar lipid bilayer - which matched those previously found through patch clamping the IMM in mitoplasts (Kirichok *et al.*, 2004) - and the first insight into its structure was determined by the finding

that the mutation to glutamine of two negatively charged residues (D260Q, E263Q) could abolish MCU activity (De Stefani *et al.*, 2011).

The initial publications suggested a topology with two transmembrane α -helices with a highly conserved DIME motif of acidic residues (EYSWDIMEP) linking the two. It has since been confirmed that both the N and C terminals are in the mitochondrial matrix, and that the DIME motif faces the intermembrane space; this has been determined through the development of genetically encoded APEX tags for electron microscopy (Martell *et al.*, 2012). An *in silico* model of the quaternary structure of the MCU suggest four identical subunits, each containing two helical membrane spanning domains and a short connecting water exposed loop containing a DIME motif (Raffaello *et al.*, 2013). This loop region contains critical negatively charged amino acids previously identified as essential to MCU function (Baughman *et al.*, 2011; De Stefani *et al.*, 2011). The structure suggests high sensitivity, with a selectivity filter containing highly conserved acidic residues, able to identify a single Ca^{2+} ion above the channel pore. It is likely that the MCU has a stable closed state conformation. Experimental investigation of this model confirmed that MCU monomers interact and form 170kD tetramers; these can be homo- or hetero-oligomers (Raffaello *et al.*, 2013), see section on MCUB below.

A variety of tissue specific work has since been done: the role of the MCU has been investigated in β -pancreatic cells (Alam *et al.*, 2012), cardiomyocytes (Drago *et al.*, 2012), and neurons (Qiu *et al.*, 2013), among others. In all of these tissues, MCU has been found to be essential for mitochondrial Ca^{2+} uptake, and to have additional tissue specific roles: in β -pancreatic cells MCU (and MICU1, see below) was found to have a role in the secretion of insulin, in neurons MCU is transcriptionally repressed by synaptic activity resulting in protection against excitotoxic cell death, and in cardiomyocytes differing levels of MCU regulates cell contraction. An MCU knockout mouse was created (Herzig *et al.*, 2013; Pan *et al.*, 2013), and the mice were found to be fully viable, although slightly smaller than usual, and the most apparent phenotypic abnormality was in their performance of high energy demand exercise – although basal metabolism was unaltered with a variety of metabolic substrates, there were some differences in the phosphorylation and activity of pyruvate dehydrogenase in MCU(-/-) mice skeletal muscle. This was surprising as Ca^{2+} plays an important role in regulating metabolism, and in a follow up paper the authors reported that

they were surprised it has been possible to breed the mice at all – due to the important role of mitochondrial Ca^{2+} in a variety of processes it had been thought that the MCU (-/-) mouse would be embryonic lethal (Murphy *et al.*, 2014), although curiously they reported that in C57 mice the knock out had been lethal during embryogenesis, at E11.5-13.5, due to unknown causes. In the CD1 outbred strain of mice used to create the knockout, the pattern of inheritance was not Mendelian and only 12-15% of mice born were MCU (-/-), rather than the expected 25%. This may suggest that in some cases it was embryonic lethal. It is unclear why the knock out was possible in CD1 mice and not C57, as there appears to be no functional compensation in the CD1s (Murphy *et al.*, 2014). In mitochondria isolated from CD1 MCU (-/-) mice, mitochondrial Ca^{2+} uptake was reduced - they were unable to rapidly uptake Ca^{2+} - but not absent, and although they appeared to lack mPTP opening, this – surprisingly - does not appear to be protective against Ca^{2+} induced cell death (Pan *et al.*, 2013). This is in contrast to expectations, and the protective role of MCU knockdown found against neuronal cell death from excitotoxicity (Qiu *et al.*, 2013). Overall the findings from the MCU (-/-) mouse have confirmed the role of the MCU for rapid mitochondrial Ca^{2+} uptake, and for activation of mPTP, but in other areas were contrary to expectations, and have raised interesting questions for further studies.

A conditional, cardiomyocyte-specific MCU knock out mouse has also been created (Kwong *et al.*, 2015; Luongo *et al.*, 2015). These data agreed with the work by Pan *et al.*, on the lack of an overt phenotype, that MCU knock out prevented mitochondrial Ca^{2+} uptake (although mitochondria would eventually load with Ca^{2+} , supporting the idea of a compensatory mechanism), and that mPTP opening was reduced. However, Kwong *et al.*, found that reduced mPTP opening led to protection from necrotic death in ischaemia reperfusion injury, as was generally expected to be the case, whereas Pan had found no protection. Additionally, it was found that MCU is necessary to match metabolic output with contractile stress, as the mice had impaired ability to perform strenuous exercise (Kwong *et al.*, 2015; Luongo *et al.*, 2015).

Although in the majority of models, the MCU by itself appears to be sufficient for mitochondrial Ca^{2+} uptake (De Stefani *et al.*, 2011), it cannot provide the fine level of control over Ca^{2+} uptake required in the cell, and it has become clear that the MCU is part of a larger and more intricate complex. This fine tuning is accounted for by other components of

the channel, MCUB and EMRE, and regulatory proteins MICU1, MICU2, MICU3, MCUR1 and SLC25A23, which together make up the MCU complex.

MCUB

Sequence analysis of CCDC109A (MCU) recently identified a new gene, CCDC109b, located on chromosome 4, which shares 50% sequence similarity with MCU, and is predicted to form a highly conserved protein (MCUB) with two transmembrane domains separated by a short loop with a slightly different DIME motif to that of MCU (Raffaello *et al.*, 2013). The gene is present in vertebrates only, suggesting a later date of evolution than MCU; the MCUB protein is expressed at a lower level than MCU across multiple tissues, and with a different expression profile.

It was found that *in vitro* expression established complete colocalization of the MCUB protein with MCU. Immunoprecipitation demonstrated that MCU interacts *in situ* with MCUB, and FRET imaging further showed that MCUB forms hetero-oligomers with MCU, and homo-oligomers with itself. MCUB can additionally form heterotetramers with MCU although the stoichiometry of these tetramers has not been determined.

Predicted structural differences in the DIME motif between MCU and MCUB, due to the amino acid substitution E256V, appear to confer different functions on the two proteins by affecting the kinetics of Ca^{2+} permeation and reducing the Ca^{2+} permeability of MCUB, as a result of removing one negative charge. Electrophysiology supported this, demonstrating that whilst MCUB forms a functional channel it is not capable of Ca^{2+} permeation, in contrast to MCU, thus suggesting a role for MCUB as a dominant negative isoform of MCU. This was confirmed by coexpression of MCUB with MCU in a 1:1 ratio, which drastically reduced the Ca^{2+} activity of the channel compared to channels containing MCU only – although in 13% of experiments, coexpression of MCUB had no effect on Ca^{2+} conductance. RNAi was used to silence or overexpress MCUB in intact cells; silencing of MCUB resulted in a significant increase of histamine induced mitochondrial Ca^{2+} peaks, whereas MCUB overexpression reduced mitochondrial Ca^{2+} peaks, without affecting levels of MCU protein, membrane potential, or cytosolic Ca^{2+} levels, confirming that MCUB specifically inhibits the function of the MCU protein (Raffaello *et al.*, 2013).

MCUb thus has been demonstrated to be a dominant negative isoform of MCU, able to specifically inhibit pore activity by incorporation into channel forming heterotetramers, and thereby regulate mitochondrial Ca^{2+} uptake. The varied expression profile of MCB suggests the level of MCB is carefully modulated depending on the degree of control over Ca^{2+} uptake necessary to the specific tissue function, suggesting an interesting and previously unknown plasticity of the MCU complex which invites further investigation.

MICU1

MICU1 was identified by integrated searching of IMM proteins in the MitoCarta database (Perocchi *et al.*, 2010). MICU1 is a 54kDa protein which has two Ca^{2+} binding EF hand domains contained in a single pass transmembrane domain, located in the intermembrane space (Lam *et al.*, 2015). MICU1 has been demonstrated to share the same evolutionary expression as MCU in a variety of mouse tissues (Bick *et al.*, 2012), being found in all major categories of eukaryotic life, although with some protozoan and fungal losses; this suggests that both MCU and MICU1 may have been an evolutionarily early feature of mitochondria. MICU1 was originally found to be a positive regulator of mitochondrial Ca^{2+} uptake: silencing of MICU1 abrogated mitochondrial Ca^{2+} entry without affecting membrane potential or respiration (Perocchi *et al.*, 2010).

However subsequent papers quickly disagreed with this role: MICU1 silencing was found to have no effect on histamine induced Ca^{2+} uptake, but significantly increased basal Ca^{2+} levels (Mallilankaraman *et al.*, 2012b), and MICU1 silencing did not prevent mitochondrial Ca^{2+} uptake. This suggested that MICU1 acts as a gatekeeper, by restricting Ca^{2+} entry during low intracellular Ca^{2+} concentrations; it was proposed that when high matrix Ca^{2+} concentrations were reached, the Ca^{2+} sensing EF hands of MICU1 would bind Ca^{2+} and inhibit MCU mediated Ca^{2+} entry, thus requiring the EF hands to lie in the mitochondrial matrix. This was supported by the finding that MICU1 localizes to the matrix side of the IMM and binds to MCU independently of the EF hands, in a homo-oligomeric form (Hoffman *et al.*, 2013). Hoffman and colleagues determined the mechanism of MICU1 interaction with MCU: the association was found to be between the coiled coil domains of MCU and the N terminal polybasic region of MICU1, and the homo-oligomerization of MICU1 was shown to be independent of this region.

Conversely, the matrix-sensitive MICU1 theory was then contested by the publication of another examination of the topology of the MCU: it was found that MICU1 faces the intermembrane space not the matrix (Csordás *et al.*, 2013), suggesting that it may primarily respond to cytosolic Ca^{2+} concentrations rather than mitochondrial. The sensitivity of MICU1 to specifically cytosolic Ca^{2+} was further supported by the findings that when MICU1 was silenced, at cytosolic $[\text{Ca}^{2+}]$ of less than $2\mu\text{M}$ the rate of mitochondrial Ca^{2+} uptake was increased but at high cytosolic $[\text{Ca}^{2+}]$ ($>4\mu\text{M}$) it was decreased (de la Fuente *et al.*, 2014), reinforcing the MICU1 as gatekeeper role. These findings suggested that MICU1 alone is responsible for the sigmoidal response of the mitochondria to cytosolic Ca^{2+} : mitochondria have a very large Ca^{2+} loading capacity at high extramitochondrial $[\text{Ca}^{2+}]$ in order to ensure rapid responses to cell events, but at resting cytosolic $[\text{Ca}^{2+}]$, the uptake is very low (see Figure 1.5). Although Csordas *et al.*, agreed with Mallilankaraman *et al.*, that MICU1 is essential to keep MCU closed (as MICU1 silencing causes mitochondrial Ca^{2+} uptake at low cytosolic $[\text{Ca}^{2+}]$, other findings by Csordas supported the original findings (Perocchi *et al.*, 2010): that MICU1 silencing abolishes mitochondrial Ca^{2+} uptake, and resting mitochondrial Ca^{2+} concentrations are unchanged. There is currently still much debate over the exact role and mechanism of MICU1, and further study is needed to confirm and refine the existing theories.

The recently derived crystal structure of MICU1 offers further insight into the mechanism by which MICU1 operates (Wang *et al.*, 2014). It was proposed that when in a Ca^{2+} -free state, MICU1 forms an inhibitory hexamer that binds to MCU; upon Ca^{2+} binding the hexamer undergoes large conformational change (especially at the EF hands) to form multiple oligomers which activate MCU – the EF hands and a C-helix are both necessary for activation (Wang *et al.*, 2014), see Figure 1.5. Modelling suggested an affinity of MICU1 for Ca^{2+} of 15-20 μM , in contrast to the low affinity of MCU, which was suggested to imply that Ca^{2+} uptake may be mediated by multiple channels governed by proteins with different Ca^{2+} affinities. Whilst this structure furthers our understanding, it also raises further questions as to where and how the other components of the MCU complex fit into this structure – something yet to be answered.

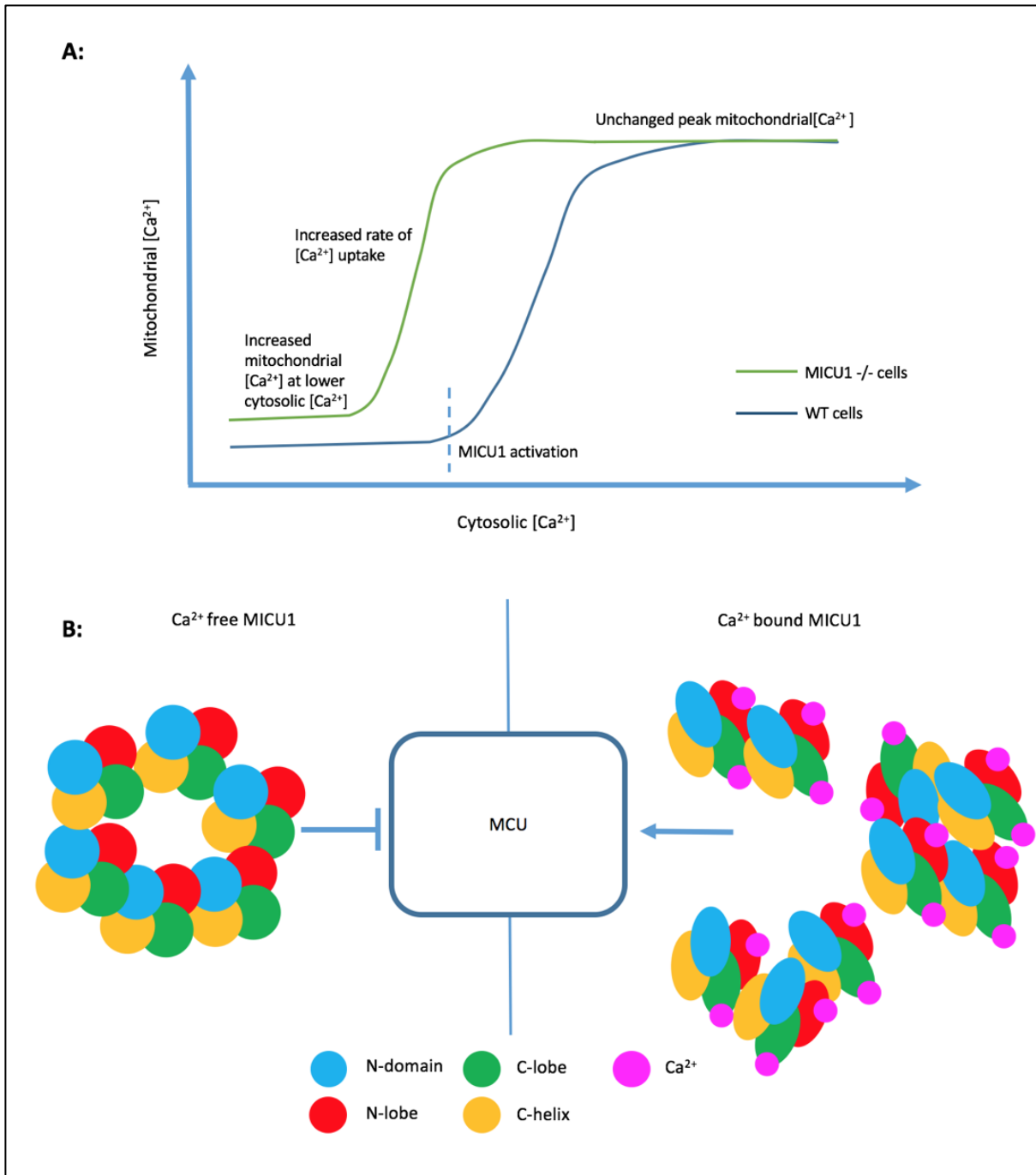


Figure 1.5: MICU1 acts as a gatekeeper, ensuring the sigmoidal response of mitochondria to cytosolic $[Ca^{2+}]$ by undergoing a conformational change on Ca^{2+} binding. Top: mitochondrial Ca^{2+} uptake is sigmoidal: at low cytosolic concentrations, mitochondrial Ca^{2+} uptake is low, after MICU1 activation and conformational change, mitochondrial Ca^{2+} uptake increases rapidly, and eventually plateaus. In MICU1^{-/-} cells, resting mitochondrial $[Ca^{2+}]$ and rate of mitochondrial Ca^{2+} uptake are higher, although peak mitochondrial $[Ca^{2+}]$ is unchanged. Bottom: Ca^{2+} binding causes a large conformational change in the MICU1 protein: in Ca^{2+} free MICU1 (left) forms a hexamer which binds to and inhibits MCU, whereas Ca^{2+} bound MICU1 (right) forms multiple MCU activating oligomers. One Ca^{2+} ion binds to the EF hand of the N-lobe, and one ion to the EF hand of the C-lobe; the C-helix is essential for the formation of the Ca^{2+} free hexamer. Models are based on Logan *et al* 2014, and Wang *et al* 2014.

A recent paper provided an interesting insight into the role of MICU1 in disease: fibroblasts from patients with MICU1 loss-of-function mutations were studied to examine Ca^{2+} uptake and mitochondrial characteristics (Logan *et al.*, 2014). The MICU1 deficient patients presented symptoms in childhood, beginning with proximal muscle weakness, elevated serum creatine kinase levels and learning difficulties. 10 of 15 subjects developed variable motor disorders with involuntary movements, and patients presented various other features indicative of mitochondrial disorders (e.g., ataxia, optic atrophy, microcephaly), although none suffered from diabetes mellitus, deafness or cardiomyopathy, which are symptoms of other mitochondrial diseases (Logan *et al.*, 2014). Muscle biopsies showed core myopathies (areas lacking mitochondria) and other myopathic features. Upon imaging the mitochondria of the patient fibroblasts, it was found that MICU1 deficiency resulted in severe mitochondrial fragmentation without affecting $\Delta\Psi_m$, and that the rate of agonist stimulated Ca^{2+} uptake was increased despite the peak mitochondrial Ca^{2+} being unchanged, suggesting an increased mitochondrial $[\text{Ca}^{2+}]$ at lower cytosolic $[\text{Ca}^{2+}]$ (see Figure 1.5). It was confirmed that the mitochondrial $[\text{Ca}^{2+}]$ was higher in MICU1 deficient cells at rest, and that the absence of MICU1 caused the loss of the typical sigmoidal curve of mitochondrial Ca^{2+} uptake. Overall oxygen consumption was not affected in the MICU1 deficient cells, although NADPH levels were higher. This complex mitochondrial phenotype suggests MICU1 has an essential role in the MCU complex, which begs further enquiry.

MICU2 and MICU3

Genome sequence analysis revealed two homologues to MICU1: EFHA1 (MICU2) and EFHA2 (MICU3), two genes which each share 25% sequence identity with MICU1, and are conserved in vertebrates (Plovanich *et al.*, 2013). Multiple sequence alignment suggests that MICU2 and MICU3 evolved from MICU1 prior to vertebrate evolution. MICU2 and MICU3 both localize to mitochondria, in the intermembrane space (Lam *et al.*, 2015), but have significantly different expression patterns; MICU1 is more broadly expressed than either of its paralogues, MICU2 is expressed most strongly in visceral organs and MICU3 predominantly in the central nervous system and skeletal muscle, and is not exclusively mitochondrial. Nothing further is yet known about MICU3.

MICU1 was suggested to stabilise MICU2: when MICU1 is knocked down, the protein level of the MICU2 is also reduced, although MICU2 mRNA levels are not affected, suggesting a post translational modification of MICU2 by MICU1; this effect appears to vary between cell types. MICU2 was demonstrated to associate with the MCU/MICU1 complex, and MICU2 silencing did not affect membrane potential or mitochondrial respiration (Plovanich *et al.*, 2013). Mitochondria isolated from mouse liver in which MICU2 or MICU1 had been silenced demonstrated impaired Ca²⁺ handling; when both MICU1 and MICU2 were silenced this effect was increased, suggesting that MICU1 and MICU2 have independent, but possibly overlapping roles. This is somewhat supported by the findings of another group, which demonstrate that loss of MICU1 or MICU2 leads to a significant reduction in Ca²⁺ uptake and an altered Ca²⁺ threshold, but that the presence of MICU1 is a requirement for the activity of MICU2, and its association with MCU (Kamer and Mootha, 2014). This suggests that both MICU1 and MICU2 act as negative regulators of Ca²⁺ transport through the pore. MICU2 was reported to have conserved EF hands similar to those of MICU1; it was found that mutation of these hands in either MICU1 or MICU2 abolishes mitochondrial Ca²⁺ uptake, suggesting they have a crucial functional role (Kamer and Mootha, 2014).

However, the function of MICU2 as suggested by Plovanich and Kamer was contested by the publication of data suggesting that MICU2 controls MCU in the opposite manner to MICU1 (Patron *et al.*, 2014); whilst this agrees with the previous papers in that MICU1 and MICU2 play non-redundant roles, the suggested role of MICU2 is entirely different. It was here demonstrated that MICU1 increases the probability of MCU opening in lipid bilayers, whereas MICU2 levels appears to inversely control MCU mediated uptake, and thus proposed that whilst MICU2 inhibits MCU activity at low [Ca²⁺], MICU1 stimulates MCU activity at high [Ca²⁺]. It was also shown that MICU1 and MICU2 form a 95kDa dimer which interacts with MCU in the DIME motif – a contrast to the 408kDa complex in which MCU, MICU1 and MICU2 were found to associate by Plovanich *et. al.*

The possibility of contrasting roles, and an interdependence of MICU1 and MICU2 protein levels could explain some of the previous conflicting data over the role of MICU1 - it is generally agreed that MICU1 silencing does not affect levels of MCU protein (Mallilankaraman *et al.*, 2012b; Csordás *et al.*, 2013), although a study in mouse liver demonstrated altered protein (but not mRNA) MCU levels when MICU1 was silenced

(Plovanich *et al.*, 2013) - perhaps MICU1 silencing also affects MICU2 levels in a tissue specific manner, giving rise to varied results. A recent paper gave more insight on the link between MICU1 and MICU2: it was found that the oxidoreductase Mia40 mediates the formation of disulphide bonds between the two proteins to form a heterodimer (Petrungaro *et al.*, 2015). It suggested that rather than one MICU protein having an activating role and one having an inhibitory, that it is their interaction which confers the action on MCU. The absence of this bond results in increased mitochondrial Ca^{2+} uptake, the presence of the bond, and thus the inhibitory dimer, is Ca^{2+} dependent: at low $[\text{Ca}^{2+}]$, the dimer associates with MCU, and at high $[\text{Ca}^{2+}]$ concentrations it dissociates. Once more, further work is needed to clarify the role of MICU1 and MICU2, and their relative functions to each other.

EMRE

Essential MCU regulator (EMRE) was identified by quantitative mass spectrometry of purified uniporter complex (Sancak *et al.*, 2013). It is a 10kD protein, predicted to have a mitochondrial targeting sequence, a transmembrane domain and an aspartate rich conserved C terminus. It appears to be expressed in all mammalian tissues. Interestingly, EMRE is metazoan specific, not being found in plants, fungi, or protozoa, whereas MCU and MICU1 are found in all eukaryotic lineages, suggesting EMRE evolved at a later point in time than MCU and MICU1.

EMRE silencing resulted in loss of mitochondrial Ca^{2+} uptake similar to that induced by silencing of MCU; mitochondrial membrane potential and the abundance of other uniplex proteins were not affected. Uptake was not recoverable by overexpression of MCU, suggesting MCU alone is not sufficient for in vivo uniporter current and that EMRE is necessary. This was confirmed by voltage clamping EMRE-deficient mitoplasts and measuring mitochondrial Ca^{2+} current, which was severely reduced in mitoplasts lacking EMRE. EMRE has an additional integral role in mediating the association between MCU and MICU1/MICU2; it is proposed that EMRE forms a link between the Ca^{2+} sensing activity of MICU1 and MICU2 in the intermembrane space, and the channel activity of MCU in the inner membrane.

In the absence of MCU, EMRE stability was found to be compromised, and in the absence of EMRE, the MCU complex was found to be smaller, suggesting that EMRE could be an essential assembly protein for the MCU complex. Supporting this idea, in a paper reconstituting the MCU complex in yeast, EMRE was a necessary component for the function of a mammalian channel, but not a fungal channel (Kovács-Bogdán *et al.*, 2014). Currently, EMRE has only been investigated in HEK293T and HeLa cells (Sancak *et al.*, 2013), and briefly in yeast (Kovács-Bogdán *et al.*, 2014), and awaits investigation in further cell lines and types.

MCUR1

Mitochondrial Ca²⁺ uniporter regulator complex 1 (MCUR1) was identified by RNAi screening of mitochondrial membrane proteins proposed to have roles in mitochondrial Ca²⁺ handling; RNAi against the gene CCDC90A was found to inhibit mitochondrial Ca²⁺ uptake (Mallilankaraman *et al.*, 2012a). CCDC90A was found to code for a 40kD protein (now designated MCUR1) that localizes to the inner mitochondrial membrane; it is predicted to contain two transmembrane helices, with the N and C termini both facing the cytosol. Using immunoprecipitation, MCUR1 was found to bind to MCU but not to MICU1 – although MICU1 was also found to bind to MCU when MCUR1 was not bound - or other endogenous inner membrane proteins.

The role of MCUR1 was investigated through the generation and testing of stable MCUR1-knockdown cell lines, which demonstrated significant inhibition of the mitochondrial Ca²⁺ rise after stimulation in intact and permeabilised cells; this inhibition was reversed by MCUR1-rescue shRNA, and MCUR1 overexpressing cells showed an increased (Na⁺/Ca²⁺ exchanger independent) mitochondrial Ca²⁺ uptake ability. The inhibition of mitochondrial Ca²⁺ uptake was proportional to the level of MCUR1 knockdown: in clones in which MCUR1 knockdown was high (>80%), Ca²⁺ uptake was almost entirely abrogated, whereas clones with only a partial knockdown of MCUR1 demonstrated an intermediate inhibition of Ca²⁺ uptake. MCUR1 mediated Ca²⁺ uptake was demonstrated to be dependent on MCU: cells overexpressing MCUR1 showed increased mitochondrial Ca²⁺ uptake, however MCU knockdown significantly reduced this uptake. MCU overexpression was not able to rescue

the reduced mitochondrial Ca^{2+} uptake seen in MCUR1 knockdown cells, showing both proteins are required for uptake.

MCUR1 was suggested to have a regulatory role in MCU mediated mitochondrial Ca^{2+} uptake: knockdown had no effect on $\Delta\Psi_m$, mitochondrial DNA copy number or MCU localization, however in MCUR1 deficient cells MCU mRNA and protein levels were increased. MCUR1 was also found to have a role in oxidative phosphorylation, as MCUR1 knockdown cells demonstrated reduced basal oxygen consumption, constitutively activated AMPK, enhanced AMP/ATP ratio (by two fold), and induced pro-survival macroautophagy, suggesting MCUR1 is essential for the preservation of typical cellular bioenergetics.

Overall, MCUR1 was identified as an essential, inner mitochondrial membrane localized protein necessary for mitochondrial Ca^{2+} uptake. Loss of MCUR1 protein reduced mitochondrial Ca^{2+} uptake in a proportional manner, and interfered with basal metabolism. MCUR1 and MCU appeared to act in a dependent manner, and were shown to bind each other in the absence of MICU1; knockdown of MCUR1 did not affect MCU localization or abundance, suggesting it has a regulatory role, and leading to the designation of the protein as the mitochondrial Ca^{2+} uniporter regulator 1 (Mallilankaraman *et al.*, 2012a).

However, in 2015, a new study was published identifying MCUR1 as a cytochrome c oxidase assembly factor, and not a direct regulator of the MCU complex (Paupe *et al.*, 2015). It was found that knocking down CCDC90A produces a specific defect in cytochrome c oxidase (COX) assembly, which resulted in decreased membrane potential and consequently decreased mitochondrial Ca^{2+} uptake. COX consists of 14 subunits, of which COXI-III are encoded by the mitochondrial genome, and form the catalytic core of the enzyme. The molecular process involved in the assembly of the COX complex is not fully understood. In this study, a MCUR1 knockdown cell line was created and the levels of the COX subunits assessed: it was found that levels of COXI and COXII were reduced, but levels of the other components of the ETC were unaffected (Paupe *et al.*, 2015). The article compared the MCUR1 knockdown cell line to patient fibroblasts from patients with a COX assembly defect, to establish that the reduced $\Delta\Psi_m$ and impaired mitochondrial Ca^{2+} uptake observed in the MCUR1 knockdowns could be caused by a COX assembly defect. It was argued that a homolog of CCDC90A, fmp32 in yeast, produces a COXIV defect, and that the reduction in

mitochondrial Ca^{2+} uptake used as evidence by Mallilankaraman of MCUR1's role as a MCU regulator is merely a consequence of the impaired $\Delta\Psi_m$, itself a consequence of the impaired oxygen consumption resulting from defective COXIV.

The paper demonstrated that whilst COX assembly rates were not affected in MCUR1 knockdown cells, COXII had a much higher turnover rate in knockdowns than in controls, and suggested an alternative function for MCUR1 as a chaperone for COXII, in order to stabilize it until the formation of the COX complex (Paupe *et al.*, 2015). However, the exact role of MCUR1 is still not clear, and requires further investigation.

Solute Carrier 25A23

The mitochondrial carrier superfamily are a family of transport proteins found mostly in the IMM, responsible for the transport of inorganic ions, amino acids, nucleotides, cofactors, and metabolites across the membrane. There are two major groups of Ca^{2+} sensitive mitochondrial solute carriers, the aspartate/glutamate carriers (Lasorsa *et al.*, 2003) and the ATP-magnesium carriers (Fiermonte *et al.*, 2004). Solute carrier SLC25A23, an Mg-ATP/Pi carrier, and its paralogues SLC25A24 and SLC25A25 contain functional, Ca^{2+} sensing, EF hands (Bassi *et al.*, 2005) and the deletion of SLC25A23 reduces oxidative phosphorylation (Amigo *et al.*, 2013). Due to these properties, and predictions that they would form multiprotein complexes located on the IMM, the SLC25 family were previously identified as being of interest during the search for the molecular identity of the MCU (Mallilankaraman *et al.*, 2012a). Similarly to the MCU, solute carriers are extensively found in eukaryotes, and SLC25A23 is highly expressed in brain, heart, skeletal muscle, liver, and small intestine (Bassi *et al.*, 2005). In 2014, the solute carriers were examined in further detail, and it was reported that knockdown of SLC25A23 reduces mitochondrial Ca^{2+} uptake while interacting with MCU and MICU1, and that the EF-hand domains of SLC25A23 are necessary for its function (Hoffman *et al.*, 2014).

Knockdown HeLa cell lines were created using shRNA targeting either SLC25A23, SLC25A24, or SLC25A25, and it was found by confocal microscopy that cells in which SLC25A23 were knocked down demonstrated reduced mitochondrial calcium uptake, and decelerated cytosolic Ca^{2+} clearance (Hoffman *et al.*, 2014). Cells in which either SLC25A24 or SLC25A25

were knocked down were not affected, and none of the knock downs altered total mitochondrial Ca^{2+} or mitochondrial Ca^{2+} efflux. Using overexpression constructs of a mutant version of SLC25A23's EF hands, it was demonstrated that the EF hands are necessary for Ca^{2+} sensing and uptake, and it was found by co-immunoprecipitation that SLC25A23 interacts with both MCU and MICU1 (Hoffman *et al.*, 2014). This is in contrast to the SILAC study which identified EMRE (Sancak *et al.*, 2013), which did not identify SLC25A23 as a part of the MCU complex.

SLC25A23 knock down did not alter mitochondrial morphology or membrane potential, demonstrating that the reduction in mitochondrial Ca^{2+} uptake was not a side effect of altered $\Delta\Psi_m$. It was also found that whilst SLC25A23 had no effect on basal mitochondrial bioenergetics or mitochondrial DNA copy number, ROS levels were decreased in knockdown cells, and levels of the antioxidant glutathione were increased (Hoffman *et al.*, 2014). Interestingly, SLC25A23 knockdown was also protective against t-butyl hydroperoxide stress in a cell death assay, suggesting SLC25A23 has a role linking mitochondrial Ca^{2+} uptake, oxidative stress, and cell death. Several other members of the SLC25 family are also known to have involvement in Ca^{2+} sensing and metabolism: SLC25A24 is involved in the regulation of the ADP/ATP ratio in the mitochondrial matrix (Traba *et al.*, 2012), and aralar (SLC25A12), which is located on the IMM, increases NAD(P)H levels in response to Ca^{2+} sensing (Satrústegui *et al.*, 2007). These observations have led to the suggestion of a mitochondrial Ca^{2+} transportome, in which the components of the MCU complex are functionally integrated with the mitochondrial solute carriers, which form a microenvironment around the uniporter (Hoffman *et al.*, 2014).

Involvement of other proteins in mitochondrial calcium uptake

Due to the surprising results from the MCU knock out mouse (Pan *et al.*, 2013), it has been suggested that there may be some functional compensation: that in the absence of MCU, mitochondria are able to utilise other pathways for Ca^{2+} uptake (Murphy *et al.*, 2014). These could include the proteins mentioned below, the reversal of the $\text{H}^+/\text{Ca}^{2+}$ and $\text{Na}^+/\text{Ca}^{2+}$ exchangers, or proteins as yet undiscovered; for review, see (Pendin *et al.*, 2014). Beyond

the MCU complex, there exist other proteins involved in mitochondrial Ca^{2+} uptake – possible candidates for involvement in any parallel system - of undefined roles, such as Letm1 and UCP2 and UCP3.

Leucine zipper EF hand-containing transmembrane protein 1 (Letm1) was identified in 1999 as a Ca^{2+} binding protein (Endele *et al.*, 1999), and later as an IMM $\text{Ca}^{2+}/\text{H}^+$ antiporter which undergoes extremely sensitive Ca^{2+} loading with slow kinetics (Jiang *et al.*, 2009). The functional role of Letm1 is unresolved, although recently a publication demonstrated that it has a role in the control of cellular bioenergetics and proliferation (Doonan *et al.*, 2014). Uncoupling proteins 2 and 3 (UCP2/3) are IMM ion transporters, which unlike uncoupling protein 1 (UCP1), UCP2/3 are not thought to have a role in heat production (Krauss *et al.*, 2005). In 2007 they were identified as being essential for mitochondrial Ca^{2+} uptake, when knockdown of either protein was found to reduce, or in some cases abolish mitochondrial Ca^{2+} uptake in response to agonist stimulation, without affecting cytosolic Ca^{2+} levels (Trenker *et al.*, 2007). However, another paper found shortly afterward that neither UCP2 or UCP3 knock out mice showed any differences in Ca^{2+} uptake in isolated mitochondria, and argued that the Trenker work used inappropriate controls and tissue samples (Brookes *et al.*, 2008).

A further study in 2011 aimed to clarify the respective role of these proteins. It was demonstrated that UCP2/3 and Letm1 mediated Ca^{2+} signals are from different Ca^{2+} sources: UCP2/3 were demonstrated to account for Ca^{2+} uptake from ER-derived intracellular Ca^{2+} release, and Letm1 for store-operated Ca^{2+} entry (SOCE) (Waldeck-Weiermair *et al.*, 2011). These paths were found to be independent of each other, as knockdown of both UCP2/3 and Letm1 had an additive effect, and knockdown of Letm1 during overexpression of UCP3 did not reduce the increased Ca^{2+} uptake caused by UCP3 overexpression. As this study was carried out prior to the identification of the MCU, the link between these pathways and the MCU was not explored, however the pathways were found to be independent of MICU1, which was then known (Waldeck-Weiermair *et al.*, 2011). Defining the exact role of these pathways, and their relation to each other and MCU, is still an outstanding question.

The mitochondrial permeability transition pore

The mitochondrial permeability transition pore (mPTP) is a non-specific pore which opens in the inner mitochondrial membrane, allowing the passage into the mitochondria of molecules <1.5kDa, an event called the mitochondrial permeability transition. The pore was first identified as such by Haworth and Hunter (Haworth and Hunter, 1979; Hunter and Haworth, 1979a, b), although it had previously been observed that exposure to high Ca^{2+} concentrations resulted in mitochondrial swelling which was partially reversible by calcium chelation (CHAPPELL and CROFTS, 1965; CROFTS and CHAPPELL, 1965). Patch clamp studies on mammalian mitoplasts followed, which revealed the presence of a high conductance channel, called the mitochondrial mega channel (MMC), which possessed all the features of the mPTP (Kinnally *et al.*, 1989) (Petronilli *et al.*, 1989). The role of mPTP in healthy cells is not yet clear. One proposal is that ageing mitochondria which are becoming more vulnerable to mPTP opening, may have transient openings of mPTP which mark them for recognition by autophagic vacuoles, thus keeping the cell's mitochondrial population healthy (Rodriguez-Enriquez *et al.*, 2004). Short term openings of the mPTP may have a physiological role in Ca^{2+} regulation (by providing a quick release mechanism), and ROS homeostasis (Petronilli *et al.*, 2001; Zorov *et al.*, 2014). In disease states in which previously healthy cells experience conditions that lead to the mitochondrial permeability transition, the opening of the mPTP is a mitochondrial catastrophe which, unless reversed, results in cell death (see Figure 1.6).

Mechanism of mPTP opening

The primary stimulus for the opening of the mPTP is matrix Ca^{2+} concentration. Although the specificity for Ca^{2+} appears to be absolute, the concentration is not – the concentration of calcium required for the opening of mPTP is highly dependent on the conditions within the cell. Factors such as oxidative stress, increased phosphate concentrations or decreased adenine nucleotide concentrations contribute to mPTP opening (Halestrap *et al.*, 2004), whereas factors such as the presence of other divalent cations (Sr^{2+} , Mn^{2+} , Ba^{2+} and Mg^{2+}), and low pH act as inhibitors (Halestrap, 1991; Bernardi *et al.*, 1992). High $[\text{Ca}^{2+}]$ is not always an essential requirement: in mitochondria isolated from MCU (-/-) mice, the extent

of necrosis after ischaemia-reperfusion injury did not differ from wild-type littermates, despite the lack of mitochondrial Ca^{2+} overload (Pan *et al.*, 2013), although in conditional MCU knock out mice there was protection against IR injury (Kwong *et al.*, 2015; Luongo *et al.*, 2015). Therefore, addition of Ca^{2+} is not always necessary for pore opening, as an agent which increases a pore inducing condition such as oxidative stress, can sensitize mitochondria to the existing matrix Ca^{2+} , and thus result in pore opening.

When the mPTP opens, protons are able to freely cross the inner mitochondrial membrane, meaning that the proton motive force, and resulting mitochondrial membrane potential are lost. Consequently, oxidative phosphorylation is uncoupled, and the ATP synthase reverses its direction of action; this means that the mitochondrion not only stops producing ATP, but consumes it. As ATP is free floating in the cell, mitochondria in which the mPTP has opened will consume the ATP produced by other mitochondria and by glycolysis, leading to a bioenergetics crisis in the cell (Halestrap *et al.*, 1998). There is also an abrupt increase in permeability: mitochondrial swelling occurs as a result of equilibration of all small molecular weight molecules between the mitochondrial matrix and the cytosol, as small molecules usually excluded from the mitochondria become able to travel through the mPTP into the mitochondrial matrix. This causes osmotic pressure which results in swelling of the mitochondrial matrix; whilst this in itself is not problematic as the cristae unfold, the swollen matrix then exerts pressure on the outer mitochondrial membrane, which will eventually rupture (Bernardi *et al.*, 2006). As the mitochondrion ruptures cytochrome c, and other pro-apoptotic proteins (such as endonuclease G and AIF) are released which may lead to apoptotic cell death (Bernardi *et al.*, 2006), although mPTP opening more commonly leads to necrotic cell death due to ATP depletion.

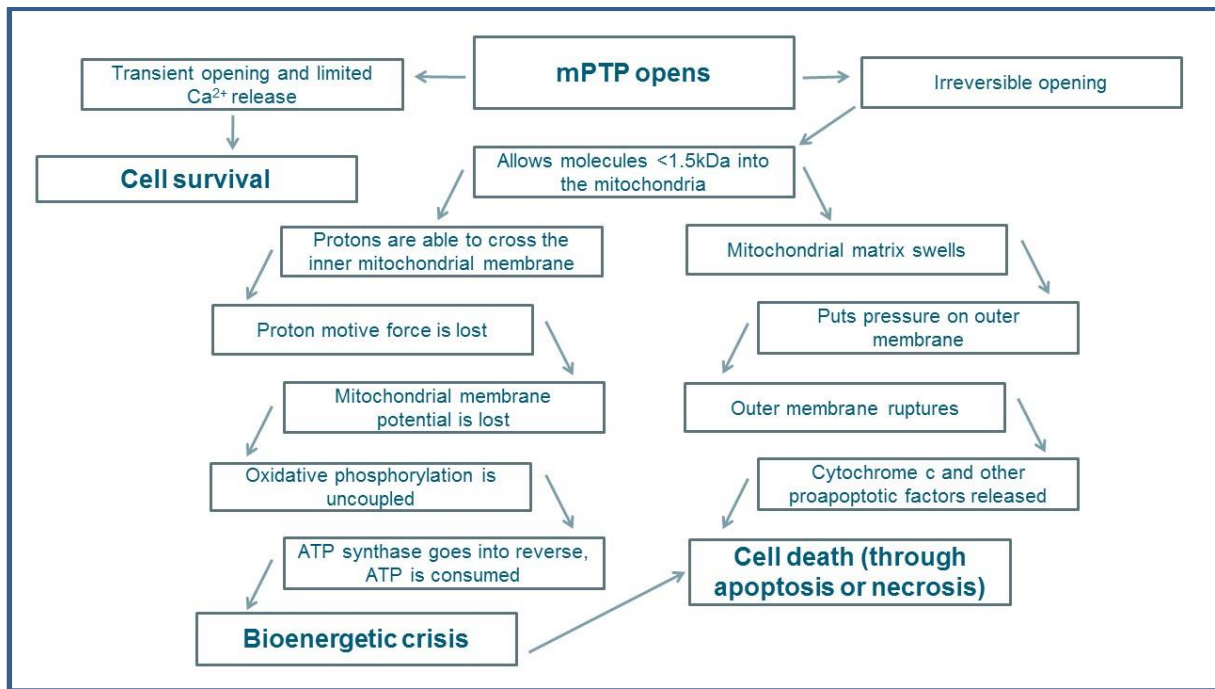


Figure 1.6: Irreversible opening of the mPTP leads to cell death.

mPTP and cell fate

There has long been evidence for transient opening of the pore (Crompton and Costi, 1990; Zoratti and Szabó, 1994). It has been hypothesized that this is a mechanism for fast Ca^{2+} induced Ca^{2+} release, and plays a role in normal cellular Ca^{2+} homeostasis (Barsukova *et al.*, 2011). Ca^{2+} uptake through the uniporter can rapidly accumulate Ca^{2+} into the mitochondria, but the efflux mechanisms (the $\text{Na}^+/\text{Ca}^{2+}$ exchanger and the $\text{H}^+/\text{Ca}^{2+}$ exchanger) are slow, meaning a sudden decrease in cytosolic Ca^{2+} cannot be immediately rectified by these pathways: transient opening of mPTP could provide a solution to this imbalance (Bernardi and Petronilli, 1996). Transient opening of the pore can be measured by rapid changes between conductance states of the pore, and does not result in cell death (see Figure 1.6) (Petronilli *et al.*, 2001; Zoratti *et al.*, 2009); a recent paper demonstrated transient (57 ± 5 seconds) opening in adult cardiac myocytes, which was suppressed by suppressing mitochondria Ca^{2+} uptake, by CsA, and in cyclophilin D knockout mice (Lu *et al.*, 2016). This work also demonstrated that the transient pore is smaller in size, with permeability of $<600\text{Da}$.

However, irreversible opening of mPTP marks a point of no return for the mitochondrion, and where widespread within the mitochondrial population, for the cell. Opening of mPTP

can lead to cell death through either necrosis or apoptosis, depending on the dynamics of opening. In order to undergo apoptosis, a cell must reach a threshold concentration of pro-apoptotic factors (released from the intermembrane space by mitochondrial swelling and rupture), whilst maintaining sufficient ATP concentrations to carry out pro-apoptotic signalling and the assembly of the apoptosome (Rasola and Bernardi, 2011). Necrotic cell death is caused by a deficiency in ATP levels, which through disruption of ionic, metabolic and Ca^{2+} homeostasis activates nucleases, phospholipases and proteases. Conditions favouring apoptotic cell death may be accomplished when mPTP opens in localised subpopulations of mitochondria, and even if mPTP opening does not happen on a large enough scale to deplete ATP levels, apoptosis may occur (Kinnally *et al.*, 2011). However, if a large portion of the mitochondria in a cell undergo mPTP opening simultaneously, this will lead to too immediate a loss of ATP to allow apoptosis, and cell death by necrosis will occur as a result of the elevated cytosolic $[\text{Ca}^{2+}]$ (Kinnally *et al.*, 2011).

Molecular identity of the mPTP

To date there has been no definitive study which identifies the mPTP, although several candidates have been suggested, and structural components of the pore have been identified.

Cyclophilin D

CypD is a protein encoded by the PPIF gene (in mice) on chromosome 10. It is synthesized in the cytosol and translocates to the mitochondria using a mitochondrial targeting sequence (Johnson *et al.*, 1999). Cyclophilin D was first identified as having a role in mPTP opening when it was observed that the potency of various CsA analogues correlated with the extent of their inhibition of a matrix peptidyl-prolyl cis-trans isomerase: cyclophilin D (Halestrap and Davidson, 1990). Whilst CypD was not suggested to form the pore itself, its role was initially unclear. This was clarified by the generation of Ppif^{-/-} mice; isolated liver, heart and brain mitochondria from the mice do not exhibit CsA sensitive mPTP opening, but do exhibit mPTP opening at higher mitochondrial $[\text{Ca}^{2+}]$, and primary hepatocytes and fibroblasts are protected from Ca^{2+} overload (Baines *et al.*, 2005; Nakagawa *et al.*, 2005), thus demonstrating that cyclophilin D has a role in conferring Ca^{2+} sensitivity on the pore. Loss of

CypD did not affect the ability of cells to undergo apoptosis, but were resistant to necrotic cell death, confirming the role of mPTP in necrosis (Nakagawa *et al.*, 2005). CypD has had an important role in the investigation of the identity of the mPTP, as interactions with it have often been used as evidence in favour of various candidates: it is accepted that whatever the identity of mPTP, it is an essential requirement that it is regulated by CypD.

A multiprotein complex: VDAC, ANT, and TSPO

For a long time, the voltage dependent anion channel (VDAC) and adenine nucleotide translocator (ANT) were considered prime candidates for the molecular identity of the mPTP. The theory was founded by the discovery that the peripheral benzodiazepine receptor (TSPO) copurified with VDAC and ANT (McEnery *et al.*, 1992). High affinity ligands of TSPO were also identified in the fractions in which these three proteins were co-expressed; this was of interest as these ligands were known to affect the electrophysiological properties of the MMC, thereby suggesting that these proteins could be structural components of mPTP (Kinnally *et al.*, 1993). This idea was further supported by the existence of OMM-IMM contact sites, which were proposed to facilitate transport of adenine nucleotides to and from the mitochondria; these contact sites included VDAC, ANT, hexokinase, and creatine kinase (Kottke *et al.*, 1988). It was shown that some of these fractions formed channels with conductance correlating to that of the mPTP, and conferred CsA-sensitive permeability to liposomes (Beutner *et al.*, 1996); these fractions were enriched in hexokinases, but not in VDAC or ANT, and also contained Bcl-2 family proteins. This led to the hypothesis that the mPTP was a multiprotein complex containing VDAC, ANT, TSPO, cyclophilin D, hexokinase and Bcl-2 family proteins (Zamzami and Kroemer, 2001).

Other groups focused on the ANT as the main candidate for the mPTP (Halestrap and Brenner, 2003). This was due to its ability to bind cyclophilin D (Crompton *et al.*, 1998; Woodfield *et al.*, 1998), the fact that decreased adenine nucleotides enhance pore opening, and that two modulators of mPTP opening, carboxyatractyloside (CAT) and bongkreikic acid (BKA) are known to act on ANT (Halestrap and Davidson, 1990). VDAC was another popular candidate: it also found able to bind cyclophilin D (Crompton *et al.*, 1998), and it was reported that ubiquinone analogues (which inhibit mPTP) bind to an IMM protein which was

identified as VDAC (Cesura *et al.*, 2003), although this was later proved erroneous (Krauskopf *et al.*, 2006).

However, these hypotheses were discredited by a range of knockout mice, in which mPTP was still found to occur in the absence of VDAC, ANT, and TSPO (Kokoszka *et al.*, 2004; Krauskopf *et al.*, 2006; Šileikytė *et al.*, 2014). Whilst these proteins may have a role in the regulation of mPTP, it is clear they are not essential structural components.

The mitochondrial phosphate carrier

Another proposition for the identity of the pore forming component was the mitochondrial phosphate carrier, PiC (Leung *et al.*, 2008). This was suggested due to the ability of the PiC to form nonspecific channels in lipid membranes, its direct interactions with CypD in the mitochondrial matrix, that mPTP-inhibiting ubiquinone analogues also inhibit PiC, and because Pi is a known activator of mPTP (Crompton *et al.*, 1988; Leung *et al.*, 2008). However, genetic deletion of the Slc25a3 gene (encoding the PiC) showed that mPTP opening could still occur without PiC, but opening was desensitized to Ca^{2+} , confirming that the PiC has a regulatory, rather than a structural role (Kwong *et al.*, 2014).

ATP synthase

Studies which tracked the interactions of matrix CypD with other mitochondrial proteins revealed another potential candidate for the mPTP: the F_1F_0 ATP synthase itself (Giorgio *et al.*, 2009) (Chinopoulos *et al.*, 2011). There are currently two theories proposing different parts of the ATP synthase as candidates.

The first suggests that the pore is formed from dimers of the ATP synthase (Giorgio *et al.*, 2013), see Figure 1.7A. In the study, in phospholipid bilayers containing reconstituted dimers of F_1F_0 ATP synthase, they detected Ca^{2+} activated channels with electrophysiological properties similar to those of mPTP. However, channel opening required the presence of ATP synthase inhibitor benzodiazepine-423 (Bz-423), and high $[\text{Ca}^{2+}]$. It was found that CypD binds to the oligomycin sensitivity conferring protein (OSCP) subunit of the ATP synthase, at the same site as the OSCP is bound by Bz-423. It was further shown that Bz-423 had a CypD like effect in sensitizing the pore to Ca^{2+} , and that decreasing protein expression of OSCP increased the Ca^{2+} sensitivity of the pore. Channel opening was inhibited by AMP-

PNP, a known inhibitor of ATP synthase, but the effects of the canonical inhibitor CsA were not investigated. In a recent review, it was also noted that mPTP opening has previously been demonstrated in PO cells lacking mtDNA for some subunits of the ATP synthase (Bonora *et al.*, 2015). An additional contradicting factor is the previous finding the dimerization of ATP synthase has previously been shown to be associated with increased efficiency of ATP synthesis (Campanella *et al.*, 2008), which is in contrast to mPTP opening, which results in cellular ATP depletion.

The second theory suggests the pore is formed by the c-subunit ring of the membrane spanning F_0 subunit of the F_1F_0 ATP synthase. This theory was first suggested by the finding in HeLa cells, that c-subunit siRNA inactivation results in cells with reduced mPTP opening (Bonora *et al.*, 2013), and c-subunit overexpression increased mPTP opening, although the actual structural role of ATP synthase was not investigated. In a second study it was demonstrated that the c-subunit ring undergoes conformational change on exposure to high matrix Ca^{2+} and becomes detached from the F_1 subunit, suggesting a mechanism for PT (Alavian *et al.*, 2014), see Figure 1.7B. The suggested model was that the sites at which CypD, CsA and Ca^{2+} modulate mPTP activity are located on the F_1 subunit, which dissociates from the c-subunit after Ca^{2+} /CypD binding, enabling the c-subunit ring to expand to form a channel, the mPTP. Reconstituted c-subunits were shown to form a voltage sensitive channel in lipid bilayers - sensitive to adenine nucleotides and anti-c-subunit antibodies - the opening of which resulted in depolarization of the IMM, although the channels conductance range was wide, and not always similar to that of mPTP. However, these channels were not sensitive to Ca^{2+} or CsA; this was further investigated by the reconstitution of F_1F_0 ATP synthase in lipid bilayers which resulted in some channel activity, which was increased by the addition of Ca^{2+} and CypD, and was prevented by CsA (although at an unusually high concentration), supporting the notion of a F_1 binding site. Additionally, sub-mitochondrial vesicles enriched in F_1F_0 formed channels sensitive to Ca^{2+} and CsA, which were not present after the removal of the OSCP and β -subunits respectively (located on the F_1 subunit). Finally, in HEK293T cells, Ca^{2+} induced opening and CsA induced closing was detected by fluorescent labelling of the c-subunit, and c-subunit depletion in HEK293T cells inhibited Ca^{2+} induced loss of $\Delta\Psi_m$ and cell death.

Currently, there is not sufficient evidence to conclude which of these theories (if either) is correct, but it is possible that both could be partially correct in an as yet unknown mechanism, perhaps involving the OSCP, which both theories agree has a role. The interaction of ATP synthase with other regulators of mPTP such as ANT and PiC has not yet been investigated, and may shed further light on the mechanism of action, and the relation between the protein's ATP synthesis activity and pore forming activity will also need investigation. Regardless of which is more accurate, it has become apparent that ATP synthase may have a role in mPTP, which has interesting implications, especially regarding ATP synthesis/hydrolysis during PT. Since publication of these theories, several responses have been published which highlight issues such as inconsistent channel activity, unusually high Ca^{2+} requirements for pore opening, and the protein purity of the sub-mitochondrial vesicles used for patch clamping (Halestrap, 2014; Chinopoulos and Szabadkai 2014; Chinopoulos and Szabadkai 2013; Szabadkai and Chinopolous 2013).

Spastic paraplegia 7

Another gene has recently been identified as being structurally involved in mPTP: spastic paraplegia 7 (SPG7) (Shanmughapriya *et al.*, 2015). Short hairpin RNA (shRNA) was used to individually silence mitochondrial proteins in HEK293T and HeLa cells, in order to assess the loss of function effect on Ca^{2+} and ROS induced mPTP opening, by measuring $\Delta\Psi_m$ and mitochondrial Ca^{2+} retention.

It was found that mitochondrial SPG7 was essential for forming the mPTP complex: ROS sensitive, Ca^{2+} induced mPTP opening was delayed in cells in which SPG7 was not present. This was also found to be the case for CyPD and VDAC1. It was demonstrated by immunoprecipitation that SPG7 interacts with both CyPD (with its matrix portion) and VDAC (with its intermembrane space portion), and that C-terminal SPG7 is essential for CyPD binding, and for mPTP formation. However, a critique of this study suggested that the screening approach is not sufficient to distinguish between core components and regulators of mPTP, and that the paper never demonstrated if the proposed VDAC and SPG7 pore forming complex was actually capable of forming a channel (Bernardi and Di Lisa, 2015).

Mitochondrial Ca²⁺ as a therapeutic target

Role of mitochondrial Ca²⁺ overload in neurodegenerative disease

Excessive mitochondrial Ca²⁺ uptake is a key step in the pathophysiology of many disease states, leading to Ca²⁺ overload and cell injury or death.

Mitochondria have an essential role in the central nervous system (CNS), even more so than in other systems: Ca²⁺ dynamics are especially important in the CNS, as signal transduction between neurons occurs through the delicate spatiotemporal organisation of local [Ca²⁺]. Mitochondria are also essential for maintaining the neuronal energy supply, which comes almost entirely from oxidative phosphorylation (rather than glycolysis), although this is to some extent dependent on the type of neural activity (Figley and Stroman, 2011; Ivanov *et al.*, 2014). Ca²⁺ also has a role in neuronal energy supply, as the rate limiting steps of the electron transport chain are Ca²⁺ dependent. It has also been suggested that the cell-type selectivity of neuronal death in different neurodegenerative diseases could be due to differences in mitochondrial Ca²⁺ handling between cell types (Duchen, 2012), as there is a huge diversity of Ca²⁺ channels and receptors within the CNS. Therefore, neurons are especially vulnerable to mitochondrial dysfunction and it is a common feature of neurodegenerative diseases: mitochondrial defects have been found in Parkinson's disease, Huntingdon's disease, Alzheimer's disease and Friedreich's ataxia, among others (for reviews see (Damiano *et al.*, 2010; Swerdlow *et al.*, 2010; Winklhofer and Haass, 2010; González-Cabo and Palau, 2013).

In 1985 it was found that prolonged exposure of neurons to glutamate resulted in Ca²⁺ induced cell death (Choi, 1985). Glutamate induced excitotoxicity is a process in which increased Ca²⁺ influx in the cell (see Figure 1.8) causes mitochondrial Ca²⁺ overload resulting in increased cell death through necrosis and apoptosis (Stout *et al.*, 1998; Abramov and Duchen, 2008). This leads to the irreversible loss of neurons which characterises neurodegenerative disease. This process occurs through the Ca²⁺ permeable glutamate receptors, the NMDA receptor and the AMPA receptor – while other receptors can also allow Ca²⁺ to enter neurons, it was discovered that there is a 'source-specificity' of Ca²⁺ toxicity, and that equal Ca²⁺ influx through other sources (for example the voltage gated Ca²⁺ channel) do not lead to toxicity and death (Tymianski *et al.*, 1993). This specificity is

due to the colocalization of these receptors with neuronal nitrous oxide synthase (nNOS), which produces the toxic nitrous oxide (NO) (Sattler *et al.*, 1999), in addition to dangerously high Ca^{2+} concentrations.

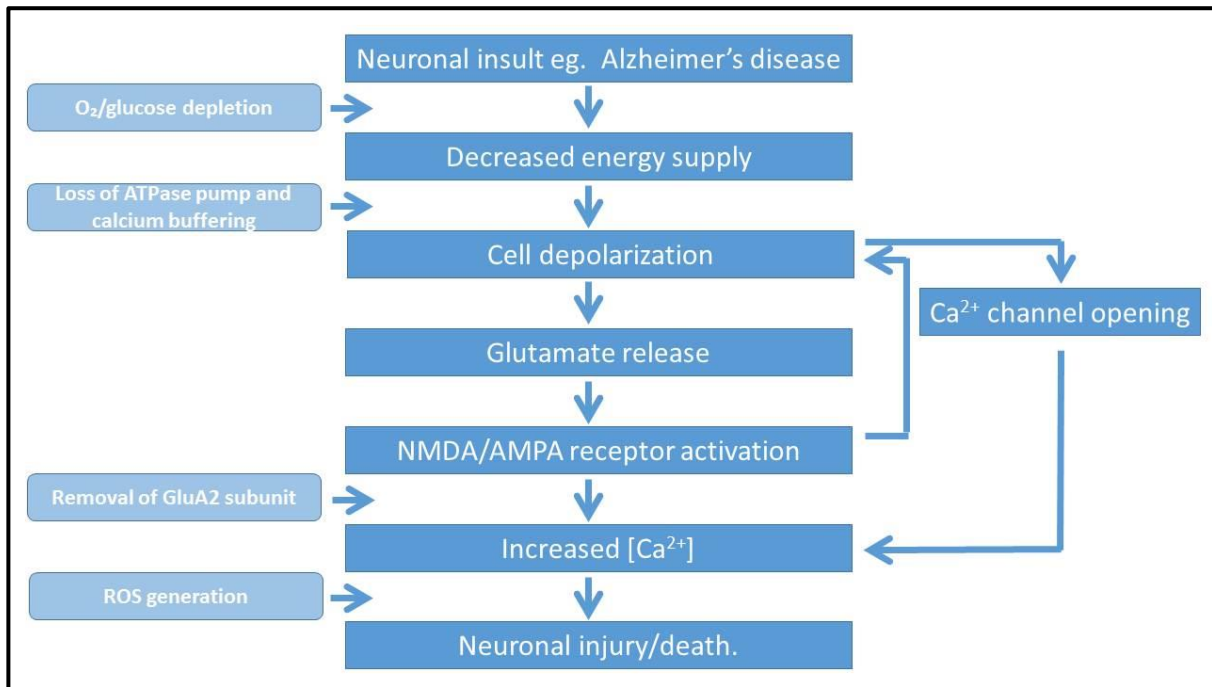


Figure 1.8: Ca^{2+} overload leads to neuronal cell death. A reduction of ATP due to neuronal insult causes a rundown of ion gradients. This leads to cell depolarization, resulting in loss of Ca^{2+} homeostasis, causing an influx of Ca^{2+} into neurons which ends in neuronal injury or death. NMDA/AMPA receptor activation by glutamate creates a feedback loop by further depolarising cells, further increasing $[\text{Ca}^{2+}]$.

The danger to mitochondria in glutamate toxicity is from the delayed calcium deregulation (DCD) which follows up to two hours after the initial glutamate exposure. The DCD is characterised by a secondary, larger Ca^{2+} rise, simultaneous to a collapse of $\Delta\Psi\text{m}$. The DCD can be prevented using nNOS inhibitors, suggesting a causal link between the glutamate induced increase in NO, and the mitochondrial failure that occurs following loss of $\Delta\Psi\text{m}$ (Keelan *et al.*, 1999; Vergun *et al.*, 1999) – due to neuronal dependence on oxidative phosphorylation and their inability to provide sufficient energy through glycolysis, this leads to neuronal death. Whilst this neuronal death is presumed to be mediated by the opening of mPTP, it has not yet been definitively proved that this is the case: although infarct size

was reduced in the CypD knockout mouse, mitochondria still underwent depolarisation after exposure to glutamate (Baines *et al.*, 2005; Abramov and Duchen, 2008). Whilst the mechanism of cell death is not clear, mitochondrial Ca^{2+} overload is clearly implicated in the pathogenesis of many neurodegenerative diseases.

As mitochondrial Ca^{2+} overload is a critical checkpoint in cell survival, it has been proposed that inhibition of mitochondrial Ca^{2+} uptake may be protective against cell death. If inhibition of mitochondrial Ca^{2+} uptake could be targeted to specific cell types or locations which were undergoing cell death then this could be a useful therapeutic intervention in diseases, such as neurodegenerative disease, which are characterized by excessive cell death. Therefore, the study of the mitochondrial Ca^{2+} uptake machinery and the expansion of our understanding of its molecular function may have great therapeutic potential for the treatment of diseases in which Ca^{2+} induced cell death is a factor.

Role of mPTP in neurodegenerative disease

Many early researchers of mPTP focused on its role within the heart, as many of the activating conditions which stimulate mPTP opening are present during reperfusion following cardiac ischaemia (Crompton *et al.*, 1987; Halestrap *et al.*, 1998). Inhibition of mPTP opening has long been the focus of intense research, and is known to be protective against cardiac cell death (Nazareth *et al.*, 1991; Griffiths and Halestrap, 1993). However, mPTP also plays an important role in the brain.

Disruption of Ca^{2+} homeostasis is a common feature in many disorders of the CNS. Ca^{2+} enters neurons through many paths: receptors, $\text{Na}^+/\text{Ca}^{2+}$ exchangers, and acid or voltage dependent ion channels (Szydłowska and Tymianski, 2010). During brain ischaemia and neurodegenerative disease, reduced reuptake of neurotransmitters causes overstimulation of their receptors, resulting in nerve depolarization and activation of voltage dependent Ca^{2+} channels (for review see (Dong *et al.*, 2009)). Neuronal excitotoxicity is characterized by an excessive influx of Ca^{2+} into neurons, which results in the activation of hydrolytic enzymes, ROS formation, mitochondrial depolarization and eventually neuronal death. mPTP opening is believed to be the cause of this neuronal death, as has been demonstrated in cultured neurons (Pivovarova *et al.*, 2004) and in mice (Schinzel *et al.*, 2005), and mPTP

inhibitor CsA has been found to be protective against hypoglycemic and IR brain injuries (Friberg *et al.*, 1998; Khaspekov *et al.*, 1999). Dysregulation of Ca^{2+} homeostasis is more common as neurons age and Ca^{2+} gradients in the cell are less tightly maintained, and in neurodegenerative disease this progressively worsens.

Calcium dysregulation has been demonstrated to have a role in many neurodegenerative diseases. For example, in Alzheimer's disease, aggregates of amyloid beta (a hallmark of the disease) can cause the formation of Ca^{2+} permeable pores in neuronal plasma membranes and affect the activity of existing Ca^{2+} channels (Supnet and Bezprozvanny, 2010). In Parkinson's disease, characterised by aggregates of α -synuclein and loss of dopaminergic neurons in the substantia nigra, α -synuclein causes neuronal Ca^{2+} accumulation; in the autosomal recessive form of Parkinson's caused by mutations in the PINK1 gene, there is dysfunction in the $\text{Na}^+ / \text{Ca}^{2+}$ exchanger of the IMM, which leads to increased mitochondrial calcium both in resting and stress conditions (Gandhi *et al.*, 2009). In Huntington's disease, caused by mutations in the gene encoding the protein Huntingtin (htt), neurons carrying this mutant gene have been found to have dysregulated mitochondrial Ca^{2+} homeostasis, reduced Ca^{2+} buffering capacity, and increased sensitivity of mPTP opening (Panov *et al.*, 2005; Gellerich *et al.*, 2008; Lim *et al.*, 2008).

Ca^{2+} dysregulation can lead to mPTP opening through the exceeding of the mitochondrial Ca^{2+} buffering capacity, resulting in excess cell death. Therefore, inhibitors which reduce mPTP opening as a result of Ca^{2+} dysregulation would be widely applicable to most neurodegenerative diseases, and mPTP is a desirable target for the treatment of these diseases.

Aims

Ca^{2+} is crucially important to mitochondrial and cellular function.

Mitochondria are capable of rapidly taking up Ca^{2+} through the MCU in response to cytosolic $[\text{Ca}^{2+}]$ increases, which affects mitochondrial energetics, morphology and autophagy, in addition to regulating localization, timing and amplitude of cytosolic Ca^{2+} waves. The MCU was identified in 2011, and a series of associated proteins and regulators have been discovered since. During pathological conditions, excessive mitochondrial Ca^{2+} uptake leads to matrix overload, stimulating the opening of the mPTP and leading to cell death.

In this thesis, I investigated aspects of the mitochondrial calcium transport system, and how it can be targeted for therapeutic use. My aims were:

- To investigate the efficacy of a group of novel compounds as inhibitors of the mPTP.
- To develop a novel screening approach to identify inhibitors of the MCU.
- To investigate the physiological and pathophysiological role of the MCU and associated proteins through genetic manipulation, and to explore the relative protein levels of MCU and associated proteins through development.

Chapter 2: Targeting the Mitochondrial Permeability Transition Pore

Introduction

Existing inhibitors of mPTP

As mPTP is a target for neuroprotection (Kristal *et al.*, 2004), it is highly desirable to develop pharmacological agents which can target mPTP opening specifically and effectively, without unwanted side effects, and which can be protective even against the most potent of mPTP inducing stimuli. Our lack of knowledge of the molecular identity of the mPTP is a bottleneck in the development of new therapeutic approaches, as it is difficult to determine the mechanism and safety of novel compounds when their target specificity cannot be assessed. However, some compounds are known to inhibit (or desensitize) pore opening.

Cyclosporin A was the first compound identified as an inhibitor of the mPTP ((Crompton *et al.*, 1988; Szabó and Zoratti, 1991; Duchen *et al.*, 1993; Griffiths and Halestrap, 1993). CsA binds to cyclophilins; CsA binds to the cytosolic molecule cyclophilin A, which inhibits the protein phosphatase calcineurin, which activates T cell immune response via NFAT, thereby giving CsA immunosuppressive properties (see Figure 2.1). It additionally binds to mitochondrial cyclophilin D, and through preventing the peptidyl prolyl isomerase activity of cyclophilin D, and preventing the binding of CypD to the adenine nucleotide transporter (ANT), thus reduces Ca^{2+} sensitivity of pore opening (Crompton *et al.*, 1988; Woodfield *et al.*, 1998). However, CsA is only effective at a narrow range of concentrations, with optimal inhibition at ~200nM (in cells), and no effect at very low or very high concentrations (Nazareth *et al.*, 1991): a biphasic response (Griffiths and Halestrap, 1993). CsA is in clinical use, most commonly to prevent organ rejection post transplantation, however it has several toxic side effects when used clinically, including nephrotoxicity, renal vascular damage and hypertension (Caramelo *et al.*, 2004), and fails to cross the BBB, making alternative compounds desirable.

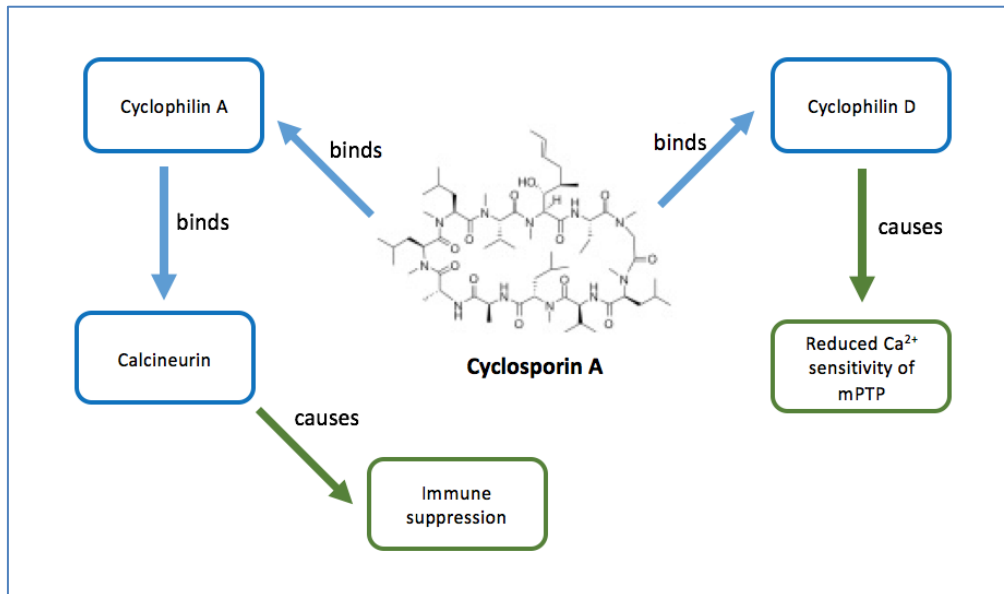


Figure 2.1: Cyclosporin A indirectly binds calcineurin and directly binds Cyclophilin D, resulting in its two effects of immunosuppression and reduced Ca²⁺ sensitivity of mPTP. Actions are shown in blue and consequences in green.

To overcome the calcineurin binding issues of CsA, several analogues have been identified or synthesized, which do not effect calcineurin, such as Sanglifehrin A, [MeAla⁶]CsA, 4-methyl-val-CsA and others (Durette *et al.*, 1988; Aebi *et al.*, 1990; Lee *et al.*, 1990; Clarke *et al.*, 2002). Sanglifehrin A was identified in 2002 as another inhibitor of mPTP opening (Clarke *et al.*, 2002). Like cyclosporin, it also binds cyclophilin A, and is an immunosuppressant, but the CypA-SfA complex does not bind calcineurin, and exerts its immunosuppressive effects by blocking T cell proliferation directly. This is an advantage for cardiac research, as calcineurin has a role in heartbeat regulation, which CsA can disrupt (Halestrap *et al.*, 2004). Whilst Sanglifehrin is as potent a pore inhibitor as CsA, it has a different mechanism, as it does not prevent CypD binding to the ANT; Sanglifehrin is not commercially available and therefore has been less widely used and studied. A problem common to both CsA and SfA is that they are not absolute inhibitors of mPTP. They reduce the sensitivity of the pore to Ca²⁺ but only decrease the probability of opening, they do not prevent it indefinitely. This is a disadvantage, because in conditions in which there is a prolonged high [Ca²⁺] or oxidative stress, these compounds will not prevent pore opening once their maximum potency has been exceeded (Clarke *et al.*, 2002). These conditions can be present in disease models in which CsA could be used, such as neurodegenerative disease, and ischaemia reperfusion (IR) injury, which could limit the utility of such

compounds: in IR injury, it has been demonstrated that the beneficial effect of CsA is due to its action during reperfusion, and not ischaemia (Halestrap *et al.*, 2004).

Other approaches to inhibiting mPTP target the stimuli which result in mPTP opening, rather than the pore itself: theoretically by modifying the prevailing conditions to an environment less favourable to mPTP opening, the likelihood of pore opening can be reduced. These methods include ischaemic pre and post conditioning (Javadov *et al.*, 2003; Gateau-Roesch *et al.*, 2006), antioxidants (Kerr *et al.*, 1999; Adlam *et al.*, 2005), and Na⁺/H⁺ exchanger inhibitors (during ischaemia the Na⁺/H⁺ exchanger is activated by a decrease in pH, leading to increased [Na⁺], which causes a reversal of the Na⁺/Ca²⁺ exchanger, resulting in Ca²⁺ accrual) (Karmazyn *et al.*, 2001; Javadov *et al.*, 2008).

A range of new compounds were developed by the Selwood laboratory at UCL, and provided to our lab for testing. These novel compounds were derived from CsA, with modifications made with the goal of reducing the immunosuppressive effects of CsA, and making the compounds selective for CypD (the mitochondrial cyclophilin) over CypA (the cytosolic cyclophilin), with a high potency as inhibitors of mPTP opening. It was also desirable to produce a molecule with a better cytotoxic profile than CsA, and the ability to reach significant brain levels, in order to be able to target neurodegeneration and, specifically, a mouse model (experimental autoimmune encephalomyelitis, or EAE) which of Multiple Sclerosis (MS) collaborators at Queen Mary University possessed. mPTP has been suggested to play a role in MS as it is a disease characterised by chronic inflammation, which results in increased levels of ROS and NO, conditions favourable to mPTP opening. The axonal degeneration found in MS has been demonstrated to feature mitochondrial damage (Su *et al.*, 2009), and the signal transduction protein p66Shc, which is associated with an increase in mPTP opening, has been shown to be protective in EAE (Savino *et al.*, 2013).

It was desirable to make the compound selective for CypD over CypA: this is difficult as the cyclophilins have very similar structures and sequences (Davis *et al.*, 2010). A potential solution to this is to enable cellular localization through structural modification. Therefore, the compound was modified to promote targeting to the mitochondria (as CypD is the mitochondrial cyclophilin variant). Previously, triphenylphosphonium (TPP⁺), a lipophilic cation that is partitioned into the matrix by the mitochondrial membrane potential, has

been used for mitochondrial targeting (Ross *et al.*, 2005), as it accumulates in the matrix at 10-100 fold the accumulation into the cytoplasm (Smith *et al.*, 2003). However, TPP has a high molecular weight and mitochondrial toxicity (Warne *et al.*, 2016), making it non-ideal so a different approach was used: the quinolinium cation was chosen due to its small molecular weight and chemical simplicity. Addition of the quinolinium moiety makes the compound more lipophilic, and more positively charged, in order to promote its concentration into the negatively charged mitochondria (Warne *et al.*, 2016).

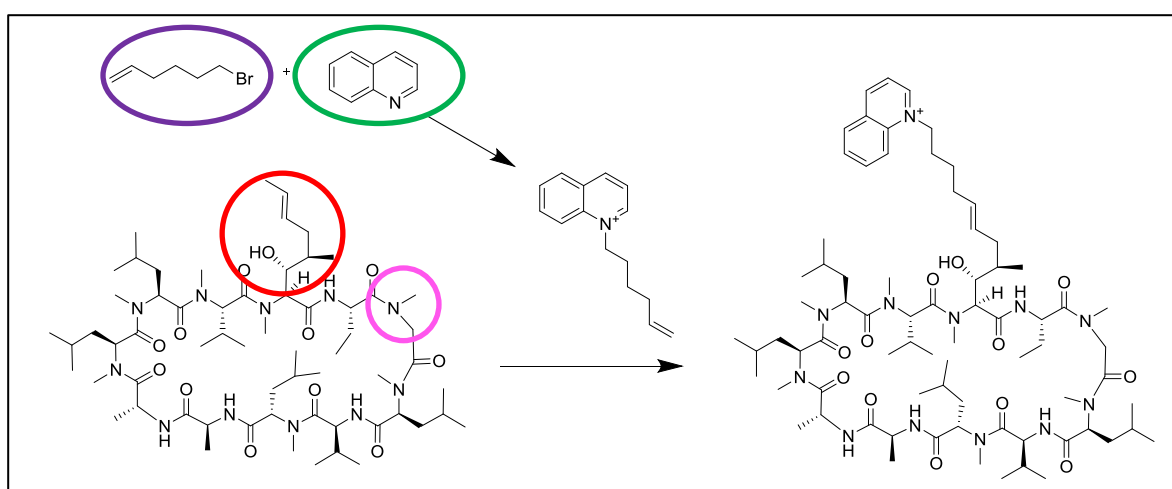


Figure 2.2: CsA was modified to produce new compounds. The chemical structure of CsA (left), of which the new compounds are derivatives, and of one of the new compounds, JW47 (right). The quinolinium cation (circled in green) was added at the the [Bmt]¹ side chain (circled in red) by olefin cross-metathesis, due to the prediction that addition at this position would have the same effect as addition at the [Sar]³ position (circled in pink). A hydrocarbon chain (circled in purple) was used as a chemical linker. Figure taken from Warne *et al.*, 2016 (with permission), and annotated.

The Selwood lab had previously created a non-immunosuppressive, non-targeted compound called SmBzCsA (Malouitre *et al.*, 2010), by adding methylbenzoate to CsA at the [Sar]³ position. The [Sar]³ position has been previously demonstrated to be necessary for calcineurin binding (Rasaiyaah 2013), but is predicted to be non-essential for cyclophilin binding. The novel compounds were constructed by modifying CsA by adding the quinolinium cation at the [Bmt]¹ side chain, which they predicted would have a similar effect to addition at the [Sar]³ position (see Figure 2.2). The immunosuppressive effects of CsA are caused by a complex of CsA, CypA and calcineurin which inhibits dephosphorylation of nuclear factors of activated T-cells (NFAT), a family of transcription factors important to

immune response (Hogan *et. al.*, 2003), so disruption of this binding complex should reduce immune suppression.

In this project, we aimed to screen an array of related novel compounds in order to assess the success of the quinolinium ion targeting approach, by investigation of their effect on mPTP opening, and by comparison of their potency with CsA; with any successful inhibitors, to investigate their molecular target, and mitochondrial toxicity profile.

Methods

Mitochondrial isolation

Subcellular fractionation was performed as previously described (Astin et al. Sci Rep 2013). C57BL/6J male mice of 3-6 months were sacrificed by cervical dislocation, and the liver was removed and placed immediately into ice-cold isolation buffer (250mM mannitol, 5mM HEPES, 0.5mM EGTA, pH 7.4). In a cold room at 4°C, the liver was rinsed in PBS to remove excess blood, and any fat and connective tissue was dissected away. PBS was then replaced with isolation buffer containing 1mM phenylmethanesulfonyl fluoride (PMSF), and the liver was chopped into pieces (approximately 2mm cubes). Tissue was then homogenized in this solution until no solid matter remained, and then centrifuged at 800G for 10 minutes at 4°C. The nuclear pellet was then discarded, and the post nuclear supernatant retained, and centrifuged at 10300G for another 10 minutes at 4°C. The post-mitochondrial supernatant was discarded, and the mitochondrial pellet was resuspended in isolation buffer and 1mM PMSF, and kept on ice. Protein levels were quantified using a ThermoScientific BCA protein quantification assay, as per manufacturer's instructions.

Calcium retention capacity assay

Isolated mitochondria were resuspended (500µg protein/ml) in MSK buffer (75mM mannitol, 25mM sucrose, 5mM potassium phosphate monobasic, 20mM Tris-HCl, 100mM KCl, and 0.1% (w/v) bovine serum albumin, pH 7.4, as previously described by (Rueda *et al.*, 2015) and others) supplemented with 10mM succinate (a Complex II substrate), 1µM rotenone (a Complex I inhibitor) and 1µM Fluo5N (a cell-impermeant calcium indicator). 200µl mitochondrial suspension per well was used in 96 well microplates. Compounds were incubated for ten minutes before the plate was assayed in a Fluostar Optima plate reader, using Ex/Em filters at 480/520nm; CaCl₂ (10µM) was injected approximately every 6.5 minutes for 80 minutes (12 total injections, final concentration of 75µM). In order to calculate % inhibition of Ca²⁺ induced pore opening, the method detailed below in Table 2 was followed. Significance was assessed by one-way ANOVA, in comparison to a CsA control. When using CypD (-/-) mice, it was found, as would be expected, the pore had much lower sensitivity to Ca²⁺, and therefore to ensure pore opening, the injected CaCl₂ was increased to 40µM (giving a final concentration of 280µM), and there were 24 total

injections rather than 12; to allow room for the additional injection volume, 100µl of mitochondria were plated per well (at 1mg/ml, to give the same total protein as in the original experiments).

Where A, B, and C represent the total fluorescence values of no Ca ²⁺ additions (A), no mitochondria (total B), and no compound (C):	
Method	Example, with sample condition "X"
1. The total fluorescence value for each condition was calculated:	➤ Sum of timepoints 1-80 (inclusive) for condition "X" = X
2. Background (no Ca ²⁺ additions trace) was subtracted from each, for background correction:	➤ $X - A = X_1$
3. The background corrected values were then divided by the "no mitochondria" control, representing the total amount of Ca ²⁺ added which remained unbuffered by mitochondria:	➤ $X_1 / B_1 = X_2$
4. Percentage inhibition for each [compound] was then calculated as the % of the corresponding value for the untreated condition	➤ % Inhibition of condition "X" = $(1 - (X_2 / C_2)) * 100$

Table 2: The method used to calculate percentage (%) inhibition for each condition of a calcium retention capacity (CRC) assay.

Preparation of rat cortical neurons in culture

17 days after first showing signs of pregnancy (a vaginal mucus plug), an adult female rat (*Rattus norvegicus*) was sacrificed according to Home Office Regulations, using the Schedule 1 technique of cervical dislocation, with confirmation of death by decapitation. The embryonic day 17 (E17) embryos were removed from the womb and the amniotic sac, decapitated, and their heads stored in 4°C phosphate buffered saline (PBS) on ice. The brains were then dissected: scissors were used to cut through the skull from the base of the brain stem in a straight line forward to the embryo's nose. The skin and skull were then peeled back using curved forceps in order to remove the brain, and the cortices were dissected from the rest of the brain. The meninges were then removed, and the cortices

gently crushed (in order to increase surface area for enzymatic digestion), and placed in fresh PBS on ice. When sufficient cortices had been dissected (usual yield 15-20million cells/embryo), the PBS was then replaced with freshly prepared papain in PBS (0.4mg/ml, 1ml/pair of cortices), and the cortices were incubated in the papain for 20 minutes at 37C. After incubation, the papain was removed and replaced with DNase (0.4mg/ml, 1ml/pair of cortices) in order to prevent viscosity in the subsequent step: using a blunt fill needle (18G x 1 ½, 1.2mm X 40mm) and a syringe the solution was gently triturated in order to dissociate the brain tissue. When the solution was sufficiently homogenous, it was then centrifuged at 500g for 5 minutes in order to form a cell pellet. After centrifugation, the supernatant was removed, and the pellet resuspended in neurobasal medium (supplemented with Glutamax (1X), B27 (1X), and penicillin/streptomycin (1% v/v)). The cells were then counted, and plated at the required density onto plates which had previously been treated with poly-L-lysine for at least 30 minutes, and then washed with distilled H₂O. Cells were grown in an incubator at 37°C with 5% CO₂ and 95% humidity. The medium was changed 48 hours after plating, and then half changed every 3-4 days.

Confocal imaging of fluorescein-tagged compound

DIV9 rat cortical neurons which had been plated at a density of 1 million cells/well, on glass coverslips (22mm) in 6 well plates, were incubated for 30 minutes at 37°C with the cell permeant cationic dye tetramethylrhodamine methyl ester (TMRM, 25nM), the nuclear marker Hoechst (5µg/ml), the L-type calcium channel blocker verapamil (40µM), and the fluorescein-tagged quinolinium compound (1µM in DMSO) in recording buffer (NaCl (150mM), KCl (4.25mM), NaH₂PO₄ (1.25mM), NaHCO₃ (4mM), CaCl₂ (1.2mM), HEPES (10mM), glucose (10mM), MgCl₂ (1.2mM)). Cells were imaged on a Zeiss 700 LSM confocal microscope, using a 63X oil objective. Hoechst fluorescence was excited at 405nm, TMRM at 555nm and fluorescein at 488nm, and measured using filters at 420-490nm, 488-555nm, and a long pass 560nm filter respectively.

Measurement of mitochondrial membrane potential (*in vitro*)

DIV 8-9 rat cortical neurons which had been plated at a density of 50000cells/well in 96 well plates, were incubated for 40 minutes at 37°C with TMRM (25nM) in recording buffer, and fluorescence was measured using the ImageXpress Micro XL system (Molecular Devices). Fluorescence was measured for 7 minutes prior to addition of DMSO, CsA or JW47 (both at

40nM and 1 μ M), and then for a further 50 minutes before the addition of the mitochondrial uncoupler carbonyl cyanide-4-(trifluoromethoxy)phenylhydrazone (FCCP, 5 μ M) as a positive control. The MetaXpress analysis software was used to calculate a mean integrated fluorescence intensity (using a customised multi-wavelength cell scoring journal). These values were normalized using the baseline reading as 100%, and the FCCP value as 0%, and then normalized to DMSO. Significance was assessed by one-way ANOVA, in comparison to DMSO control.

Measurement of mitochondrial membrane potential (*ex vivo*)

Freshly isolated mouse liver mitochondria were suspended in MSK buffer containing 10 μ g/ml rhodamine123 (dequench mode), at a concentration of 500 μ g/ml, and plated in an opaque black 96 well plate. Baseline fluorescence was then measured every 60 seconds for 5 minutes in a Fluostar Optima (Ex480/Em520) before manual addition of compounds (concentrations as specified). Fluorescence measurements were continued for 45 minutes until the addition of 2 μ M FCCP, followed by a further 10 minutes of fluorescence readings. Data were then normalized, using the baseline as 100% and the FCCP value as 0% and normalized to DMSO. Significance was assessed by one-way ANOVA, in comparison to DMSO control.

Respirometry: Oroboros

Oxygen consumption was measured using Oroboros Oxygraph-2K as previously described (Astin et al. Sci Rep 2013). Prior to the assay, the Oxygraph chambers were calibrated with Miro5 buffer (0.5mM EGTA, 3mM MgCl₂.6H₂O, 60mM K-lactobionate, 20mM taurine, 10mM KH₂PO₄, 20mM HEPES, 110mM sucrose, 1g/l BSA (essentially fatty acid free)). Isolated mitochondria were suspended in Miro5 (at 100-200 μ g/ml), loaded into the chamber together with substrates (L-malate, 2mM; L-glutamate, 10mM), and the O₂ flow signal was allowed to stabilise to the basal respiration rate (approx. 10 min). Compounds were added to the chambers at the following concentrations and order: DMSO/CsA/JW47 (concentration as indicated) to produce basal rate after compound (basal AC), ADP (2.5mM) to give state 3 respiration, oligomycin (2.5 μ M) to give leak respiration, FCCP (titrated to produce maximal respiratory capacity), and antimycin A (2.5 μ M) to give non-mitochondrial respiration. Data were analysed by subtracting the antimycin A respiration rate to give mitochondrial specific O₂ consumption, and were then expressed as a percentage of the

basal O₂ consumption. Significance was assessed by one-way ANOVA, in comparison to DMSO control.

Respirometry: Seahorse

Seahorse assays were carried out using the Seahorse XF FluxPack 24well kit, consisting of a cell plate, a probe plate (containing the fluorescent probes which measure cell responses), a drug plate, and calibration medium. Seahorse 24 well cell plates were coated for 30 minutes with poly-L-lysine, which was then removed, and the plates washed with sterile dH₂O. Then freshly prepared embryonic cortical rat neurons were plated at a density of 125000 cells/well, in all wells except control wells (A1, B4, C3, D6), in 200µl neurobasal medium (supplemented with Glutamax (1X), B27 (1X), and penicillin/streptomycin (1% v/v)). Cells were grown in a 5% CO₂, 95% humidity, 37C incubator. 48 hours after plating, the medium was replaced, and then half replaced after a further 72 hours. 24 hours prior to assay, calibration medium (1ml) was added to each well of the probe plate, and this was incubated at 37°C. Immediately prior to calibration, neurobasal medium was gently removed from the cell plate, and replaced with 600µl seahorse medium (DMEM powder (8.3g/L, final composition 0.83% w/v), pyruvate (1mM), glucose (5.5mM), glutamax (1X), sodium bicarbonate (44mM), FBS (10% v/v), pH 7.4). Compounds were then prepared and loaded into the drug plate, in order to add (in the following order) either DMSO/JW47/CsA (at concentrations specified), oligomycin (5µM), FCCP (2.5µM), and Antimycin A (5µM). The drug plate was then fitted on top of the fluorescent probe plate, and these two plates were then loaded into the machine, and the calibration protocol run. Subsequent to calibration, the probe plate was removed, and replaced with the cell plate, and the acquisition protocol run. After the acquisition was complete, total protein in each well was quantified using a ThermoScientific BCA protein quantification assay, as per manufacturer's instructions, and the oxygen consumption normalized to protein content.

Measurement of ATP

Freshly isolated mitochondria were resuspended in MSK buffer (containing 10mM L-glutamate and 2mM L-malate) at 1mg/ml and plated in opaque white 96 well plates, or for neuronal assays, neurons were used 9 days after plating at 15000 cells/well. Drugs (DMSO, CsA, JW47, oligomycin or IAA) were added at the concentrations specified, and for mitochondrial assays were incubated for ten minutes before addition of ADP (5mM),

followed by another 45 minutes. For neuronal assays, drugs were added in neurobasal medium and incubated for 60 minutes. Cell Titer Glo reagent was then added, and the plate shaken for 2 minutes in the dark to lyse cells/mitochondria and release ATP. The plates were incubated a further ten minutes and then luminescence values read using an Optima FluoStar. Data were normalised to DMSO control, and significance assessed by one-way ANOVA.

Results

Initial assessment of compounds

Four novel compounds were provided from the laboratory of David Selwood in order to be screened to assess their efficacy as inhibitors of mPTP. In order to do this, the calcium retention capacity (CRC) assay was used, a classical assay for measuring Ca^{2+} mediated pore opening in which isolated mouse liver mitochondria are suspended with the membrane impermeable low affinity ($K_d \sim 90\mu\text{M}$) calcium indicator Fluo-5N and subjected to repeated boluses of CaCl_2 . After each CaCl_2 addition, an increase in fluorescence is apparent, followed by an immediate decrease as the Ca^{2+} is taken up by the mitochondria (Figure 2.3A). This is repeated until the mitochondria exceed their maximum buffering capacity, upon which mPTP opens, which is visible as an uncontrolled rise in fluorescence as Ca^{2+} is released from the mitochondria (marked by red arrows), followed by a lack of buffering of subsequent CaCl_2 boluses. Successful inhibition is visible as a delay in pore opening compared to untreated controls, as shown by the CsA treated trace in Fig2.3A.

To assess the efficacy of these novel compounds, they were tested at three concentrations using the CRC assay, with CsA as a positive control. The previously published non-immunosuppressive, non-targeted SmBzCsA (8MB2) (Malouitre *et al.*, 2010) was used as a control in the initial screening, in order to investigate whether the quinolinium targeting method was successful. % inhibition was calculated for each compound and normalised to the % inhibition demonstrated by CsA. It was found that all compounds were as effective as CsA at higher concentrations ($5\mu\text{M}$ and $1\mu\text{M}$), but that at 200nM – which is the optimal concentration for CsA - two compounds, JW47 and JW115 were significantly more potent than CsA, whereas the inhibition provided by the other two compounds JW65.2 and 8MB2 decreased sharply (Figure 2.3B). As compound JW47 was the most effective at 200nM , this was selected for further study.

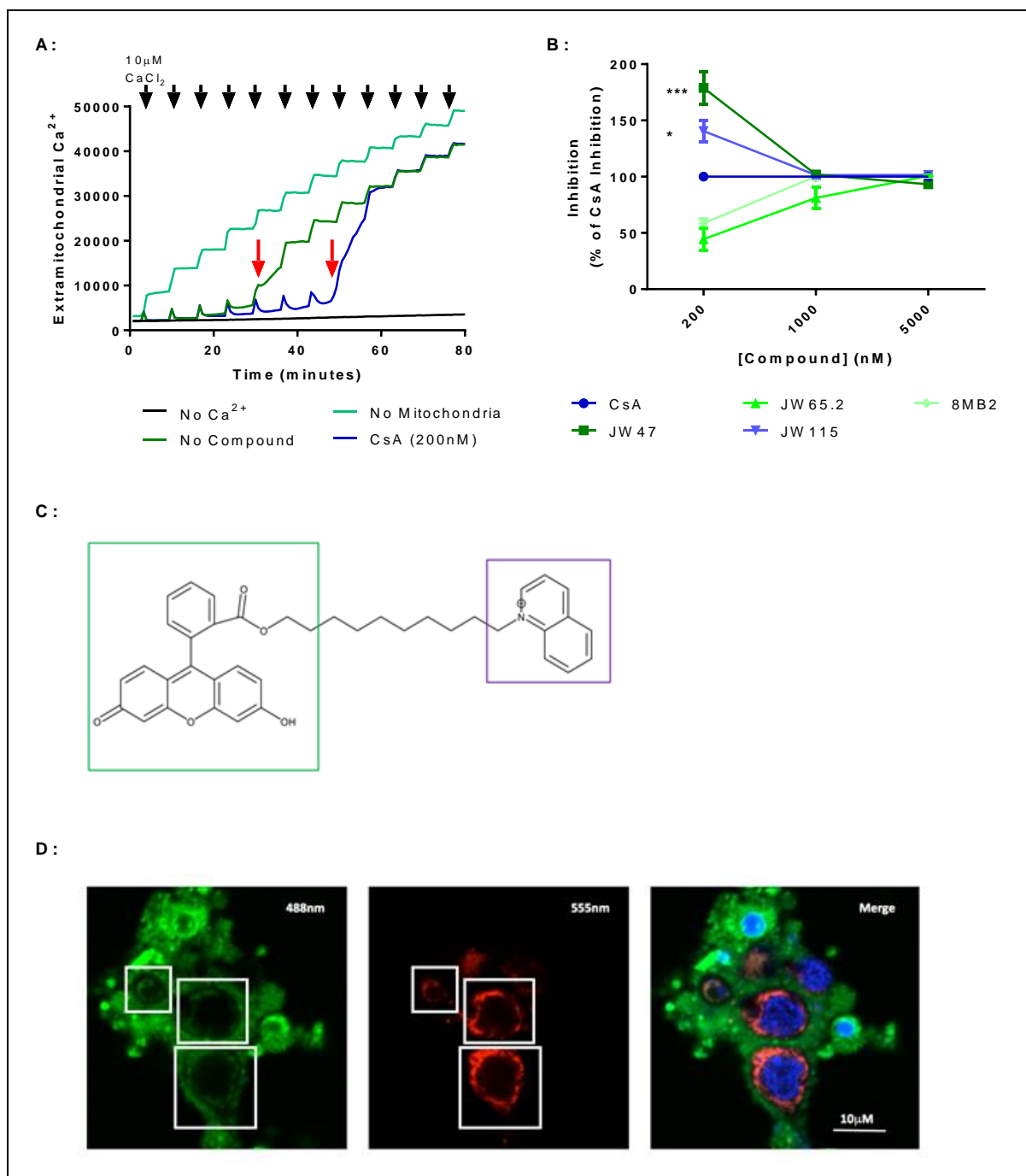


Figure 2.3: Novel compound JW47 was an effective inhibitor of mPTP opening. A: Representative trace of the CRC assay. Red arrows mark mPTP opening, which is delayed by addition of CsA. B: When assessed by CRC assay, all compounds inhibited pore opening to the same extent as CsA at 5 μM and 1 μM. At 200 nM, Compounds JW47 and JW115 were significantly more potent inhibitors of mPTP opening than CsA. Significance was assessed by one-way ANOVA, * denotes significance. * = p value < 0.05, *** = p value < 0.005. N of 3, error bars shown are standard error of the mean (SEM). C: Structure of fluorescein-tagged quinolinium. Fluorescein is boxed in green, and quinolinium in purple. Structure used with permission of David Selwood. D: Fluorescein-tagged quinolinium (488 nm) colocalized with mitochondria labelled with TMRM (555nm) in DIV10 rat cortical neurons.

To demonstrate that the quinolinium modification causes mitochondrial targeting, a fluorescein-tagged quinolinium molecule was created by the Selwood laboratory (Figure 2.3C), and its cellular localization was examined. It was found that when the fluorescein-tagged quinolinium entered the cell, it localised to the mitochondria, as shown by the colocalization of the fluorescein fluorescence with TMRM (see Figure 2.3D, and for line intensity profile plots of the colocalisation, Appendix A1), demonstrating that the quinolinium targeting approach was successful. However, a large proportion of the dye did not enter the cells, and formed a clear delineation of the cell membrane, suggesting there could be some issues with the permeability of this molecule.

Investigation of JW47 efficacy and target

A dose response was then carried out by CRC assay to compare the inhibition profile of CsA with JW47. Compounds were tested at concentrations from 0.32nM to 1 μ M; JW47 showed half maximal potency at ~10nM compared to ~40nM for CsA (Figure 2.4), showing that JW47 is approximately a 4 fold more potent inhibitor than CsA of Ca²⁺ mediated mPTP opening. Interestingly, there was no apparent difference between JW47 and CsA at 200nM, in contrast to the initial dose response at which there was a significant difference.

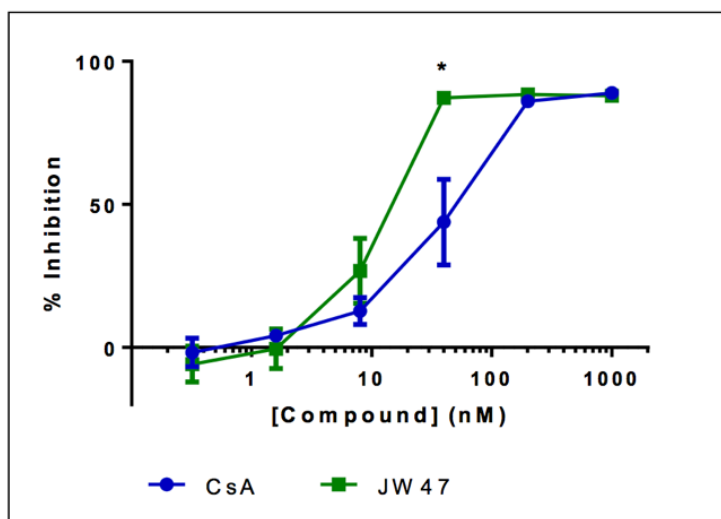


Figure 2.4: At 40nM JW47 was a significantly more potent inhibitor of mPTP opening than CsA. JW47 retained inhibitory activity at lower concentrations than CsA, with the maximal difference at 40nM. N of 4. Significance was assessed by one-way ANOVA. * denotes significance, p value <0.05. Error bars are SEM.

In order to confirm that JW47 is selective for CypD and that the mechanism of action is to reduce Ca^{2+} sensitivity by binding CypD, the compound was then tested on mitochondria isolated from CypD knockout mice. The mice were confirmed to be CypD $-/-$ by the absence of a band at $\sim 20kDa$ in a Western blot using anti-CypD antibody (see Figure 2.5B and 2.5C).

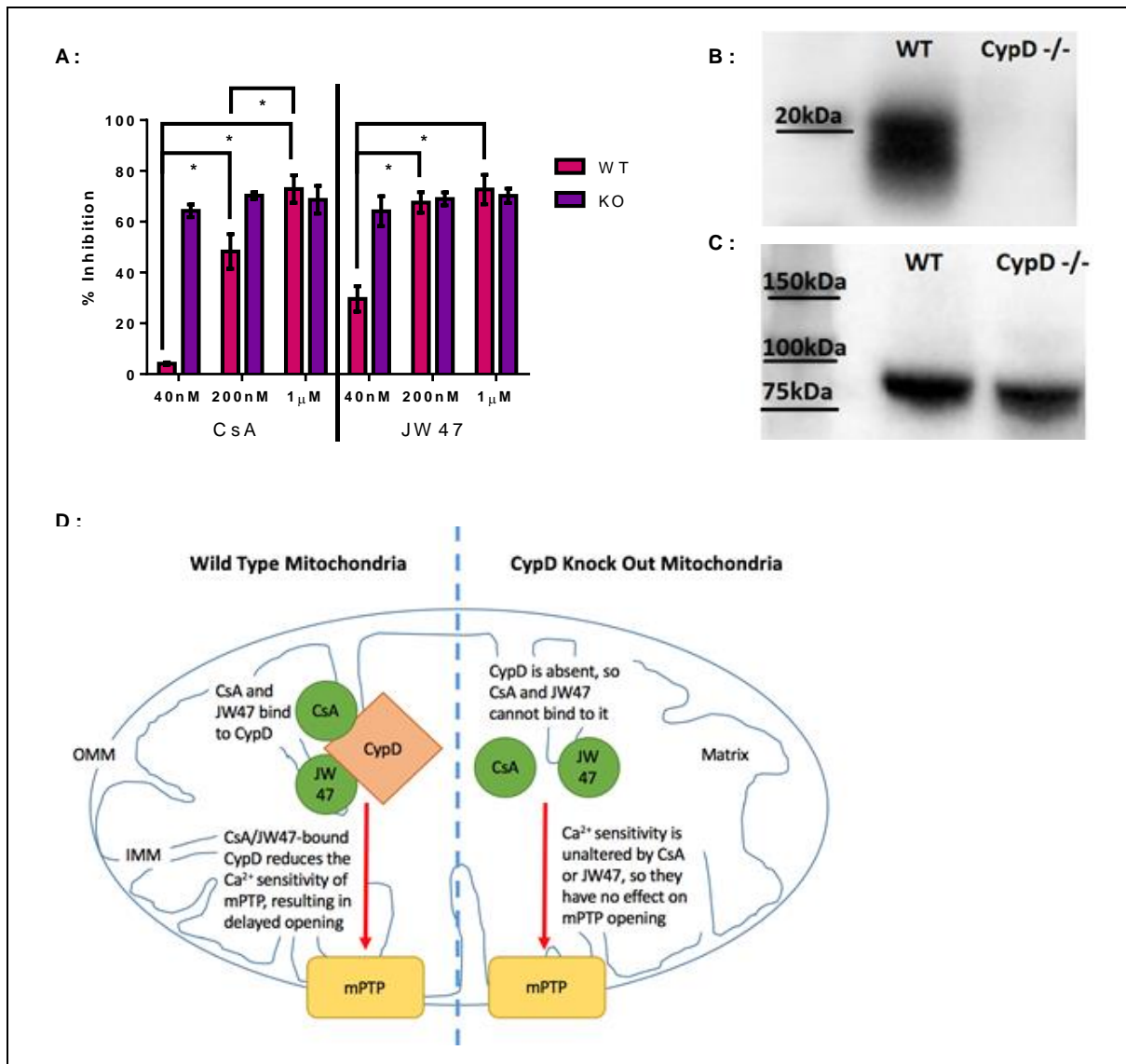


Figure 2.5: JW47 inhibits mPTP opening by binding CypD and reducing Ca^{2+} sensitivity of the pore. A) In mitochondria isolated from WT mice, pore opening was inhibited by both CsA and JW47 in a dose dependent manner, whereas in mitochondria isolated from CypD KO mice neither drug had any effect. N of 3. Significance was assessed by one-way ANOVA. * denotes significance, p value < 0.05. Error bars are SEM. B) CypD was not present in a Western blot of mitochondria isolated from CypD $-/-$ mice, in contrast to the WT control, in which there was a band of $\sim 20kDa$. C) Mitochondrial heatshock protein GRP75 was present in both WT and CypD $-/-$ samples, demonstrating there was mitochondrial content in both samples. D) in wild type mitochondria (left), JW47 inhibits mPTP opening by binding CypD and reducing Ca^{2+} sensitivity of the pore. In CypD KO mitochondria (right), JW47 has no effect due to the absence of CypD.

It was found that neither CsA nor JW47 had any effect on the CRC assay in mitochondria from CypD KO mice, at any concentration (see Figure 2.5A), whereas in the mitochondria from WT mice there were significant differences between all concentrations of CsA, and between 40nM and 200nM JW47 (there was no difference between 200nM and 1µM JW47, having attained maximal inhibition by 200nM). This demonstrated that, as in the absence of the CypD protein JW47 and CsA had no effect, the target of these compounds is CypD. In order to induce pore opening in CypD $-/-$ mice, it was necessary to increase the concentration and number of CaCl₂ injections, reiterating that it is CypD which confers Ca²⁺ sensitivity on the pore, and that therefore these compounds can be said to work by decreasing the Ca²⁺ sensitivity of the pore via CypD.

Investigation of the effect of JW47 on mitochondrial parameters

Next, essential mitochondrial parameters were measured in order to assess possible adverse effects of JW47. CsA has been shown to induce mitochondrial toxicity (Rodríguez *et al.*, 2007), so it is desirable that any derivatives do not possess these toxic properties. Parameters were measured both in isolated mitochondria and in primary cortical neurons, at concentrations causing maximal (40nM) and supramaximal (200nM, 1µM) inhibition of mPTP.

Treatment of isolated liver mitochondria with JW47 had no significant effect at any concentration, on mitochondrial membrane potential (Figure 2.6A), ATP production (Figure 2.6B), or oxygen consumption (Figure 2.6C and 2.6D).

In rat cortical neurons (at DIV8-9), 40nM and 200nM treatment with JW47 had no effect on mitochondrial membrane potential (Figure 2.7A), ATP production (Figure 2.7B), or oxygen consumption (Figure 2.7C), however at supramaximal concentration (1µM), JW47 significantly reduced mitochondrial membrane potential. Whilst JW47 at 1µM did not produce significant affects in the other measures of mitochondrial function, there was a visible, but not significant, reduction in ATP production in both cortical neurons and isolated mitochondria, and in state 3 and maximal respiration in isolated mitochondria. Whilst it is clear that JW47 does show some adverse affects on mitochondrial function, this

demonstrates that these effects take place at least an order of magnitude higher than the maximal concentrations for inhibition of mPTP, and there is a wide safety window.

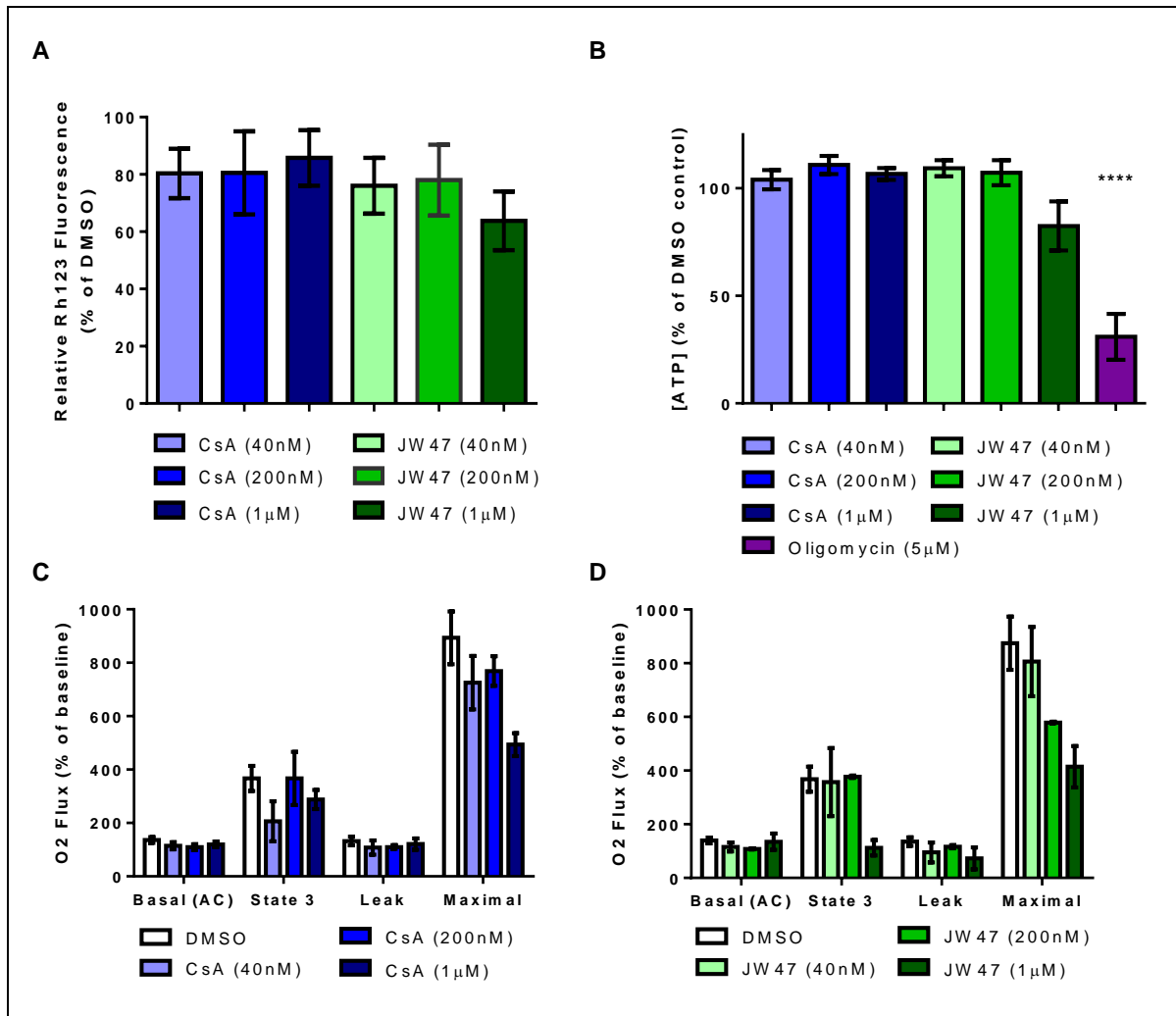


Figure 2.6: At low concentrations, JW47 has no effect on mitochondrial membrane potential, oxygen consumption or ATP production in isolated mitochondria. A: Neither CsA or JW47 affected mitochondrial membrane potential. N of 3. B: Neither CsA nor JW47 had a significant effect on ATP production. N of 4. C: Respiration was not significantly affected by CsA at any concentration, although it visibly reduced maximal respiration at 1µM. N of 3. D: Respiration was not significantly affected by JW47 at any concentration, however at 200nM and 1µM maximal respiration was visibly reduced. N of 4. Significance was tested by one-way ANOVA. * denotes significance, **** = p value <0.001. All error bars are SEM.

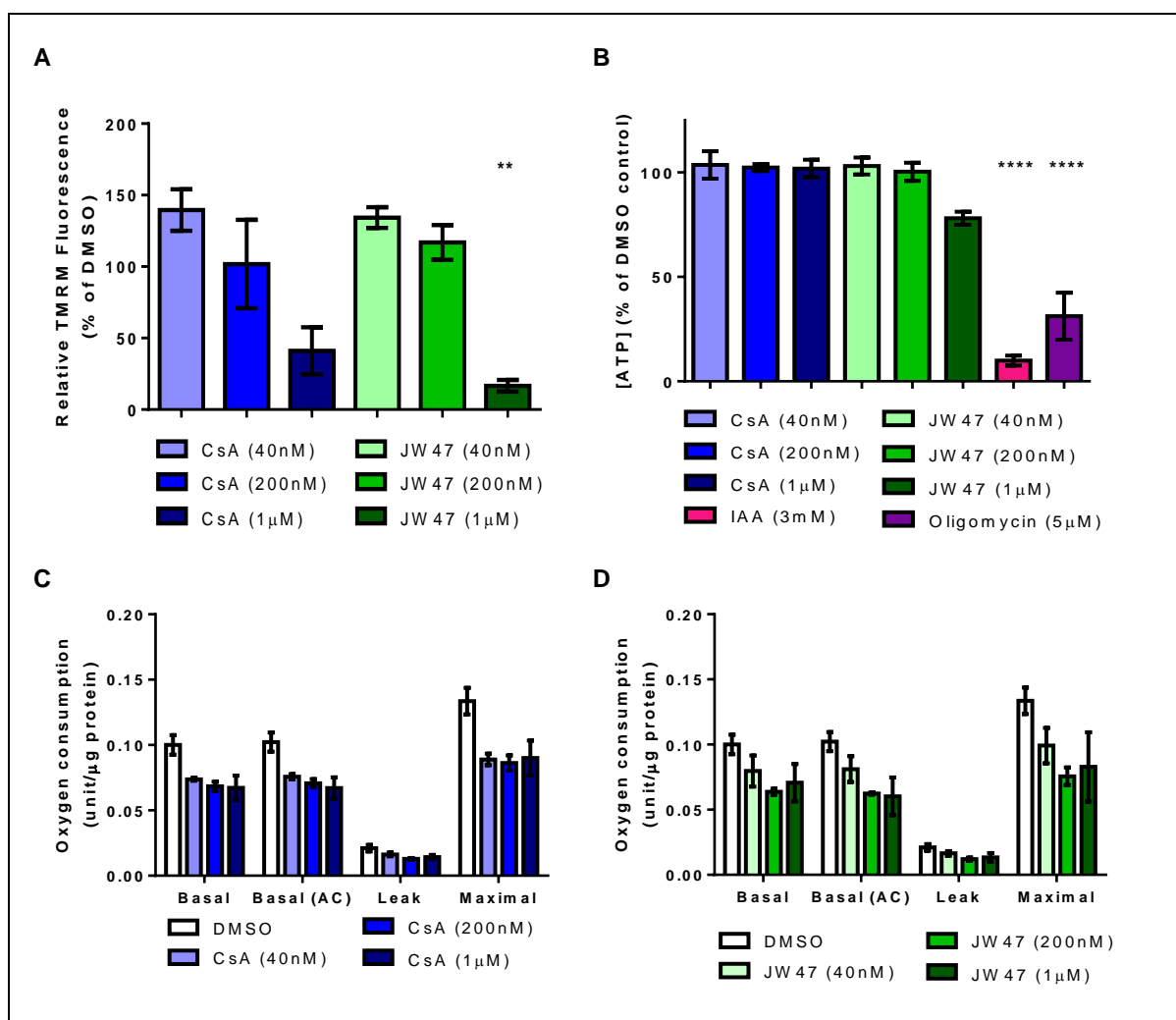


Figure 2.7: At low concentrations, JW47 has no effect on mitochondrial membrane potential, oxygen consumption or ATP production in rat cortical neurons. A: CsA did not reduce mitochondrial membrane potential at any concentration. At 40nM and 200nM, JW47 had no effect, however at 1µM JW47 membrane potential was significantly reduced. N of 4. B: In cortical neurons, neither CsA nor JW47 had a significant effect on ATP production. N of 3. C: Respiration was not significantly affected by CsA at any concentration, although at all concentrations it appeared to cause some reduction in oxygen consumption. N of 3. D: Respiration was not significantly affected by JW47 at any concentration. N of 3. Significance was tested by one-way ANOVA. * denotes significance, ** = p value <0.01, **** = p value <0.001. All error bars are SEM.

Investigation of second generation compounds

Lastly, further compounds were provided for testing from the Selwood laboratory. These compounds were also CsA derivatives, modified according to the success of JW47, and were tested on isolated mouse liver mitochondria using the CRC assay. These were tested only at

lower concentrations (40nM and 8nM), as it had been found that differences were more detectable at low concentrations. CsA is only at half maximal inhibition at 40nM, therefore JW47 was used as a control in these experiments. It was found that at 40nM there were three compounds (JW28, JW76 and JW83) which were able to inhibit pore opening to the same extent as JW47, whilst the other compounds had no effect on pore opening (see Fig 2.8A). At 8nM, JW47 no longer effectively inhibited pore opening. However, at 8nM the three new compounds were found to inhibit pore opening to a similar extent as at 40nM (Fig 7B), suggesting these compounds are even more efficacious than JW47.

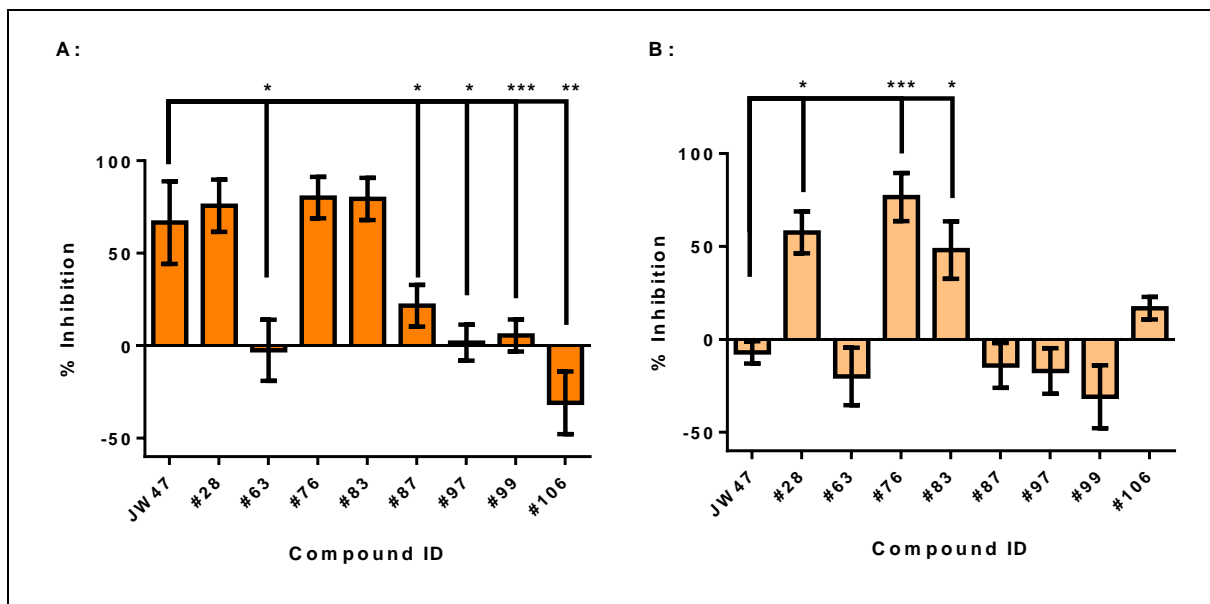


Figure 2.8: Three derivatives of JW47 were effective inhibitors of mPTP opening. A: When assessed by CRC assay at 40nM, novel compounds #28, #76 and #83 inhibited mPTP opening to the same extent as JW47, although several of the other compounds did not inhibit mPTP opening at all. N of 3. B: At 8nM, compounds #28, #76, and #83 were significantly more effective inhibitors than JW47. N of 3. . Significance was tested by one-way ANOVA. * denotes significance, * = p value <0.05, *** = p value <0.005. All error bars are SEM.

Summary

Four novel compounds were screened using the CRC assay and two of them were found to be more potent inhibitors of mPTP opening than CsA at 200nM. A fluorescein-tagged quinolinium molecule was demonstrated to co-localize with mitochondria in cortical

neurons, suggesting that this is a successful mitochondrial targeting approach, and explaining the increased potency of the CsA derivatives. The most potent compound, JW47 was further investigated and found to act by binding CypD. JW47 was shown by dose response to be approximately a 4X more potent inhibitor than CsA, with a half maximal concentration of ~10nM. In isolated mitochondria, JW47 did not significantly affect membrane potential, ATP production, or oxygen consumption at any concentration. JW47 was found to inhibit mitochondrial membrane potential in rat cortical neurons at supramaximal concentrations but to have no effect at 40nM or 200nM. A new range of compounds which are derivatives of JW47 were found to be more effective than JW47 at low concentrations, providing a promising future direction for this investigation.

Discussion

The initial compound screen demonstrated that JW47 is an effective inhibitor of mPTP, and at low concentration (200nM) is more potent than CsA. This would suggest that the chemical modification of the structure to optimize CypD targeting was successful: the modification using the quinolinium ion appears to have successfully localized the compound to the mitochondria due to its negative membrane potential, as demonstrated by the much higher efficacy of JW47 than CsA and 8MB2 (a compound without mitochondrial targeting). This was also confirmed by colocalization of a fluorescein-tagged quinolinium probe with TMRM labelled mitochondria; however, not all of the fluorescein compound entered the cells, suggesting there may be issues with the membrane permeability of this molecule. This does not necessarily mean that there are issues with the permeability of JW47, as the structures differ, (the compound used here was only quinolinium attached to fluorescein, without the rest of the JW47 structure), however it would be useful to check this by creating a fluorescently tagged JW47. It would also be useful to verify the effectiveness of quinolinium in conferring mitochondrial specificity on a compound: to do this, a fluorescein-tagged JW47 without the quinolinium ion could be used, to investigate the localization of the compound without the mitochondrial targeting.

A drawback to this approach is the use of liver mitochondria: as the compounds are of interest as potential therapeutics for a neurological condition, it would be more clinically relevant to investigate their efficacy using brain mitochondria. However, liver mitochondria are more commonly used, are easy to isolate, and are known to be robust and give high yield, and this was our justification for using them. In future work it would be useful to confirm the efficacy of these compounds on mitochondria isolated from the brain, as some properties (substrate transport, respiration and ROS production) of mitochondria from the brain have been shown to differ to those of mitochondria isolated from the liver (Gusdon *et al.*, 2015).

Mitochondria isolated from CypD knock out mice did not show CsA or JW47 sensitive pore opening at any CsA/JW47 concentration, whereas wild type litter mates showed a dose-dependent inhibition for both drugs. This confirms that JW47 targets CypD, as is expected

as a derivative of CsA, and demonstrates that the chemical modifications to the structure did not ablate CypD binding. It was also shown by other groups that in an X-ray structure of JW47, the CypD binding complex is conserved, that JW47 has reduced CypA binding in comparison to CsA, and is less immunosuppressive (inhibits T cell proliferation to a lesser extent) than CsA (Warne *et al.*, 2016).

The dose response curve showed that JW47 is approximately 4X more potent than CsA at inhibiting mPTP opening, with a half maximal inhibition for JW47 of 10nM, compared to CsA at 40nM, supporting the use of the quinolinium ion as a mitochondrial targeting aid. However, the dose response raised an interesting point in that no significant difference was observed between CsA and JW47 at 200nM, whereas in the initial screen there had been one. This is likely due to instability of JW47 – during experiments it was noted that JW47 appeared to become less efficient after multiple freeze thaws, whereas CsA was not affected. This could be a potential issue with the therapeutic use of the compound, causing issues with mass production and storage, however no effect was noted when tested *in vivo*: JW47 was tested *in vivo* (see Appendix Figure A2) by the Baker lab at Queen Mary University, and was found to be neuroprotective in a mouse model of MS (Warne *et al.*, 2016). JW47 treatment did not prevent the onset or severity of MS relapses, but significantly improved the clinical score post relapse in comparison to vehicle treated mice. JW47 treated mice also performed significantly better in a rotarod test (a measure of motor skills) than vehicle treated mice; no side effects were observed in JW47 treated mice.

It would have been desirable to demonstrate that JW47 prevented pore opening *in vitro*, in rat cortical neurons, however, the mPTP is notoriously difficult to measure reproducibly in cells and cell lines. Different methods were attempted to quantify the effect of JW47 and CsA on mPTP *in vitro*, in cortical rat neurons, however these were without success.

The first method, the calcein cobalt assay, has previously been described (Petronilli *et al.*, 1999) as a method with which to measure transitory and permanent pore opening. The assay selectively labels mitochondria using calcein AM, the acetoxymethyl ester of calcein dye - a colourless, non-fluorescent substance - and CoCl_2 , which quenches calcein fluorescence. Calcein AM diffuses throughout the cell and accumulates throughout the cytosol and mitochondria; inside the cell esterases cleave the ester group thus preventing

further diffusion of the dye, so that the dye which has spread to the mitochondria is then trapped. CoCl_2 is then added, which quenches the cytosolic calcein fluorescence, but not the mitochondrial, as Co^{2+} cannot permeate the IMM. Upon opening of mPTP, Co^{2+} gains access to the mitochondrial-sequestered dye, and quenches mitochondrial calcein fluorescence, which can be rescued by CsA (Petronilli *et al.*, 1999). However, this technique was immediately challenged (Lemasters and Nieminen, 1999), in a letter to the editors which claimed that calcein loading was not mitochondrial, and that Petronilli had been mistaken in identifying mitochondria, which Lemasters said exclude calcein and appear as dark voids in the cytosolic fluorescence. They also noted a strong temperature dependence of calcein loading: at 37°C cytosolic esterases are so active that the calcein AM is cleaved before entry to the mitochondria, although they noted that this may vary between cell types. The mPTP is also sensitive to temperature preconditioning (Khaliulin *et al.*, 2007), and temperature sensitivity was also found during our CRC assay optimization. The calcein cobalt assay continues to be used (Quintanilla *et al.*, 2013), however there are many difficulties with it: cobalt is a heavy metal ion, known to be toxic to cells (Jones *et al.*, 2002), calcein does not universally enter mitochondria (Lemasters *et al.*, 1998), and the technique cannot distinguish between calcein release from mitochondria and CoCl_2 entry. In our experiments, it was found that cytosolic quenching in rat cortical neurons did not result in fluorescent mitochondria: most cells were found to have a combination of non specific staining and dark voids, with only some clear mitochondrial staining.

Modulation of mPTP using photostimulation, has long been described: the pore can be inhibited using photostimulation in combination with hematoporphyrin (Salet *et al.*, 1997), or can be activated using high levels of radiation, in order to decrease mitochondrial calcium retention capacity (Hüser *et al.*, 1998; Petronilli *et al.*, 2009; Blanchet *et al.*, 2014), representing photoactivation of mPTP. The technique of photoactivation was used for the second approach of monitoring mPTP *in vitro*: the method we used was to load the cells with a high ($1\mu\text{M}$) concentration of TMRM, a fluorescent lipophilic cation which partitions specifically in the mitochondria, dependent on $\Delta\Psi\text{m}$. During imaging, high laser power is used to excite TMRM, causing the local generation of free radicals, which cause mPTP opening (De Giorgi *et al.*, 2002). As TMRM accumulation is dependent on $\Delta\Psi\text{m}$, it can be used to measure this; therefore, in this assay TMRM is used both as the trigger and the

measure of mPTP. mPTP opening is marked by a sudden decrease in $\Delta\Psi_m$, represented by a sharp increase in TMRM fluorescence. However, this technique also has issues: depolarization can be caused by a variety of events besides mPTP opening (e.g. increased ATP demand). When this assay was tried (on a Zeiss Confocal LSM 500, and a Molecular devices ImageXpress MicroXL), it was found to be very difficult to attenuate the light exposure in order to give a sufficient delay in pore opening such that compounds could be assessed – the pore opened (represented by a sudden increase in TMRM fluorescence) within seconds of exposure, was found to be highly variable between different cell populations, and even within cell populations there was significant time delay between pore opening in different cells. Therefore, neither of these assays produced sufficiently reproducible data to be used to investigate the effect of JW47 on pore opening in cells *in vitro*.

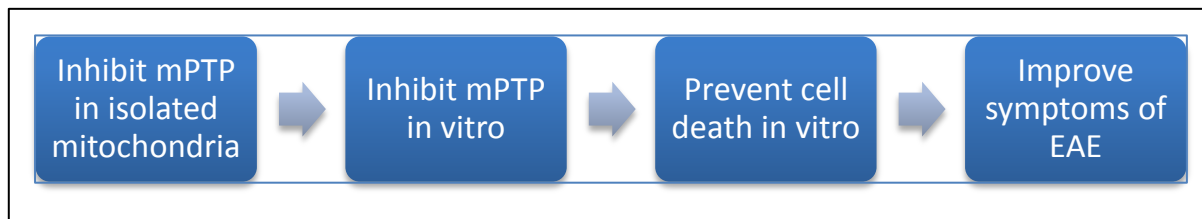


Figure 2.9: a flowchart for the presumed mechanism of action of JW47.

An alternative approach could be - rather than demonstrating that JW47 inhibits mPTP opening *in vitro* - to investigate whether JW47 inhibits cell death, as cell death is the supposed consequence of mPTP opening. If it could be demonstrated that JW47 inhibits cell death, this would nicely demonstrate the presumed mechanism by which it is able to improve symptoms of EAE (see Figure 2.9). In order to test this, an ischemia-reperfusion assay could be used, in which cells are kept in anoxic conditions, typically using argon gas to displace oxygen, in order to mimic ischemia and produce cell death during reperfusion – for review see (White *et al.*, 2000). Alternatively, neurons could be treated with glutamate, in order to cause Ca^{2+} influx through voltage gated Ca^{2+} channels, and NMDA receptors, and cause Ca^{2+} induced cell death. If using a glutamate assay, it would be necessary to use older neurons than have been used in this project, as glutamate sensitivity changes throughout development, with young (DIV6-8) neurons able to recover from glutamate stimulation,

whereas older (DIV11-17) neurons are more vulnerable to glutamate induced injury (Adamec *et al.*, 1998; Vergun *et al.*, 1999). H₂O₂ could also be used to induce cell death.

In *in vivo* work done by the Baker group, JW47 was found at nanomolar concentrations in the brain of EAE animals following a 10mg/kg dose, demonstrating it is able to enter the brain. This does not demonstrate that it can cross the blood brain barrier however, as it has been found that the lesions formed in the brain in the EAE model of Multiple Sclerosis cause a local malfunction of p-glycoprotein, which is usually responsible for the extrusion of any solutes which manage to cross the BBB (Al-Izki *et al.*, 2014). This means that compounds are able to cross the BBB at the sites at which they are most necessary; further work would be needed to establish whether the compound can cross the BBB in other circumstances. This could be established by removing the brains of healthy mice after treatment, and using mass spectrometry to investigate the presence of JW47.

The assays of the basic mitochondrial function demonstrated that JW47 does have a toxic effect at high, supramaximal concentration (1 μ M), at which it significantly reduces membrane potential, and appears to reduce state 3 and maximal respiration and ATP production, although these were not significantly affected. Whilst this toxicity is clearly an issue, as toxic side effects will reduce the usefulness of the compound as a therapeutic pharmaceutical, the lack of toxic effect at 200nM or 40nM demonstrates that there is a wide margin for error between relevant concentrations and the threshold for toxicity. The effects of the drug on membrane potential, respirometry, and ATP production can be easily linked, as $\Delta\Psi_m$ is defined by the proton gradient across the IMM generated by oxidative phosphorylation; therefore if oxidative phosphorylation is reduced, as demonstrated by reduced oxygen consumption, it is logical that $\Delta\Psi_m$ would decline also. ATP production is the end product of oxidative phosphorylation so it is consistent that lower oxygen consumption would be accompanied by lower ATP production. The effect of the compound on the P/O ratio could be investigated; this ratio is the amount of ATP produced by the movement of two electrons (from an oxygen atom) through the ETC. $\Delta\Psi_m$ was significantly affected in cells only (not in isolated mitochondria), suggesting the reduction in membrane potential may be due to off target effects on other cellular components, such as substrate supply. Conversely, the reduction of mitochondrial membrane potential could also potentially contribute to the efficacy of the drug: specific Ca²⁺ uptake through MCU is

dependent on $\Delta\Psi_m$, so if $\Delta\Psi_m$ is reduced then Ca^{2+} uptake would also reduce, therefore reducing the mitochondrial Ca^{2+} overload which leads to mPTP opening. However, inhibition of mPTP was seen at concentrations of JW47 which do not cause mitochondrial depolarisation, so it is unlikely that this mechanism is in effect. It would be interesting to investigate the toxic side effects of JW47 at high concentration further, using immunoprecipitation to investigate whether the drug binds to other components of the cell.

Screening of the second round of compounds demonstrated that three compounds were as effective as JW47 at 40nM, and significantly more effective than JW47 at 8nM. As full structural data is not yet available for these compounds it cannot be hypothesized why they are more efficacious. Whilst toxicity studies have not been done with these compounds, it would be hoped that even if they share the same toxic side effects as JW47 at higher concentrations, their effective concentrations would be even further removed from the toxicity threshold, thereby making them even more suitable as potential therapeutic agents. It would be interesting to investigate whether they have similar side effects to JW47 as it would provide some insight into the cause of these effects, whether they are associated with regions that differ between these compounds and JW47, or the regions that have remained the same.

In conclusion, JW47 was found to be a more efficacious inhibitor of mPTP than the classic inhibitor CsA, and was active at lower concentrations. This is likely due to the mitochondrial localization caused by the use of the quinolinium ion. JW47 was found to be non toxic to mitochondrial membrane potential, ATP production, or oxygen consumption in both isolated liver mitochondria and rat cortical neurons at nanomolar concentrations, but it significantly reduced membrane potential in neurons at 1 μ M. Future work should include screening the compounds in mitochondria isolated from brains in order to confirm they have the same effect, and experiments to confirm that JW47 can delay mPTP opening or reduce necrotic cell death *in vitro*, in order to investigate the mechanism by which JW47 is able to improve clinical symptoms of EAE. The newest compounds need further investigation in order to find their optimal concentrations, and investigating for mitochondrial toxicity but are promising in terms of their higher efficacy in comparison to JW47. Further work is also needed to investigate whether the compound can cross the BBB;

if so then JW47 and the range of new compounds have broad therapeutic potential for the treatment of neurodegenerative disease.

Chapter 3: Developing an Aequorin-based Screening Approach to Identify Inhibitors of MCU

Introduction

Mitochondria as drug targets

Mitochondrial dysfunction is implicated in an ever increasing number of major diseases, for example, in neurodegenerative disease mitochondrial dysfunction is a common feature, and in cancer cells, mitochondria play an important role in allowing cell survival and proliferation (Camara *et al.*, 2010). Increased understanding of the pathways that cause dysfunction opens the way to development of new pharmaceutical approaches which can specifically target mitochondrial functions, which presents a challenge in drug discovery: it is necessary to differentiate between the mitochondrial and cytosolic effects of drugs, as some effects seen on mitochondria may be downstream consequences of the effects of a drug on the cytosol.

The MCU in particular is an interesting therapeutic target in diseases in which there is excessive cell death, such as neurodegenerative disease - as discussed in depth the introduction to this thesis, it has been proposed that inhibition of mitochondrial Ca^{2+} uptake may be protective against cell death, as mitochondrial Ca^{2+} overload is a critical checkpoint in cell survival. Existing MCU inhibitors are difficult to work with, and all have off target effects (see below), so it is desirable to find other MCU-specific, small molecule, cell and BBB permeable inhibitors, both as an alternative experimental tool to using genetic manipulation to study MCU function, and as potential therapeutics to reduce mitochondrial Ca^{2+} overload induced cell death.

Existing MCU-targeting compounds

For many years preceding the discovery of the molecular identity of MCU, ruthenium red (RuR) and ruthenium 360 (Ru360) - derivatives of ruthenium - have been used as inhibitors of the MCU. RuR potently inhibits mitochondrial Ca^{2+} uptake in isolated mitochondria with no major off target effects, however in intact cells it has a wide selectivity and also targets (amongst others), VDAC, L-type plasmalemmal Ca^{2+} channels, Ry-R (Duchen, 1992; Lukyanenko *et al.*, 2000). An additional difficulty with the use of RuR in intact cells is its high charge, which makes it unlikely to cross the plasma membrane, although it has been reported to do so (McCormack and England, 1983). Ru360 is reportedly a more potent inhibitor of MCU, and more readily enters intact cells, where it does not inhibit the RyR (Matlib *et al.*, 1998), however it has been found that in many cell types, neither RuR or Ru360 are effective in intact cells and that cell type specific validation of their efficacy is needed (Hajnóczky *et al.*, 2006). In one of the original MCU identifying papers it was established that Ru360 acts directly on the channel protein: a point mutation of MCU at S259A confers resistance to Ru360 (Baughman *et al.*, 2011). Lanthanides are also able to inhibit mitochondrial Ca^{2+} uptake in isolated mitochondria, but not in intact cells (Mela, 1969). The drug KB-R7943 has also been demonstrated to inhibit the MCU, but simultaneously inhibits NCLX (Santo-Domingo *et al.*, 2007); the polyamine spermine has historically been suggested as an MCU activator (Nicchitta and Williamson, 1984; McCormack, 1989), as has kaempferol, which is also known to have other cellular targets (Montero *et al.*, 2004). No drugs have yet been proposed to effect components of the MCU complex besides the MCU itself; this could be an interesting approach to modulating, rather than ablating, mitochondrial Ca^{2+} uptake.

Ca^{2+} signalling can be used to identify mitochondrial specific inhibitors, as Ca^{2+} can be measured specifically in different cellular compartments by using targeted aequorin. This provides the benefit, when searching for MCU specific inhibitors, of direct insight into the impact of compounds on mitochondrial Ca^{2+} uptake. Therefore, an aequorin-based approach was used to develop a method of screening for mitochondrial-specific compounds.

Aequorin

Aequorin is a 21kDa Ca^{2+} sensitive bioluminescent protein, first isolated from the jellyfish *Aequorea Victoria* in 1962 (SHIMOMURA *et al.*, 1962). It is a coelenterate protein which is inactive in its apoprotein form; it requires reconstitution with the hydrophobic prosthetic group coelenterazine, to which it binds covalently, in order to function as a Ca^{2+} indicator. It was initially used as a purified protein which had to be microinjected into cells (Ridgway and Ashley, 1967; Allen and Blinks, 1978), thereby limiting its use to large and robust cells, and due to this it became a secondary technique to small molecule fluorescent Ca^{2+} indicator dyes. However, the cloning of aequorin cDNA (Inouye *et al.*, 1985; Prasher *et al.*, 1985) opened the way to the more widespread use of aequorin, as it could then be transfected into a wider variety of cells.

A further discovery which popularized the use of aequorin was the ability to target it to cellular compartments and organelles. This was first demonstrated in 1992 (Rizzuto *et al.*, 1992), when the cDNA encoding subunit VIII of human cytochrome c oxidase was ligated to the aequorin cDNA in order to target aequorin to the mitochondria. It has since been targeted also to the endoplasmic reticulum (Kendall *et al.*, 1992a), the nucleus (Brini *et al.*, 1993) and the Golgi apparatus (Pinton *et al.*, 1998), among others. These cDNA constructs can then be transfected (or, when packaged in a viral vector, transduced) into cells in order to measure intracellular Ca^{2+} in specific compartments. Mutant versions of both the aequorin protein and coelenterazine have also been made, in which the affinity for Ca^{2+} has been altered (Kendall *et al.*, 1992b; Shimomura *et al.*, 1993). These mutant versions can be used in combination (mutant aequorin cDNA with mutant coelenterazine), or with wild type counterparts (wild type aequorin with mutant coelenterazine or vice versa).

Aequorin measurements can be made using a cuvette in a spectrophotometer, or for higher throughput, in a plate reader able to measure luminescence. A typical aequorin assay consists of a two-hour incubation with coelenterazine in order to form the active photoprotein, followed by a baseline measurement, an addition of (cell type appropriate) agonist to induce a Ca^{2+} response, and then a permeabilizing agent such as digitonin with a

saturating concentration of Ca^{2+} . The digitonin and excess Ca^{2+} is in order to provide a maximal light value (L_{max}), which can then be used to calibrate the agonist-induced response into a micromolar Ca^{2+} concentration (see Figure 3.1); L_{max} can also be used to assess the transfection efficiency of the experiment.

1. A ratio is made using the formula:

$$\text{Ratio} = ((L1 - \text{MIN}(L1:LX)) / \text{SUM}(L1:LX))^{(1/n)}$$

Where:

L1 = first light measurement of the time course (in counts per second)

LX = last light measurement of the time course (n counts per second)

n = 2.99

2. This is then calibrated into a micromolar Ca^{2+} value using the formula:

$$[\text{Ca}^{2+}] (\mu\text{M}) = (\text{Ratio} + (\text{Ratio} * K_{\text{TR}} - 1)) / (K_{\text{R}} - (\text{Ratio} * K_{\text{R}})) * 10^6$$

Where:

$K_{\text{TR}} = 120$

$K_{\text{R}} = 10366185$

Figure 3.1: An explanation of aequorin calibration, from measurements made using wild type aequorin reconstituted with wild type coelenterazine, measured at 37°C. Note: under these conditions, the rate constant is 1.0 sec^{-1} (Allen and Blinks, 1978), and therefore is not included in the equations.

The constants used to calibrate the measurements in a $[\text{Ca}^{2+}]$ value were derived using a model in which each of the aequorin protein's Ca^{2+} binding site has two possible states, R and T (Allen *et al.*, 1977). It is assumed that Ca^{2+} only binds to the R state, and light is emitted when every site is in the R state, and therefore the equilibrium is in favour of the R state. There are four constants used in the calibration of aequorin: n (the number of Ca^{2+} binding sites), K_{R} (the Ca^{2+} association constant), $K_{\text{TR}} (= [\text{T}]/[\text{R}])$, and Rate (rate constant of aequorin consumption at saturating $[\text{Ca}^{2+}]$). These constants vary between the different

types of aequorin (wild type or mutant), and the different types of coelenterazine (wild type and mutant). The K_R constant also varies depending on the temperature at which the experiment is carried out (usually 37°C) (Brini *et al.*, 1995), so this is important to note during experiments.

The major limitation of aequorin is its poor ability to emit light (Ottolini *et al.*, 2014), which limits its use: it has to be expressed at a sufficiently high level to emit enough light to be measurable, and therefore can mostly only be used in easily transfectable cell lines, although recently GFP-aequorin conjugates have been produced to overcome this issue (Baubet *et al.*, 2000). Another factor which has to be considered is the consumption of aequorin through the experiment, which prevents its use in lengthy time courses (although it has been demonstrated to give continuous signals for up to 70 minutes (Woods *et al.*, 1986), and the necessity of a time consuming reconstitution with coelenterazine. A final consideration is that due to the single wavelength of light emitted, signals from different compartments cannot be measured in parallel, as there is no way to distinguish the source of the light. However, the advantages of aequorin make it an appropriate choice for large scale screening experiments: the specificity of the targeting allows measurements from whole population, and consequently the analysis is much simpler than single cell measurements where regions of interest (ROIs) have to be defined manually. Additionally the calibration can be largely automated, using Excel templates or R code to make the process faster, which is especially advantageous for screening many compounds. Lastly, aequorin has a large dynamic range, which makes it suitable for work with compounds which have unknown effects on Ca^{2+} signalling, and could produce a wide range of changes in $[Ca^{2+}]$.

Designing an aequorin-based screening approach for inhibitors of MCU

A useful approach to finding new inhibitors is to screen a compound library of drugs already in clinical use; therefore any drugs found to be MCU inhibitors would already be known to be safe for human use. However this means it is necessary to design a screening approach which will be able to identify mitochondrial specific inhibitors, and this is what we aimed to

do in the work described in this chapter. This project aimed to develop an aequorin based screening approach in order to screen the NINDS-2 compound library (see Appendix 2): compounds were screened initially using mitochondrial-targeted aequorin, and then with cytosolic aequorin, to ensure that changes in mitochondrial signal were not secondary to changes in the cytosolic calcium signal. Different experimental approaches were used to confirm the results, and investigations were made of the compounds other effects on mitochondrial parameters.

Methods

Tissue culture

Tissue culture was carried out in a laminar flow cabinet in order to maintain a sterile environment and prevent contamination of the cells; before and after use the cabinet was cleaned with Virkon, and all items used for tissue culture were sprayed with 70% ethanol before being placed in the cabinet. Lab coats and gloves were worn, and gloves were sprayed with 70% ethanol before placing hands in the cabinet. After use, the cabinet was closed, the laminar airflow turned off, and sterilised with UV light. Human embryonic kidney (HEK 293T) cells were cultured in Dulbecco's Modified Eagles Medium (DMEM) with 10% (v/v) Fetal Bovine Serum (FBS), in 10cm tissue culture treated sterile plates. Cells were cultured in a 37°C incubator with 5% CO₂ and 95% humidity. HEK 293T cells were passaged every 2-3 days using trypsin: when cells were 80-90% confluent, media was removed, and cells were gently washed with PBS (5ml). Trypsin (0.25% w/v, 2ml) was then added to the dish, and incubated for 1-2 minutes, until the cells began to lift from the plate. DMEM + FBS (4ml) was then added to the plate to inactivate the trypsin and halt digestion, and the media was triturated to ensure the cells were all dislodged. The cell suspension was then centrifuged at 500g for 5 minutes, in order to form a cell pellet free of all trypsin, and then resuspended in DMEM + FBS, counted if necessary, and plated as appropriate into a fresh 10cm plate. When it was necessary to plate a specific number of cells, 10µl of cell suspension were mixed with 10µl of trypan blue, and 10µl of this mixture were pipetted onto a haemocytometer. Four counts were then made – one of each shaded section (see Figure 3.2) – and an average count calculated. This value was then multiplied by 2 (to account for the dilution with trypan blue), and then by 10000, in order to give an average number of cells/ml.

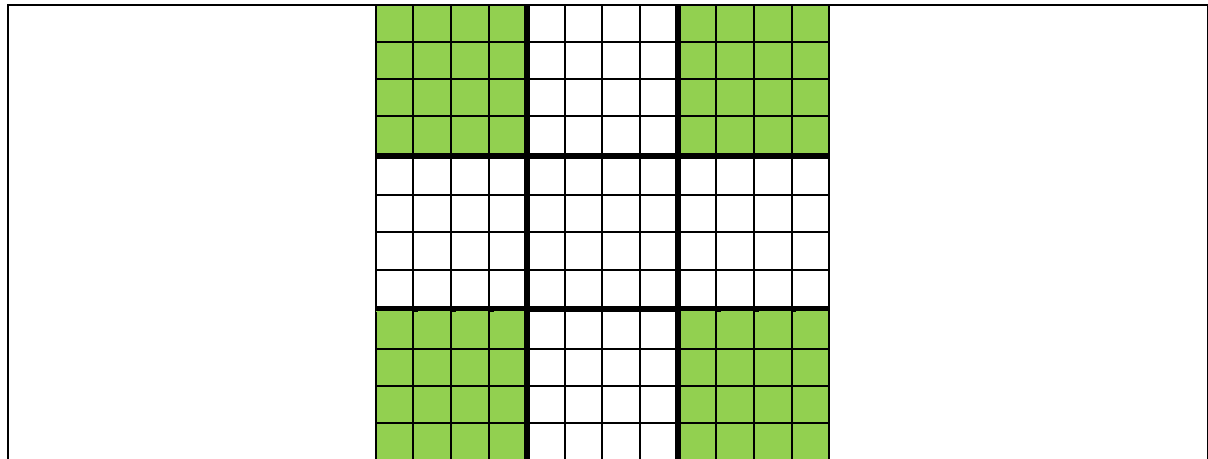


Figure 3.2: A haemocytometer. Live cells in each shaded section were counted using a 20X microscope, and then an average cell number calculated.

Transient Transfection with Aequorin cDNA

HEK 293T cells were transfected using Fugene transfection reagent. By splitting and counting the cells as described above, cells were plated into 6 well plates at a density of 1 million cells/well. After 24 hours, cells were transfected: per well to be transfected, 12 μ l Fugene was added to 200 μ l Optimem and mixed. 4 μ l DNA (1 μ g/ μ l) was then added and mixed, and the mixture incubated for 15 minutes at room temperature, during which time the cell media (DMEM + 10% FBS (v/v)) was replaced. After incubation the transfection mixture was added dropwise to the cells. Transfection reactions and media were removed after 24 hours, and cells were split, and plated into 96 well plates at a density of 50000 cells/well. Aequorin assays were carried out after a further 24 hours (48 hours after transfection). The mitochondrial aequorin construct is in the commercially available pcDNA3 plasmid (with ampicillin resistance), and the cytosolic aequorin construct is in the VR1012 plasmid (with kanomycin resistance (Hartikka *et al.*, 1996)). Both constructs are wild type, and the mitochondrial construct targeting sequence is subunit VIII of human cytochrome c oxidase, as described in (Rizzuto *et al.*, 1992).

Viral Transduction with Aequorin Adenovirus

All viral work was carried out in a designated Biosafety Level III laboratory, using laminar flow cabinets and appropriate disposal methods. HEK293T cells were transduced using wild type mitochondrial aequorin cDNA packaged in an adenoviral vector (kind gift from R. Rizzuto, Padova). 72 hours prior to assay, HEK293T cells at 80-90% confluency were split,

counted, and plated in opaque white 96 well plates at a density of 20000 cells/well. This density was chosen as HEK293T cells will double in number approximately every 24 hours, but after addition of virus their growth slows dramatically; 20000 cells/well was found to produce an appropriate level of confluency on day of assay. Extra wells were plated at the same density on a transparent 96 well plate in order to monitor the cell health and growth before and after addition of the virus. 24 hours after plating, cells were transduced with the viral aequorin: media was removed from the cells, and fresh DMEM containing the virus was added. After a further 24 hours, the media was removed from the cells, and replaced with fresh DMEM. As the viral concentration was unknown, the volume of virus was titrated in order to ensure a sufficient expression level of the aequorin protein, and the optimum volume was found to be 2 μ l of the mitochondrial aequorin virus per well, and the optimum volume of cytosolic virus was 10 μ l/well.

Aequorin Assays

Transfected HEK293T cells were plated in opaque white 96 well plates at a density of 50000cells/well, 24 hours prior to assay (transduced cells were plated as described above). Aequorin is expressed in an inactive form; to reconstitute the active protein, cells were incubated with the lipophilic prosthetic group coelenterazine (5 μ M) for 2 hours prior to assay at 37°C, in Krebs buffer (125mM NaCl, 5mM KCl, 1mM Na₃PO₄, 1mM MgSO₄, 1g/l glucose, 20mM HEPES) plus 1mM CaCl₂ or DMEM/HEPES buffer (1 bottle DMEM powder, 4.5g/L glucose, 1mM sodium pyruvate, 2mM L-glutamine, 15mM HEPES), as specified. Coelenterazine was then removed and replaced with Krebs buffer or DMEM/HEPES as appropriate. Cells were placed in a BMG Labtech Fluostar Optima plate reader to readjust to 37°C for at least 10 minutes (longer where drug treatments were required) and then assayed. Standardly, cells were measured for 10 seconds before stimulation with ATP (100 μ M) and then a further 20 seconds before the addition of digitonin (1mM) and CaCl₂ (100mM) in dH₂O, in order to produce L_{max}. For the high throughput screen these timings were reduced to ATP injection at 4 seconds, and digitonin at 13 seconds (total timecourse 18 seconds). Data were then calibrated using the appropriate constants (dependent on temperature and type of aequorin used), as described in Figure 3.1, or for the 18 second timecourse a ratio was made using the equation $ratio = M/T$, where M is the maximum ATP-induced luminescence value, and T is the sum of all luminescence values after the digitonin

injection, see Figure 3.4. For the initial high throughput screen, automated drug additions were carried out with the assistance of the Ketteler lab of the UCL Laboratory of Molecular and Cellular Biology, who also provided the NINDS-2 compound library. Data were then analysed by B-score by Dr Janos Kriston-Vizi of the same lab, using the *CellHTS2* analysis package, available from Bioconductor.

Fluo4-am Assays

Cytosolic Ca^{2+} responses to drugs were also assessed using Fluo4-AM, a cell permeant dye which, once diffused into the cell, is cleaved by cellular esterases into Fluo4 free acid and an AM group, leaving the charged Fluo4 trapped within the cell. Cells were plated in an opaque black 96 well plate at 50 000 cells/well. 30 minutes prior to assay, cells were loaded with 5 μM Fluo4-AM with 0.002% v/v pluronic acid and 1.4mM probenecid (to inhibit anionic transporters that may transport the dye from the cell) in Krebs buffer at 37°C, and drug concentrations as specified in results; cells were then washed and the buffer replaced with Krebs buffer + 200 μM EGTA. Fluorescence was measured with a BMG Labtech Fluostar Optima plate reader (Ex/Em 480/520); after 10 seconds baseline measurement, 100 μM ATP was injected, followed by 2 μM ionomycin after a further 20 seconds. Measurements were calibrated by subtracting background counts, and then using the equation: $[\text{Ca}^{2+}] = K_d \times (F/F_{\text{max}} - 1/R_f)/(1 - F/F_{\text{max}})$, where the K_d is 350nM, F_{max} is maximum fluorescence (post ionomycin addition) and R_f is 100 (Maravall *et al.*, 2000).

Measuring $\Delta\Psi_m$ using an ImageXpress Micro-XL

Cells were imaged on a Molecular Devices ImageXpress Micro-XL. Cells were plated in clear bottomed black 96 well plates at a density of 50000/well, 24 hours before assay. Cells were loaded for 30 minutes before assay with 25nM TMRM and 5 $\mu\text{g}/\text{ml}$ Hoechst in Krebs buffer at 37°C. Ex/Em 377/50 and 531/540 and a 20X objective were used, and 9 sites were taken per well. Basal levels were measured for 20 minutes before the addition of compounds. Fluorescence signals were then measured for a further 40 minutes before the addition of 5 μM FCCP to all wells, using the fluidics application, in order to give a minimum TMRM fluorescence value. After acquisition, the mean cell integrated intensity of the TMRM was calculated for each well over the time course, using the MicroXpress High Content Image Acquisition and Analysis software. Each time series was then expressed as a percentage of the average of its 20 minute baseline, and the minimum fluorescence value measured after

the addition of compound, before the addition of FCCP was used to assess the effect of the compound on membrane potential.

Mitochondrial Isolation and Calcium Retention Capacity Assay

Mitochondrial isolation and CRC assays were carried out as detailed elsewhere (Chapter 2, p66) in this thesis.

Respirometry: Seahorse XF24 Extracellular Flux Analyzer

Respirometry was carried out using a Seahorse XF 24 Extracellular Flux Analyzer as described elsewhere in this thesis (Chapter 2, p70). HEK293T cells were plated 24 hours ahead of assay, at a density of 50000 cells/well. Cells were incubated with the compounds (10 μ M) for 30 minutes prior to assay (during the calibration of the fluorescent probes), and the drug additions were: oligomycin (5 μ M), FCCP (2 μ M), FCCP (2 μ M), Antimycin A (5 μ M).

Results

Initial Screening of the NINDS-2 compound library

HEK293T cells were transiently transfected with mitochondrial-targeted aequorin in order to assess the effect of the NINDS-2 compound library on mitochondrial calcium accumulation (see Appendix 2). Cells were stimulated with 100 μ M ATP to generate a Ca²⁺ peak and then 1mM digitonin and saturating CaCl₂ to produce a maximal luminescence value. In order to screen large numbers of compounds, steps were taken to reduce assay time; this was due to a desire for efficiency (with a standard time course of 50 seconds, each 96 well plate would take 80 minutes, with 1040 compounds on 13 plates this would take 52 hours of assay time to screen the whole library in triplicate, not including reconstitution and other preparations), and additionally the observation that there was a time dependent effect on the magnitude of aequorin signals.

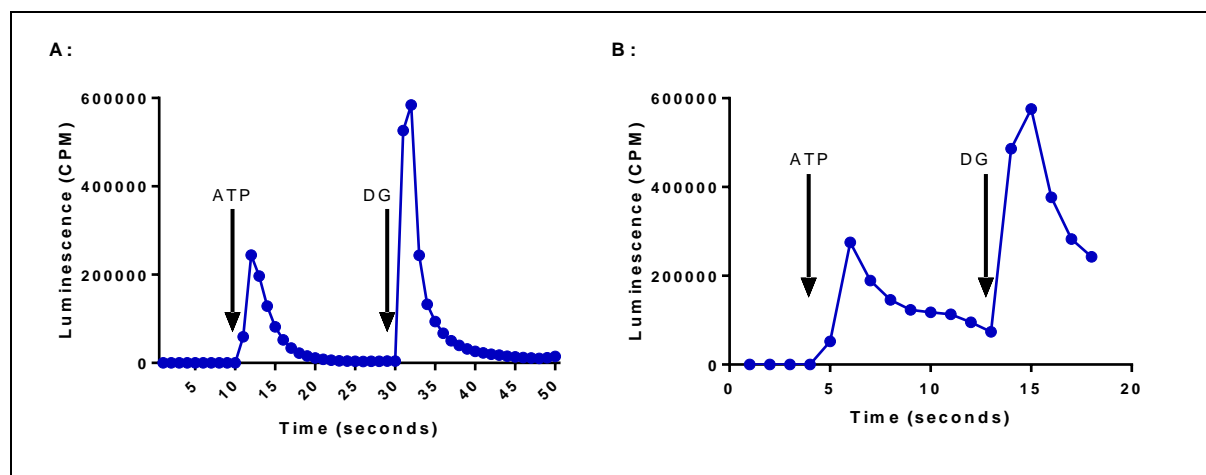


Figure 3.3: The time resolution of the signal for each well was reduced to enable high throughput screening. A: Typical experiments run for 50 seconds, with ATP injected at 10 seconds and digitonin (DG) injected at 30 seconds. B: The reduced temporal resolution gave a run of 18 seconds, with the ATP injection at 4 seconds and the digitonin at 13 seconds.

One option to overcome this was to change the format in which the plate was read; instead of reading one well continuously for 50 seconds (well mode), it is possible to take one

measurement from each well and repeat this cycle multiple times (plate mode). However, in plate mode, the lag time between cycles was found to be too long to capture the fast Ca^{2+} dynamics. Therefore, it was decided to reduce the overall measurement time, in order to use well mode within reasonable time limits. Initially, a 13 second measurement was trialled, with an ATP injection at 4 seconds, and no digitonin injection. However, this was dismissed, as without an L_{max} value, it cannot be said definitively that reductions in agonist-induced response are due to the effect of the compounds, rather than lower aequorin expression. Consequently it was decided to extend the timecourse to 18 seconds, in order to allow for an L_{max} measurement (See Figure 3.3).

	Time (seconds)	Luminescence (CPS)	Ratio
	1	243	=MAX(C6:C15)/SUM(C16:C20)
	2	248	
	3	320	
ATP >	4	257	
	5	52269	
	6	275440	
	7	189390	
	8	145590	
	9	123495	
	10	117721	
	11	113040	
	12	95376	
DG >	13	73576	
	14	486166	
	15	575837	
	16	376738	
	17	282560	
	18	242663	

Figure 3.4: An example of how the ratio values were calculated for the 18 second timecourse. Using the luminescence values from the timecourse in Figure 3.3, a ratio was calculated between the maximum ATP induced luminescence value and the total digitonin-induced luminescence values.

This was found to be adequate to measure both responses. However, as the digitonin peak does not return to baseline levels within this timecourse, the L_{\max} value is not a true L_{\max} as it doesn't measure the total maximum light emitted in response to digitonin, and therefore cannot be used to calibrate the luminescence values into $[Ca^{2+}]$. For the purposes of the screening however, it was not deemed necessary to calibrate into an actual $[Ca^{2+}]$, as long as the total luminescence is still taken into account; the effect of the compounds can be assessed by their effect relative to control compounds, rather than the absolute $[Ca^{2+}]$ produced. Therefore a ratio was made, of the peak value after ATP stimulation divided by the total luminescence after digitonin injection (See Figure 3.4).

The full drug library was then screened, using HEK293T cells transiently transfected with mitochondrial-targeted aequorin in order to assess the effect of the compounds. Prior to assay, cells were treated with 10 μ M compounds or DMSO as a negative control; they were incubated with the compounds for 30 minutes at 37°C and then assayed in a BMG FluoStar plate reader.

Out of 1040 compounds, 65 compounds were found which inhibited mitochondrial Ca^{2+} by more than two standard deviations from the mean (see Figure 3.5A). Two standard deviations from the mean was arbitrarily selected for the purpose of keeping the number of compounds manageable, and the threshold could be raised or lowered as necessary. It is also important to consider the total aequorin luminescence: compounds in which there was a significantly decreased total luminescence were likely to be raising Ca^{2+} concentration prior to the assay, and thus exhausting the aequorin supply, or it might indicate cell death induction by the compound. This would suggest they have off target effects, and are not suitable, therefore only compounds which did not deviate in total aequorin luminescence by more than two standard deviations from the mean were considered for further investigation. The top 21 compounds which most strongly inhibited mitochondrial $[Ca^{2+}]$ without affecting total luminescence were selected for the next stage of the screen.

It is notable that in the mitochondrial screen, the controls appear skewed to the upper left quadrant of the plot of peak $[Ca^{2+}]$ against total aequorin luminescence – this is due to the normalization method used to acquire these data. The data were normalized by Dr Janos

Kriston-Vizi using B-score normalization (Brideau *et al.*, 2003). B-score is a sample-based normalization method recommended for high throughput screening (Malo *et al.*, 2006), in which it is assumed that the majority of screened compounds will have no effect on phenotype, and the samples are therefore used as controls. B-score is a measure of variability within each plate, and eliminates positional bias (Brideau *et al.*, 2003).

HEK293T cells were then transiently transfected with cytosolic aequorin in order to assess the effect of compounds on cytosolic $[Ca^{2+}]$. In order to ensure mitochondrial specificity, successful compounds should have no effect on cytosolic $[Ca^{2+}]$ as it is likely that compounds which reduce cytosolic $[Ca^{2+}]$ are false positives: the reduced mitochondrial $[Ca^{2+}]$ in these instances would be a downstream effect of a reduced cytosolic $[Ca^{2+}]$ transient. Therefore, in this secondary screen, compounds were selected for which the $[Ca^{2+}]$ signal did not differ from the controls (see Figure 3.5B). This applied to only 3 of the 21 compounds screened. These were aminosalicylate sodium, cetylpyridinium chloride (also known as hexadecylpyridinium chloride) and desipramine hydrochloride (see Figure 3.6), hereafter designated as Drug A, H and D respectively.

These compounds were found in different positions on the compound plates, suggesting that there was not a positional bias in the assay. They have diverse uses: Drug A is an anti-bacterial and tuberculostatic compound, Drug H is a topical anti-infective compound, and Drug D is an antidepressant (see Appendix 2).

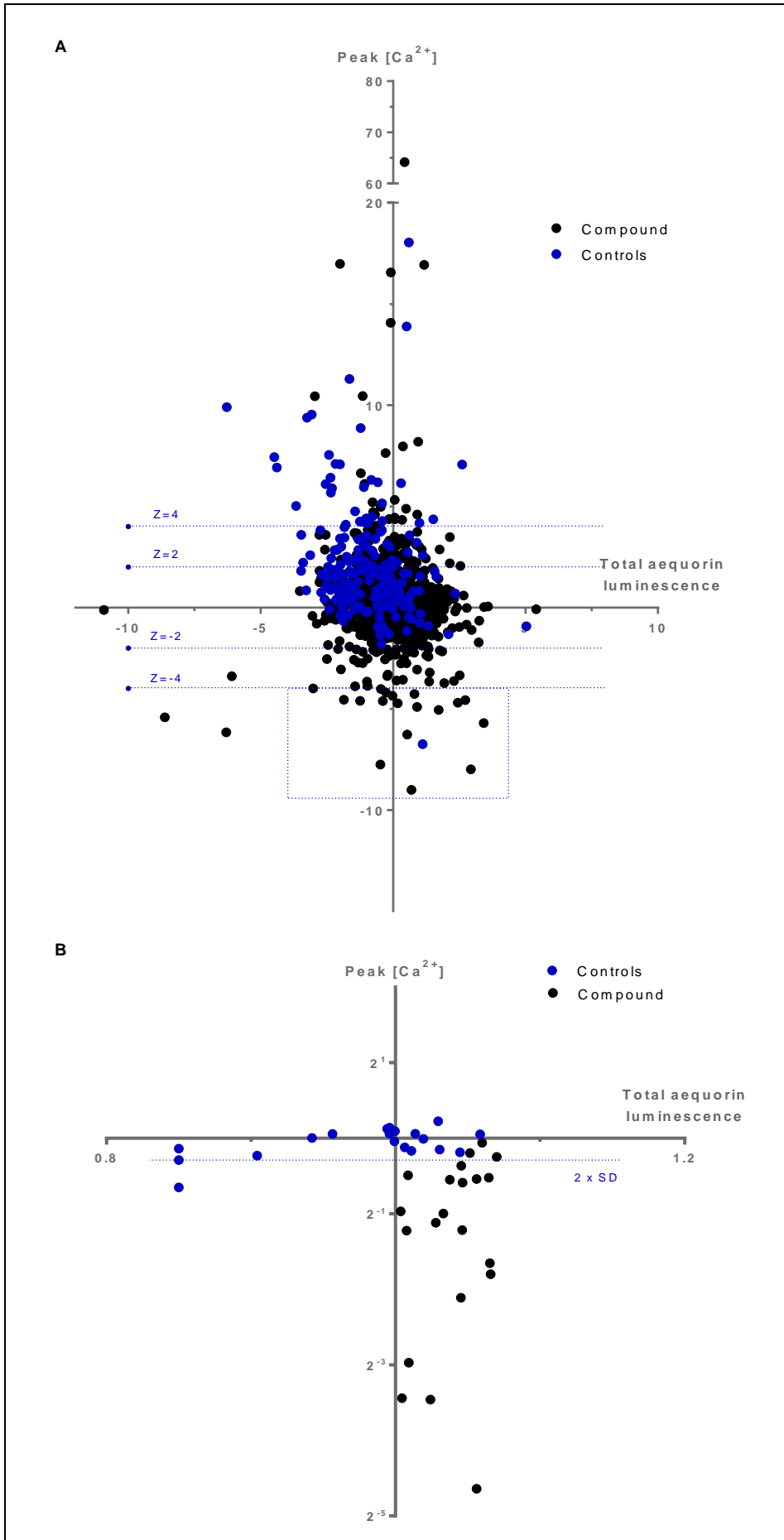


Figure 3.5: Aequorin based screening of the NINDS-2 drug library.

A: an initial screen of 1040 compounds at 10 μM using mitochondrial targeted aequorin found 65 compounds which inhibited mitochondrial calcium concentration by more than two standard deviation from the mean. The dotted box represents those compounds which inhibit mitochondrial [Ca^{2+}] by more than four standard deviations, without affecting total luminescence. N = 3.

B: a secondary screen of the top 21 compounds (at 10 μM) selected from the initial screen, using cytosolic aequorin to find compounds which do not affect cytosolic [Ca^{2+}]. Three compounds were found to inhibit cytosolic [Ca^{2+}] by less than two standard deviations from the mean. N = 3.

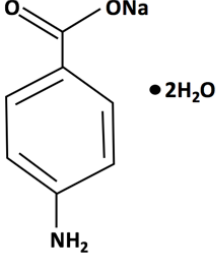
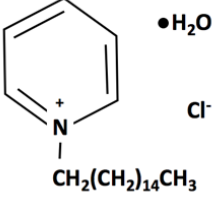
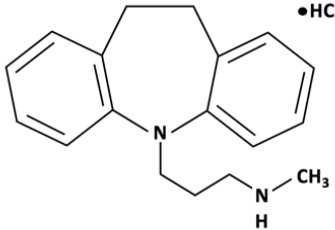
Compound Name	Aminosaliclylate sodium	Desipramine hydrochloride	(Hexa)cetylpyridinium chloride
Designation	Drug A	Drug D	Drug H
Plate	001	002	001
Well	F03	D03	A04
Compound Type	Anti-bacterial, tuberculostatic	Anti-depressant	Anti-infective (topical)
Chemical Structure			

Figure 3.6: Three compounds were identified as specific inhibitors of mitochondrial Ca^{2+} uptake. These compounds were aminosaliclylate sodium (Drug A), cetylpyridinium chloride (Drug H), and desipramine hydrochloride (Drug D). Chemical structures own drawings (information from Sigma-Aldrich).

Reconfirming screening results

The next step was to reconfirm the actions of these compounds by other methods, to investigate whether the screen had been a robust method of detecting specific reductions in mitochondrial $[\text{Ca}^{2+}]$. Initially, retroviral aequorin was used: as some cell lines do not transfect with a high enough efficiency to be practical, retroviral aequorin was used to transduce cells to investigate whether this could be an appropriate screening strategy for these cell lines. FCCP (carbonyl cyanide-4-(trifluoromethoxy)phenylhydrazone) was used as a positive control for the mitochondrial aequorin and a negative control for the cytosolic. FCCP is a mitochondrial uncoupler which dissipates $\Delta\Psi_m$ by equilibrating H^+ ions across the mitochondrial membrane. As a result of its effect on $\Delta\Psi_m$, FCCP inhibits mitochondrial calcium uptake through the MCU (which is $\Delta\Psi_m$ dependent), but does not affect the agonist stimulated cytosolic $[\text{Ca}^{2+}]$ response, although it can cause an increase in resting cytosolic $[\text{Ca}^{2+}]$ (Luo *et al.*, 1997). It was found that Drugs D and H significantly reduced mitochondrial $[\text{Ca}^{2+}]$ responses in comparison to the DMSO control (see Figure 3.7A), but Drug A did not –

a contrast to the initial screening in which all these drugs significantly inhibited mitochondrial Ca^{2+} uptake.

Drug D was also found to significantly inhibit cytosolic $[\text{Ca}^{2+}]$ responses in comparison to the DMSO control (see Figure 3.7B). However, the cytosolic $[\text{Ca}^{2+}]$ responses shown in Figure 3.7B are very unusual: they range from 2-9 μM which is much higher than the standard cytosolic $[\text{Ca}^{2+}]$ response, which is in the nM range (Rizzuto and Pozzan, 2006). This calls into serious doubt the validity of the cytosolic aequorin virus, and raises questions about whether the construct is truly cytosolic: these concentrations are much more typical of mitochondria. Therefore, these results have been discounted, and an alternative approach was taken to confirm the effect of the compounds on cytosolic $[\text{Ca}^{2+}]$: the fluorescent calcium indicator Fluo4-AM was used to measure cytosolic $[\text{Ca}^{2+}]$ in response to ATP stimulation (see Figure 3.7C), and it was found that none of the drugs were significantly different to DMSO control.

A calcium retention capacity assay was also used on liver mitochondria isolated from adult C57/Black mice to investigate the effect of the compounds on mPTP opening (see Figure 3.7D and 3.7E). CsA was used as a positive control, as it is known to desensitize the pore to Ca^{2+} , thereby delaying its opening. It was found that Drugs A and D both inhibited pore opening, as the responses were not significantly different to CsA, but that Drug H potentiated pore opening in comparison to the DMSO control (0%), and was significantly different to CsA, Drug D and Drug A. Inhibition of mPTP correlates with inhibition of MCU: it is logical that reduced mitochondrial Ca^{2+} uptake would be expected to delay mPTP opening, which is caused by mitochondrial Ca^{2+} overload, as was demonstrated in the MCU knock out mouse (Pan *et al.*, 2013). This contrasts with the data shown in Figure 3.7A, in which Drug A was found to not significantly reduce mitochondrial $[\text{Ca}^{2+}]$, whereas Drug H did.

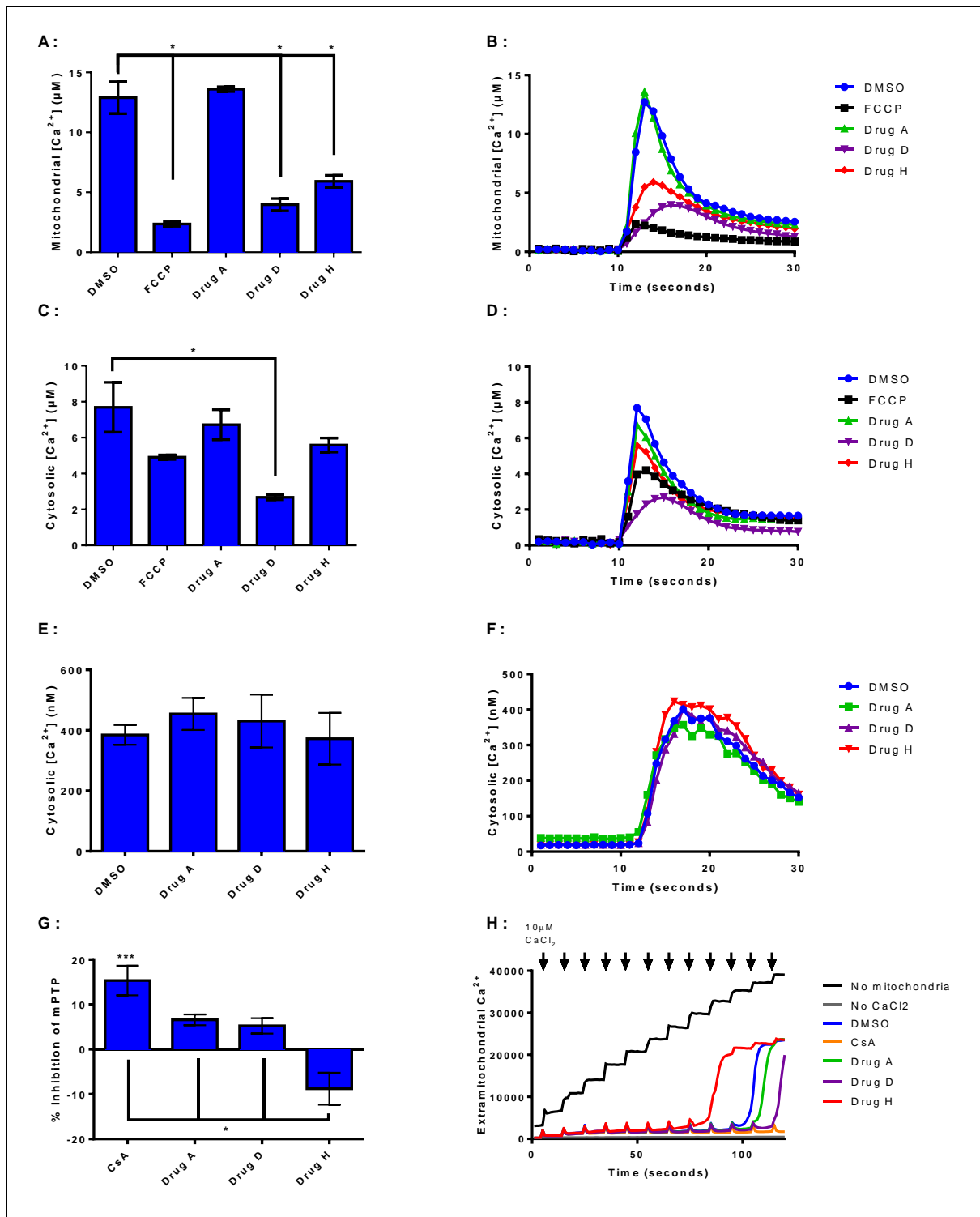


Figure 3.7: Reconfirming the results of the initial screen. A: Using the mitochondrial aequorin virus, FCCP (5 μM), Drug D and Drug H significantly reduced mitochondrial $[Ca^{2+}]$. N of 3. B: Representative mitochondrial $[Ca^{2+}]$ trace using the mitochondrial aequorin virus. C: Using the cytosolic aequorin virus, Drug D was found to significantly reduce $[Ca^{2+}]$, however these results were discounted due to doubt over the identity of aequorin construct. N of 3. D: Representative cytosolic $[Ca^{2+}]$ trace using the cytosolic aequorin virus. E: None of the drugs affected cytosolic $[Ca^{2+}]$ when measured using the calcium indicator dye Fluo4-AM. N of 3. F: Representative cytosolic $[Ca^{2+}]$ trace using Fluo4-AM. G: A CRC assay showed that only CsA (1 μM) was significantly different to DMSO (0%), but that Drug A and D had an inhibitory effect while

Drug H potentiated mPTP opening. N of 5. H: A representative trace of the CRC assay. * denotes significance as assessed by one way ANOVA * = p value <0.05, *** = p value < 0.005. Drugs A, D and H were used at 10 μ M for all these experiments. Error Bars are SEM.

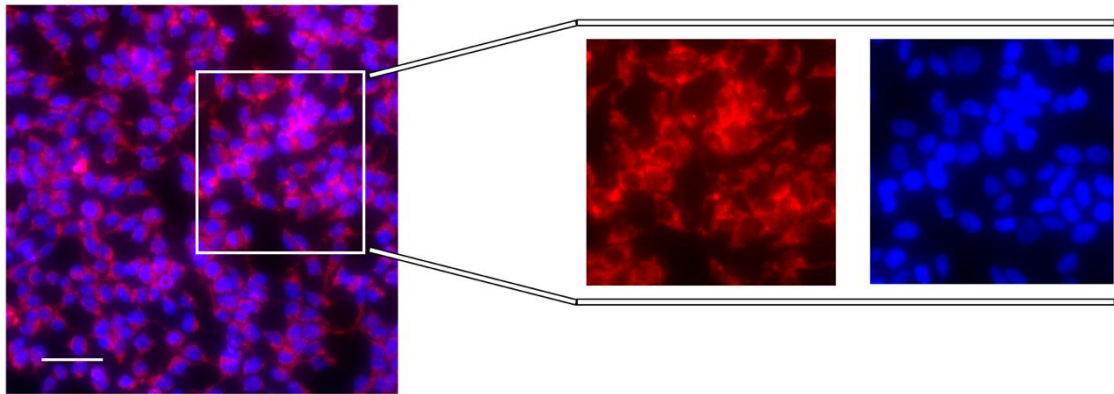
Investigating the effect of compounds on other mitochondrial parameters

In order to further investigate the mechanism of action of the three compounds, their effect on mitochondrial membrane potential ($\Delta\Psi_m$) was examined using the cationic fluorescent dye TMRM (Figure 3.8A). As mitochondrial calcium uptake through the MCU is dependent on mitochondrial $\Delta\Psi_m$, any drugs which dissipate $\Delta\Psi_m$ (visible as a reduction in TMRM) will reduce mitochondrial calcium uptake independently of any action on the MCU, as a downstream effect of the reduction in $\Delta\Psi_m$. FCCP was used as a positive control.

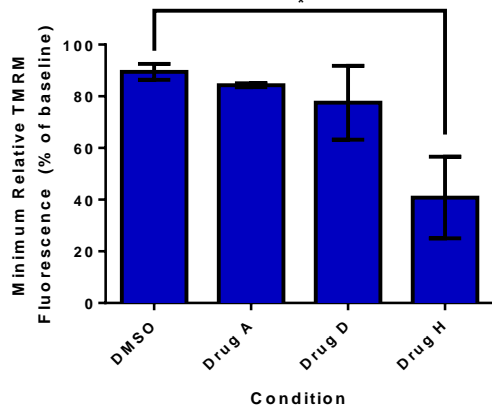
TMRM intensity was found to be significantly reduced in comparison to DMSO control in HEK293T cells treated with Drug H (see Figure 3.8B), whereas it was not significantly different in cells treated with Drug A or D. This confirms that the inhibition of mitochondrial calcium uptake by Drugs A and D is not a consequence of inhibition of $\Delta\Psi_m$, but that Drug H may be working indirectly on MCU, via $\Delta\Psi_m$. In all conditions FCCP ablated TMRM intensity when added after 40 minutes incubation with the compounds of interest, confirming loss of TMRM fluorescence corresponds to a drop in $\Delta\Psi_m$.

The effect of the compounds on oxygen consumption was then investigated, using a Seahorse XF Flux Analyzer (Figure 3.8D). Drugs A and D had no effect in comparison to DMSO, but Drug H significantly reduced basal oxygen consumption, although it had no effect on leak respiration, and no significant effect on maximal consumption, though it appeared reduced. This suggests that the reduction of $\Delta\Psi_m$ seen in Figure 8B may be due to inhibition of respiration, as $\Delta\Psi_m$ is generated by the activity of the electron transport chain.

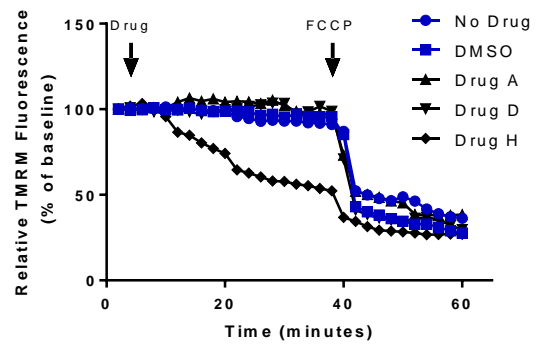
A:



B:



C:



D:

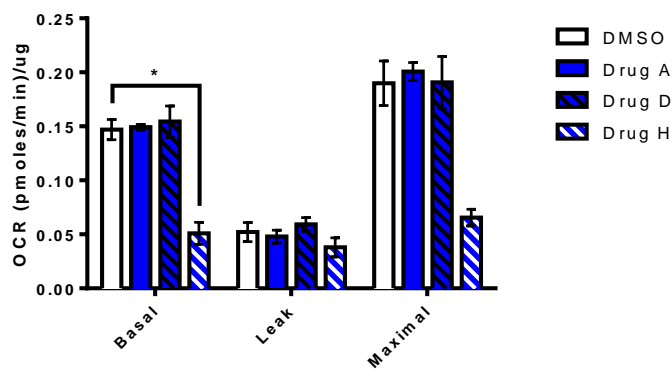


Figure 3.8: Drugs A and D act independently of mitochondrial membrane potential, and do not affect oxygen consumption. A: HEK293T cells stained with Hoechst and TMRM prior to drug addition. B: TMRM fluorescence (relative to baseline) was significantly reduced by addition of Drug H in HEK293T cells, but not affected by addition of any other drugs in HEK293T cells. N of 3. C: Representative trace of TMRM intensity after 10 μ M drug addition in HEK293T cells. D: Basal oxygen consumption was significantly reduced by Drug H (in comparison to DMSO), but not affected by Drugs A or D. N of 3. Significance was assessed by one-way ANOVA, * denotes significance. * = p value <0.05. Error bars are SEM.

Summary

Overall, it was demonstrated that an aequorin based screening approach can be used to find mitochondrial specific inhibitors of mitochondrial Ca^{2+} uptake: of the NINDS-2 compound library, the initial mitochondrial and cytosolic aequorin screens identified three compounds, Drug A, D and H, which inhibited mitochondrial $[\text{Ca}^{2+}]$ uptake and did not affect cytosolic $[\text{Ca}^{2+}]$ responses. Screening with viral aequorin to verify the actions of these compounds was carried out, and revealed that Drug A had no effect on mitochondrial $[\text{Ca}^{2+}]$ uptake, and that the cytosolic aequorin construct was likely contaminated. Fluo4-AM was found to be a simple alternative method for assessing impact on cytosolic $[\text{Ca}^{2+}]$, and reconfirmed that the compounds did not affect cytosolic $[\text{Ca}^{2+}]$, and a calcium retention capacity assay was found to be another possible approach. Imaging with TMRM was shown to be an essential step to verify the specificity of inhibition, and Drug H was shown to significantly reduce $\Delta\Psi_m$, and therefore be indirectly reducing mitochondrial $[\text{Ca}^{2+}]$ uptake rather than directly inhibiting MCU. Measurement of oxygen consumption cast further light on the mechanism of action of the compounds.

Discussion

The initial screen using mitochondrial targeted aequorin was a successful approach, enabling the screening of a large library relatively easily and quickly (at the rate of 84 compounds an hour, or the entire library in 13 hours). A moderately high number of compounds were found to be of interest in this screen: 65 compounds were found to inhibit mitochondrial $[Ca^{2+}]$ by more than two standard deviations from the mean. It would have been useful to have positive controls included in this part of the screen, however this was not possible due to the automated drug addition (necessary to maintain the efficiency of screening) and the lack of a suitable control – whilst FCCP has been used elsewhere in this study it does not directly inhibit the MCU, which would be desirable in an optimal control.

Although there were 65 positive hits from the mitochondrial screen, only 21 were used for the next step; this was in order to keep the cost of screening low, whilst the screening method was still in development, these other compounds could be screened in future investigations. From the top 21 mitochondrial Ca^{2+} inhibitors, only 3 were found not to have affected cytosolic $[Ca^{2+}]$ responses. An alternative approach could have been to start the screen with a cytosolic screen and so eliminate all compounds which did affect cytosolic $[Ca^{2+}]$ before proceeding to the mitochondrial screen – this may have been a more efficient approach, as 85% of the compounds reduced cytosolic $[Ca^{2+}]$, and these compounds could be immediately eliminated from the screen.

Another approach would be to screen all compounds with both mitochondrial and cytosolic aequorin simultaneously; whilst this approach would have been the most thorough it would also significantly increase the time necessary for screening, using the 96 well plate reader method. Alternatively, a FLIPR device could be used for screening: this enables the simultaneous measurement of every well in a 96 well plate; therefore the original 50 seconds timecourse could be used, and the screening of the entire library in triplicate would take only ~32 minutes of assay time, significantly reducing screening time. This would be highly advantageous to increase the throughput of screening, and would be recommended

for any further library screens, however no luminescence-capable FLIPR was available for this project.

When reconfirming the effect of the drugs using a virally transduced mitochondrial-targeted aequorin (Figure 3.7), it was found that only Drugs D and H were significantly different to the DMSO control, and that Drug A did not reduce mitochondrial $[Ca^{2+}]$ at all.

There was clearly an issue with the results from the viral cytosolic aequorin: the $[Ca^{2+}]$ responses found in these experiments were much higher than would be expected in the cytosol, and therefore these data were completely discounted, as the method cannot be relied upon. It is possible that the cytosolic virus may have been confused or contaminated with the mitochondrial virus during transit, as the $[Ca^{2+}]$ values are much more representative of mitochondrial $[Ca^{2+}]$; in order to establish which aequorin this is, it could be tested with FCCP: if it is a mitochondria-targeted construct, FCCP should significantly decrease $[Ca^{2+}]$ due to its effects as an uncoupler, whereas if it is really a cytosolic construct FCCP should have no effect. Another method of establishing the identity of the cDNA would be to sequence it to identify whether the mitochondrial COX targeting sequence is present. Alternatively, this could be due to low transduction efficiency: if a low level of aequorin was expressed, a large proportion may be used up in the initial agonist-induced response, meaning that the aequorin could be entirely consumed before the peak digitonin-induced response was reached, meaning it would not be representative of true L_{max} , and therefore the calibration would be skewed.

When assessed using Fluo4-AM, ATP-induced cytosolic Ca^{2+} signals did not differ between conditions. Fluo4-AM could be an acceptable alternative for the initial cytosolic screen, especially for cells which do not easily transfect or transduce. Although the timecourse of a Fluo4-AM experiment is too long (1 minute/well) to enable high throughput screening, this could be reduced, as was the aequorin timecourse, or a FLIPR could be used to measure all wells simultaneously. If a FLIPR device could be acquired which was capable of measuring luminescence and fluorescence simultaneously, Fluo4-AM could even be used in the same cells as mitochondrial-targeted aequorin – Fluo4-AM is excited at 480nm and emits at 510nm, whereas aequorin luminesces at 465nm - in order to measure mitochondrial and

cytosolic Ca^{2+} together. Another method of dual measurement, using luminescence and fluorescence, would be to simultaneously measure mitochondrial aequorin and TMRM in order to measure mitochondrial membrane potential and mitochondrial Ca^{2+} together.

The CRC assay showed that Drug A and Drug D inhibited mPTP opening to a similar extent as CsA. It would be expected that MCU inhibitors would inhibit mPTP opening, as they would reduce mitochondrial Ca^{2+} uptake, and therefore mitochondrial $[\text{Ca}^{2+}]$, which is the critical trigger for mPTP opening. Interestingly however, Drug A has previously been shown in Figure 3.7A to not significantly reduce mitochondrial $[\text{Ca}^{2+}]$, and Drug H had been shown to significantly reduce it, whereas in this experiment Drug H was not inhibiting mPTP opening, and was in fact potentiating it. These contrasting results suggest that Drug H could be having other effects which are causing the earlier opening of mPTP, as mitochondrial Ca^{2+} overload is not the only cause of mPTP opening; it was demonstrated that Drug H also significantly reduced mitochondrial membrane potential and oxygen consumption. Mitochondria can produce reactive oxygen species (ROS) such as superoxide, which is produced by the reduction by one electron of O_2 (Murphy, 2009). Superoxide flux is determined by both the availability of electron donors, and the local O_2 concentration, which has been demonstrated to be altered by Drug H: this suggests that Drug H could be potentiating mPTP opening through production of ROS. This could be tested by FACS or confocal imaging with a ROS sensitive dye, such as dihydroethidium (DHE), to investigate whether Drug H increases ROS production above basal levels. This would not be necessary to include as part of an initial screen for mitochondria-specific inhibitors, but could be a useful secondary step for determining mechanism of action.

Drug H was found to significantly reduce TMRM fluorescence (and therefore $\Delta\Psi_m$) in comparison to a DMSO control (Figure 3.8). This demonstrates that Drug H is not acting directly on the MCU – it is indirectly inhibiting mitochondrial Ca^{2+} uptake by reducing mitochondrial membrane potential, upon which MCU mediated uptake relies. This shows that this is an important step of the screening, to check the specificity of the compounds.

The effect of the compounds on oxygen consumption was also investigated – ATP production via oxidative phosphorylation is the primary function of mitochondria, and

therefore it is important that any potential inhibitors do not affect oxygen consumption. Drugs A and D were found to have no significant affect on oxygen consumption, whereas Drug H significantly reduced basal levels in comparison to DMSO controls. This is not a surprising result, as Drug H was found to significantly reduce $\Delta\Psi_m$, which is generated by the passage of protons across the inner membrane by the electron transport chain, therefore a reduction in basal oxygen consumption would directly account for the reduced $\Delta\Psi_m$. This demonstrates that Drug H is conclusively not an MCU specific inhibitor.

From the NINDS-2 library screened in this study, 3 drugs were found which in a preliminary screen significantly reduced mitochondrial $[Ca^{2+}]$ without affecting cytosolic $[Ca^{2+}]$ responses; using mitochondrial-targeted aequorin was a useful approach for determining drug specificity. When reconfirmed using viral aequorin, Drug A was found to not inhibit mitochondrial $[Ca^{2+}]$, and when the effect of the compounds on $\Delta\Psi_m$ was investigated, Drug H was found to significantly reduce membrane potential and oxygen consumption, and to potentiate mPTP opening. In this screen, Drug D was found to specifically inhibit mitochondrial Ca^{2+} without affecting cytosolic Ca^{2+} responses, although it was not a particularly potent inhibitor; this was reconfirmed using viral aequorin, Fluo4-AM, and the CRC assay. It did not affect mitochondrial membrane potential or oxygen consumption, important measurements of mitochondrial health. Further work would be to do dose response experiments, and to investigate the pharmacokinetics and methods of action of Drug D, in addition to more work on possible side effects, such as ROS production. It would also be interesting to test these drugs in cells from the MCU knock out mouse to verify their specificity for the MCU.

Finding an inhibitor of the MCU would provide an invaluable research tool and has considerable translational potential for pathologies involving calcium overload. Overall, this screening approach appears to be a good preliminary method of screening large numbers of compounds before progressing to more in depth analysis of any positive hits, and could be used to screen other compound libraries in order to identify such inhibitors.

Chapter 4: Investigating the role of the MCU *in vitro*.

Introduction

The Mitochondrial Calcium Uniporter (MCU)

Until recently, the molecular components of the mitochondrial calcium uniporter complex were unknown. A variety of components have now been identified: MCU (Baughman *et al.*, 2011; De Stefani *et al.*, 2011), MCUB (Raffaello *et al.*, 2013), MICU1/2/3 (Perocchi *et al.*, 2010; Plovanich *et al.*, 2013), EMRE (Sancak *et al.*, 2013), MCUR1 (Mallilankaraman *et al.*, 2012a), and SLC25A23 (Hoffman *et al.*, 2014). Investigations into the role and function of these proteins have begun (see Chapter 1, “the mitochondrial Ca²⁺ uptake complex” p33-47), but much work is still needed to fully understand the function of the individual proteins, the function of the entire complex in health and disease, the composition of the complex, and the manner of its regulation. Investigating the role of each of the components is too large a task for one project, therefore it was decided to focus initially on MCU, as the central component of the pore and the MCU complex.

To recap, in the original studies identifying MCU, MCU knockdown was found to cause no differences in mitochondrial volume or number, $\Delta\Psi_m$, or basal and uncoupled respiration, but to significantly reduce agonist stimulated mitochondrial Ca²⁺ uptake (Baughman *et al.*, 2011; De Stefani *et al.*, 2011). Overexpression was found to increase H₂O₂ mediated cell death, and the DIME motif was identified as being essential for Ca²⁺ uptake. The knock out mouse did not have an overt phenotype, and the most notable difference (beyond ablation of mitochondrial Ca²⁺ uptake) was that the MCU ^{-/-} mice performed worse in high intensity exercise tests (Pan *et al.*, 2013). There have been contradicting reports on the effect of MCU knock out on cell death, with the original knockout mouse paper reporting there was no effect (Pan *et al.*, 2013), and the latter conditional knockout showing protection (Kwong *et al.*, 2015; Luongo *et al.*, 2015).

Many more studies have been published in the intervening years since the identification of the gene *CCDC109a* as the MCU. These studies have found a plethora of functions in which MCU is involved, in diverse areas and organisms. For example, MCU knockdown has been found to increase autophagy (Mallilankaraman *et al.*, 2012b), and to regulate metabolism in the heart, coupling energy supply and demand (Kwong *et al.*, 2015; Luongo *et al.*, 2015; Wu *et al.*, 2015). It has also been found to be involved in ROS mediated wound closure in *C. elegans* (Xu and Chisholm, 2014), to play a role in NMDA induced toxicity – against which MCU knockdown is protective (Qiu *et al.*, 2013) – and to be important for the development of the notochord and anteroposterior stages during gastrulation in zebrafish development (Prudent *et al.*, 2013). MCU also has an increasing number of roles in cancer cells: it has been found to mediate breast cancer cell progression via transcription factor HIF-1 α (Tosatto *et al.*, 2016), to have a role in regulating passage into and out from senescence (Wiel *et al.*, 2014), and in mediating cerastol-induced paraptosis (cell death characterized by extensive vacuolization) in breast cancer cells (Yoon *et al.*, 2014). Despite these discoveries, MCU function is still relatively uncharacterized, and further investigation is warranted, to confirm these data and to expand upon them.

Protein function can be examined chemically, using drugs to inhibit or potentiate function, or genetically, by reducing or removing gene expression and therefore protein function. Due to the issues (lack of specificity and permeability) with the existing inhibitors of the MCU, as described elsewhere in this thesis (Chapter 3, p88), it was decided to investigate the function of the MCU genetically, by transfecting cells with constructs targeting the *CCDC109a* gene.

Transfection

Transfection is a powerful tool for the study of gene and protein function: it is a procedure which produces genetically altered cells through the use of transfection reagents which introduce foreign nucleic acids (DNA and RNA) to the cell. The goal of transfection is to study the function of specific genes and the gene products, by either enhancing or inhibiting gene expression. Transfection is an alternative to the use of transgenic animals as it allows the study of gene function without the need for housing, breeding and sacrificing animals, thus complying with the replacement principle of using non animal methods to achieve the same scientific aims, although animals are still useful to demonstrate how genetic

alterations impact within a multicellular organism rather than the more simplistic cell culture model.

Cells can be transfected either transiently or stably; stable transfections require a selection marker, usually an antibiotic resistance gene, and will continue to express transgenes in future generations of cells. Transient transfections do not require selection and transgenes are only temporarily expressed, typically for up to 72 hours after transfection, although some methods provide longer expression. Transiently transfected cells will not express the transgene in future generations (Kim and Eberwine, 2010), as the introduced nucleic acid is not integrated into the genome, so it will be diluted through mitosis, and degraded. Both have their advantages and should be selected depending on the experimental requirements.

DNA and RNA can be transfected into cells, although usually with opposite purpose: transfection with DNA is usually to express a new protein, or overexpress an existing protein, whereas transfection with RNA is often to prevent protein expression through gene knockdown with RNA interference (RNAi). RNAi was first used in 1998 (Fire *et al.*, 1998); it allows the knockdown of gene expression and has a variety of applications, such as the study of protein function, pathway analysis and drug target discovery. RNAi can be used in a wide variety of cells, and also *in vivo*. There are different types of RNAi including short interfering RNA (siRNA), and short hairpin RNA (shRNA), amongst others.

siRNAs are double stranded RNAs (dsRNAs) of 21-25bp, with dinucleotide 3' overhangs. They induce gene knockdown through the RNA-induced silencing complex (RISC): the antisense strand of the siRNA is incorporated into RISC and acts as a targeting sequence to identify the corresponding mRNA. RISC then cleaves the matching mRNA and marks it for degradation, resulting in loss of protein expression, as no further protein encoded by that mRNA will be synthesized (for overview, (Sen and Blau, 2006)). shRNA (contained in DNA vectors) is a subset of RNAi used for stable gene knockdown. shRNA can be introduced to the cell through transfection or transduction, and can integrate into the host cell DNA. They consist of two 19-22bp RNA sequences linked by a short "hairpin" loop of 4-11 nucleotides. After transcription, the shRNA is exported to the cytosol, where it is processed into siRNA by the enzyme Dicer, and is incorporated into RISC, which binds to the target sequence, and marks it for degradation (Paddison *et al.*, 2002).

Methods of transfection

Unfortunately, there is not one methodology which works for all cell types and nucleic acid types. Multiple methods of transfection exist, and each of them need optimizing for different cell types in order to produce maximum transfection efficiency. Optimization of the transfection method aims to achieve high and reproducible transfection efficiency with minimal cell toxicity.

One of the main challenges in optimizing transfection is reducing toxicity to the cell: in order to deliver genetic material (most commonly to the nucleus, although other parts of the cell can also be targeted), it is generally necessary to disrupt the plasma membrane. This can cause membrane leakiness and activate stress response pathways, which can impact cell health and sometimes lead to cell death. Many transfection reagents require a serum-free medium, which can also damage cell health.

Transfection methods can be either chemical, physical, or biological. Each method has advantages and disadvantages; these are summarised in Table 3. This is not an exhaustive list: other methods also exist, such as direct injection of genetic material into cells, laser irradiation to disrupt the plasma membrane, and the use of nanoparticles for delivery into the cell.

Transfection method	Type of method	Advantages	Disadvantages
Lipofection E.g. Fugene, Lipofectamine, Viafect, Effectene	Chemical: uses positively charged cationic liposomes which form complexes with negatively charged DNA, and are thus able to fuse to cell membranes.	Easy to use Widely available Low cost Applicable to a wide range of immortalized cell lines	Requires extensive optimization to find optimum lipofection agent:DNA ratio (Recillas-Targa, 2006)
Calcium phosphate	Chemical: forms a precipitate of positively charged	Inexpensive	Batch dependent efficiency (Graham and van der Eb, 1973)

	calcium and negatively charged phosphate which binds DNA on its surface.		
Morpholino	Chemical: an oligomer with a backbone of morpholino rings, targets specific mRNA sequences and prevents translation by steric blocking.	Does not require additional reagents	Must be designed and synthesized specially Expensive (Summerton, 1999)
Electroporation E.g. nucleofection	Physical: uses an electrical pulse to permeabilize the cell membrane, allowing the transfer of genetic material inside the cell.	Does not require vector Can be used <i>in vivo</i> Uses small amounts of DNA	High rate of cell death Requires special equipment (Neumann <i>et al.</i> , 1982)
Viral transduction E.g. Lentiviral, retroviral	Biological: viral vector carrying nucleic acid infects host cell, and NA is integrated into the nuclear genome, replicated and transcribed.	High efficiency Can infect non dividing cells	Biohazard, requires GM license and Level 2 containment laboratories (Akkina <i>et al.</i> , 1996) Can have high cell toxicity

Table 3: a summary of the primary advantages and disadvantages of a range of transfection techniques.

Transfecting primary cultures

Primary cultures are cells isolated directly from tissue, which may initially contain more than one cell type, as opposed to cell lines, which are cells of one type which are either naturally

immortal (such as cancer cell lines) or have been genetically altered to inhibit genes involved in senescence (Stacey, 2006).

Primary cells are a more relevant model than immortalized cell lines, as they more closely retain the characteristics of cells *in vivo* than immortalized cell lines, which are either cancer cell lines or cell lines with extreme genetic modifications. However, primary cells are more labour intensive to prepare, and they can only be kept in culture for a limited time before entering senescence and dying – this is as described by the Hayflick Limit, which is the number of times which a population of human cells will divide, before entering senescence (HAYFLICK and MOORHEAD, 1961). This is dependent on cell type, and is linked to the length of telomeres, which shorten after each cycle of cell division, and eventually induce apoptosis after reaching a specified length. Primary cells are also more vulnerable, requiring specific media containing growth factors and cytokines, and requiring more expertise to culture than immortalized cell lines (ATCC, 2012). With minor exceptions, primary neurons do not divide (Fishel *et al.*, 2007), and therefore it is not possible to generate stably transfected neuronal lines (Zeitelhofer *et al.*, 2009). They can with difficulty be transiently transfected or transduced, but this is harder to achieve than in immortalized cell lines, and they are also more vulnerable to transfection-induced toxicity and cell death.

HEK293T cells were selected for initial study: they are a widely used and easy to transfect cell line, and the MCU gene is highly expressed in the kidney (Mallilankaraman *et al.*, 2012a), making these kidney derived cells appropriate for the study of MCU function. In this project, the properties of the MCU were investigated through the creation of a stable MCU knockdown cell line in HEK293T cells, created through the lipofection of HEK293T cells with shRNA constructs. Mitochondrial and cytosolic $[Ca^{2+}]$, at rest and under stimulation, mitochondrial morphology and membrane potential, oxygen consumption, cell growth and cell death were then investigated.

Methods

Tissue culture

Tissue culture of HEK293T cells was carried out as described elsewhere (Chapter 3, p93) in this thesis.

Transient Fugene Transfection

Transient Fugene transfections were carried out as described elsewhere (Chapter 3, p94) in this thesis. The shRNA constructs used were obtained from OpenBioSystems, and the sequences were as follows:

Identified in text:	OpenBioSystems Nomenclature:	Sequence (mature antisense):	Target	GC Content
#58	V3LHS_410058	TTTCATACACAATGATCCC	3' UTR	36.8%
#62	V3LHS_370862	TGAGTGGAAGTACAGCG	ORF	52.6%
#86	V2LHS_37186	GACAATATTCCTAAGCCC	ORF	52.6%

Table 4: identities, sequences and details of the shRNA constructs used to create transient knockdown of MCU.

Constructs were received as bacterial stabs, and were amplified by the Central Lab facility at UCL, run (at the time of use) by Mary Rahman.

Stable Transfection

HEK 293T cells were transfected using Fugene transfection reagent, as described in Chapter 3. However, 24 hours after transfection cells were split at low confluency into 10cm plates; this and all subsequent steps were simultaneously done with cells which had not been transfected. After another 48 hours, media was removed and replaced with selection media (DMEM + 10% v/v FBS + 1µg/µl puromycin). Once all non-transfected cells had died (approximately 5-7 days after the addition of selection media), single colonies were picked and grown in 96 well plates, and numbered according to the order in which they were picked. Once confluent in a 96 well plate, they were transferred to and grown in 6 well plates. Cells were maintained in selection media until freezing (3-6 passages), and then in DMEM + 10% v/v FBS only; cells were reselected with puromycin every 10-20 passages to ensure the population was still transfected.

Protein sample collection

Protein samples were collected from cells grown in 6 well plates: tissue culture media was removed from cells and they were rinsed gently with PBS. 100µl of RIPA buffer (150mM NaCl, 0.5% (v/v) sodium deoxycholic acid, 0.1% (v/v) SDS, 1% (v/v) Triton X-100, 50mM Tris pH 8.0, 1mM PMSF) were added per well and solubilised cells were collected using a rubber spatula; this was then transferred to an Eppendorf (on ice) and spun at 13200g for 10 minutes at 4°C, then the protein containing supernatant was removed and stored, and the pellet discarded. Samples were stored at -20°C until use.

Western blot

Protein samples were quantified using a Qiagen BCA protein quantification kit according to manufacturer's instructions. Samples were prepared with loading buffer and boiled as appropriate per antibody (for anti-MCU and anti-MCUB antibodies this was for 5 minutes at 100°C, for the oxphos cocktail antibody this was for 5 minutes at 55°C). 10% NuPAGE gels were loaded with 15-50µg (usually 30µg) protein per well and run at 120V in MES running buffer until sufficient separation was achieved. Blotting pads were pre-soaked in transfer buffer, and PVDF membranes were cut to size, activated in methanol, and then soaked in transfer buffer. Transfer apparatus was then assembled, and gels were transferred onto a PVDF membrane using a semi-dry transfer at 20V; protein transfer was checked with Ponceau-S, and then membranes were blocked for one hour at room temperature in PBS-Tween containing 5% (w/v) milk. Primary antibodies were applied overnight at 4°C, at appropriate dilutions (see Materials); membranes were then washed 3X for 5 minutes each with PBS-Tween before application of a suitable horseradish peroxidase-conjugated secondary antibody for 1 hour at room temperature in PBS-Tween and 5% (w/v) milk. Membranes were washed 3X for 5 minutes each with PBS-Tween, then imaged on a BioRAD ChemiDoc system using BioRAD ECL. Where a loading control was necessary, membranes were then further washed 3X for 5 minutes each with PBS-Tween before repeating the primary and secondary antibody steps with an appropriate loading control (usually beta-actin). Images were analysed using ImageJ, and relative intensities were normalized to loading controls.

Aequorin assays

Aequorin assays were carried out as detailed elsewhere (Chapter 3, p95) in this thesis.

Fluo4 Assays

Responses to drugs were also assessed by measuring cytosolic $[Ca^{2+}]$ by the Fluo4 fluorescent dye. Cells were plated in an opaque black 96 well plate at 50 000 cells/well. 30 minutes prior to assay, cells were loaded with 5 μ M Fluo4-AM with 0.002% (v/v) pluronic acid and 1.4mM probenecid in Krebs buffer at 37°C, and drug concentrations as specified in results; cells were then washed and the buffer replaced with Krebs buffer. Fluorescence was measured with a BMG Labtech Fluostar Optima plate reader; after 10 seconds baseline measurement, 100 μ M ATP was injected, followed by 2 μ M ionomycin after a further 20 seconds. Measurements were calibrated by subtracting background counts, and then using the equation: $[Ca^{2+}] = Kd \times (F/F_{max} - 1/Rf)/(1 - F/F_{max})$, where the Kd is 350nM, Fmax is maximum fluorescence (post ionomycin addition) and Rf is 100 (Maravall *et al.*, 2000).

Respirometry: Oroboros

Oxygen consumption rates were measured using an Oroboros Oxygraph-2K system. Confluent cells (grown in 10cm plates for 48 hours prior to assay) were trypsinized, counted, and diluted to 1 million cells/ml in DMEM/HEPES (as described in Chapter 3). Prior to assay, electrode air calibration was performed were calibrated with DMEM/HEPES, as suggested by manufacturer's protocol. 2ml of cell suspension were added to each chamber, and the O2 flow signal allowed to stabilise to the routine respiration rate. Drugs were added to the chambers using Hamilton syringes at the following concentrations and order: histamine (100 μ M, to one chamber only), oligomycin (2.5 μ M), FCCP (titrated 1 μ l at a time from 1mM stock, to produce maximal respiratory capacity), and antimycin A (2.5 μ M). Data were then extracted and analysed using O2K cell analysis template, in order to give oxygen consumption per unit cells. For the galactose experiments, cells were grown in galactose media (DMEM powder (8.3g/L), pyruvate (1mM), galactose (5.5mM), glutamax, sodium bicarbonate (44mM), FBS (10% v/v), penicillin/streptomycin (1% v/v)), for a minimum of two weeks prior to measurement, and galactose media was used throughout the experiment (to calibrate the chambers, resuspend the cells).

ImageXpress - measurement of mitochondrial membrane potential

Cells were imaged on a Molecular Devices ImageXpress Micro-XL. Cells were plated 24 hours before assay, and loaded for 30 minutes before assay with 30nM TMRM and 5 μ g/ml Hoechst in Krebs buffer at 37°C. Steady state TMRM intensities were measured for 20

minutes before the addition of 5 μ M FCCP to all wells. The mean cell integrated intensity of TMRM was calculated for each well over the time course, using the MetaXpress High Content Image Acquisition and Analysis software, and averaged for each cell type.

ImageXpress – measurement of transfection efficiency and cell death

Cells were imaged on a Molecular Devices ImageXpress Micro-XL. Cells were transfected 48 hours before assay with cDNA for red fluorescent protein (RFP), as a marker of successful transfection, and loaded for 15 minutes before assay with Sytox Green (40nM), a marker of cell death and 5 μ g/ml Hoechst (to mark total cell number) in recording buffer at 37°C. Images were taken using a 20X objective, and excitation wavelengths 377nm (Hoechst), 562nm (RFP) and 462 nm (Sytox Green). MicroXpress High Content Image Acquisition and Analysis software was used to analyse the images: multi-wavelength cell scoring was used to count the number of cells positive for each wavelength, and percentages were made of cell death (Sytox Green positive cells divided by total cells) and of transfection efficiency (RFP positive cells divided by total cells). In all transfection methods, non-transfected cells were used as controls; % cell death in non-transfected cells was subtracted from % cell death in transfected cells, to give the % cell death caused specifically by transfection.

ImageXpress – measurement of thapsigargin induced cell death

Cells were plated into a 96 well plate at a density of 10000 cells/well. 24 hours after plating, media was removed and replaced with either DMEM + DMSO or DMEM + thapsigargin (1 μ M) for half of the cells in the plate (48 hour treatment). After a further 24 hours, media was removed and replaced with either DMEM + DMSO or DMEM + thapsigargin (1 μ M) for the other half of the plate (24 hour treatment). After another 24 hours, cells were imaged using the Molecular Devices ImageXpress XL: cells were loaded for 15 minutes before assay with Sytox Green (40nM), and 5 μ g/ml Hoechst in recording buffer at 37°C. Images were taken using a 20X objective, and excitation wavelengths 377nm (Hoechst), and 462 nm (Sytox Green). MicroXpress High Content Image Acquisition and Analysis software was used to analyse the images: multi-wavelength cell scoring was used to count the number of cells positive for each wavelength, and a percentage was made of Sytox Green positive cells divided by total cells to indicate % cell death.

Mitochondrial morphology

Cells were plated on glass coverslips (22mm) 24 hours in advance of imaging, at a density of 1 million cells/coverslip. 30 minutes prior to imaging, cells were loaded in recording buffer with TMRM (25nM) and Hoechst (5 μ g/ml). Cells were imaged on a Zeiss 700 LSM using a 63X oil objective, and single images were taken. These images were visually scored, and each cell was awarded a score of 1-3, using the following criteria: for cells in which all of the mitochondria were fragmented, a score of 1 was given. For cells in which all of the mitochondria were fused, a score of 3 was given, and for cells in which some mitochondria were fragmented, and some were fused, a score of 2 was given. Images were compared to other images of fused and fragmented mitochondria (see for example Logan et. al., 2013, Figure 4) to identify which score was appropriate.

4mtGCaMP6m experiments

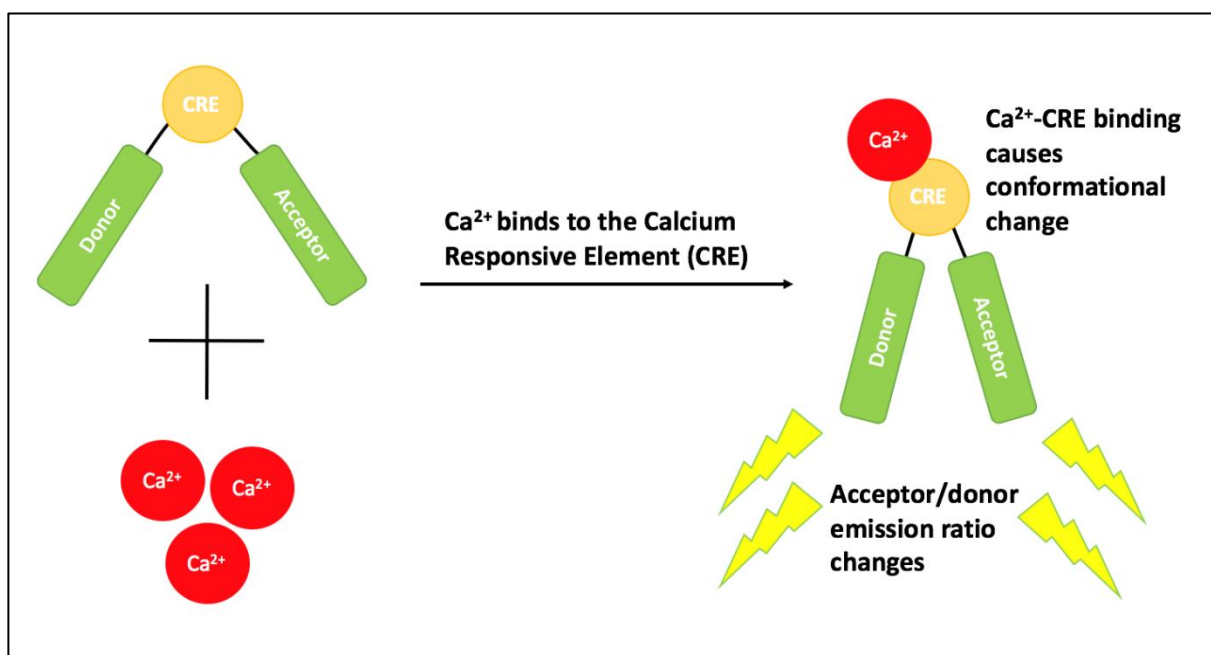


Figure 4.0: A simplified mechanism of 4mtGCaMP6m fluorescence. A donor and acceptor are separated by a Ca²⁺ responsive element (CRE). Ca²⁺ binding to CRE causes conformational change and alters the FRET efficiency, leading to a change in the acceptor/donor emission ratio (Hill et al., 2014).

48 hours prior to imaging, cells were transiently transfected with mitochondrial targeted 4mtGCaMP6m cDNA (Logan et al., 2014) using Fugene (as described in Chapter 3). 24 hours after transfection, the cells were plated onto glass coverslips (22mm) at a density of 1

million cells/cover slip. They were imaged using an Olympus TH4-200 microscope, controlled using Metafluor software, and using a 20X air objective. Cells were imaged in recording buffer. GCaMP was excited at 410nm and 480nm and images were collected every 5 seconds. A baseline was recorded for 30 seconds, followed by the addition of ionomycin (2 μ M) and imaging for a further 60 seconds. The background was subtracted from both wavelengths, and regions of interest drawn around cells showing fluorescence. A ratio was made of the 480:410 fluorescence intensity (see Figure 4.0), and this was calibrated into a [Ca²⁺] using the equation:

$$[\text{Ca}^{2+}] = Kd \times (F/F_{\text{max}} - 1/Rf) / (1 - F/F_{\text{max}})$$

Where Kd is 167, F is fluorescence value, and Fmax is the maximum fluorescence value in the time course. These data were then averaged and significance tested by one-way ANOVA.

Growth assay

HEK293T cells were plated at a density of 5000 cells/well of a 96 well plate in DMEM. 4 plates were prepared per experiment. After 24 hours the growth medium was replaced with fresh DMEM, and simultaneously, one plate was fixed with paraformaldehyde (PFA) to give a 0-hour time point. 24 hours later, another plate was fixed (24 hour timepoint), and this was repeated at 48 and 72 hours after medium change. To fix the cells, 4% (v/v) paraformaldehyde was prepared in PBS. DMEM was removed from the cells, and they were gently rinsed in PBS, which was removed and replaced with 100 μ l of 4% (v/v) PFA per well. This was incubated for 30 minutes at room temperature before being removed and replaced with PBS containing Hoechst (5 μ g/ml). This was incubated for 10 minutes at room temperature, after which the cells were rinsed 3X with PBS, and stored in PBS at 4 $^{\circ}$ C until imaged. Plates were imaged using the Molecular Devices ImageXpress XL, using a 10X objective and Ex/Em 377/447nm. 16 images were taken per well, to ensure that the entire surface area was imaged to give an accurate total cell count. MicroXpress High Content Image Acquisition and Analysis software was used to analyse the images by creating a specification of nuclei size and intensity, in order to ensure recognition of all nuclei and avoid double counting. These data were then averaged and tested for significance by one-way ANOVA.

Fluorescence activated cell sorting (FACS)

Cells were plated into a 24 well plate 48 hours prior to assay. Cells were incubated with either DMSO or 1 μ M A23187 (a Ca²⁺ ionophore) in DMEM (no FBS) for 12 hours overnight. After incubation, media was removed and kept, and cells were trypsinized. Trypsin was inactivated with DMEM + FBS, and the cells triturated and added to the previously removed media. Control samples were run on an Accuri C-Flow Plus FACS machine with no dye in order to gate the whole cell population and exclude debris; this was done by measuring forward scattering versus side scattering. Control samples were then run with 1 μ g/ml propidium iodide (PI) to determine where to establish the division between the live and dead cell populations. Samples were then loaded with PI and run until 5000 events occurred within the gate.

Immunocytochemistry

DIV 7 primary neuronal cells grown in 96 well plates were fixed with 4% (v/v) paraformaldehyde in PBS and then permeabilized for 5 minutes with TritonX (0.2% v/v). Blocking was carried out in PBS + 3% (w/v) BSA for 1 hour at 25°C and then incubated at 4°C overnight with anti-MAP2 primary antibody (1 in 2000). Cells were then washed 3X with PBS, and incubated with a 488 conjugated donkey anti-mouse antibody in PBS + 3% (w/v) BSA (1 in 4000) for 3 hours at 25°C. Cells were then washed 3X with PBS, and then incubated with Hoechst (5 μ g/ml) for 5 minutes. Cells were again washed with PBS and then stored at 4°C. Primary and secondary antibody specificity was ensured by inclusion of both no primary, and no secondary antibody controls. To quantify staining, cells were imaged on a Molecular Devices ImageXpress MicroXL, using excitation/emission 377/460nm for Hoechst and 472/520nm for MAP2 staining, and data were analysed using the multiwavelength cell scoring application on MetaXpress software.

Lipofectamine LTX transfection

Neurons were prepared as described in Chapter 2 of this thesis, and grown in 96 well plates. Cells were transfected at DIV5. To prepare the transfection mix, DNA (4 μ g per well of a 6 well plate) was added to Optimem (500 μ l/well) and flicked to mix. Lipofectamine Plus reagent (4 μ l/well) was then added and gently mixed; this was then incubated at room temperature for 5 minutes. Lipofectamine LTX reagent (4 μ l/well) was then added and flicked to mix; this was then incubated at room temperature for 5 minutes, during which

time the media on the cells was changed to Neurobasal (Glutamax and B27 only). After incubation the transfection mix was added dropwise to the cells and incubated overnight at 37°C, 5% CO₂, after which the media was removed and replaced. Transfection efficiency was measured 48 hours after transfection.

Calcium phosphate transfection

Neurons were prepared as described in Chapter 2 of this thesis, and grown in 96 well plates. Cells were transfected at DIV5. 48 hours prior to assay, the transfection mixture was prepared: CaCl₂ (10µl of 2.5M stock) was mixed with DNA (8µg) and mQH₂O (100µl), and then 2X HBS (100µl, 280mM NaCl, 1.5mM Na₂HPO₄, 50mM HEPES, pH 7.12) was added by vortexing, and the mixture was incubated for 10 minutes at room temperature, during which time the cell media was removed and replaced with fresh media. The transfection mixture was then added dropwise onto cells, and incubated overnight. Media was removed, cells were washed with PBS, and fresh media was added. Measurements given are per well of a 6 well plate.

Viafect transfection

Neurons were prepared as described in Chapter 2 of this thesis, and grown in 96 well plates. Cells were transfected at DIV5. 48 hours prior to assay, the transfection mixture was prepared: DNA:Viafect in a ratio of 1:3. These were mixed together and incubated at room temperature for 25 minutes, then added dropwise directly onto cells (at 10µl/well of a 96 well plate); Viafect does not require removal of serum or media replacement (before or after transfection). Cells were then incubated at 37°C/5% CO₂ until assay.

Nucleofection

Neurons were prepared as described in Chapter 2 of this thesis, and grown in 96 well plates. Cells were transfected at DIV5. Primary cortical neurons were prepared as described elsewhere in this thesis (Chapter 2, p67). 96 well plates which had been coated with polylysine were pre-incubated (containing 100µl neurobasal medium/well) in a 37°C/5% CO₂ incubator, as was additional neurobasal medium. Prior to plating, cells were nucleofected with RFP cDNA using a Lonza nucleofector: 5x10⁶ cells per sample were centrifuged at 500 g for 5 minutes at room temperature. The supernatant was discarded, and the pellet was resuspended in 100µl room temperature Nucleofector Solution per

sample. This cell suspension was then combined with 2µg of DNA, and the mixture was transferred into a Nucleofector cuvette. On the nucleofector itself, the program O-003 (for primary rat neurons) was selected, and the cuvette was inserted into the Nucleofector, and the program run. When the program finished, the cuvette was removed, and 500µl of the pre-incubated neurobasal medium was added to the cuvette. This was then transferred directly into the prepared 96 well plate, and the cells incubated at 37°C/5% CO₂. After 4 hours the medium was carefully replaced with fresh neurobasal medium in order to remove cell debris, and the medium was replaced again after a further 24 hours. Cells were imaged to assess % transfection and % cell death 48 hours after nucleofection.

Endoporter transfection

Neurons were prepared as described in Chapter 2 of this thesis, and grown in 96 well plates. Cells were transfected at DIV5. 48 hours prior to assay, the media was completely removed and replaced with fresh neurobasal. The endoporter was supplied with a fluorescent tag; this was used at the recommended concentration (5µM). In 500µl of neurobasal medium, 2.5µl of the fluorescent tag were added, and mixed, followed by 3µl of endoporter (again as recommended), and mixed again. This was then added dropwise to the cells (at 50µl per well of a 96 well plate). Cells were imaged to assess % transfection and % cell death 48 hours after transfection.

Morpholino

Neurons were prepared as described in Chapter 2 of this thesis, and grown in 96 well plates. Cells were treated at DIV5. A 500µM morpholino stock was kept at RT. 2X solutions were prepared in Neurobasal medium (see Figure 4.10 for concentration range used), and 50% of the media of the neurons to be treated was removed, and replaced with an equal volume of 2X morpholino. After 24 hours, this media was removed and replaced, and after another 24 hours cells were assayed. The sequence of the morpholino used was GTCCACGTCATTAATGTTCTTCAGG, which targets the mouse MICU1 gene. The morpholino was a kind gift of Dr Haiyan Zhou at the Institute of Child Health, and was of her own design (ordered from Gene Tools).

Results

Transient transfections with MCU targeted shRNA

HEK293T cells were transiently transfected with MCU shRNA knockdown constructs to investigate the effect of reduced levels of MCU protein.

Firstly, the effect of the shRNA constructs on MCU protein level was assessed by Western blot. As shown in Figure 4.1A, no significant difference was found in the MCU protein level between control cells (transfected with scrambled shRNA vector, or the vector alone pGIPZ) and MCU-knockdown cells. This suggests the transfection efficiency of the knockdown construct may be too low to be able to see its functional effects. To verify this, these cells were transiently transfected with either mitochondrial-targeted or cytosolic aequorin in order to assess whether there had been any functional consequence of the constructs on mitochondrial Ca^{2+} uptake. Cells were transfected with a mitochondrial-targeted or cytosolic aequorin construct and assayed in a plate reader using stimulation with 100 μM ATP to generate a Ca^{2+} signal, which was calibrated into $[\text{Ca}^{2+}]$ using a total luminescence value provided by the later addition of digitonin (not shown, see Methods). As shown in Figure 4.1C and 4.1D, there was no difference in either mitochondrial or cytosolic Ca^{2+} signal, confirming the lack of knockdown.

In transient transfections, transgenes are only expressed for up to 72 hours after transfection, therefore if the protein turnover for MCU is longer than this, a transient transfection may not impact the cell's current proteome. Therefore, it was decided to make a stable monoclonal MCU-knockdown cell line in order to produce a significant knockdown of MCU protein. In stable cell lines, the transgene is continually expressed, and therefore will affect the cell's protein population. Knockdown construct #58 was chosen for the production of a stable cell line, as it had given the lowest level of MCU protein, despite not reaching significance.

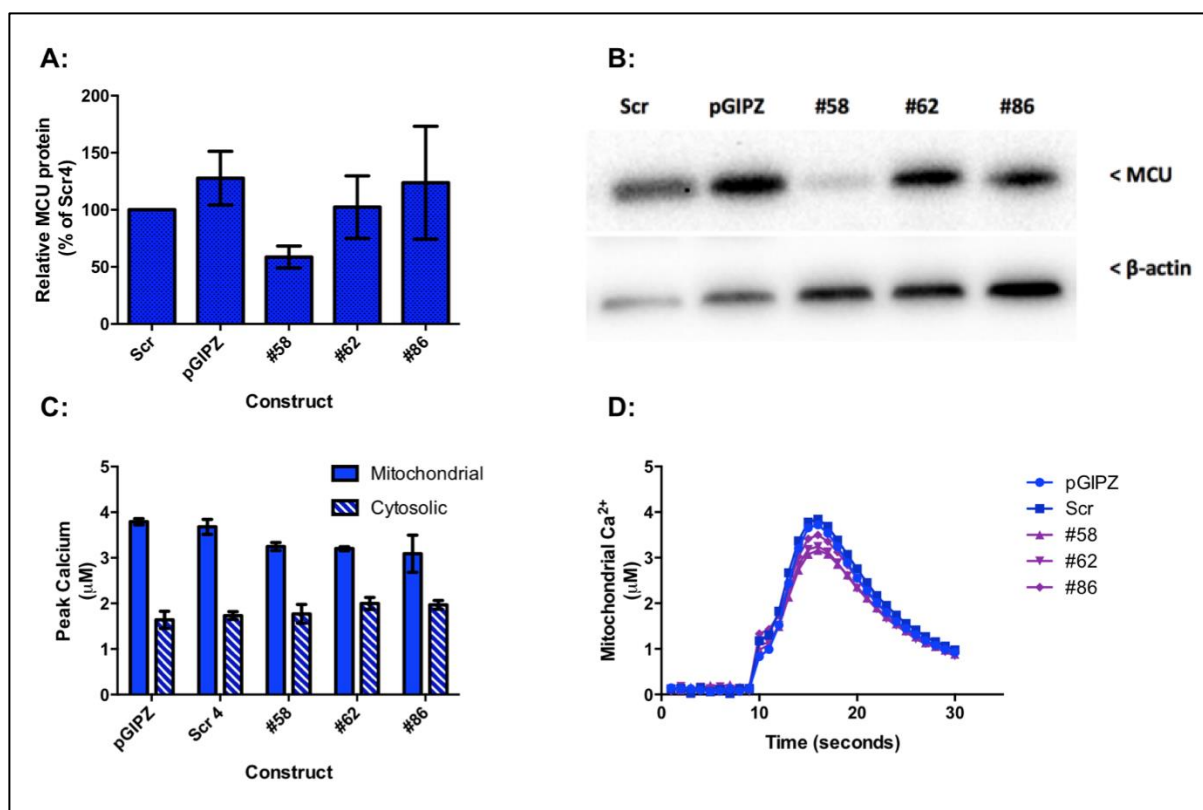


Figure 4.1: HEK293T cells transiently transfected with MCU knockdown constructs do not show different MCU protein levels, or altered mitochondrial or cytosolic Ca^{2+} levels. A: MCU knockdown construct #58 is most effective at reducing MCU protein levels compared to scrambled and pGIPZ controls; no significant difference between any conditions. N of 3. B: a representative Western blot of the transient transfections. C: peak Ca^{2+} concentration reached after stimulation with 100μ M ATP. Transiently transfected cells were not significantly different to scrambled or pGIPZ controls. N of 3. D: representative trace of an ATP-induced Ca^{2+} response. Significance was assessed by one-way ANOVA. Error bars are SEM.

Creating and characterizing a stable MCU knockdown cell line

Next, cell lines stably expressing MCU shRNA knockdown were established using construct #58, as described in the methods, and monoclonal cells selected, also as described in the methods. Monoclonal cells are a group of cells which have all been replicated from a single common ancestor, meaning they are genetically identical to each other, and genetically distinct to monoclonal cells derived from a different common ancestor; therefore it is of use to test more than one monoclonal cell in case their genetic variation causes functional variation. MCU protein levels of several control (scr) and knockdown (KD) monoclonal cells were assessed by Western blot (see Figure 4.2A and 4.2B), and it was found that three MCU-knockdown

monoclonal – KD7, KD33 and KD36 – showed significantly lower MCU expression than scrambled controls and these were therefore selected for further testing.

It was recently shown that altered MCU complex component expression can result in alterations to the protein levels of other complex components ((Kamer and Mootha, 2014), therefore protein levels of MCUB were also investigated in the MCU-knockdown monoclonal (Figure 4.2C and 4.2D), and it was found that MCUB protein levels were not significantly affected in any of the monoclonal; knockdown resulted in a change in the MCU:MCUB ratio of one order of magnitude: the average ratio for the SCR clones being 1.09, and for the MCU KD clones being 0.11.

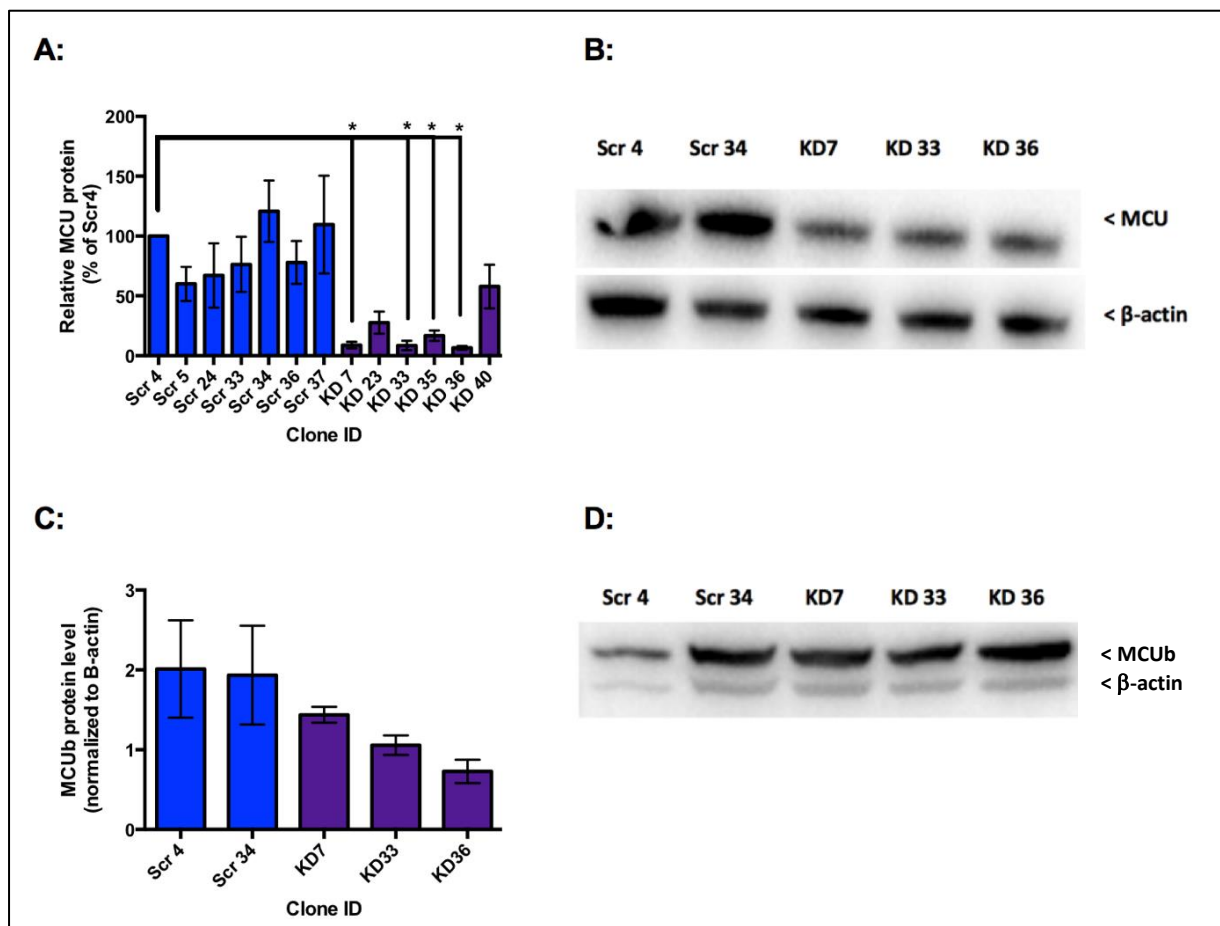


Figure 4.2: MCU protein levels in HEK293T cells can be significantly reduced by stable transfection. A: Relative levels of MCU protein in monoclonal of HEK293T cells stably transfected with construct #58. * denotes significant difference in comparison to Scr 4 control as assessed by one-way ANOVA, $p < 0.05$. KD 7, KD 33, KD 35, and KD 36 were all also significantly different to Scr 34 control, $p < 0.05$. N of 3. B: a representative Western blot of the clones which were chosen for further study. C; relative protein levels of MCUB in stably transfected MCU knockdown cells and scrambled controls. N of 3. D: a representative Western blot of MCUB protein levels. Error bars are SEM.

The effect of MCU knockdown in stable clones was then explored. Initially, the effect of MCU knockdown on Ca^{2+} signalling was investigated: cells were again transiently transfected with mitochondrial-targeted or cytosolic aequorin construct and their response to $100\mu\text{M}$ ATP measured. MCU knockdown significantly reduced mitochondrial Ca^{2+} peak concentration: all three knockdown clones had significantly lower peak mitochondrial Ca^{2+} concentrations than the two scrambled controls, with maximum $[\text{Ca}^{2+}]$ of 43-55% of control (see Figure 4.3), whereas cytosolic Ca^{2+} peak concentrations were unaffected. Therefore, MCU knockdown specifically reduces mitochondrial Ca^{2+} uptake.

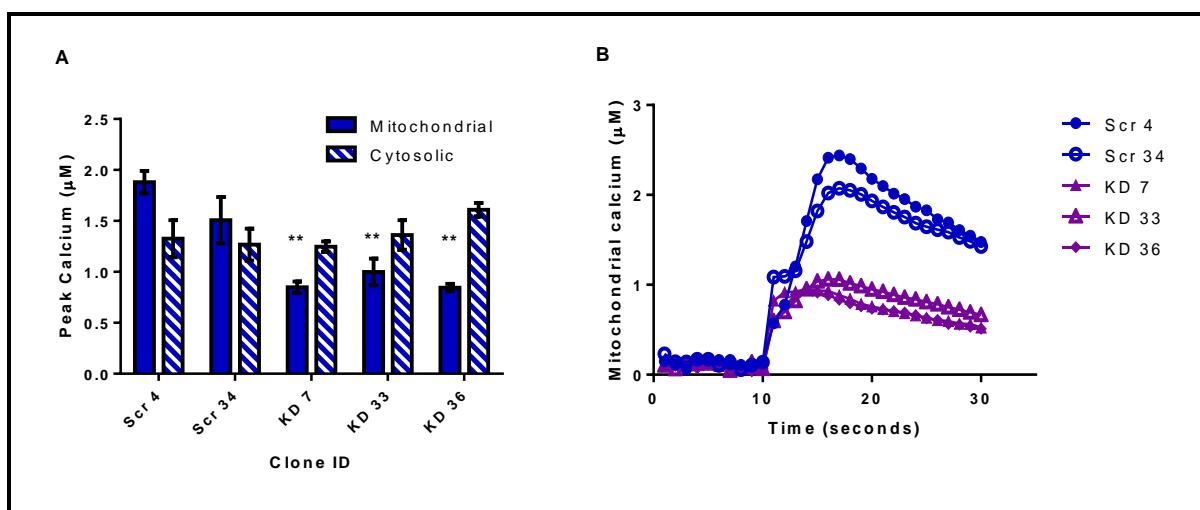


Figure 4.3: HEK293T cells stably transfected with MCU knockdown constructs show significantly reduced mitochondrial, but not cytosolic agonist-induced Ca^{2+} concentration in comparison to controls. A: peak Ca^{2+} concentration reached after stimulation with $100\mu\text{M}$ ATP. All three knockdown clones (KD 7, 33, 36) had significantly lower mitochondrial Ca^{2+} concentrations in comparison to both scrambled controls (p value <0.001), whereas cytosolic Ca^{2+} concentrations were unchanged. N of 3. B: representative trace of an ATP-induced Ca^{2+} response. Significance was assessed by one-way ANOVA, * denotes significance. ** = p value <0.01 . Error bars are SEM.

Next, mitochondrial membrane potential and morphology were examined. Mitochondrial Ca^{2+} uptake is dependent on $\Delta\Psi_m$, so it is an important parameter to consider: it was found that MCU knockdown had no effect on membrane potential (Figure 4.4A), showing that the reduced mitochondrial Ca^{2+} uptake demonstrated in Figure 2 was not due to reduced mitochondrial membrane potential. Mitochondrial morphology was scored per cell, as all fragmented (1), all fused (3), or a mixture of both (3) (see Figure 4.4C). MCU knockdown

had no effect on morphology (Figure 4.4B), there was no difference in mitochondria morphology between the scrambled and MCU knockdown cells.

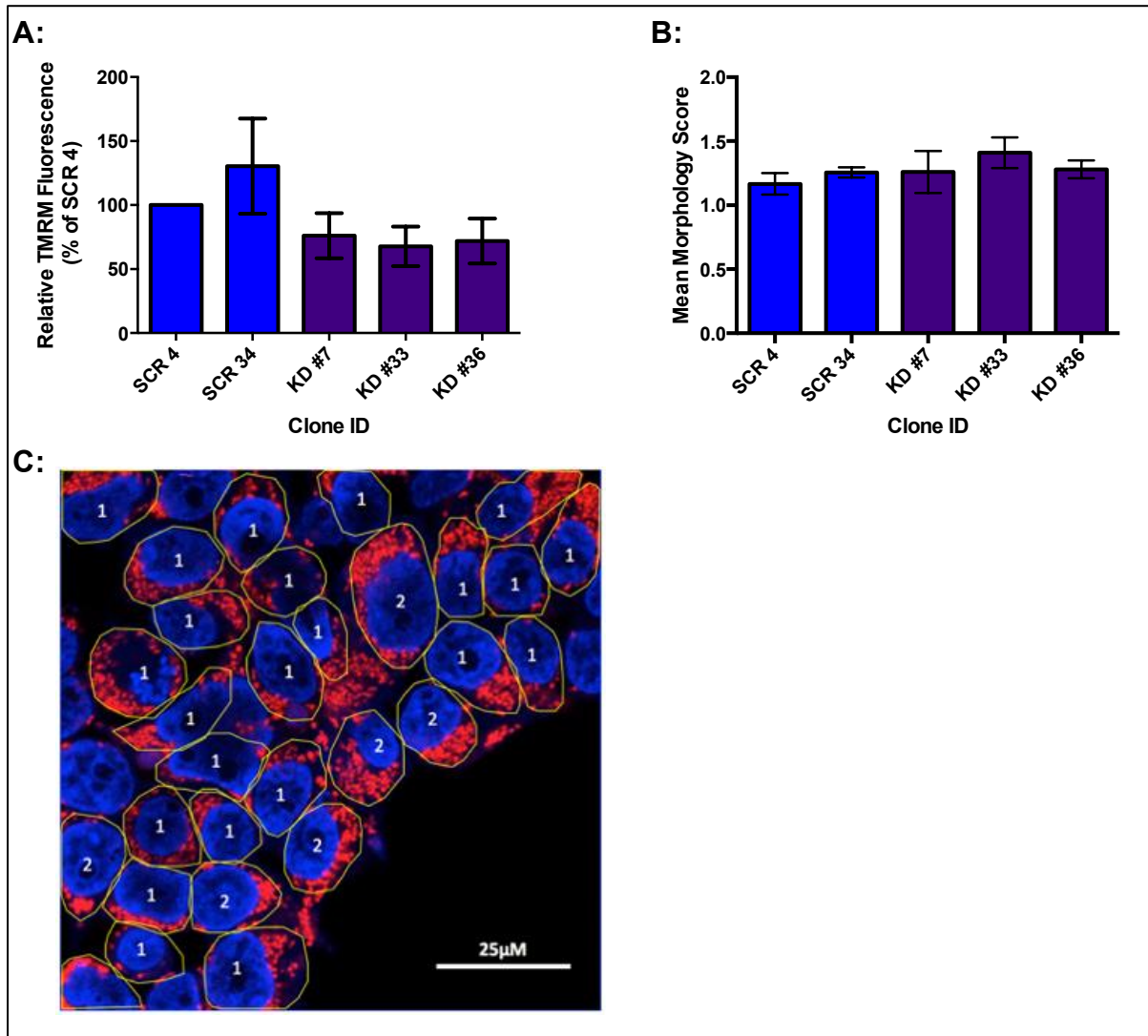


Figure 4.4: Mitochondrial membrane potential and morphology were not affected. A: Mitochondrial membrane potential was not affected by MCU knockdown. N of 4. B: Mitochondrial morphology was not affected by MCU knockdown. Each cell was scored either 1 (all fragmented), 2 (some fragmented, some fused) or 3 (all fused) and an average taken for each clone of ~60 cells from a total of 3 images per clone (n of 3). C: Representative image to demonstrate morphology scoring method. Significance was assessed by one-way ANOVA. Error bars are SEM.

Basal mitochondrial $[Ca^{2+}]$ was measured using 4mtGCaMP6m, and basal cytosolic $[Ca^{2+}]$ was measured using the calcium indicator dye Fluo4-AM (Figure 4.5). Basal Ca^{2+} concentrations in MCU knockdown clones were not significantly different from scrambled

clones in either experiment, although basal cytosolic Ca^{2+} concentrations were unusually high in all clones. This shows that MCU knockdown does not result in lower resting mitochondrial $[\text{Ca}^{2+}]$, and that it is only reduces Ca^{2+} uptake when stimulated.

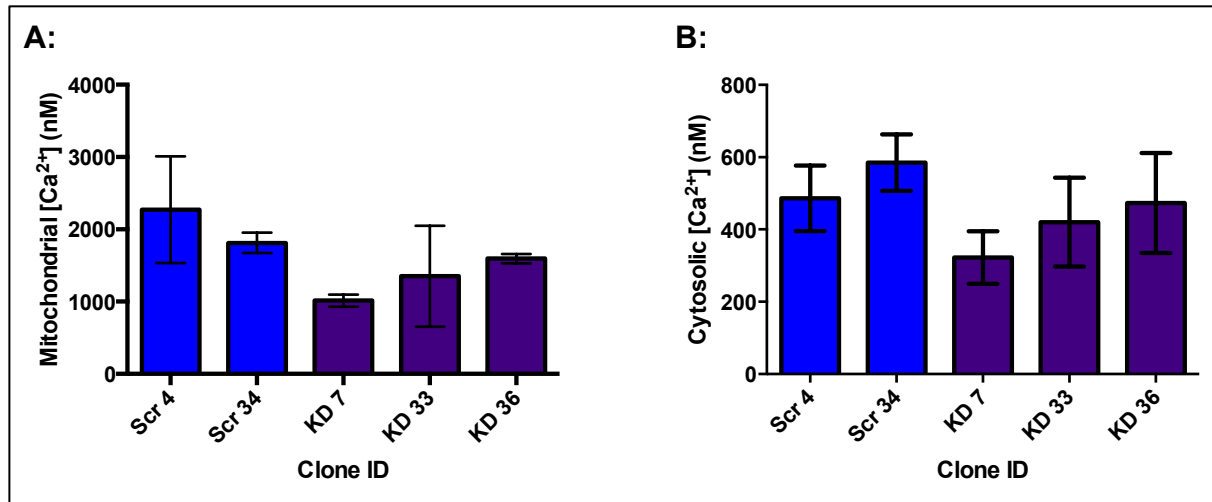


Figure 4.5: Basal mitochondrial and cytosolic $[\text{Ca}^{2+}]$. A: Basal mitochondrial $[\text{Ca}^{2+}]$ measured using GCaMP was not significantly different between control and knockdown cells. N of 3. B: Basal cytosolic $[\text{Ca}^{2+}]$ measured using Fluo4-AM was not significantly different between control and knockdown cells. N of 4. Significance was assessed by one-way ANOVA. Error bars are SEM.

In order to investigate the downstream consequences of MCU KD, Ca^{2+} stimulated respiration was examined in the stable MCU KD clones. Oxygen consumption of control and MCU knockdown cells was assessed in different respiratory states using an Oroboros O2K Oxygraph. Routine (steady state) oxygen consumption was measured prior to any drug addition, once respiration had stabilised (Figure 4.6A and 4.6B). Leak respiration was measured after the addition of oligomycin, an inhibitor of ATP synthase which allows assessment of the rate of proton leak through the membrane (Figure 4.6C and 4.6D); a high leak state is indicative of increased proton leak across the inner mitochondrial membrane, and can be due to a loss of membrane integrity. Maximal electron transfer system (ETS), capacity was measured after the addition of the uncoupler FCCP (Figure 4.6E and 4.6F). It was found that oxygen consumption did not differ significantly between MCU knockdown cells and SCR control cells in any respiratory state, with or without the addition of histamine.

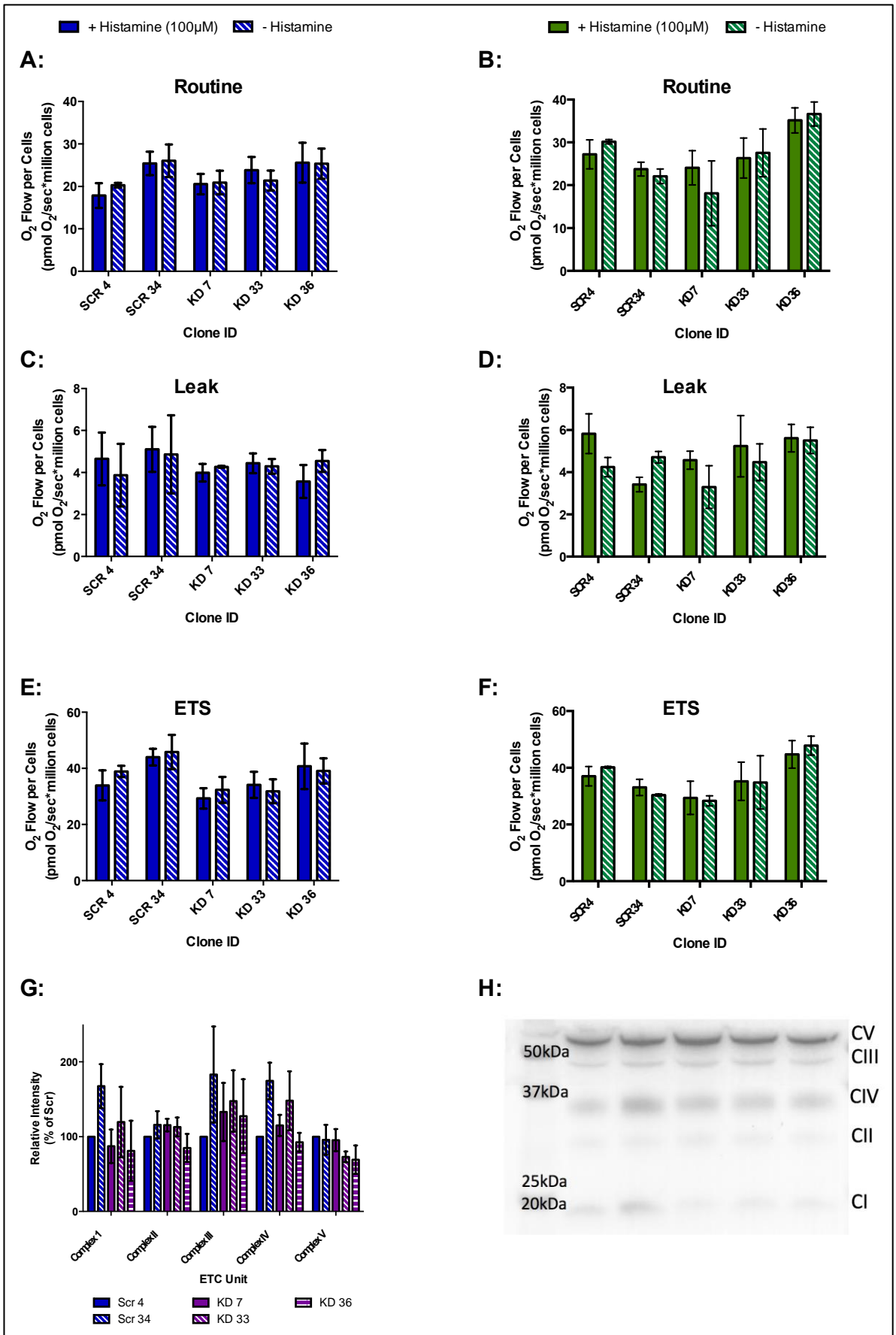


Figure 4.6 (previous page): MCU knockdown does not affect the rate of respiration, or the protein level of electron transport chain protein complexes I-V. Respiration with and without the addition of 100 μ M histamine: Routine respiration in glucose media. B: Routine respiration in galactose media. C: Leak respiration in glucose media. C: Leak respiration in galactose media. D: ETS respiration in glucose media. E: ETS respiration in galactose media. In all conditions, and with both media, O₂ flow does not differ between MCU knockdown cells and SCR controls, and the addition of histamine does not cause any significant differences. G: Relative levels of protein of complexes I-V of the ETC was assessed by Western blot and there were no significant differences between MCU knockdown cells and SCR controls. H: Representative Western blot of ETC complexes. All panels are n of 3 (except H). Significance assessed by one-way ANOVA. Error bars are SEM.

The respirometry experiments were done in both glucose and galactose based media; many cell lines, and those derived from cancer tissues in particular, derive their ATP supply from glycolysis rather than oxidative phosphorylation (Bensinger and Christofk, 2012), and consequently, effects on OXPHOS of modifications to mitochondrial proteins may be harder to see in these models. To overcome this, cells can be grown using galactose rather than glucose, which suppresses glycolysis and shifts the energy dependency toward oxidative phosphorylation (Reitzer *et al.*, 1979; MacVicar and Lane, 2014). However, there were still no significant differences between MCU knockdown cells and SCR controls in any respiratory state. Protein levels of the ETC complexes were also assessed, and there was no detectable difference between samples from SCR control and MCU knockdown cells (Figure 4.6G and H).

Cell growth was also measured: cells were plated at low density in 96 well plates, and cell number was recorded at 0, 24, 48 and 72 hours after a media change (24 hours after plating) in order to monitor the effect of MCU knockdown on growth. There were no differences in the growth rate between MCU knockdown cells and scrambled control cells at any time point (Figure 4.7). In support of this, another experiment, done by Dr Aleck Jones (not shown) demonstrated there were no significant differences in the rate at which the cells progressed through the cell cycle between SCR and KD clones.

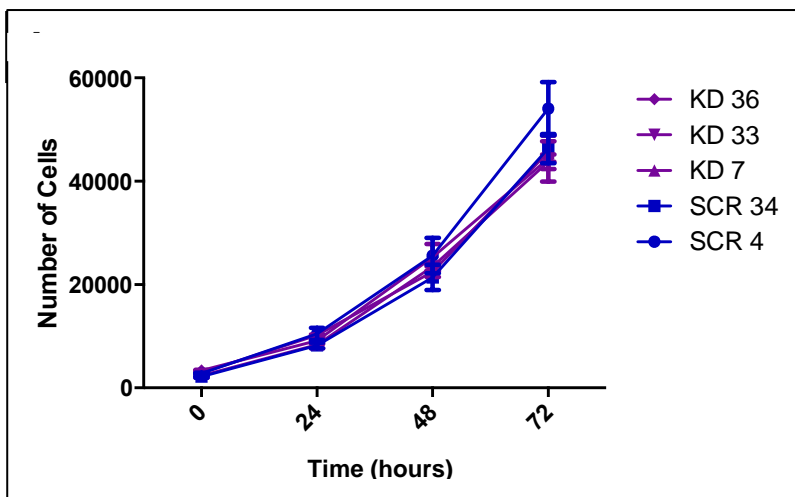


Figure 4.7: Rates of cell growth in SCR and MCU KD cells. A: Medium was changed at 0 hours, and cells were fixed and imaged at 0, 24, 48 and 72 hours, and there were no significant difference in cell number between SCR and KD cells. N of 4. Significance was tested by one-way ANOVA. Error bars are SEM.

Next, cell death was investigated. Firstly, to verify that increased $[Ca^{2+}]$ causes death in these cells, the calcium ionophore A23187 was used to raise intracellular $[Ca^{2+}]$ by enabling Ca^{2+} cations to equilibrate across the cell and mitochondrial membrane (Pressman, 1976), bypassing the MCU. Cell death was significantly increased by the ionophore in all clones treated, and there was no significant difference between responses in scrambled controls and MCU knockdowns (as would be expected), as the Ca^{2+} overload is MCU independent (see Figure 4.8A). This confirms that increased $[Ca^{2+}]$ causes cell death, and that this can be measured by FACS.

Then, cells were tested using thapsigargin (TG), an inhibitor of SERCA which causes Ca^{2+} release from the ER, in order to produce mitochondrial Ca^{2+} overload in an MCU-dependent manner. However, this approach was unsuccessful: after both 24 (Figure 4.8B) and 48 hours (Figure 4.8C) treatment with TG ($1\mu M$), only 1-4% cell death was apparent in both DMSO treated and TG treated cells, suggesting that TG treatment had no effect. TG treatment did not trigger Ca^{2+} dependent cell death, and therefore it was not possible to determine at this time whether MCU knockdown is protective against cell death, when Ca^{2+} is transported into mitochondria by the MCU.

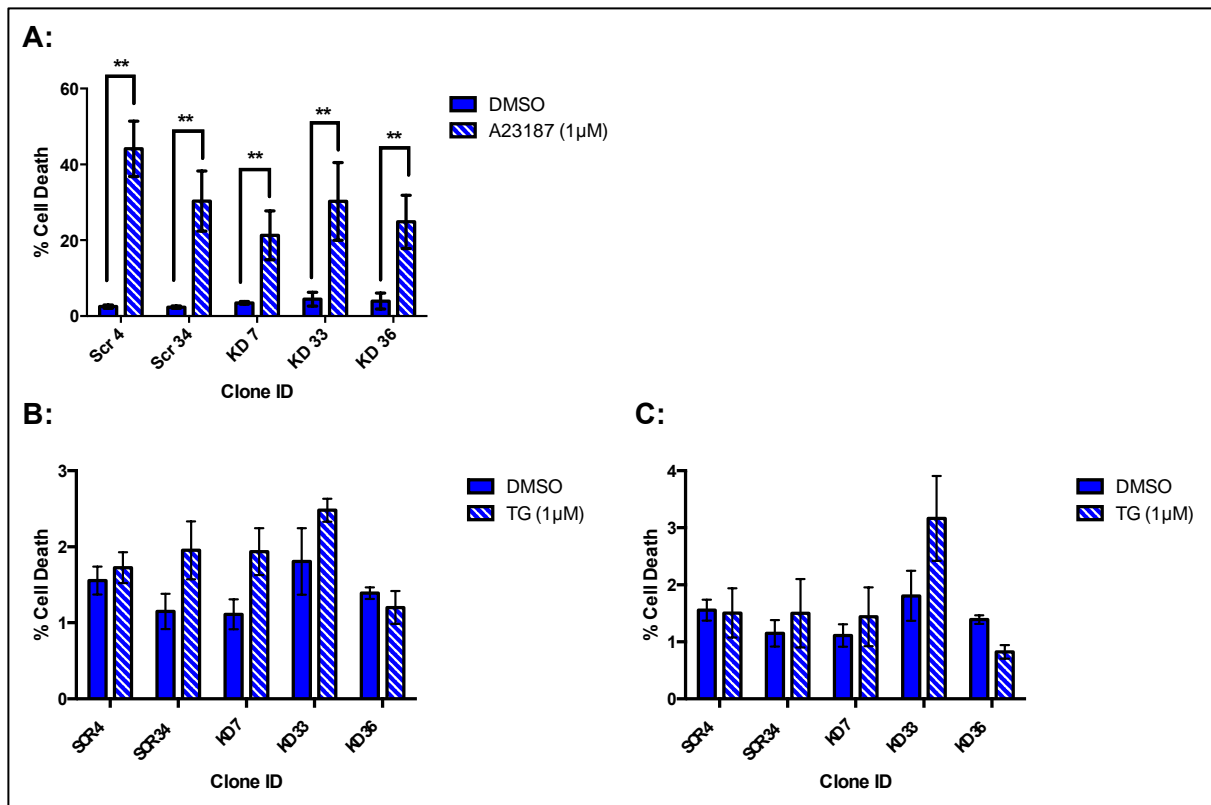


Figure 4.8: An MCU independent Ca^{2+} increase causes Ca^{2+} induced cell death. A: Cells were treated with the Ca^{2+} ionophore A23187 (1µM) for 12 hours overnight, and cells were assayed by FACS, using Propidium Iodide (PI) as a marker of cells death. There is a significant increase in cell death in treated cells compared to untreated cells in all clones; but there is no difference in cell death between MCU knockdown clones and controls, as would be expected. N of 3. B and C: Cells were treated with either DMSO or Thapsigargin (TG, 1µM) for 24 (B) or 48 (C) hours, and cells were imaged using Sytox Green as a marker of cell death, using the Molecular Devices Image Xpress. No significant differences were found between treated and untreated, or SCR and MCU KD cells at either timepoint. Both N of 3, * marks significance as tested by one-way ANOVA, ** = p value < 0.01. Error bars are SEM.

Summary

Overall, transient transfection was shown to be insufficient to investigate the effect of MCU knockdown. In stably transfected HEK293T monoclonal cells, MCU knockdown was shown to significantly reduce stimulated mitochondrial Ca^{2+} levels, without affecting stimulated cytosolic Ca^{2+} concentration; and to have no effect on respiration or on levels of respiratory chain proteins, or cell growth. The effect of MCU knockdown on cell death was not determined.

HEK293Ts are a useful model system for preliminary studies, however they have limitations: as they are an immortalized, cancerous cell lines they are not always representative of how

normal cells would behave. Therefore, it is useful to consider using other model systems, such as primary cells and animal models, in order to generate more physiologically relevant data.

Transfecting primary neurons

It was decided to investigate the role of MCU in primary neuronal cultures, by knocking down MCU expression; Ca^{2+} signalling is especially important in the brain, so MCU is of special interest in this model. In addition to characterizing the effect of MCU knockdown in primary neuronal cultures on general mitochondrial properties, it would be of particular interest to investigate glutamate excitotoxicity and delayed calcium deregulation (DCD, see page 57) in neurons with reduced MCU expression. For this purpose, a method for measuring DCD was developed and optimised (see Appendix 4, Figure A3).

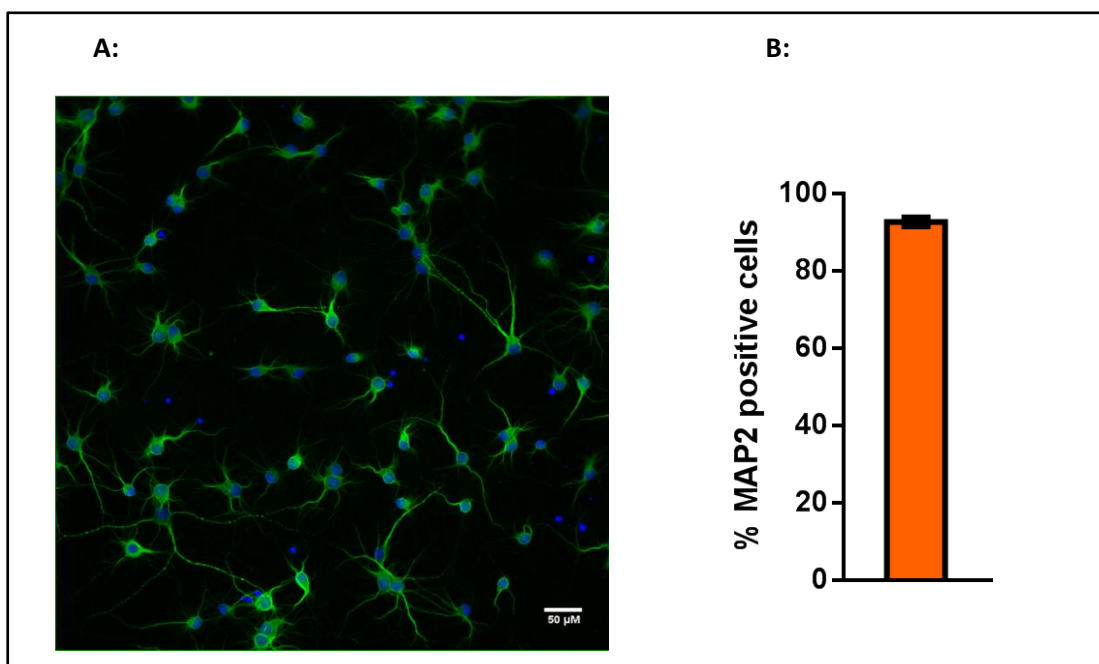


Figure 4.9: 92.6% of cells were neurons. A – cultures stained with Hoechst and MAP2. B – Quantification of staining showed that 92.6% of cells stained with Hoechst were also stained with MAP2. Error bars are SEM.

All transfection conditions were optimised using DIV 5-7 primary cortical neurons from E17 rat embryos. These were used as it is possible to get nearly entirely pure neuronal cultures without the use of cell division inhibitors such as cytarabine (AraC). The percentage of neuronal cells within the cultures was investigated using microtubule associated protein 2 (MAP2) staining; MAP2 is a neuron specific cytoskeletal protein which is not present in astrocytes and glial cells (NCBI Gene, 2015); cultures were on average 92.6% neuronal cells, see Figure 4.9.

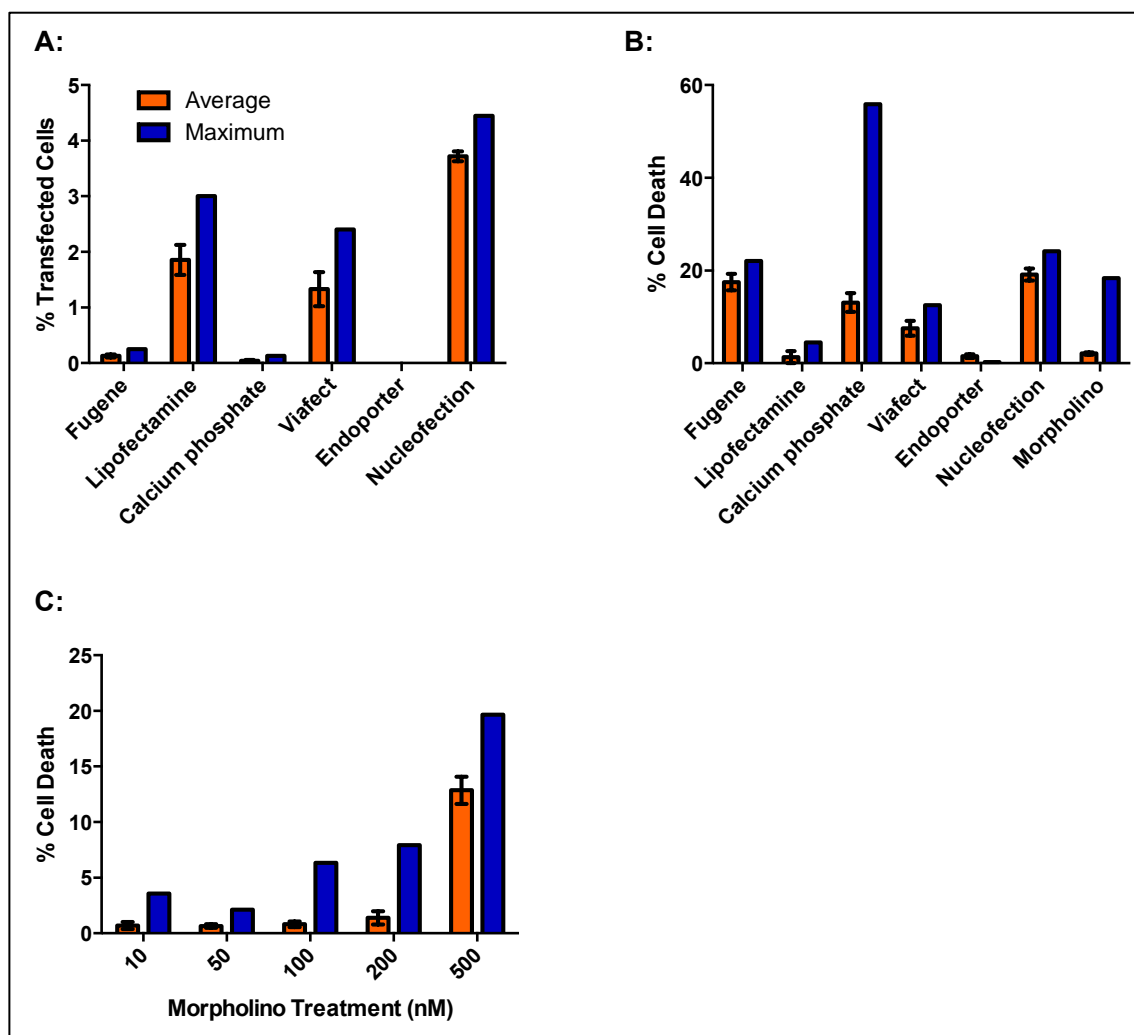


Figure 4.10: Assessment of efficiency and toxicity of different transfection techniques. A: Transfection efficiency using a variety of transfection techniques. B: Quantification of cell death using different transfection techniques. C: Cell death increased proportionately to concentration of morpholino treatment.

As primary cells are more difficult to transfect, a variety of transfection techniques were tried, in order to provide maximum transfection efficiency. To assess efficiency of transfection using different techniques, neurons were transfected with cDNA encoding red fluorescent protein (RFP), using the optimised technique for each transfection method. Transfection efficiency was calculated by measuring the total number of transfected cells as a percentage of total cells, and average efficiencies are shown in Figure 4.10A. The transfection procedures were found to be extremely variable between different experimental repeats, therefore the maximal transfection efficiency found in any experiment is also shown in Figure 4.10A, although this was generally not replicable. It is clear that nucleofection was the most efficient transfection method, however this still only had an average efficiency of 3.8%, and a maximal efficiency of 4.5%. Additionally, all transfection procedures caused considerable cell death (Figure 4.10B); this ranged from 5-60%, with calcium phosphate being the most toxic transfection method, and the endporter the least. Cell death increased with morpholino concentration (Figure 4.10C) and at the manufacturer recommended concentrations (200-500nM) was between 2-20%.

The low transfection levels found with each of these techniques is not sufficient for whole cell-population studies, or for confocal imaging, and as time did not permit further optimization, further studies were not undertaken in primary neuronal cultures.

Discussion

Considering the low level of protein knockdown in transiently transfected HEK293T cells, as demonstrated by Western blot in Figure 4.1A, it is not surprising that there was no significant difference in peak mitochondrial Ca^{2+} levels between MCU knockdown and control cells (Figure 4.1C). Transfection efficiency of HEK 293T cells by Fugene has previously been found to be approximately 60% (data not shown), so it may have been expected that some knockdown would be apparent; in cells transfected with construct #58, there was some visible reduction in protein level, although this was not significant. Knockdown is also dependent on the efficacy of the knockdown constructs, explaining the disparity between the three different constructs. This can depend on factors such as which splice variant (if there are more than one) the shRNA targets, whether the target site has previously been validated, if the construct contains sequences which could trigger premature termination, whether the target site overlaps any regions of single nucleotide polymorphisms (SNPs), amongst others (Moore *et al.*, 2010). These shRNA constructs were ordered from OpenBioSystems (see Methods for details), who do not publish their construct design strategy, however these constructs have not been previously confirmed. An alternative approach to MCU knockdown could be to overexpress MCUB, the dominant negative isoform of MCU (Raffaello *et al.*, 2013), as this would also result in reduced mitochondrial Ca^{2+} uptake, and allow examination of the effects of this on the cell.

Stable transfection was markedly more successful at reducing levels of MCU protein; in Figure 4.2A the levels of MCU protein in clone numbers #7, #33, and #36 were reduced to 6-8% of SCR control.

MCUB protein levels (Figure 4.2C) were not significantly affected by MCU knockdown. MCUB has been shown to form an oligomer with MCU (Raffaello 2013), so it was interesting to investigate whether MCU knockdown would also cause a reduction in MCUB levels, to keep the ratio of MCU:MCUB the same. This did not happen, and the MCU:MCUB ratio changed significantly between the SCR (ratio of 1.09) and MCU KD (ratio of 0.11) clones.

The mitochondrial Ca^{2+} peaks in response to ATP were also significantly reduced, see Figure 4.3; however the peak $[\text{Ca}^{2+}]$ was only reduced to approximately 50% of scrambled control.

This is surprising considering the extent to which the protein level is reduced, as previous work suggests the effects of MCU knockdown increases with longer exposure to genetic modifying agents: it was previously found that in HeLa cells, MCU silencing by siRNA reduced mitochondrial $[Ca^{2+}]$ responses by 75% 72 hours after transfection, but only by 50% after 48 hours (De Stefani *et al.*, 2011). As in these cells, the knockdown is stable, it would be hoped that the functional knockdown would be more complete. This could suggest that the other proteins of the MCU complex (or other mitochondrial proteins) are able to compensate for reduced expression of MCU in order to prevent loss of function; to test this theory it would be interesting to create multiple knockdown cells lines in which MCU and another component could be targeted, in order to see which, if any component causes the compensation for loss of MCU. As the MCUb protein levels did not change with MCU knockdown, this is unlikely to be a compensatory component. It would also be useful to investigate the mRNA levels using quantitative PCR (qPCR), to determine the extent to which the shRNA resulted in degradation of MCU mRNA.

Mitochondrial membrane potential and morphology were not affected by MCU knockdown (Figure 4.4). Membrane potential is an important parameter to check, as mitochondrial Ca^{2+} uptake is dependent on it, therefore it is essential to know that it is unaffected in order to conclude that the reduction in mitochondrial Ca^{2+} uptake is specifically due to MCU knockdown. For absolute verification of this, it would have been useful to measure membrane potential concurrently with Ca^{2+} signals, rather than separately. Mitochondrial morphology changes in response to the cellular environment, and the bioenergetics demands of such conditions. Previous studies have suggested that increased resting mitochondrial $[Ca^{2+}]$ is associated with mitochondrial fragmentation (Logan *et al.*, 2014), however no change was seen with MCU knockdown in this case. This was supported by the finding that there was no change in resting mitochondrial or cytosolic $[Ca^{2+}]$ between SCR and MCU KD cells (Figure 4.5), unlike MICU1 $-/-$ patient fibroblasts, in which mitochondria were fragmented, basal mitochondrial $[Ca^{2+}]$ was higher, and basal cytosolic $[Ca^{2+}]$ was lower than in controls (Logan *et al.*, 2014). However, basal cytosolic Ca^{2+} was unusually high (300-600nM, compared to usual basal concentrations of ~ 100 nM) in all clones, which calls these data into question.

MCU knockdown does not appear to have any effect on routine, leak or ETS respiration states, in either glucose or galactose-based media. Moreover, the relative protein levels of the oxidative phosphorylation complexes were not affected by MCU knockdown (Figure 4.6). It might be expected that altered levels of mitochondrial Ca^{2+} may have some effect on respiration due to the stimulation of the dehydrogenases of the TCA cycle by mitochondrial Ca^{2+} ; this is somewhat supported by findings in the MCU knockout mouse in which basal metabolism was unaltered but there were differences in the phosphorylation and activity of pyruvate dehydrogenase (Pan *et al.*, 2013). This supports the unaltered basal rate seen here. Pyruvate dehydrogenase phosphorylation and activity was not investigated in this cell line; but it would be interesting to study.

The electron transfer system capacity (ETS) (in which an uncoupler is used to dissipate membrane potential in order to induce the maximal rate of respiration by the ETC) was not examined in the knockout mouse. It might be expected that there would be no difference in ETS between control and MCU knockdown: as the membrane potential is dissipated the MCU would cease to function even in control cells, unless there were differences in complex protein levels. Histamine had no measurable effect on respiratory rate in control or MCU-knock down cells. Previously, in MICU1 knockdown cells, low (10 μM) histamine increased respiration, whereas high (100 μM) histamine did not (Mallilankaraman *et al.*, 2012b); as my experiments used 100 μM histamine it is possible some effect might be seen using a lower histamine concentration, although the differences seen by Mallilankaraman *et. al.*, may be an effect of the altered uptake curve of MICU1, and therefore not apply.

Cell growth was also examined; there was no difference between SCR and MCU KD cells in cell number, or in cell cycle progression (data not shown). It was noted that the MCU knockout mouse was smaller than the wild type (Pan *et al.*, 2013), although this is a common feature of knockout mice (Reed *et al.*, 2008), and may therefore not necessarily be an MCU specific trait.

Previous work has shown conflicting results over the role of MCU knockdown in protection from Ca^{2+} induced cell death: it has been found to be protective against NMDA induced excitotoxicity in neuronal cells (Qiu *et al.*, 2013), and against ischaemia reperfusion injury in a conditional MCU knock out mouse (Kwong *et al.*, 2015), although a different MCU

knockout mouse showed no protection against coronary ischaemia induced necrosis, contrary to expectations (Pan *et al.*, 2013). The ionophore A23187 raises intracellular $[Ca^{2+}]$ by enabling Ca^{2+} cations to equilibrate across the cell membrane (Pressman, 1976). Therefore, in cells treated with this compound, it would be expected that MCU knockdown would have no effect - as Ca^{2+} is being transported directly into the matrix bypassing the mitochondrial calcium transport machinery – but that cell death would result from the Ca^{2+} overload. This is what was seen in the experiments in Figure 4.8: there was no effect of MCU knockdown on A23187 induced cell death, and it was found that increasing mitochondrial $[Ca^{2+}]$ does result in significant cell death. Furthermore, the effect of MCU dependent mitochondrial $[Ca^{2+}]$ increases on cell death was investigated. This was tested using a (non-ionophore) drug to induce cytosolic $[Ca^{2+}]$ increase, thapsigargin. As thapsigargin causes Ca^{2+} release from the ER, cytosolic $[Ca^{2+}]$ will rise, and therefore mitochondrial $[Ca^{2+}]$ should rise – in an MCU dependent manner - with risk of Ca^{2+} overload and resultant cell death (Rogers *et al.*, 1995). However, it was found that TG did not induce significant levels of cell death, and the level of cell death was not sufficient to establish whether MCU knockdown was protective, and so this question remains open. This is unusual, as TG is well established as a treatment for causing Ca^{2+} induced cell death (Nath *et al.*, 1997; Takadera and Ohyashiki, 1998), therefore it is likely that with optimization of this procedure, a sufficient level of cell death could be produced.

Overall, MCU knockdown in HEK293T cells was found to have little effect, beyond reducing mitochondrial $[Ca^{2+}]$ when cells were stimulated. There was no effect on MCUB protein level, mitochondrial membrane potential, morphology, basal mitochondrial or cytosolic $[Ca^{2+}]$, respiration, or cell growth, and the effect on cell death could not be determined. Therefore, it was decided that it could be interesting to examine the effects in a different type of cell: rather than using an immortalized human cancer cell line, primary neuronal cells were utilized. Immortalized cell lines, whilst easy to grow and well characterized, are not representative of *in vivo* conditions, or even of normal cells, as they are typically taken from tumours, which are known to have altered mitochondrial properties (Vander Heiden *et al.*, 2009). Primary cells (cells cultured directly from the tissue of living animals) are more physiologically relevant than immortalized cell lines, although they are more difficult to culture and have a limited life span.

The effect of MCU knockdown in primary cortical neurons has previously been examined (Qiu *et al.*, 2013), however it would be interesting to expand on this work, and to examine the effect of other MCU complex components (such as MICU1, the absence of which causes severe learning difficulties in humans (Logan *et al.*, 2014) in this model. In order to do this, a variety of approaches were taken to transfect primary neurons.

It is useful to quantify the percentage of cultures which are neurons, as glial cells transfect more easily, as they continue to undergo division in culture, unlike neurons. Therefore, if there is a high percentage of non-neuronal cells in a culture, transfection efficiency is likely to increase, but will not actually be targeting the desired cells, so to ensure any effects of transfection are neuron-specific it is useful to have a high percentage of neuronal cells. In Figure 4.9, immunocytochemistry using the antibody anti-MAP2 showed that 92.6% of cells were neurons. However, as shown in Figure 4.10, all transfection methods tested were unsuccessful, with a maximum transfection efficiency of 4% across all techniques, and cell death of up to 60%. This is not entirely surprising as neurons are notoriously difficult to transfect, however, it has previously been done with success (Jiang and Chen, 2006; Zeitelhofer *et al.*, 2009; Qiu *et al.*, 2013; Sariyer, 2013) and should be possible. Nevertheless, even when methods have been completely optimized and neurons have been successfully transfected, the transfection efficiency still tends to be lower than that of immortalized cell lines.

An alternative to transfection is transduction, which uses a viral vector to infect cells with nucleic acids. This has the advantage of being able to infect non-dividing cells and has a high efficiency, but can also cause high toxicity, so would still require further optimizing, as well as the construction of the virus, but this could be considered a future avenue.

A possible alternative approach to the genetic modification of cells, would be to examine MCU protein function chemically, using desipramine hydrochloride (Drug D), identified in Chapter 3 as a potential MCU-specific inhibitor. This would also be interesting to further examine the effects of Drug D in a different cell type (primary neuronal cultures) to that in which it was initially tested (HEK293T). Another alternative approach, and possibly more physiologically relevant is to use tissue from a knockout animal (knockout animals can form compensatory mechanisms to overcome the issues caused by the loss of the knockout gene,

and therefore mask these effects, for reviews see (Barbaric *et al.*, 2007; Liang and Li, 2009), thus making their physiological relevance debated). Whilst there is confusion over the MCU knockout mouse – in C57 mice the knockout was embryonic lethal, but in CD1 mice the knockout was viable, although non-Mendelian inheritance of the knockout suggested a more complex picture (Murphy *et al.*, 2014) - mice lacking other components of the MCU complex have been, and are being developed, although no work has yet been published.

Chapter 5: Investigating expression levels of the MCU complex during development

Introduction

Cellular protein levels are dynamic. They can be up and down regulated, either by the up/down regulation of mRNA, or by post-translational modifications that can mark the translated protein for activation or destruction, depending on the cell's needs (Doherty *et al.*, 2009; Farkash-Amar *et al.*, 2012; Han *et al.*, 2014). Housekeeping proteins (proteins which have an essential function in the cell, such as β -actin, a cytoskeletal actin with a role in cell structure and integrity) tend to have a constant expression level at all stages of development and under all cellular conditions, making them useful measures of total protein content, although care has to be taken to select appropriate proteins (Ferguson *et al.*, 2005). Some proteins have constant expression levels, however, the majority of proteins will vary in expression level, dependent on factors such as cell type, developmental stage, cell environment and cellular health.

Ca^{2+} signalling has long been known to play a role during development, beginning with the activation of the egg (Heilbrunn *et al.*, 1937). During fertilization and the early stages of embryogenesis, Ca^{2+} signalling is intracellular, consisting of blips, quarks, puffs, (Ca^{2+} signals resulting from a single IP_3 receptor, a single or group of ryanodine receptors, groups of IP_3 receptors respectively) and intracellular Ca^{2+} waves; for a review, see (Webb and Miller, 2003). During the blastula phase of embryo development when cell number is increasing and cell size is decreasing, the Ca^{2+} signalling shifts from intracellular to localized intercellular, due to the requirement for coordinated activity (Reinhard *et al.*, 1995). This then shifts again to pan-embryonic intercellular signalling as the embryo establishes the body axes and develops a polarized structure, which necessitates coordination on a whole embryo scale (Gilland *et al.*, 1999), and then finally back to localized intercellular signalling

for organ and tissue formation (Webb and Miller, 2003). Confirming the importance of Ca^{2+} regulation in these processes, in an MCU knock down zebrafish model, it was found that the maturation of the notochord, and development of the anteroposterior axis during gastrulation were disrupted (Prudent *et al.*, 2013).

In addition to the many different types of Ca^{2+} signalling during development, Ca^{2+} signalling also has many functions during development; it has been demonstrated to be involved with the axis specification (Kume *et al.*, 2000; Palma *et al.*, 2001), cell motility (Gilland *et al.*, 1999), and organogenesis: heart, muscle and kidney formation (Godin *et al.*, 1998; Mesaeli *et al.*, 1999; De Deyne, 2000), and the development of the nervous system (Leclerc *et al.*, 2003), such as synapse formation and axon growth (Lohmann, 2009).

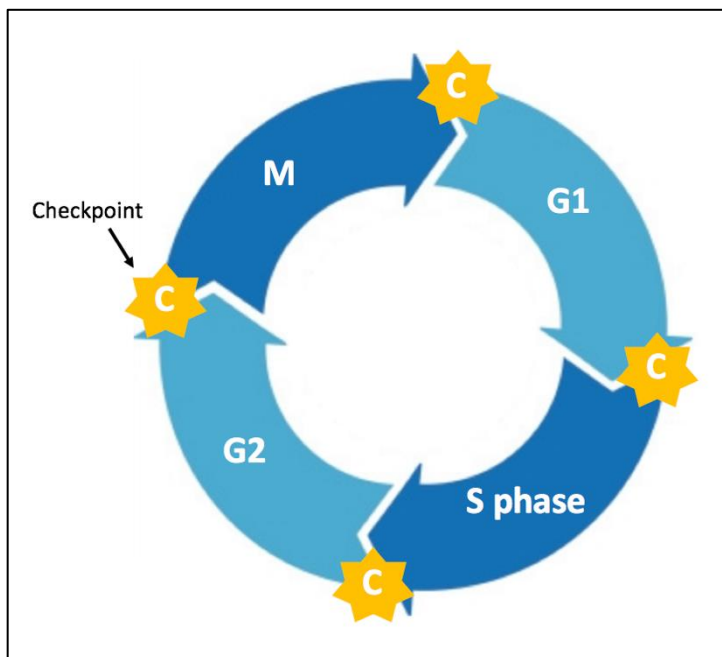


Figure 5.0: the cell cycle. The cell division cycle has four stages: Gap 1 (G1), DNA synthesis (S phase), Gap 2 (G2) and mitosis (M). There are checkpoints between each of these stages, which either allow or prevent the passage of cells to the next stage.

Ca^{2+} signalling also has a role in cell growth and division in somatic cells, although this role is not entirely clear: it was first suggested that Ca^{2+} may play a role when it was identified that microtubules are Ca^{2+} sensitive (Hepler, 1989; Whitaker, 1997). The cell division cycle has four stages: Gap 1 (G1), DNA synthesis (S phase), Gap 2 (G2) and mitosis (M), see Figure 5.0. This cycle is governed by a complex signalling network: prior to entering each stage, the cell pauses at checkpoints. Checkpoints either allow or prevent passage of the cell into the next stage, by the flicking of a chemical switch, to ensure that any cells containing errors are not

allowed to progress (Whitaker, 2006). Errors can occur due to the mis-segregation of chromosomes, mistakes made by DNA polymerase, and damage sustained during the life of the cell by oxidative stress or UV radiation. The role of Ca^{2+} in this process is thought to be in triggering the chemical switch. It has been demonstrated that in sea urchins there are Ca^{2+} signals at these cell cycle checkpoints (Poenie *et al.*, 1985), and that microinjection of Ca^{2+} can induce entry into mitosis (Steinhardt and Alderton, 1988). In frog embryos, injection of Ca^{2+} chelators prevents entry into mitosis (Han *et al.*, 1992) and in mice, large Ca^{2+} signals coincide with mitosis (Tombes *et al.*, 1992).

As Ca^{2+} signalling is important to cell health, life and death, and mitochondria play an important role in cellular Ca^{2+} homeostasis, it would be expected that the components of the MCU complex would be widely expressed, in order to enable mitochondrial Ca^{2+} handling and control in cells. This has been found to be true, as homologues of MCU are present in nearly all plants and metazoa, in some fungi and protozoa, and a few bacterial species (Bick 2012). In metazoa, plants and protozoa, where MCU homologues exist, there are also MICU1 homologues, but in fungi this is not true: MCU-containing organisms typically do not express MICU1, suggesting they have alternative regulatory mechanisms. Interestingly, EMRE has been found to be metazoan-specific (Sancak *et al.*, 2013). Studies of different cell types and mouse tissues have found that MCU, MICU1, MICU2, EMRE and MCUR1 are ubiquitously expressed in mammalian tissues, at various levels: mRNA has been identified in the skeletal muscle, heart, kidney, liver, brain, lung, large intestine, small intestine, thymus, bone marrow, spleen, adipose tissue, pancreas, spinal cord and lymph nodes (De Stefani *et al.*, 2011; Mallilankaraman *et al.*, 2012a; Sancak *et al.*, 2013), with the highest levels in skeletal muscle and kidney. MCUB is also ubiquitously expressed, although at a different expression profile to MCU (Raffaello *et al.*, 2013). SLC25A23 mRNA was found in human tissue samples from brain, heart, skeletal muscle, liver and the small intestine (Bassi *et al.*, 2005).

Studies by the Allen Mouse Brain Atlas (Lein *et al.*, 2007) have explored the expression of MCU in different structures of the adult mouse brain: MCU was identified in the olfactory areas, hippocampal formation, thalamus, pons, medulla, (Allen Mouse Brain Atlas, 2015), and MICU1 and SLC25A23 were found in all areas examined: the isocortex, hippocampal formation, olfactory areas, cortical subplate, striatum, pallidum, thalamus, hypothalamus,

midbrain, pons, medulla, and cerebellum (Allen Mouse Brain Atlas, 2015). Data were not available for EMRE, MCUB, MICU2, MICU3, or MCUR1, and no data were available for the developing mouse brain for these proteins.

However, all of the existing work on the expression of the MCU complex has been done using either tissue taken from adult mice, or HEK293T and HeLa cell lines. As Ca^{2+} plays such an important role in development and growth, we aimed to perform a preliminary investigation to explore how the expression level and structure of the MCU complex varies during development. Therefore, in this project, protein samples were prepared from the brains of rats at eight different developmental stages, ranging from embryonic to adult, and the protein levels of MCU, MCUB, MICU1, and MCUR1 were investigated.

Methods

Sample preparation

Rats were sacrificed according to Home Office Schedule 1 procedure: rats of age P21 and below by cervical dislocation, confirmed by beheading, older rats by CO₂, confirmed by beheading. Scissors were then used to break open the skull, and the brain was removed using curved forceps.

Brains were then placed into sample tubes, and roughly chopped with scissors into rice grain-size pieces, and snap frozen in liquid nitrogen to preserve protein stability. Samples were then removed and thawed on ice. RIPA buffer was added (as described in Chapter 4); volumes were adjusted according to sample size, between 200µl-2ml) and the tissue was manually homogenized using a Potter-Elvehjem homogenizer. Samples were then centrifuged for 10 minutes at 13200g at 4°C. The supernatant was transferred to a fresh tube, the protein concentration quantified, and then frozen at -20°C until use. Protein concentrations were calculated using protein standards of 0-2000µg/ml in RIPA buffer, using a ThermoFisher Scientific BCA assay kit, according to manufacturer's instructions.

Western blot

Western blots were carried out as previously described (Chapter 4). 50µg protein sample were loaded for each blot and for all antibodies except GRP75, samples were boiled to denature prior to loading on the gel. For GRP75 samples were heated to 55°C for 5 minutes. After images of the blots were acquired on a BioRad ChemiDoc Imager, protein levels were quantified using ImageJ: the image was inverted in order to make bands more visible, and the rectangular selection tool was used to draw a rectangle which fully included all of one band. This was fixed into a y position on the blot using the command "Select First Lane" (Control + 1). Identical rectangles (in the same y axis position) were used to cover each band, and were each fixed into place using the command "Select Second Lane" (Control + 2). The command "Plot Lanes" (Control +3) was then used to open plots of the intensity of each area, and the straight line tool used to mark off the peak caused by the band within each plot. The wand tool was then used to measure the area of each peak, and these data were recorded, and normalized to area of the B-actin band in the corresponding lane.

Results

Brain protein samples were prepared from rats at eight different developmental stages: two embryonic stages (E12.5 and E17), at birth and shortly after birth (p0 and p2), during childhood (p10 and p21), at sexual maturity (2.5 months old), and in older adults (6 months old) (Sengupta, 2013).

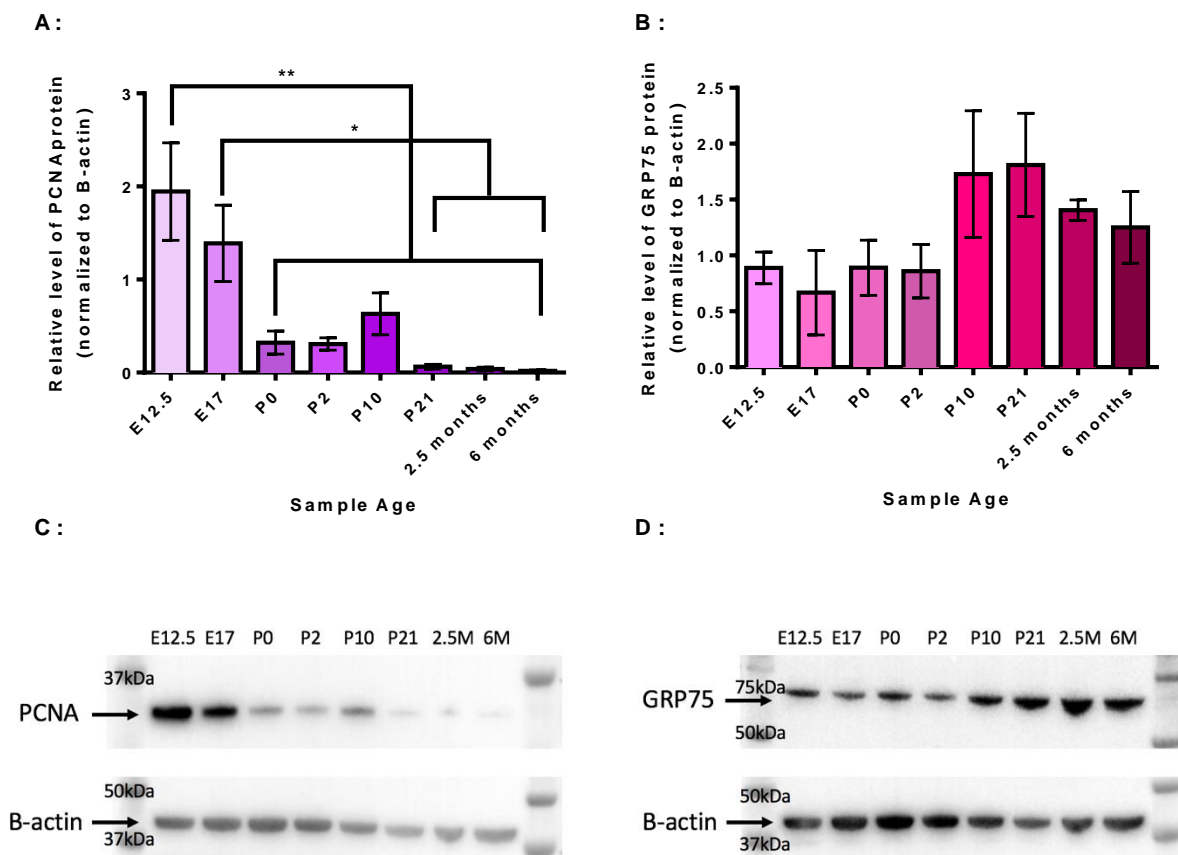


Figure 5.1: Monitoring expression of developmental and mitochondrial markers. A: Relative PCNA protein levels in brain samples of different ages. N of 3. B: Relative GRP75 protein levels in brain samples of different ages. N of 3. C: Representative blot of PCNA and B-actin. D: Representative blot of GRP75 and B-actin. P0, P2, P10 and P21 refer to sample age in number of postnatal days. 2.5M and 6M refer to sample age in months. Significance was assessed by one-way ANOVA. * denotes significance, * = p value < 0.05, ** = p value < 0.01. Error bars are SEM.

Initially, to demonstrate the change in developmental stage between the samples, Western blots were carried out using an anti-proliferating cell nuclear antigen (PCNA) antibody (Figure 5.1A and 5.1C). PCNA is an essential component of DNA replication machinery

(Kelman, 1997), and is only found in dividing cells, so can be used as a marker of development and proliferation. Blots were also run using an anti-GRP75 antibody, a member of the heat shock protein 70 (HSP-70) family (Wadhwa *et al.*, 1993), a family of heat shock proteins which act as molecular chaperones in the import of nuclear encoded mitochondrial proteins. GRP75 is expressed solely in the mitochondrial matrix, and therefore can be used as a marker of mitochondrial content.

It was found that levels of PCNA decreased as the age of the sample increased (Figure 5.1A): PCNA protein levels at E12.5 were significantly different to that at P0, P2, P10, P21, 2.5 and 6 months, and PCNA protein at E17 was significantly different to that at P21, 2.5 and 6 months. By P21, PCNA was barely detectable, demonstrating that the range of sample ages chosen represents both the developing and developed brain. GRP75 was found to remain relatively constant throughout development, with a non-significant trend to increase after P2 (Figure 5.1B); this can be used to normalize the expression levels of the MCU complex, in order to examine whether their expression level remains consistent with mitochondrial load throughout development, or increases or decreases relative to mitochondrial load.

Then, the protein expression levels of components of the MCU complex were examined by Western blot: levels of MCU were found to increase significantly across development (Figure 5.2A). Relative MCU protein at E12.5 and E17 was significantly different to P10, and E12.5, E17 and P0 were all significantly different to P21, 2.5 months and 6 months. However, when normalized to GRP75 (Figure 5.2B), there were no significant differences between any sample ages, suggesting that MCU expression increases only proportionally with mitochondrial content.

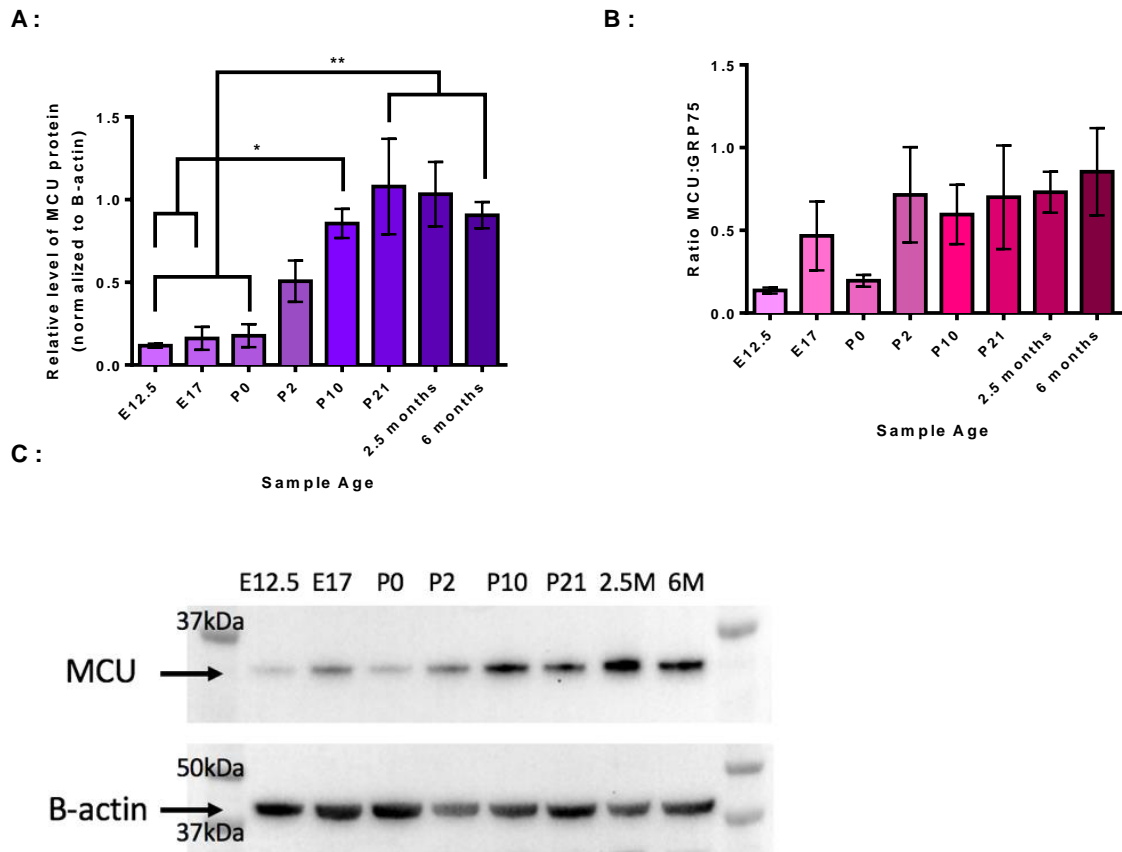


Figure 5.2: Level of MCU protein expression at different developmental stages. A: Level of MCU protein normalized to B-actin. N of 3. B: Ratio of (B-actin normalized) MCU: (B-actin normalized) GRP75. N of 3. C: Representative Western blot of MCU protein. P0, P2, P10 and P21 refer to sample age in number of postnatal days. 2.5M and 6M refer to sample age in months. Significance was assessed by one-way ANOVA. * denotes significance, * = p value <0.05, ** = p value < 0.01. Error bars are SEM.

Levels of MCUB were next investigated and were found to progressively increase across development (Figure 5.3). Relative MCUB protein expression at E17, P0 and P2 was significantly different to protein levels at 2.5 months and 6 months; protein levels at E17 were also significantly different to protein levels at 2.5 months and 6 months; protein levels at E12.5 were actually higher than protein levels at E17, P0 and P2, in contrast to the overall effect of increasing MCUB levels with age, and therefore, only differed significantly to protein at 6 months. However, when normalized to GRP75 (Figure 5.3B), there were no significant differences between any sample ages, suggesting that MCUB expression increases proportionally with mitochondrial content.

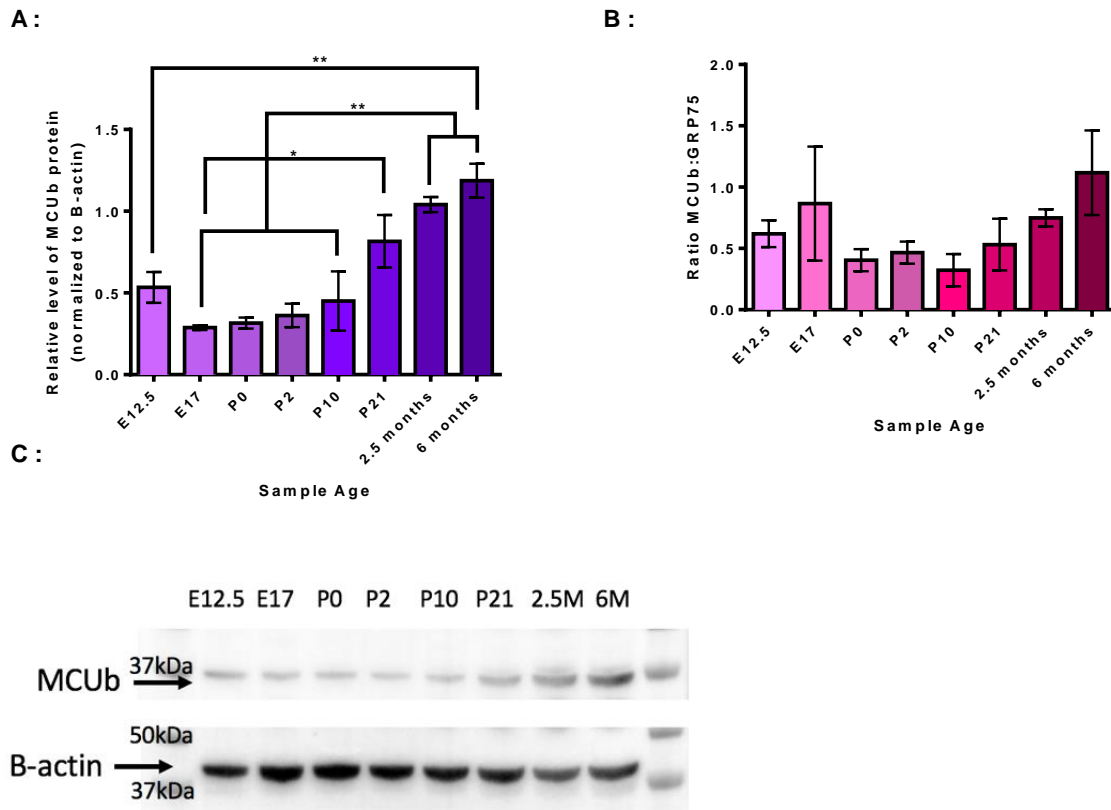


Figure 5.3: Level of MCUB protein expression at different developmental stages. A: Level of MCUB protein normalized to B-actin. N of 3. B: Ratio of (B-actin normalized) MCUB: (B-actin normalized) GRP75. N of 3. C: Representative Western blot of MCUB protein. P0, P2, P10 and P21 refer to sample age in number of postnatal days. 2.5M and 6M refer to sample age in months. Significance was assessed by one-way ANOVA. * denotes significance, * = p value <0.05, ** = p value < 0.01. Error bars are SEM.

Levels of MICU1 expression were then investigated and it was found that they did not alter significantly across development (Figure 5.4A). The MICU1 antibody was not highly specific, with several non-specific bands observed; to ensure the correct band was used for analysis, samples were included from MICU1-deficient patient fibroblasts and control fibroblasts (Logan *et al.*, 2014), and only the band in which there was protein present in the control, and absent in the patient, was used. There appeared to be a general trend of increasing MICU1 content with sample age, although as the standard error was very large, this apparent increase failed to be significant. When normalized to GRP75 (Figure 5.4B), there were no significant differences between any sample ages, suggesting that MICU1 expression also increases only proportionally with mitochondrial content.

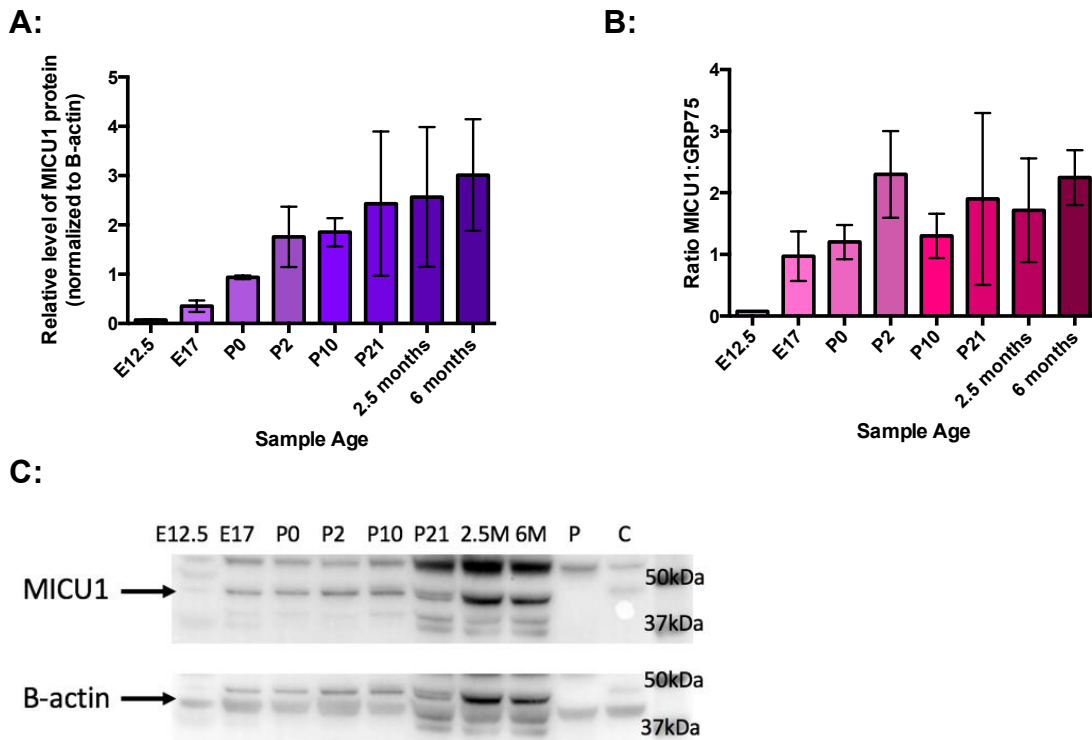


Figure 5.4: Level of MICU1 protein expression at different developmental stages. A: Level of MICU1 protein normalized to B-actin. N of 3. B: Ratio of (B-actin normalized) MICU1: (B-actin normalized) GRP75. N of 3. C: Representative Western blot of MICU1 protein. Lane P contains samples from MICU1 $-/-$ patients, Lane C contains samples from control patients. P0, P2, P10 and P21 refer to sample age in number of postnatal days. 2.5M and 6M refer to sample age in months. Significance was assessed by one-way ANOVA and no differences were found. Error bars are SEM.

Levels of MCUR1 expression were then investigated and it was found that they did not alter significantly across development (Figure 5.5A). There appeared to be very low protein levels of MCUR1 in early development and around birth (E12.5, E17, P0 and P2), with a trend to increase after P10; however this was not significant, and when normalized to GRP75 (Figure 5.5B), there were no significant differences between any sample ages, suggesting that MCUR1 also increases only proportionally with mitochondrial content.

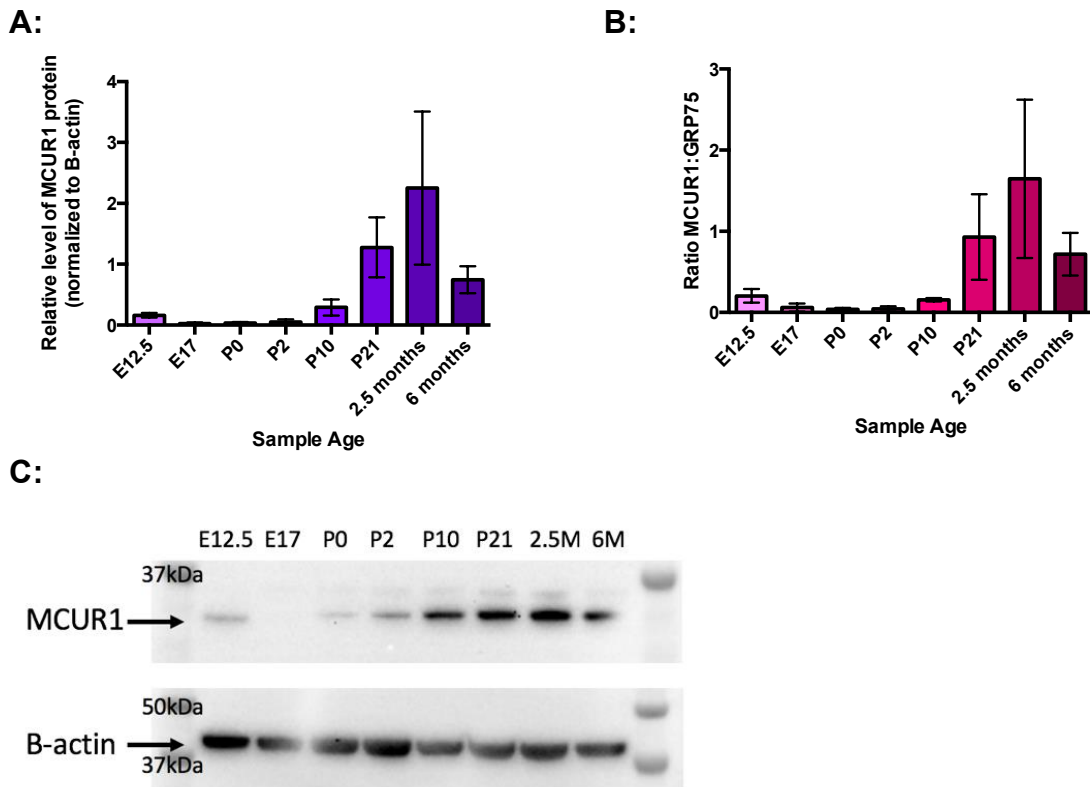
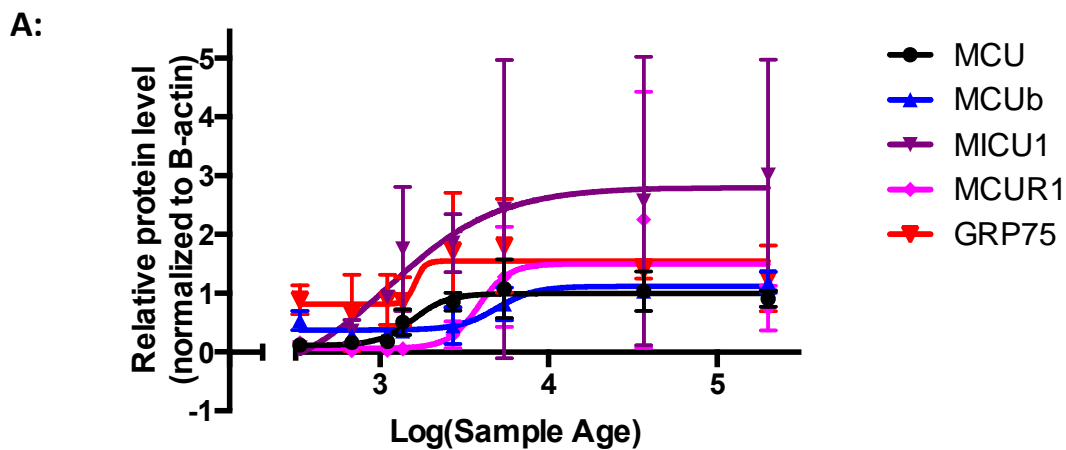


Figure 5.5: Level of MCUR1 protein expression at different developmental stages. A: Level of MCUR1 protein normalized to B-actin. N of 3. B: Ratio of (B-actin normalized) MCUR1: (B-actin normalized) GRP75. N of 3. C: Representative Western blot of MCUR1 protein. P0, P2, P10 and P21 refer to sample age in number of postnatal days. 2.5M and 6M refer to sample age in months. Significance was assessed by one-way ANOVA and no differences were found. Error bars are SEM.

Next, in order to compare the pattern of expression between the different proteins, each were plotted onto one graph, and a sigmoidal non-linear regression curve was added to them (Figure 5.6A). This allowed comparison through the K_m (the day at which half of the maximal protein level was reached) and the slope factor (a measure of the steepness of the curve, which gives measure of the rate at which maximal protein level is achieved). The K_m of GRP75 was 24.77 days post conception (Figure 5.6B), showing that half of the maximal mitochondrial content is achieved three days after birth. The K_m for MCU and MICU1 were very similar to this, of 24.43 and 21.09 respectively, whereas for MCUB and MCUR1 they were higher, of 40.16 and 36.05 respectively. This could suggest that the regulatory subunits develop slightly later than MCU, the pore forming subunit, and MICU1, the essential gatekeeper. The slope factor of GRP75 was 15.21, in contrast to the slope factor of

the MCU complex components, which varied from 1.33 (MICU1) to 4.86 (MCUR1). A higher slope factor value represents a steeper curve, so this shows that the sigmoidal curve of GRP75 was considerably more steep than that of the MCU complex components, due to the abrupt increase in GRP75 expression levels between P2 and P10. However, the error bars were extremely large, and the confidence intervals overlapped between all proteins, so no conclusions can be drawn from this.



B:

	Km (day after conception)	Slope Factor (AU)
MCU	24.43	4.19
MCUb	40.16	3.85
MICU1	21.09	1.33
MCUR1	36.05	4.86
GRP75	24.77	15.21

Figure 5.6: Comparing relative protein levels of MCU, MCUb, MICU1, MCUR1 and GRP75. A: Relative protein levels of each of the examined components and GRP75. B: Km and Slope Factor for each of the examined components and GRP75. Error bars are SEM.

Summary

Overall, it was found that none of the components of the MCU complex which were examined by Western blot changed significantly during development, in comparison to mitochondrial content. Levels of MCU and MCUb protein both significantly increased during

development, but when normalized to GRP75 their increase was not significant. MCU and MICU1 had very similar K_m values to GRP75, whilst the K_m of MCUB and MCUR1 were higher. GRP75 had a considerably higher slope factor value than any of the MCU complex components.

Discussion

Expression levels of GRP75, MICU1 and MCUR1 showed high standard errors, especially at the later stages of development, and therefore the apparent differences in expression levels failed to reach significance. This is likely due to the limitations of Western blots in quantifying protein levels, and insufficient powering of the experiment to produce significant results: all experiments only had an n of 3. With highly variable results between different samples, and semi-quantitative techniques such as Western blots (see below), these experiments have low power. Power is the ability of an experiment to detect an effect, if an effect is present, and low powered experiments need higher sample numbers in order to assess whether there is an effect; this is exaggerated if the expected effect is only small. Therefore, in these experiments, as the size of the effect (if present) is unknown, more replicates should be done in order to give the experiment sufficient power.

Western blots are useful in order to examine what is happening at a protein level (which is more likely to give insight into protein function than the mRNA level), but are of limited use for quantification of proteins – they can provide relative protein levels but not absolute protein concentration (Mahmood and Yang, 2012). This is because of variations in loading and transfer between different blots, and because the signal generated for detection is not linear, which will have contributed to the high level of variation seen between samples in these experiments. Whilst relative protein level is sufficient for a comparison within blots of the same protein at different ages, it would be useful to quantify this more precisely; for this qPCR could be used to measure mRNA levels. This would also be interesting to investigate whether there are differences between the mRNA and protein levels, which would give an indication of whether the proteins are regulated at an mRNA level, or by post-translational modification.

It was found that the protein levels all of the examined components of the MCU complex had a trend of increase over time, with significant increase in MCU and MCUB protein expression levels between the earlier and later developmental stages studied. However, expression levels of GRP75 also increased over development, although with large standard error, so there were no significant differences in mitochondrial content at any development

age. A possible source of this variability is GRP75's role as a heat shock protein: GRP75 levels are variable in response to cellular stress, so if stress conditions were present in the tissues before isolation, then GRP75 levels may not be constant. It would be useful to consider other approaches to quantifying mitochondrial content to eliminate this high variability. This could be done using antibodies with alternative markers of mitochondrial content, such as cytochrome c oxidase (COX), or by quantifying mitochondrial DNA copy number with qPCR.

This large standard error contributed to the lack of significant effect found when MCU complex components were normalized to levels of GRP75: once normalized to mitochondrial content, there were no significant differences between the developmental stages of any of the components. This would suggest that each complex increases proportionally to the mitochondrial content, rather than any component being especially highly expressed in different stages, which could indicate a more important role of the component at that stage. Interestingly, although the protein expression levels were not different, there were some differences in the expression dynamics, although due to large standard error and overlapping confidence intervals (resulting from the issues discussed above) these differences were not significant: the K_m values of MCU and MICU1 were very similar to that of GRP75, whereas the K_m values of MCUB and MCUR1 were higher by at least 50%. This suggests that they have a slightly altered expression profile, with half-maximal protein levels being reached 12-16 days later in development than MCU, MCUB and GRP75. This could indicate that fine regulation of mitochondrial Ca^{2+} uptake develops slightly later than the basic ability to uptake Ca^{2+} . This could be supported by the less broad expression of MCU regulators: MCUB is present in vertebrates but not other lineages (such as plants, Nematoda and kinetoplastids) (Raffaello *et al.*, 2013), whereas the conservation of MCUR1 between species has not been described. Another regulatory component, EMRE, is metazoan specific (Sancak *et al.*, 2013); this limited abundance of regulatory components is in contrast to MCU and MICU1 which are present in metazoan, plants and protozoa (and MCU-only in fungi). The reduced abundance of the regulatory subunits between species suggests that MCU regulation might not be essential for earlier life, which could explain the later development of these components as suggested by the data presented here.

It would be useful to examine the other known components of the complex, EMRE and SLC25A23, however, antibodies were not available for these proteins. In adult mice, protein expression was quite different between the components in different areas of the brain (Allen Mouse Brain Atlas, 2015), with some (MICU1 and SLC25A23) being ubiquitously expressed and others (MCU) being more area specific. This could suggest that whole brain samples, as were used here, may not give an accurate view, at least for components which are not ubiquitously expressed. Therefore, it would also be interesting to examine specific areas of the brain, in order to have a more thorough picture of component expression, and to be able to compare this to the published data for adult mice.

Another interesting avenue to investigate could be to attempt to clarify the role of MCUR1 – its identity as part of the MCU complex has been contested by a recent paper suggesting it is a cytochrome c oxidase assembly factor (Paupé *et al.*, 2015). To do this, cytochrome c oxidase protein expression could also be measured, to see whether protein levels between this and MCUR1 correlate – if it is an assembly factor then it could reasonably be assumed that its expression levels would correlate with the expression level of the protein it helps to assemble. While this would not be an absolute proof of the role of MCUR1, it would be another piece of evidence to support one theory or the other.

Overall, it was found that protein levels of MCU and MCUB increased significantly during development, and protein levels of MICU1 and MCUR1 increased but were not significant. When normalized to GRP75 as a marker of mitochondrial content, there were no significant differences between developmental stages of any components. This is likely due to insufficient powering of the experiment: due to the variability of samples between experiments, and the limitations of Western blotting, a higher n number is needed to overcome the difficulty in assessing whether there are any differences. Additionally, it would be advantageous to consider other markers of mitochondrial content, as GRP75 may not be consistently expressed. Expression profiles of MCU and MICU1 were found to differ to those of MCUR1 and MCUB, suggesting it is possible that regulatory proteins may develop later, however these are not reliable conclusions due to the high variability of these data. Further work is needed to clarify how the MCU complex develops in the brain.

Chapter 6: Conclusions and Future Work

The purpose of the work described in this thesis was to investigate mitochondrial Ca^{2+} uptake pathways, and the associated pathology, mPTP, as potential therapeutic targets. This is because Ca^{2+} is essential to mitochondrial and cellular function. Mitochondrial Ca^{2+} uptake through the MCU (in response to increased cytosolic $[\text{Ca}^{2+}]$) upregulates mitochondrial energetics, alters morphology and suppresses mitophagy, in addition to regulating the localization, timing and amplitude of cytosolic Ca^{2+} waves (see Introduction, p27-28 for further detail). During pathological conditions, excessive mitochondrial Ca^{2+} uptake resulting in matrix overload may cause cell death as a result of mPTP opening. In order to examine the potential of mitochondrial Ca^{2+} uptake pathways as therapeutic targets, the following aims were followed:

1. To investigate the efficacy of a group of novel compounds as inhibitors of the mPTP.
2. To develop a novel screening approach to identify inhibitors of the MCU.
3. To investigate the physiological and pathophysiological role of the MCU and associated proteins through genetic manipulation, and to explore the relative protein levels of MCU and associated proteins through development.

Each chapter of the thesis has addressed one of these aims.

Rather than focus on preventing or reducing mitochondrial Ca^{2+} uptake as a therapeutic strategy, in Chapter 2 I focused on inhibition of the mPTP – the downstream consequence of excessive mitochondrial Ca^{2+} uptake and matrix overload and the direct cause of cell death. mPTP represents a potentially exciting therapeutic target as it appears to serve as the final common path to cell death in a wide number of pathologies, regardless of the source or method of excess mitochondrial Ca^{2+} uptake. In order to identify inhibitors of the mPTP, I screened derivatives of CsA, with an added quinolinium ion for mitochondrial targeting, and with edited side chains to remove CyPA binding capability and improve CyPD binding. The

quinolinium targeting was found to be a successful approach, resulting in mitochondrial localization, and led to inhibition of mPTP at lower concentrations than CsA: the mitochondrial targeting has a concentrating effect on the compounds, so that therapeutic dose can be reduced, and off target effects avoided. The most effective compound, JW47, was further investigated and found to be approximately 4X more potent than CsA, non toxic to mitochondrial membrane potential, ATP production, or oxygen consumption in both isolated liver mitochondria and rat cortical neurons at nanomolar concentrations, although it significantly reduced membrane potential in neurons at 1 μ M. Three further compounds were identified as effective inhibitors at even lower concentrations than JW47. The work described in this chapter did not directly demonstrate that the compound prevents cell death: although the animal study conducted by Gareth Pryce in parallel (see Appendix 2) demonstrates that JW47 has potential therapeutic benefit, and the inference is that this is due to reduced cell death, this needs to be proved, and would be a useful addition to this study. Work is continuing in the Duchen/Szabadkai lab on developing cell based mPTP assays with which to test JW47 and other compounds. In the animal study the effect of JW47 was not compared to that of CsA, which would also be a crucial piece of work to demonstrate that the advantages of quinolinium targeting translate to *in vivo* studies. Future work should seek to clarify these two issues, and additionally demonstrate that the compound is capable of crossing the BBB, which is essential for it to have therapeutic value in neurological disease. The three second generation compounds identified as more efficacious than JW47 should also be investigated further, as their higher efficacy presents a chance to further minimize possible toxicity. It is hoped that these compounds will undergo pre-clinical testing, with a view to progressing to clinical trial if safety parameters are met.

In Chapter 3, I addressed the current lack of MCU specific inhibitors – if the MCU is to be considered a therapeutic target, it is necessary to develop inhibitors which are MCU specific and cell permeable, and therefore methods are needed with which to screen for such compounds. Additionally, MCU specific, permeable inhibitors would be a useful research tool with which to further investigate the function of MCU. In Chapter 3, I described the development of a novel aequorin-based screening approach as a methodology to identify MCU specific inhibitors. I used the NINDS-2 compound library as a starting point, and used

mitochondrial-targeted aequorin to identify compounds affecting mitochondrial Ca^{2+} uptake, followed by a screen measuring cytosolic $[\text{Ca}^{2+}]$ to determine which of these compounds were specific to mitochondria. Of the 1040 compounds screened, the initial mitochondrial and cytosolic aequorin screens identified three compounds, Drug A, D and H, which inhibited mitochondrial $[\text{Ca}^{2+}]$ but did not affect cytosolic $[\text{Ca}^{2+}]$. The specificity of these compounds were reconfirmed using other approaches (viral aequorin, Fluo4-AM, and a calcium retention capacity assay), which revealed that Drug A may not significantly affect mitochondrial Ca^{2+} uptake, and that Drug H potentiated mPTP opening, demonstrating the importance of validation. $\Delta\Psi_m$ and oxygen consumption were also measured, and Drug H was found to reduce both, suggesting Drug H is a non-specific inhibitor of MCU, and acts through another mechanism (e.g. through ROS production). Overall this approach was successful, and one mitochondria specific compound, Drug D, was identified. Positive controls (compounds known to reduce mitochondrial Ca^{2+} uptake) could not be included in the initial screen, due to a lack of permeable, MCU specific inhibitors, thus only a DMSO control was included. If appropriate positive controls were available, they would be useful to give a comparative efficiency of any inhibitors identified. In this work, I identified a pipeline that can be used to develop MCU specific inhibitors, with three hits in the initial screen. It would be interesting to develop this work both to identify further compounds and also to explore their potential therapeutic value. In order to do this, future work would need to develop Drug D by further investigating its mechanism of action and possible side effects, establishing its K_d , and assessing the bioavailability, efficacy and safety in animals. An additional use of this screening approach which could develop from this work is the identification of activators of MCU; this could easily be done by reanalyzing the initial screen for compounds which increased mitochondrial Ca^{2+} concentration but which did not affect cytosolic $[\text{Ca}^{2+}]$.

The work described in Chapters 4 and 5 then sought to investigate the MCU further as a therapeutic target by investigating its role in cell life, death and development. In Chapter 4, an MCU knockdown cell line was created in HEK 293T cells, and its effects investigated. MCU knockdown was found to reduce mitochondrial $[\text{Ca}^{2+}]$ uptake when cells were stimulated, although only to around 50% of control, despite a high level of protein

knockdown. There was no effect on MCUB protein level, mitochondrial membrane potential, morphology, basal mitochondrial or cytosolic $[Ca^{2+}]$, respiration, or cell growth, and the effect on cell death could not be determined. To determine the use of the model in the possibility of MCU being a therapeutic target, it would be useful to explore the effect of MCU knockdown on cell death. This would be crucial to carry out as future work, as the current literature on whether reduced MCU protein is protective against cell death has been controversial; work is continuing in the lab to develop better Ca^{2+} induced cell death assays. It could also be useful to combine this knockdown cell line with inhibitors of MCU in order to completely ablate the mitochondrial Ca^{2+} uptake, as it is possible the limited effects of MCU knockdown are due to the remaining 50% mitochondrial Ca^{2+} uptake – the cumulative effect of knockdown and inhibitors may give a more accurate picture of the role of MCU. The inhibitor identified in Chapter 3, Drug D, could be used for this purpose, for example. In Chapter 4, I also attempted to optimize transfection of neuronal cultures, in order to investigate the effects of knockdown of MCU (and other components) in a primary cell system, as this would be a more therapeutically relevant model to use than an immortalized cell line. However, this was not successful, and would therefore be another avenue for future work. In Chapter 5, the relative protein levels of the MCU complex components were analysed in the rat brain at 8 stages throughout development, from embryonic day 12 to 6 month adults. This demonstrated that although protein levels of all components examined – MCU, MICU1, MCUB and MCUR1 - increase in proportion with mitochondrial content throughout development, MCUB and MCUR1 have a considerably later half maximal value, suggesting the possibility that regulation of MCU develops later. It would be useful to confirm the results by qPCR, as Western blots cannot provide absolute quantification, only relative. However, qPCR gives information on mRNA level, and not protein expression level, which is more indicative of function. It would also be of use to quantify the other protein components of the MCU complex, EMRE, MICU2/3 and SLC25A23, in order to provide further insight about the possible differential development of regulatory subunits.

Overall, this work contributes to the literature by identifying several new inhibitors of mPTP, and examining one in detail, by introducing a mechanism by which to screen for MCU-specific inhibitors, and by further investigating the role of MCU in HEK293T cells, and during

development. This should help to provide further background about the properties of the MCU for future work to build upon, and offer new pharmacological tools to aid the study of the physiological and pathophysiological roles of the MCU and the mPTP in addition to their potential use as therapeutics. It is crucial for the application of this research to establish the extent to which MCU is a therapeutic target, and to directly link inhibition of mPTP to a reduction in cell death, however, it is clear that mitochondrial Ca^{2+} transport pathways have an important role in cell life and death, and it is important to continue to investigate their therapeutic potential.

References

- Abramov AY, Duchen MR. Mechanisms underlying the loss of mitochondrial membrane potential in glutamate excitotoxicity. *Biochim Biophys Acta* 2008; 1777(7-8): 953-64.
- Adamec E, Didier M, Nixon RA. Developmental regulation of the recovery process following glutamate-induced calcium rise in rodent primary neuronal cultures. *Brain Res Dev Brain Res* 1998; 108(1-2): 101-10.
- Adlam VJ, Harrison JC, Porteous CM, James AM, Smith RA, Murphy MP, *et al.* Targeting an antioxidant to mitochondria decreases cardiac ischemia-reperfusion injury. *FASEB J* 2005; 19(9): 1088-95.
- Aebi JD, Deyo DT, Sun CQ, Guillaume D, Dunlap B, Rich DH. Synthesis, conformation, and immunosuppressive activities of three analogues of cyclosporin A modified in the 1-position. *J Med Chem* 1990; 33(3): 999-1009.
- Akkina RK, Walton RM, Chen ML, Li QX, Planelles V, Chen IS. High-efficiency gene transfer into CD34+ cells with a human immunodeficiency virus type 1-based retroviral vector pseudotyped with vesicular stomatitis virus envelope glycoprotein G. *J Virol* 1996; 70(4): 2581-5.
- Al-Izki S, Pryce G, Hankey DJ, Lidster K, von Kutzleben SM, Browne L, *et al.* Lesional-targeting of neuroprotection to the inflammatory penumbra in experimental multiple sclerosis. *Brain* 2014; 137(Pt 1): 92-108.
- Alam MR, Groschner LN, Parichatikanond W, Kuo L, Bondarenko AI, Rost R, *et al.* Mitochondrial Ca²⁺ Uptake 1 (MICU1) and Mitochondrial Ca²⁺ Uniporter (MCU) Contribute to Metabolism-Secretion Coupling in Clonal Pancreatic beta-Cells. *The Journal of biological chemistry* 2012; 287(41).
- Alavian KN, Beutner G, Lazrove E, Sacchetti S, Park HA, Licznerski P, *et al.* An uncoupling channel within the c-subunit ring of the F1FO ATP synthase is the mitochondrial permeability transition pore. *Proc Natl Acad Sci U S A* 2014; 111(29): 10580-5.
- Allen DG, Blinks JR. Calcium transients in aequorin-injected frog cardiac muscle. *Nature* 1978; 273(5663): 509-13.
- Allen DG, Blinks JR, Prendergast FG. Aequorin luminescence: relation of light emission to calcium concentration--a calcium-independent component. *Science* 1977; 195(4282): 996-8.
- Allen Mouse Brain Atlas. 2015. Gene ccdc109a. [ONLINE] Available at: <http://mouse.brain-map.org/gene/show/84886>. [Accessed 18 December 15].
- Allen Mouse Brain Atlas. 2015. Gene Micu1. [ONLINE] Available at: <http://mouse.brain-map.org/gene/show/84887>. [Accessed 18 December 15].

- Allen Mouse Brain Atlas. 2015. Gene slc25a23. [ONLINE] Available at: <http://mouse.brain-map.org/gene/show/42815>. [Accessed 18 December 15].
- Amigo I, Traba J, González-Barroso MM, Rueda CB, Fernández M, Rial E, *et al.* Glucagon regulation of oxidative phosphorylation requires an increase in matrix adenine nucleotide content through Ca²⁺ activation of the mitochondrial ATP-Mg/Pi carrier SCaMC-3. *J Biol Chem* 2013; 288(11): 7791-802.
- Anderson S, Bankier AT, Barrell BG, de Bruijn MH, Coulson AR, Drouin J, *et al.* Sequence and organization of the human mitochondrial genome. *Nature* 1981; 290(5806): 457-65.
- Andersson SG, Kurland CG. Ancient and recent horizontal transfer events: the origins of mitochondria. *APMIS Suppl* 1998; 84: 5-14.
- Andersson SG, Zomorodipour A, Andersson JO, Sicheritz-Pontén T, Alsmark UC, Podowski RM, *et al.* The genome sequence of *Rickettsia prowazekii* and the origin of mitochondria. *Nature* 1998; 396(6707): 133-40.
- ATCC. 2012. ATCC Primary Cell Culture Guide. [ONLINE] Available at: http://www.atcc.org/~media/PDFs/Culture%20Guides/Primary_Cell_Culture_Guide.ashx. [Accessed 18 December 15].
- Baines CP, Kaiser RA, Purcell NH, Blair NS, Osinska H, Hambleton MA, *et al.* Loss of cyclophilin D reveals a critical role for mitochondrial permeability transition in cell death. *Nature* 2005; 434(7033): 658-62.
- Balaban RS. The role of Ca²⁺ signaling in the coordination of mitochondrial ATP production with cardiac work. *Biochim Biophys Acta* 2009; 1787(11): 1334-41.
- Barbaric I, Miller G, Dear TN. Appearances can be deceiving: phenotypes of knockout mice. *Brief Funct Genomic Proteomic* 2007; 6(2): 91-103.
- Barsukova A, Komarov A, Hajnóczky G, Bernardi P, Bourdette D, Forte M. Activation of the mitochondrial permeability transition pore modulates Ca²⁺ responses to physiological stimuli in adult neurons. *Eur J Neurosci* 2011; 33(5): 831-42.
- Bassi MT, Manzoni M, Bresciani R, Pizzo MT, Della Monica A, Barlati S, *et al.* Cellular expression and alternative splicing of SLC25A23, a member of the mitochondrial Ca²⁺-dependent solute carrier gene family. *Gene* 2005; 345(2): 173-82.
- Baubet V, Le Mouellic H, Campbell AK, Lucas-Meunier E, Fossier P, Brúlet P. Chimeric green fluorescent protein-aequorin as bioluminescent Ca²⁺ reporters at the single-cell level. *Proc Natl Acad Sci U S A* 2000; 97(13): 7260-5.
- Baughman JM, Perocchi F, Girgis HS, Plovanich M, Belcher-Timme CA, Sancak Y, *et al.* Integrative genomics identifies MCU as an essential component of the mitochondrial calcium uniporter. *Nature* 2011; 476(7360).
- Bensinger SJ, Christofk HR. New aspects of the Warburg effect in cancer cell biology. *Semin Cell Dev Biol* 2012; 23(4): 352-61.

Bernardi P, Di Lisa F. The mitochondrial permeability transition pore: molecular nature and role as a target in cardioprotection. *J Mol Cell Cardiol* 2015; 78: 100-6.

Bernardi P, Krauskopf A, Basso E, Petronilli V, Blachly-Dyson E, Blalchy-Dyson E, *et al.* The mitochondrial permeability transition from in vitro artifact to disease target. *FEBS J* 2006; 273(10): 2077-99.

Bernardi P, Petronilli V. The permeability transition pore as a mitochondrial calcium release channel: a critical appraisal. *J Bioenerg Biomembr* 1996; 28(2): 131-8.

Bernardi P, Vassanelli S, Veronese P, Colonna R, Szabó I, Zoratti M. Modulation of the mitochondrial permeability transition pore. Effect of protons and divalent cations. *J Biol Chem* 1992; 267(5): 2934-9.

Beutner G, Ruck A, Riede B, Welte W, Brdiczka D. Complexes between kinases, mitochondrial porin and adenylate translocator in rat brain resemble the permeability transition pore. *FEBS Lett* 1996; 396(2-3): 189-95.

Bick AG, Calvo SE, Mootha VK. Evolutionary Diversity of the Mitochondrial Calcium Uniporter. *Science* 2012; 336(6083): 886-.

Blanchet L, Grefte S, Smeitink JA, Willems PH, Koopman WJ. Photo-induction and automated quantification of reversible mitochondrial permeability transition pore opening in primary mouse myotubes. *PLoS One* 2014; 9(11): e114090.

Boerries M, Most P, Gledhill JR, Walker JE, Katus HA, Koch WJ, *et al.* Ca²⁺-dependent interaction of S100A1 with F1-ATPase leads to an increased ATP content in cardiomyocytes. *Mol Cell Biol* 2007; 27(12): 4365-73.

Boitier E, Rea R, Duchen MR. Mitochondria exert a negative feedback on the propagation of intracellular Ca²⁺ waves in rat cortical astrocytes. *J Cell Biol* 1999; 145(4): 795-808.

Bonora M, Bononi A, De Marchi E, Giorgi C, Lebedzinska M, Marchi S, *et al.* Role of the c subunit of the FO ATP synthase in mitochondrial permeability transition. *Cell Cycle* 2013; 12(4): 674-83.

Bonora M, Wieckowski MR, Chinopoulos C, Kepp O, Kroemer G, Galluzzi L, *et al.* Molecular mechanisms of cell death: central implication of ATP synthase in mitochondrial permeability transition. *Oncogene* 2015; 34(12): 1608.

Breckenridge DG, Stojanovic M, Marcellus RC, Shore GC. Caspase cleavage product of BAP31 induces mitochondrial fission through endoplasmic reticulum calcium signals, enhancing cytochrome c release to the cytosol. *J Cell Biol* 2003; 160(7): 1115-27.

Brideau C, Gunter B, Pikounis B, Liaw A. Improved statistical methods for hit selection in high-throughput screening. *J Biomol Screen* 2003; 8(6): 634-47.

Brini M, Marsault R, Bastianutto C, Alvarez J, Pozzan T, Rizzuto R. Transfected aequorin in the measurement of cytosolic Ca²⁺ concentration ([Ca²⁺]_c). A critical evaluation. *J Biol Chem* 1995; 270(17): 9896-903.

Brini M, Murgia M, Pasti L, Picard D, Pozzan T, Rizzuto R. Nuclear Ca²⁺ concentration measured with specifically targeted recombinant aequorin. *EMBO J* 1993; 12(12): 4813-9.

Brookes PS, Parker N, Buckingham JA, Vidal-Puig A, Halestrap AP, Gunter TE, *et al.* UCPs--unlikely calcium porters. *Nat Cell Biol* 2008; 10(11): 1235-7; author reply 7-40.

Camara AK, Lesnefsky EJ, Stowe DF. Potential therapeutic benefits of strategies directed to mitochondria. *Antioxid Redox Signal* 2010; 13(3): 279-347.

Campanella M, Casswell E, Chong S, Farah Z, Wieckowski MR, Abramov AY, *et al.* Regulation of mitochondrial structure and function by the F₁F₀-ATPase inhibitor protein, IF1. *Cell Metab* 2008; 8(1): 13-25.

Caramelo C, Alvarez-Arroyo MV, Yagüe S, Suzuki Y, Castilla MA, Velasco L, *et al.* Cyclosporin A toxicity, and more: vascular endothelial growth factor (VEGF) steps forward. *Nephrol Dial Transplant* 2004; 19(2): 285-8.

Cesura AM, Pinard E, Schubeneil R, Goetschy V, Friedlein A, Langen H, *et al.* The voltage-dependent anion channel is the target for a new class of inhibitors of the mitochondrial permeability transition pore. *J Biol Chem* 2003; 278(50): 49812-8.

CHAPPELL JB, CROFTS AR. CALCIUM ION ACCUMULATION AND VOLUME CHANGES OF ISOLATED LIVER MITOCHONDRIA. CALCIUM ION-INDUCED SWELLING. *Biochem J* 1965; 95: 378-86.

Chen H, Chomyn A, Chan DC. Disruption of fusion results in mitochondrial heterogeneity and dysfunction. *J Biol Chem* 2005; 280(28): 26185-92.

Chen H, Detmer SA, Ewald AJ, Griffin EE, Fraser SE, Chan DC. Mitofusins Mfn1 and Mfn2 coordinately regulate mitochondrial fusion and are essential for embryonic development. *J Cell Biol* 2003; 160(2): 189-200.

Chinopoulos C, Konràd C, Kiss G, Metelkin E, Töröcsik B, Zhang SF, *et al.* Modulation of F₀F₁-ATP synthase activity by cyclophilin D regulates matrix adenine nucleotide levels. *FEBS J* 2011; 278(7): 1112-25.

Chinopoulos C, Szabadkai G. What Makes You Can Also Break You: Mitochondrial Permeability Transition Pore Formation by Dimers of the F₁F₀ ATP-Synthase? *Front Oncol* 2013; 3:25

Chinopoulos C, Szabadkai G. What Makes You Can Also Break You, Part III: Mitochondrial Permeability Transition Pore Formation by Dimers of the F₁F₀ ATP-Synthase? *Front Oncol* 2014; 4:235

Chlystun M, Campanella M, Law AL, Duchon MR, Fatimathas L, Levine TP, *et al.* Regulation of mitochondrial morphogenesis by annexin A6. *PLoS One* 2013; 8(1): e53774.

Choi DW. Glutamate neurotoxicity in cortical cell culture is calcium dependent. *Neurosci Lett* 1985; 58(3): 293-7.

Chomyn A, Cleeter MW, Ragan CI, Riley M, Doolittle RF, Attardi G. URF6, last unidentified reading frame of human mtDNA, codes for an NADH dehydrogenase subunit. *Science* 1986; 234(4776): 614-8.

Chomyn A, Mariottini P, Cleeter MW, Ragan CI, Matsuno-Yagi A, Hatefi Y, *et al.* Six unidentified reading frames of human mitochondrial DNA encode components of the respiratory-chain NADH dehydrogenase. *Nature* 1985; 314(6012): 592-7.

Clarke SJ, McStay GP, Halestrap AP. Sangliffehrin A acts as a potent inhibitor of the mitochondrial permeability transition and reperfusion injury of the heart by binding to cyclophilin-D at a different site from cyclosporin A. *J Biol Chem* 2002; 277(38): 34793-9.

CROFTS AR, CHAPPELL JB. CALCIUM ION ACCUMULATION AND VOLUME CHANGES OF ISOLATED LIVER MITOCHONDRIA. REVERSAL OF CALCIUM ION-INDUCED SWELLING. *Biochem J* 1965; 95: 387-92.

Crompton M, Costi A. A heart mitochondrial Ca²⁺-dependent pore of possible relevance to reperfusion-induced injury. Evidence that ADP facilitates pore interconversion between the closed and open states. *Biochem J* 1990; 266(1): 33-9.

Crompton M, Costi A, Hayat L. Evidence for the presence of a reversible Ca²⁺-dependent pore activated by oxidative stress in heart mitochondria. *Biochem J* 1987; 245(3): 915-8.

Crompton M, Ellinger H, Costi A. Inhibition by cyclosporin A of a Ca²⁺-dependent pore in heart mitochondria activated by inorganic phosphate and oxidative stress. *Biochem J* 1988; 255(1): 357-60.

Crompton M, Virji S, Ward JM. Cyclophilin-D binds strongly to complexes of the voltage-dependent anion channel and the adenine nucleotide translocase to form the permeability transition pore. *Eur J Biochem* 1998; 258(2): 729-35.

Csordás G, Golenár T, Seifert EL, Kamer KJ, Sancak Y, Perocchi F, *et al.* MICU1 Controls Both the Threshold and Cooperative Activation of the Mitochondrial Ca²⁺ Uniporter. *Cell Metab* 2013; 17(6): 976-87.

Cárdenas C, Foskett JK. Mitochondrial Ca²⁺ signals in autophagy. *Cell Calcium* 2012; 52(1): 44-51.

Cárdenas C, Miller RA, Smith I, Bui T, Molgó J, Müller M, *et al.* Essential regulation of cell bioenergetics by constitutive InsP₃ receptor Ca²⁺ transfer to mitochondria. *Cell* 2010; 142(2): 270-83.

Damiano M, Galvan L, Déglon N, Brouillet E. Mitochondria in Huntington's disease. *Biochim Biophys Acta* 2010; 1802(1): 52-61.

David G, Barrett JN, Barrett EF. Evidence that mitochondria buffer physiological Ca²⁺ loads in lizard motor nerve terminals. *J Physiol* 1998; 509 (Pt 1): 59-65.

Davis TL, Walker JR, Campagna-Slater V, Finerty PJ, Paramanathan R, Bernstein G, *et al.* Structural and biochemical characterization of the human cyclophilin family of peptidyl-prolyl isomerases. *PLoS Biol* 2010; 8(7): e1000439.

De Deyne PG. Formation of sarcomeres in developing myotubes: role of mechanical stretch and contractile activation. *Am J Physiol Cell Physiol* 2000; 279(6): C1801-11.

De Giorgi F, Lartigue L, Bauer MK, Schubert A, Grimm S, Hanson GT, *et al.* The permeability transition pore signals apoptosis by directing Bax translocation and multimerization. *FASEB J* 2002; 16(6): 607-9.

de la Fuente S, Matesanz-Isabel J, Fonteriz RI, Montero M, Alvarez J. Dynamics of mitochondrial Ca²⁺ uptake in MICU1-knockdown cells. *Biochem J* 2014; 458(1): 33-40.

De Stefani D, Raffaello A, Teardo E, Szabo I, Rizzuto R. A forty-kilodalton protein of the inner membrane is the mitochondrial calcium uniporter. *Nature* 2011; 476(7360).

DELUCA HF, ENGSTROM GW. Calcium uptake by rat kidney mitochondria. *Proc Natl Acad Sci U S A* 1961; 47: 1744-50.

Denton RM, Randle PJ, Martin BR. Stimulation by calcium ions of pyruvate dehydrogenase phosphate phosphatase. *Biochem J* 1972; 128(1): 161-3.

Denton RM, Richards DA, Chin JG. Calcium ions and the regulation of NAD⁺-linked isocitrate dehydrogenase from the mitochondria of rat heart and other tissues. *Biochem J* 1978; 176(3): 899-906.

Doherty MK, Hammond DE, Clague MJ, Gaskell SJ, Beynon RJ. Turnover of the human proteome: determination of protein intracellular stability by dynamic SILAC. *J Proteome Res* 2009; 8(1): 104-12.

Dong XX, Wang Y, Qin ZH. Molecular mechanisms of excitotoxicity and their relevance to pathogenesis of neurodegenerative diseases. *Acta Pharmacol Sin* 2009; 30(4): 379-87.

Doonan PJ, Chandramoorthy HC, Hoffman NE, Zhang X, Cárdenas C, Shanmughapriya S, *et al.* LETM1-dependent mitochondrial Ca²⁺ flux modulates cellular bioenergetics and proliferation. *FASEB J* 2014; 28(11): 4936-49.

Drago I, De Stefani D, Rizzuto R, Pozzan T. Mitochondrial Ca²⁺ uptake contributes to buffering cytoplasmic Ca²⁺ peaks in cardiomyocytes. *Proceedings of the National Academy of Sciences of the United States of America* 2012; 109(32).

Duchen MR. Ca²⁺-dependent changes in the mitochondrial energetics in single dissociated mouse sensory neurons. *Biochem J* 1992; 283 (Pt 1): 41-50.

Duchen MR. Mitochondria, calcium-dependent neuronal death and neurodegenerative disease. *Pflugers Archiv-European Journal of Physiology* 2012; 464(1).

Duchen MR, McGuinness O, Brown LA, Crompton M. On the involvement of a cyclosporin A sensitive mitochondrial pore in myocardial reperfusion injury. *Cardiovasc Res* 1993; 27(10): 1790-4.

Dumollard R, Hammar K, Porterfield M, Smith PJ, Cibert C, Rouvière C, *et al.* Mitochondrial respiration and Ca²⁺ waves are linked during fertilization and meiosis completion. *Development* 2003; 130(4): 683-92.

Durette PL, Boger J, Dumont F, Firestone R, Frankshun RA, Koprak SL, *et al.* A study of the correlation between cyclophilin binding and in vitro immunosuppressive activity of cyclosporine A and analogues. *Transplant Proc* 1988; 20(2 Suppl 2): 51-7.

Endele S, Fuhry M, Pak SJ, Zabel BU, Winterpacht A. LETM1, a novel gene encoding a putative EF-hand Ca²⁺-binding protein, flanks the Wolf-Hirschhorn syndrome (WHS) critical region and is deleted in most WHS patients. *Genomics* 1999; 60(2): 218-25.

Farkash-Amar S, Eden E, Cohen A, Geva-Zatorsky N, Cohen L, Milo R, *et al.* Dynamic proteomics of human protein level and localization across the cell cycle. *PLoS One* 2012; 7(11): e48722.

Ferguson RE, Carroll HP, Harris A, Maher ER, Selby PJ, Banks RE. Housekeeping proteins: a preliminary study illustrating some limitations as useful references in protein expression studies. *Proteomics* 2005; 5(2): 566-71.

Fiermonte G, De Leonardis F, Todisco S, Palmieri L, Lasorsa FM, Palmieri F. Identification of the mitochondrial ATP-Mg/Pi transporter. Bacterial expression, reconstitution, functional characterization, and tissue distribution. *J Biol Chem* 2004; 279(29): 30722-30.

Figley CR, Stroman PW. The role(s) of astrocytes and astrocyte activity in neurometabolism, neurovascular coupling, and the production of functional neuroimaging signals. *Eur J Neurosci* 2011; 33(4): 577-88.

Fire A, Xu S, Montgomery MK, Kostas SA, Driver SE, Mello CC. Potent and specific genetic interference by double-stranded RNA in *Caenorhabditis elegans*. *Nature* 1998; 391(6669): 806-11.

Fishel ML, Vasko MR, Kelley MR. DNA repair in neurons: so if they don't divide what's to repair? *Mutat Res* 2007; 614(1-2): 24-36.

Fransson S, Ruusala A, Aspenström P. The atypical Rho GTPases Miro-1 and Miro-2 have essential roles in mitochondrial trafficking. *Biochem Biophys Res Commun* 2006; 344(2): 500-10.

Friberg H, Ferrand-Drake M, Bengtsson F, Halestrap AP, Wieloch T. Cyclosporin A, but not FK 506, protects mitochondria and neurons against hypoglycemic damage and implicates the mitochondrial permeability transition in cell death. *J Neurosci* 1998; 18(14): 5151-9.

Gandhi S, Wood-Kaczmar A, Yao Z, Plun-Favreau H, Deas E, Klupsch K, *et al.* PINK1-associated Parkinson's disease is caused by neuronal vulnerability to calcium-induced cell death. *Mol Cell* 2009; 33(5): 627-38.

Gateau-Roesch O, Argaud L, Ovize M. Mitochondrial permeability transition pore and postconditioning. *Cardiovasc Res* 2006; 70(2): 264-73.

Geissler A, Krimmer T, Bömer U, Guiard B, Rassow J, Pfanner N. Membrane potential-driven protein import into mitochondria. The sorting sequence of cytochrome b(2) modulates the $\Delta\psi$ -dependence of translocation of the matrix-targeting sequence. *Mol Biol Cell* 2000; 11(11): 3977-91.

Gellerich FN, Gizatullina Z, Nguyen HP, Trumbeckaite S, Vielhaber S, Seppet E, *et al.* Impaired regulation of brain mitochondria by extramitochondrial Ca²⁺ in transgenic Huntington disease rats. *J Biol Chem* 2008; 283(45): 30715-24.

Gilland E, Miller AL, Karplus E, Baker R, Webb SE. Imaging of multicellular large-scale rhythmic calcium waves during zebrafish gastrulation. *Proc Natl Acad Sci U S A* 1999; 96(1): 157-61.

Giorgio V, Bisetto E, Soriano ME, Dabbeni-Sala F, Basso E, Petronilli V, *et al.* Cyclophilin D modulates mitochondrial FOF1-ATP synthase by interacting with the lateral stalk of the complex. *J Biol Chem* 2009; 284(49): 33982-8.

Giorgio V, von Stockum S, Antoniel M, Fabbro A, Fogolari F, Forte M, *et al.* Dimers of mitochondrial ATP synthase form the permeability transition pore. *Proc Natl Acad Sci U S A* 2013; 110(15): 5887-92.

Glitsch MD, Bakowski D, Parekh AB. Store-operated Ca²⁺ entry depends on mitochondrial Ca²⁺ uptake. *EMBO J* 2002; 21(24): 6744-54.

Godin RE, Takaesu NT, Robertson EJ, Dudley AT. Regulation of BMP7 expression during kidney development. *Development* 1998; 125(17): 3473-82.

González-Cabo P, Palau F. Mitochondrial pathophysiology in Friedreich's ataxia. *J Neurochem* 2013; 126 Suppl 1: 53-64.

Graham FL, van der Eb AJ. A new technique for the assay of infectivity of human adenovirus 5 DNA. *Virology* 1973; 52(2): 456-67.

Griffiths EJ, Halestrap AP. Protection by Cyclosporin A of ischemia/reperfusion-induced damage in isolated rat hearts. *J Mol Cell Cardiol* 1993; 25(12): 1461-9.

Gunter TE, Buntinas L, Sparagna G, Eliseev R, Gunter K. Mitochondrial calcium transport: mechanisms and functions. *Cell Calcium* 2000; 28(5-6): 285-96.

Gusdon AM, Fernandez-Bueno GA, Wohlgemuth S, Fernandez J, Chen J, Mathews CE. Respiration and substrate transport rates as well as reactive oxygen species production distinguish mitochondria from brain and liver. *BMC Biochem* 2015; 16: 22.

Hajnóczky G, Csordás G, Das S, Garcia-Perez C, Saotome M, Sinha Roy S, *et al.* Mitochondrial calcium signalling and cell death: approaches for assessing the role of mitochondrial Ca²⁺ uptake in apoptosis. *Cell Calcium* 2006; 40(5-6): 553-60.

Halestrap AP. 2014. The C Ring of the F1Fo ATP Synthase Forms the Mitochondrial Permeability Transition Pore: A Critical Appraisal. *Front Oncol* 2014; 4:234

Halestrap AP. Calcium-dependent opening of a non-specific pore in the mitochondrial inner membrane is inhibited at pH values below 7. Implications for the protective effect of low pH against chemical and hypoxic cell damage. *Biochem J* 1991; 278 (Pt 3): 715-9.

Halestrap AP, Brenner C. The adenine nucleotide translocase: a central component of the mitochondrial permeability transition pore and key player in cell death. *Curr Med Chem* 2003; 10(16): 1507-25.

Halestrap AP, Clarke SJ, Javadov SA. Mitochondrial permeability transition pore opening during myocardial reperfusion--a target for cardioprotection. *Cardiovasc Res* 2004; 61(3): 372-85.

Halestrap AP, Davidson AM. Inhibition of Ca²⁺(+)-induced large-amplitude swelling of liver and heart mitochondria by cyclosporin is probably caused by the inhibitor binding to mitochondrial-matrix

peptidyl-prolyl cis-trans isomerase and preventing it interacting with the adenine nucleotide translocase. *Biochem J* 1990; 268(1): 153-60.

Halestrap AP, Kerr PM, Javadov S, Woodfield KY. Elucidating the molecular mechanism of the permeability transition pore and its role in reperfusion injury of the heart. *Biochim Biophys Acta* 1998; 1366(1-2): 79-94.

Han JK, Fukami K, Nuccitelli R. Reducing inositol lipid hydrolysis, Ins(1,4,5)P₃ receptor availability, or Ca²⁺ gradients lengthens the duration of the cell cycle in *Xenopus laevis* blastomeres. *J Cell Biol* 1992; 116(1): 147-56.

Han K, Jaimovich A, Dey G, Ruggero D, Meyuhas O, Sonenberg N, *et al.* Parallel measurement of dynamic changes in translation rates in single cells. *Nat Methods* 2014; 11(1): 86-93.

Hartikka J, Sawdey M, Cornefert-Jensen F, Margalith M, Barnhart K, Nolasco M, *et al.* An improved plasmid DNA expression vector for direct injection into skeletal muscle. *Hum Gene Ther* 1996; 7(10): 1205-17.

Haworth RA, Hunter DR. The Ca²⁺-induced membrane transition in mitochondria. II. Nature of the Ca²⁺ trigger site. *Arch Biochem Biophys* 1979; 195(2): 460-7.

HAYFLICK L, MOORHEAD PS. The serial cultivation of human diploid cell strains. *Exp Cell Res* 1961; 25: 585-621.

Heilbrunn, L. V. & Wilbur, K. M. Stimulation and nuclear breakdown in the *Nereis* egg (1937) *Biol. Bull.* **73**, 557–567

Hepler PK. Calcium transients during mitosis: observations in flux. *J Cell Biol* 1989; 109(6 Pt 1): 2567-73.

Herzig S, Maundrell K, Martinou JC. Life without the mitochondrial calcium uniporter. *Nat Cell Biol* 2013; 15(12): 1398-400.

Hill JM, De Stefani D, Jones AW, Ruiz A, Rizzuto R, Szabadkai G. Measuring baseline Ca²⁺ levels in subcellular compartments using genetically engineered fluorescent indicators. *Methods Enzymol* 2014; 543: 47-72.

Hoffman NE, Chandramoorthy HC, Shamugapriya S, Zhang X, Rajan S, Mallilankaraman K, *et al.* MICU1 Motifs Define Mitochondrial Calcium Uniporter Binding and Activity. *Cell Rep* 2013; 5(6): 1576-88.

Hoffman NE, Chandramoorthy HC, Shanmughapriya S, Zhang XQ, Vallem S, Doonan PJ, *et al.* SLC25A23 augments mitochondrial Ca²⁺ uptake, interacts with MCU, and induces oxidative stress-mediated cell death. *Mol Biol Cell* 2014; 25(6): 936-47.

Hogan PG, Chen L, Nardone J, Rao A. Transcriptional regulation by calcium, calcineurin, and NFAT. *Genes Dev* 2003; 17(18): 2205-32.

Hoth M, Fanger CM, Lewis RS. Mitochondrial regulation of store-operated calcium signaling in T lymphocytes. *J Cell Biol* 1997; 137(3): 633-48.

Hunter DR, Haworth RA. The Ca²⁺-induced membrane transition in mitochondria. I. The protective mechanisms. *Arch Biochem Biophys* 1979a; 195(2): 453-9.

Hunter DR, Haworth RA. The Ca²⁺-induced membrane transition in mitochondria. III. Transitional Ca²⁺ release. *Arch Biochem Biophys* 1979b; 195(2): 468-77.

Høyer-Hansen M, Bastholm L, Szyniarowski P, Campanella M, Szabadkai G, Farkas T, *et al.* Control of macroautophagy by calcium, calmodulin-dependent kinase kinase-beta, and Bcl-2. *Mol Cell* 2007; 25(2): 193-205.

Hüser J, Rechenmacher CE, Blatter LA. Imaging the permeability pore transition in single mitochondria. *Biophys J* 1998; 74(4): 2129-37.

Inouye S, Noguchi M, Sakaki Y, Takagi Y, Miyata T, Iwanaga S, *et al.* Cloning and sequence analysis of cDNA for the luminescent protein aequorin. *Proc Natl Acad Sci U S A* 1985; 82(10): 3154-8.

Ivanov AI, Malkov AE, Waseem T, Mukhtarov M, Buldakova S, Gubkina O, *et al.* Glycolysis and oxidative phosphorylation in neurons and astrocytes during network activity in hippocampal slices. *J Cereb Blood Flow Metab* 2014; 34(3): 397-407.

Javadov S, Choi A, Rajapurohitam V, Zeidan A, Basnakian AG, Karmazyn M. NHE-1 inhibition-induced cardioprotection against ischaemia/reperfusion is associated with attenuation of the mitochondrial permeability transition. *Cardiovasc Res* 2008; 77(2): 416-24.

Javadov SA, Clarke S, Das M, Griffiths EJ, Lim KH, Halestrap AP. Ischaemic preconditioning inhibits opening of mitochondrial permeability transition pores in the reperfused rat heart. *J Physiol* 2003; 549(Pt 2): 513-24.

Jiang D, Zhao L, Clapham DE. Genome-wide RNAi screen identifies Letm1 as a mitochondrial Ca²⁺/H⁺ antiporter. *Science* 2009; 326(5949): 144-7.

Jiang M, Chen G. High Ca²⁺-phosphate transfection efficiency in low-density neuronal cultures. *Nat Protoc* 2006; 1(2): 695-700.

Johnson N, Khan A, Virji S, Ward JM, Crompton M. Import and processing of heart mitochondrial cyclophilin D. *Eur J Biochem* 1999; 263(2): 353-9.

Jones RA, Smail A, Wilson MR. Detecting mitochondrial permeability transition by confocal imaging of intact cells pinocytically loaded with calcein. *Eur J Biochem* 2002; 269(16): 3990-7.

Jouaville LS, Pinton P, Bastianutto C, Rutter GA, Rizzuto R. Regulation of mitochondrial ATP synthesis by calcium: evidence for a long-term metabolic priming. *Proc Natl Acad Sci U S A* 1999; 96(24): 13807-12.

Kamer KJ, Mootha VK. MICU1 and MICU2 play nonredundant roles in the regulation of the mitochondrial calcium uniporter. *EMBO Rep* 2014; 15(3): 299-307.

Karmazyn M, Sostaric JV, Gan XT. The myocardial Na⁺/H⁺ exchanger: a potential therapeutic target for the prevention of myocardial ischaemic and reperfusion injury and attenuation of postinfarction heart failure. *Drugs* 2001; 61(3): 375-89.

Keelan J, Vergun O, Duchen MR. Excitotoxic mitochondrial depolarisation requires both calcium and nitric oxide in rat hippocampal neurons. *J Physiol* 1999; 520 Pt 3: 797-813.

Kelman Z. PCNA: structure, functions and interactions. *Oncogene* 1997; 14(6): 629-40.

Kendall JM, Dormer RL, Campbell AK. Targeting aequorin to the endoplasmic reticulum of living cells. *Biochem Biophys Res Commun* 1992a; 189(2): 1008-16.

Kendall JM, Sala-Newby G, Ghalaut V, Dormer RL, Campbell AK. Engineering the CA(2+)-activated photoprotein aequorin with reduced affinity for calcium. *Biochem Biophys Res Commun* 1992b; 187(2): 1091-7.

Kerr JF, Wyllie AH, Currie AR. Apoptosis: a basic biological phenomenon with wide-ranging implications in tissue kinetics. *Br J Cancer* 1972; 26(4): 239-57.

Kerr PM, Suleiman MS, Halestrap AP. Reversal of permeability transition during recovery of hearts from ischemia and its enhancement by pyruvate. *Am J Physiol* 1999; 276(2 Pt 2): H496-502.

Khaliulin I, Clarke SJ, Lin H, Parker J, Suleiman MS, Halestrap AP. Temperature preconditioning of isolated rat hearts--a potent cardioprotective mechanism involving a reduction in oxidative stress and inhibition of the mitochondrial permeability transition pore. *J Physiol* 2007; 581(Pt 3): 1147-61.

Khaspekov L, Friberg H, Halestrap A, Viktorov I, Wieloch T. Cyclosporin A and its nonimmunosuppressive analogue N-Me-Val-4-cyclosporin A mitigate glucose/oxygen deprivation-induced damage to rat cultured hippocampal neurons. *Eur J Neurosci* 1999; 11(9): 3194-8.

Kim TK, Eberwine JH. Mammalian cell transfection: the present and the future. *Anal Bioanal Chem* 2010; 397(8): 3173-8.

Kinnally KW, Campo ML, Tedeschi H. Mitochondrial channel activity studied by patch-clamping mitoplasts. *J Bioenerg Biomembr* 1989; 21(4): 497-506.

Kinnally KW, Peixoto PM, Ryu SY, Dejean LM. Is mPTP the gatekeeper for necrosis, apoptosis, or both? *Biochim Biophys Acta* 2011; 1813(4): 616-22.

Kinnally KW, Zorov DB, Antonenko YN, Snyder SH, McEnery MW, Tedeschi H. Mitochondrial benzodiazepine receptor linked to inner membrane ion channels by nanomolar actions of ligands. *Proc Natl Acad Sci U S A* 1993; 90(4): 1374-8.

Kirichok Y, Krapivinsky G, Clapham DE. The mitochondrial calcium uniporter is a highly selective ion channel. *Nature* 2004; 427(6972): 360-4.

Kokoszka JE, Waymire KG, Levy SE, Sligh JE, Cai J, Jones DP, *et al.* The ADP/ATP translocator is not essential for the mitochondrial permeability transition pore. *Nature* 2004; 427(6973): 461-5.

Kottke M, Adam V, Riesinger I, Bremm G, Bosch W, Brdiczka D, *et al.* Mitochondrial boundary membrane contact sites in brain: points of hexokinase and creatine kinase location, and control of Ca²⁺ transport. *Biochim Biophys Acta* 1988; 935(1): 87-102.

Kovács-Bogdán E, Sancak Y, Kamer KJ, Plovanich M, Jambhekar A, Huber RJ, *et al.* Reconstitution of the mitochondrial calcium uniporter in yeast. *Proc Natl Acad Sci U S A* 2014; 111(24): 8985-90.

Krauskopf A, Eriksson O, Craigen WJ, Forte MA, Bernardi P. Properties of the permeability transition in VDAC1(-/-) mitochondria. *Biochim Biophys Acta* 2006; 1757(5-6): 590-5.

Krauss S, Zhang CY, Lowell BB. The mitochondrial uncoupling-protein homologues. *Nat Rev Mol Cell Biol* 2005; 6(3): 248-61.

Kristal BS, Stavrovskaya IG, Narayanan MV, Krasnikov BF, Brown AM, Beal MF, *et al.* The mitochondrial permeability transition as a target for neuroprotection. *J Bioenerg Biomembr* 2004; 36(4): 309-12.

Kukat C, Wurm CA, Spåhr H, Falkenberg M, Larsson NG, Jakobs S. Super-resolution microscopy reveals that mammalian mitochondrial nucleoids have a uniform size and frequently contain a single copy of mtDNA. *Proc Natl Acad Sci U S A* 2011; 108(33): 13534-9.

Kume S, Saneyoshi T, Mikoshiba K. Desensitization of IP3-induced Ca²⁺ release by overexpression of a constitutively active Gqalpha protein converts ventral to dorsal fate in *Xenopus* early embryos. *Dev Growth Differ* 2000; 42(4): 327-35.

Kwong JQ, Davis J, Baines CP, Sargent MA, Karch J, Wang X, *et al.* Genetic deletion of the mitochondrial phosphate carrier desensitizes the mitochondrial permeability transition pore and causes cardiomyopathy. *Cell Death Differ* 2014; 21(8): 1209-17.

Kwong JQ, Lu X, Correll RN, Schwanekamp JA, Vagnozzi RJ, Sargent MA, *et al.* The Mitochondrial Calcium Uniporter Selectively Matches Metabolic Output to Acute Contractile Stress in the Heart. *Cell Rep* 2015; 12(1): 15-22.

Lam SS, Martell JD, Kamer KJ, Deerinck TJ, Ellisman MH, Mootha VK, *et al.* Directed evolution of APEX2 for electron microscopy and proximity labeling. *Nat Methods* 2015; 12(1): 51-4.

Lasorsa FM, Pinton P, Palmieri L, Fiermonte G, Rizzuto R, Palmieri F. Recombinant expression of the Ca(2+)-sensitive aspartate/glutamate carrier increases mitochondrial ATP production in agonist-stimulated Chinese hamster ovary cells. *J Biol Chem* 2003; 278(40): 38686-92.

Lawlis VB, Roche TE. Effect of micromolar Ca²⁺ on NADH inhibition of bovine kidney alpha-ketoglutarate dehydrogenase complex and possible role of Ca²⁺ in signal amplification. *Mol Cell Biochem* 1980; 32(3): 147-52.

Leclerc C, Lee M, Webb SE, Moreau M, Miller AL. Calcium transients triggered by planar signals induce the expression of ZIC3 gene during neural induction in *Xenopus*. *Dev Biol* 2003; 261(2): 381-90.

Lee JP, Dunlap B, Rich DH. Synthesis and immunosuppressive activities of conformationally restricted cyclosporin lactam analogues. *Int J Pept Protein Res* 1990; 35(5): 481-94.

Lein, E.S. *et al.* (2007) Genome-wide atlas of gene expression in the adult mouse brain, *Nature* 445: 168-176.

Leist M, Single B, Castoldi AF, Kühnle S, Nicotera P. Intracellular adenosine triphosphate (ATP) concentration: a switch in the decision between apoptosis and necrosis. *J Exp Med* 1997; 185(8): 1481-6.

Lemasters JJ. Modulation of mitochondrial membrane permeability in pathogenesis, autophagy and control of metabolism. *J Gastroenterol Hepatol* 2007; 22 Suppl 1: S31-7.

Lemasters JJ, Nieminen AL. Negative contrast imaging of mitochondria by confocal microscopy. *Biophys J* 1999; 77(3): 1747-50.

Lemasters JJ, Nieminen AL, Qian T, Trost LC, Elmore SP, Nishimura Y, *et al.* The mitochondrial permeability transition in cell death: a common mechanism in necrosis, apoptosis and autophagy. *Biochim Biophys Acta* 1998; 1366(1-2): 177-96.

Leung AW, Varanyuwatana P, Halestrap AP. The mitochondrial phosphate carrier interacts with cyclophilin D and may play a key role in the permeability transition. *J Biol Chem* 2008; 283(39): 26312-23.

Li Z, Okamoto K, Hayashi Y, Sheng M. The importance of dendritic mitochondria in the morphogenesis and plasticity of spines and synapses. *Cell* 2004; 119(6): 873-87.

Liang H, Li WH. Functional compensation by duplicated genes in mouse. *Trends Genet* 2009; 25(10): 441-2.

Lim D, Fedrizzi L, Tartari M, Zuccato C, Cattaneo E, Brini M, *et al.* Calcium homeostasis and mitochondrial dysfunction in striatal neurons of Huntington disease. *J Biol Chem* 2008; 283(9): 5780-9.

Logan CV, Szabadkai G, Sharpe JA, Parry DA, Torelli S, Childs AM, *et al.* Loss-of-function mutations in MICU1 cause a brain and muscle disorder linked to primary alterations in mitochondrial calcium signaling. *Nat Genet* 2014; 46(2): 188-93.

Lohmann C. Calcium signaling and the development of specific neuronal connections. *Prog Brain Res* 2009; 175: 443-52.

Lu X, Kwong JQ, Molkentin JD, Bers DM. Individual Cardiac Mitochondria Undergo Rare Transient Permeability Transition Pore Openings. *Circ Res* 2016; 118(5): 834-41.

Lukyanenko V, Györke I, Subramanian S, Smirnov A, Wiesner TF, Györke S. Inhibition of Ca(2+) sparks by ruthenium red in permeabilized rat ventricular myocytes. *Biophys J* 2000; 79(3): 1273-84.

Luo Y, Bond JD, Ingram VM. Compromised mitochondrial function leads to increased cytosolic calcium and to activation of MAP kinases. *Proc Natl Acad Sci U S A* 1997; 94(18): 9705-10.

Luongo TS, Lambert JP, Yuan A, Zhang X, Gross P, Song J, *et al.* The Mitochondrial Calcium Uniporter Matches Energetic Supply with Cardiac Workload during Stress and Modulates Permeability Transition. *Cell Rep* 2015; 12(1): 23-34.

Macaskill AF, Rinholm JE, Twelvetrees AE, Arancibia-Carcamo IL, Muir J, Fransson A, *et al.* Miro1 is a calcium sensor for glutamate receptor-dependent localization of mitochondria at synapses. *Neuron* 2009; 61(4): 541-55.

Macreadie IG, Novitski CE, Maxwell RJ, John U, Ooi BG, McMullen GL, *et al.* Biogenesis of mitochondria: the mitochondrial gene (*aap1*) coding for mitochondrial ATPase subunit 8 in *Saccharomyces cerevisiae*. *Nucleic Acids Res* 1983; 11(13): 4435-51.

MacVicar TD, Lane JD. Impaired OMA1-dependent cleavage of OPA1 and reduced DRP1 fission activity combine to prevent mitophagy in cells that are dependent on oxidative phosphorylation. *J Cell Sci* 2014; 127(Pt 10): 2313-25.

Mahmood T, Yang PC. Western blot: technique, theory, and trouble shooting. *N Am J Med Sci* 2012; 4(9): 429-34.

Mallilankaraman K, Cardenas C, Doonan PJ, Chandramoorthy HC, Irrinki KM, Golenar T, *et al.* MCUR1 is an essential component of mitochondrial Ca²⁺ uptake that regulates cellular metabolism. *Nature cell biology* 2012a; 14(12).

Mallilankaraman K, Doonan P, Cardenas C, Chandramoorthy HC, Mueller M, Miller R, *et al.* MICU1 Is an Essential Gatekeeper for MCU-Mediated Mitochondrial Ca²⁺ Uptake that Regulates Cell Survival. *Cell* 2012b; 151(3).

Malo N, Hanley JA, Cerquozzi S, Pelletier J, Nadon R. Statistical practice in high-throughput screening data analysis. *Nat Biotechnol* 2006; 24(2): 167-75.

Malouitre S, Dube H, Selwood D, Crompton M. Mitochondrial targeting of cyclosporin A enables selective inhibition of cyclophilin-D and enhanced cytoprotection after glucose and oxygen deprivation. *Biochem J* 2010; 425(1): 137-48.

Mannella CA. Structure and dynamics of the mitochondrial inner membrane cristae. *Biochim Biophys Acta* 2006; 1763(5-6): 542-8.

Maravall M, Mainen ZF, Sabatini BL, Svoboda K. Estimating intracellular calcium concentrations and buffering without wavelength ratioing. *Biophys J* 2000; 78(5): 2655-67.

Marchi S, Pinton P. The mitochondrial calcium uniporter complex: molecular components, structure and physiopathological implications. *J Physiol* 2014; 592(Pt 5): 829-39.

Martell JD, Deerinck TJ, Sancak Y, Poulos TL, Mootha VK, Sosinsky GE, *et al.* Engineered ascorbate peroxidase as a genetically encoded reporter for electron microscopy. *Nat Biotechnol* 2012; 30(11): 1143-8.

Matlib MA, Zhou Z, Knight S, Ahmed S, Choi KM, Krause-Bauer J, *et al.* Oxygen-bridged dinuclear ruthenium amine complex specifically inhibits Ca²⁺ uptake into mitochondria in vitro and in situ in single cardiac myocytes. *J Biol Chem* 1998; 273(17): 10223-31.

- McCormack JG. Effects of spermine on mitochondrial Ca²⁺ transport and the ranges of extramitochondrial Ca²⁺ to which the matrix Ca²⁺-sensitive dehydrogenases respond. *Biochem J* 1989; 264(1): 167-74.
- McCormack JG, England PJ. Ruthenium Red inhibits the activation of pyruvate dehydrogenase caused by positive inotropic agents in the perfused rat heart. *Biochem J* 1983; 214(2): 581-5.
- McEnery MW, Snowman AM, Trifiletti RR, Snyder SH. Isolation of the mitochondrial benzodiazepine receptor: association with the voltage-dependent anion channel and the adenine nucleotide carrier. *Proc Natl Acad Sci U S A* 1992; 89(8): 3170-4.
- Mela L. Inhibition and activation of calcium transport in mitochondria. Effect of lanthanides and local anesthetic drugs. *Biochemistry* 1969; 8(6): 2481-6.
- Mesaeli N, Nakamura K, Zvaritch E, Dickie P, Dziak E, Krause KH, *et al.* Calreticulin is essential for cardiac development. *J Cell Biol* 1999; 144(5): 857-68.
- Mitchell P, Moyle J. Chemiosmotic hypothesis of oxidative phosphorylation. *Nature* 1967; 213(5072): 137-9.
- Montero M, Alonso MT, Carnicero E, Cuchillo-Ibáñez I, Albillos A, García AG, *et al.* Chromaffin-cell stimulation triggers fast millimolar mitochondrial Ca²⁺ transients that modulate secretion. *Nat Cell Biol* 2000; 2(2): 57-61.
- Montero M, Lobatón CD, Hernández-Sanmiguel E, Santodomingo J, Vay L, Moreno A, *et al.* Direct activation of the mitochondrial calcium uniporter by natural plant flavonoids. *Biochem J* 2004; 384(Pt 1): 19-24.
- Moore CB, Guthrie EH, Huang MT, Taxman DJ. Short hairpin RNA (shRNA): design, delivery, and assessment of gene knockdown. *Methods Mol Biol* 2010; 629: 141-58.
- Murphy E, Pan X, Nguyen T, Liu J, Holmström KM, Finkel T. Unresolved questions from the analysis of mice lacking MCU expression. *Biochem Biophys Res Commun* 2014; 449(4): 384-5.
- Murphy MP. How mitochondria produce reactive oxygen species. *Biochem J* 2009; 417(1): 1-13.
- Nakagawa T, Shimizu S, Watanabe T, Yamaguchi O, Otsu K, Yamagata H, *et al.* Cyclophilin D-dependent mitochondrial permeability transition regulates some necrotic but not apoptotic cell death. *Nature* 2005; 434(7033): 652-8.
- Nath R, Raser KJ, Hajimohammadreza I, Wang KK. Thapsigargin induces apoptosis in SH-SY5Y neuroblastoma cells and cerebrocortical cultures. *Biochem Mol Biol Int* 1997; 43(1): 197-205.
- Nazareth W, Yafei N, Crompton M. Inhibition of anoxia-induced injury in heart myocytes by cyclosporin A. *J Mol Cell Cardiol* 1991; 23(12): 1351-4.
- NCBI Gene. 2015. MAP2 microtubule associated protein 2 [Homo sapiens (human)]. [ONLINE] Available at: <http://www.ncbi.nlm.nih.gov/gene/4133>. [Accessed 18 December 15].

Neumann E, Schaefer-Ridder M, Wang Y, Hofschneider PH. Gene transfer into mouse lymphoma cells by electroporation in high electric fields. *EMBO J* 1982; 1(7): 841-5.

Nicchitta CV, Williamson JR. Spermine. A regulator of mitochondrial calcium cycling. *J Biol Chem* 1984; 259(21): 12978-83.

Orrenius S, Zhivotovsky B, Nicotera P. Regulation of cell death: the calcium-apoptosis link. *Nat Rev Mol Cell Biol* 2003; 4(7): 552-65.

Ottolini D, Cali T, Brini M. Methods to measure intracellular Ca²⁺ fluxes with organelle-targeted aequorin-based probes. *Methods Enzymol* 2014; 543: 21-45.

Paddison PJ, Caudy AA, Bernstein E, Hannon GJ, Conklin DS. Short hairpin RNAs (shRNAs) induce sequence-specific silencing in mammalian cells. *Genes Dev* 2002; 16(8): 948-58.

Pagliarini DJ, Calvo SE, Chang B, Sheth SA, Vafai SB, Ong SE, *et al.* A mitochondrial protein compendium elucidates complex I disease biology. *Cell* 2008; 134(1): 112-23.

Palma V, Kukuljan M, Mayor R. Calcium mediates dorsoventral patterning of mesoderm in *Xenopus*. *Curr Biol* 2001; 11(20): 1606-10.

Pan X, Liu J, Nguyen T, Liu C, Sun J, Teng Y, *et al.* The physiological role of mitochondrial calcium revealed by mice lacking the mitochondrial calcium uniporter. *Nat Cell Biol* 2013; 15(12): 1464-72.

Panov AV, Lund S, Greenamyre JT. Ca²⁺-induced permeability transition in human lymphoblastoid cell mitochondria from normal and Huntington's disease individuals. *Mol Cell Biochem* 2005; 269(1-2): 143-52.

Patron M, Checchetto V, Raffaello A, Teardo E, Vecellio Reane D, Mantoan M, *et al.* MICU1 and MICU2 finely tune the mitochondrial Ca²⁺ uniporter by exerting opposite effects on MCU activity. *Mol Cell* 2014; 53(5): 726-37.

Paupe V, Prudent J, Dassa EP, Rendon OZ, Shoubridge EA. CCDC90A (MCUR1) Is a Cytochrome c Oxidase Assembly Factor and Not a Regulator of the Mitochondrial Calcium Uniporter. *Cell Metab* 2015; 21(1): 109-16.

Pendin D, Greotti E, Pozzan T. The elusive importance of being a mitochondrial Ca²⁺ uniporter. *Cell Calcium* 2014; 55(3): 139-45.

Perocchi F, Gohil VM, Girgis HS, Bao XR, McCombs JE, Palmer AE, *et al.* MICU1 encodes a mitochondrial EF hand protein required for Ca²⁺ uptake. *Nature* 2010; 467(7313).

Perry SW, Norman JP, Barbieri J, Brown EB, Gelbard HA. Mitochondrial membrane potential probes and the proton gradient: a practical usage guide. *Biotechniques* 2011; 50(2): 98-115.

Petronilli V, Miotto G, Canton M, Brini M, Colonna R, Bernardi P, *et al.* Transient and long-lasting openings of the mitochondrial permeability transition pore can be monitored directly in intact cells by changes in mitochondrial calcein fluorescence. *Biophys J* 1999; 76(2): 725-34.

Petronilli V, Penzo D, Scorrano L, Bernardi P, Di Lisa F. The mitochondrial permeability transition, release of cytochrome c and cell death. Correlation with the duration of pore openings in situ. *J Biol Chem* 2001; 276(15): 12030-4.

Petronilli V, Sileikyte J, Zulian A, Dabbeni-Sala F, Jori G, Gobbo S, *et al.* Switch from inhibition to activation of the mitochondrial permeability transition during hematoporphyrin-mediated photooxidative stress. Unmasking pore-regulating external thiols. *Biochim Biophys Acta* 2009; 1787(7): 897-904.

Petronilli V, Szabò I, Zoratti M. The inner mitochondrial membrane contains ion-conducting channels similar to those found in bacteria. *FEBS Lett* 1989; 259(1): 137-43.

Petrungaro C, Zimmermann KM, Küttner V, Fischer M, Dengjel J, Bogeski I, *et al.* The Ca(2+)-Dependent Release of the Mia40-Induced MICU1-MICU2 Dimer from MCU Regulates Mitochondrial Ca(2+) Uptake. *Cell Metab* 2015.

Pinton P, Giorgi C, Siviero R, Zecchini E, Rizzuto R. Calcium and apoptosis: ER-mitochondria Ca²⁺ transfer in the control of apoptosis. *Oncogene* 2008; 27(50): 6407-18.

Pinton P, Pozzan T, Rizzuto R. The Golgi apparatus is an inositol 1,4,5-trisphosphate-sensitive Ca²⁺ store, with functional properties distinct from those of the endoplasmic reticulum. *EMBO J* 1998; 17(18): 5298-308.

Pivovarova NB, Nguyen HV, Winters CA, Brantner CA, Smith CL, Andrews SB. Excitotoxic calcium overload in a subpopulation of mitochondria triggers delayed death in hippocampal neurons. *J Neurosci* 2004; 24(24): 5611-22.

Plovanich M, Bogorad RL, Sancak Y, Kamer KJ, Strittmatter L, Li AA, *et al.* MICU2, a paralog of MICU1, resides within the mitochondrial uniporter complex to regulate calcium handling. *PLoS One* 2013; 8(2): e55785.

Poenie M, Alderton J, Tsien RY, Steinhardt RA. Changes of free calcium levels with stages of the cell division cycle. *Nature* 1985; 315(6015): 147-9.

Prasher D, McCann RO, Cormier MJ. Cloning and expression of the cDNA coding for aequorin, a bioluminescent calcium-binding protein. *Biochem Biophys Res Commun* 1985; 126(3): 1259-68.

Pressman BC. Biological applications of ionophores. *Annu Rev Biochem* 1976; 45: 501-30.

Prudent J, Popgeorgiev N, Bonneau B, Thibaut J, Gadet R, Lopez J, *et al.* Bcl-wav and the mitochondrial calcium uniporter drive gastrula morphogenesis in zebrafish. *Nat Commun* 2013; 4: 2330.

Qiu J, Tan YW, Hagenston AM, Martel MA, Kneisel N, Skehel PA, *et al.* Mitochondrial calcium uniporter Mcu controls excitotoxicity and is transcriptionally repressed by neuroprotective nuclear calcium signals. *Nat Commun* 2013; 4: 2034.

Quintanilla RA, Jin YN, von Bernhardi R, Johnson GV. Mitochondrial permeability transition pore induces mitochondria injury in Huntington disease. *Mol Neurodegener* 2013; 8: 45.

Raffaello A, De Stefani D, Sabbadin D, Teardo E, Merli G, Picard A, *et al.* The mitochondrial calcium uniporter is a multimer that can include a dominant-negative pore-forming subunit. *EMBO J* 2013; 32(17): 2362-76.

Rasola A, Bernardi P. Mitochondrial permeability transition in Ca²⁺-dependent apoptosis and necrosis. *Cell Calcium* 2011; 50(3): 222-33.

Recillas-Targa F. Multiple strategies for gene transfer, expression, knockdown, and chromatin influence in mammalian cell lines and transgenic animals. *Mol Biotechnol* 2006; 34(3): 337-54.

Reed DR, Lawler MP, Tordoff MG. Reduced body weight is a common effect of gene knockout in mice. *BMC Genet* 2008; 9: 4.

Reinhard E, Yokoe H, Niebling KR, Allbritton NL, Kuhn MA, Meyer T. Localized calcium signals in early zebrafish development. *Dev Biol* 1995; 170(1): 50-61.

Reitzer LJ, Wice BM, Kennell D. Evidence that glutamine, not sugar, is the major energy source for cultured HeLa cells. *J Biol Chem* 1979; 254(8): 2669-76.

Rich PR. The molecular machinery of Keilin's respiratory chain. *Biochem Soc Trans* 2003; 31(Pt 6): 1095-105.

Ridgway EB, Ashley CC. Calcium transients in single muscle fibers. *Biochem Biophys Res Commun* 1967; 29(2): 229-34.

Ringer S. A third contribution regarding the Influence of the Inorganic Constituents of the Blood on the Ventricular Contraction. *J Physiol* 1883; 4(2-3): 222-5.

Rizzuto R, Pozzan T. Microdomains of intracellular Ca²⁺: molecular determinants and functional consequences. *Physiol Rev* 2006; 86(1): 369-408.

Rizzuto R, Simpson AW, Brini M, Pozzan T. Rapid changes of mitochondrial Ca²⁺ revealed by specifically targeted recombinant aequorin. *Nature* 1992; 358(6384): 325-7.

Rodríguez-Enriquez S, He L, Lemasters JJ. Role of mitochondrial permeability transition pores in mitochondrial autophagy. *Int J Biochem Cell Biol* 2004; 36(12): 2463-72.

Rodríguez LC, Araujo CR, Posleman SE, Rey MeR. Hepatotoxic effect of cyclosporin A in the mitochondrial respiratory chain. *J Appl Toxicol* 2007; 27(4): 310-7.

Rogers TB, Inesi G, Wade R, Lederer WJ. Use of thapsigargin to study Ca²⁺ homeostasis in cardiac cells. *Biosci Rep* 1995; 15(5): 341-9.

Ross MF, Kelso GF, Blaikie FH, James AM, Cochemé HM, Filipovska A, *et al.* Lipophilic triphenylphosphonium cations as tools in mitochondrial bioenergetics and free radical biology. *Biochemistry (Mosc)* 2005; 70(2): 222-30.

Rouzier C, Bannwarth S, Chaussonot A, Chevrollier A, Verschueren A, Bonello-Palot N, *et al.* The MFN2 gene is responsible for mitochondrial DNA instability and optic atrophy 'plus' phenotype. *Brain* 2012; 135(Pt 1): 23-34.

Rueda CB, Traba J, Amigo I, Llorente-Folch I, González-Sánchez P, Pardo B, *et al.* Mitochondrial ATP-Mg/Pi carrier S_{Ca}MC-3/Slc25a23 counteracts PARP-1-dependent fall in mitochondrial ATP caused by excitotoxic insults in neurons. *J Neurosci* 2015; 35(8): 3566-81.

Salet C, Moreno G, Ricchelli F, Bernardi P. Singlet oxygen produced by photodynamic action causes inactivation of the mitochondrial permeability transition pore. *J Biol Chem* 1997; 272(35): 21938-43.

Sancak Y, Markhard AL, Kitami T, Kovács-Bogdán E, Kamer KJ, Udeshi ND, *et al.* EMRE is an essential component of the mitochondrial calcium uniporter complex. *Science* 2013; 342(6164): 1379-82.

Santo-Domingo J, Vay L, Hernández-Sanmiguel E, Lobatón CD, Moreno A, Montero M, *et al.* The plasma membrane Na⁺/Ca²⁺ exchange inhibitor KB-R7943 is also a potent inhibitor of the mitochondrial Ca²⁺ uniporter. *Br J Pharmacol* 2007; 151(5): 647-54.

Saotome M, Safiulina D, Szabadkai G, Das S, Fransson A, Aspenstrom P, *et al.* Bidirectional Ca²⁺-dependent control of mitochondrial dynamics by the Miro GTPase. *Proc Natl Acad Sci U S A* 2008; 105(52): 20728-33.

Sariyer IK. Transfection of neuronal cultures. *Methods Mol Biol* 2013; 1078: 133-9.

Satrústegui J, Contreras L, Ramos M, Marmol P, del Arco A, Saheki T, *et al.* Role of aralar, the mitochondrial transporter of aspartate-glutamate, in brain N-acetylaspartate formation and Ca(2+) signaling in neuronal mitochondria. *J Neurosci Res* 2007; 85(15): 3359-66.

Sattler R, Xiong Z, Lu WY, Hafner M, MacDonald JF, Tymianski M. Specific coupling of NMDA receptor activation to nitric oxide neurotoxicity by PSD-95 protein. *Science* 1999; 284(5421): 1845-8.

Savino C, Pelicci P, Giorgio M. The P66Shc/mitochondrial permeability transition pore pathway determines neurodegeneration. *Oxid Med Cell Longev* 2013; 2013: 719407.

Schinzel AC, Takeuchi O, Huang Z, Fisher JK, Zhou Z, Rubens J, *et al.* Cyclophilin D is a component of mitochondrial permeability transition and mediates neuronal cell death after focal cerebral ischemia. *Proc Natl Acad Sci U S A* 2005; 102(34): 12005-10.

Sen GL, Blau HM. A brief history of RNAi: the silence of the genes. *FASEB J* 2006; 20(9): 1293-9.

Sengupta P. The Laboratory Rat: Relating Its Age With Human's. *Int J Prev Med* 2013; 4(6): 624-30.

Shanmughapriya S, Rajan S, Hoffman NE, Higgins AM, Tomar D, Nemani N, *et al.* SPG7 Is an Essential and Conserved Component of the Mitochondrial Permeability Transition Pore. *Mol Cell* 2015; 60(1): 47-62.

SHIMOMURA O, JOHNSON FH, SAIGA Y. Extraction, purification and properties of aequorin, a bioluminescent protein from the luminous hydromedusan, Aequorea. *J Cell Comp Physiol* 1962; 59: 223-39.

Shimomura O, Musicki B, Kishi Y, Inouye S. Light-emitting properties of recombinant semi-synthetic aequorins and recombinant fluorescein-conjugated aequorin for measuring cellular calcium. *Cell Calcium* 1993; 14(5): 373-8.

- Šileikytė, J., Blachly-Dyson, E., Sewell, R., Carpi, A., Menabò, R., Di Lisa, F., . . . Forte, M. (2014). Regulation of the mitochondrial permeability transition pore by the outer membrane does not involve the peripheral benzodiazepine receptor (Translocator Protein of 18 kDa (TSPO)). *J Biol Chem*, 289(20), 13769-13781. doi:10.1074/jbc.M114.549634
- Smith, R. A., Porteous, C. M., Gane, A. M., & Murphy, M. P. (2003). Delivery of bioactive molecules to mitochondria in vivo. *Proc Natl Acad Sci U S A*, 100(9), 5407-5412. doi:10.1073/pnas.0931245100
- Stacey, G., (2006) Primary Cell Cultures and Immortal Cell Lines. In: eLS. John Wiley & Sons Ltd, Chichester. Available at: <http://www.els.net/WileyCDA/ElsArticle/refId-a0002564.html> [Accessed 18 December 15]
- Steinhardt RA, Alderton J. Intracellular free calcium rise triggers nuclear envelope breakdown in the sea urchin embryo. *Nature* 1988; 332(6162): 364-6.
- Stout AK, Raphael HM, Kanterewicz BI, Klann E, Reynolds IJ. Glutamate-induced neuron death requires mitochondrial calcium uptake. *Nature Neuroscience* 1998; 1(5): 366-73.
- Su KG, Banker G, Bourdette D, Forte M. Axonal degeneration in multiple sclerosis: the mitochondrial hypothesis. *Curr Neurol Neurosci Rep* 2009; 9(5): 411-7.
- Summerton J. Morpholino antisense oligomers: the case for an RNase H-independent structural type. *Biochim Biophys Acta* 1999; 1489(1): 141-58.
- Supnet C, Bezprozvanny I. The dysregulation of intracellular calcium in Alzheimer disease. *Cell Calcium* 2010; 47(2): 183-9.
- Swerdlow RH, Burns JM, Khan SM. The Alzheimer's disease mitochondrial cascade hypothesis. *J Alzheimers Dis* 2010; 20 Suppl 2: S265-79.
- Szabadkai G, Duchen MR. Mitochondria: the hub of cellular Ca²⁺ signaling. *Physiology (Bethesda)* 2008; 23: 84-94.
- Szabadkai G, Chinopoulos C. What Makes You Can Also Break You, Part II: Mitochondrial Permeability Transition Pore Formation by Dimers of the F1FO ATP-Synthase? *Front Oncol* 2013; 3:140
- Szabó I, Zoratti M. The giant channel of the inner mitochondrial membrane is inhibited by cyclosporin A. *J Biol Chem* 1991; 266(6): 3376-9.
- Szalai G, Krishnamurthy R, Hajnóczky G. Apoptosis driven by IP(3)-linked mitochondrial calcium signals. *EMBO J* 1999; 18(22): 6349-61.
- Szydłowska K, Tymianski M. Calcium, ischemia and excitotoxicity. *Cell Calcium* 2010; 47(2): 122-9.
- Takadera T, Ohyashiki T. Apoptotic cell death and CPP32-like activation induced by thapsigargin and their prevention by nerve growth factor in PC12 cells. *Biochim Biophys Acta* 1998; 1401(1): 63-71.
- Tinel H, Cancela JM, Mogami H, Gerasimenko JV, Gerasimenko OV, Tepikin AV, *et al.* Active mitochondria surrounding the pancreatic acinar granule region prevent spreading of inositol trisphosphate-evoked local cytosolic Ca(2+) signals. *EMBO J* 1999; 18(18): 4999-5008.

Tombes RM, Simerly C, Borisy GG, Schatten G. Meiosis, egg activation, and nuclear envelope breakdown are differentially reliant on Ca²⁺, whereas germinal vesicle breakdown is Ca²⁺ independent in the mouse oocyte. *J Cell Biol* 1992; 117(4): 799-811.

Tosatto A, Sommaggio R, Kummerow C, Bentham RB, Blacker TS, *et al.* The mitochondrial calcium uniporter regulates breast cancer progression via HIF-1 α . *EMBO Mol. Med.* (2016) *In press.*

Traba J, Del Arco A, Duchen MR, Szabadkai G, Satrústegui J. SCaMC-1 promotes cancer cell survival by desensitizing mitochondrial permeability transition via ATP/ADP-mediated matrix Ca²⁺ buffering. *Cell Death Differ* 2012; 19(4): 650-60.

Trenker M, Malli R, Fertschai I, Levak-Frank S, Graier WF. Uncoupling proteins 2 and 3 are fundamental for mitochondrial Ca²⁺ uniport. *Nat Cell Biol* 2007; 9(4): 445-52.

Twig G, Elorza A, Molina AJ, Mohamed H, Wikstrom JD, Walzer G, *et al.* Fission and selective fusion govern mitochondrial segregation and elimination by autophagy. *EMBO J* 2008; 27(2): 433-46.

Tymianski M, Charlton MP, Carlen PL, Tator CH. Source specificity of early calcium neurotoxicity in cultured embryonic spinal neurons. *J Neurosci* 1993; 13(5): 2085-104.

Vandenabeele P, Galluzzi L, Vanden Berghe T, Kroemer G. Molecular mechanisms of necroptosis: an ordered cellular explosion. *Nat Rev Mol Cell Biol* 2010; 11(10): 700-14.

Vander Heiden MG, Cantley LC, Thompson CB. Understanding the Warburg effect: the metabolic requirements of cell proliferation. *Science* 2009; 324(5930): 1029-33.

Vergun O, Keelan J, Khodorov BI, Duchen MR. Glutamate-induced mitochondrial depolarisation and perturbation of calcium homeostasis in cultured rat hippocampal neurones. *J Physiol* 1999; 519 Pt 2: 451-66.

Verstreken P, Ly CV, Venken KJ, Koh TW, Zhou Y, Bellen HJ. Synaptic mitochondria are critical for mobilization of reserve pool vesicles at *Drosophila* neuromuscular junctions. *Neuron* 2005; 47(3): 365-78.

Wadhwa R, Kaul SC, Ikawa Y, Sugimoto Y. Identification of a novel member of mouse hsp70 family. Its association with cellular mortal phenotype. *J Biol Chem* 1993; 268(9): 6615-21.

Waldeck-Weiermair M, Jean-Quartier C, Rost R, Khan MJ, Vishnu N, Bondarenko AI, *et al.* Leucine zipper EF hand-containing transmembrane protein 1 (Letm1) and uncoupling proteins 2 and 3 (UCP2/3) contribute to two distinct mitochondrial Ca²⁺ uptake pathways. *J Biol Chem* 2011; 286(32): 28444-55.

Wang L, Yang X, Li S, Wang Z, Liu Y, Feng J, *et al.* Structural and mechanistic insights into MICU1 regulation of mitochondrial calcium uptake. *EMBO J* 2014; 33(6): 594-604.

Warne J, Pryce G, Hill JM, Shi X, Lennerås F, Puentes F, *et al.* Selective Inhibition of the Mitochondrial Permeability Transition Pore Protects against Neurodegeneration in Experimental Multiple Sclerosis. *J Biol Chem* 2016; 291(9): 4356-73.

Webb SE, Miller AL. Calcium signalling during embryonic development. *Nat Rev Mol Cell Biol* 2003; 4(7): 539-51.

Whitaker M. Calcium and mitosis. *Prog Cell Cycle Res* 1997; 3: 261-9.

Whitaker M. Calcium microdomains and cell cycle control. *Cell Calcium* 2006; 40(5-6): 585-92.

White BC, Sullivan JM, DeGracia DJ, O'Neil BJ, Neumar RW, Grossman LI, *et al.* Brain ischemia and reperfusion: molecular mechanisms of neuronal injury. *J Neurol Sci* 2000; 179(S 1-2): 1-33.

Wiel C, Lallet-Daher H, Gitenay D, Gras B, Le Calvé B, Augert A, *et al.* Endoplasmic reticulum calcium release through ITPR2 channels leads to mitochondrial calcium accumulation and senescence. *Nat Commun* 2014; 5: 3792.

Winklhofer KF, Haass C. Mitochondrial dysfunction in Parkinson's disease. *Biochim Biophys Acta* 2010; 1802(1): 29-44.

Woodfield K, Rück A, Brdiczka D, Halestrap AP. Direct demonstration of a specific interaction between cyclophilin-D and the adenine nucleotide translocase confirms their role in the mitochondrial permeability transition. *Biochem J* 1998; 336 (Pt 2): 287-90.

Woods NM, Cuthbertson KS, Cobbold PH. Repetitive transient rises in cytoplasmic free calcium in hormone-stimulated hepatocytes. *Nature* 1986; 319(6054): 600-2.

Wu Y, Rasmussen TP, Koval OM, Joiner ML, Hall DD, Chen B, *et al.* The mitochondrial uniporter controls fight or flight heart rate increases. *Nat Commun* 2015; 6: 6081.

Xu S, Chisholm AD. *C. elegans* epidermal wounding induces a mitochondrial ROS burst that promotes wound repair. *Dev Cell* 2014; 31(1): 48-60.

Yang D, Oyaizu Y, Oyaizu H, Olsen GJ, Woese CR. Mitochondrial origins. *Proc Natl Acad Sci U S A* 1985; 82(13): 4443-7.

Yoon MJ, Lee AR, Jeong SA, Kim YS, Kim JY, Kwon YJ, *et al.* Release of Ca²⁺ from the endoplasmic reticulum and its subsequent influx into mitochondria trigger celastrol-induced paraptosis in cancer cells. *Oncotarget* 2014; 5(16): 6816-31.

Zamzami N, Kroemer G. The mitochondrion in apoptosis: how Pandora's box opens. *Nat Rev Mol Cell Biol* 2001; 2(1): 67-71.

Zeitelhofer M, Karra D, Vessey JP, Jaskic E, Macchi P, Thomas S, *et al.* High-efficiency transfection of short hairpin RNAs-encoding plasmids into primary hippocampal neurons. *J Neurosci Res* 2009; 87(1): 289-300.

Zinser E, Sperka-Gottlieb CD, Fasch EV, Kohlwein SD, Paltauf F, Daum G. Phospholipid synthesis and lipid composition of subcellular membranes in the unicellular eukaryote *Saccharomyces cerevisiae*. *J Bacteriol* 1991; 173(6): 2026-34.

Zoratti M, De Marchi U, Gulbins E, Szabò I. Novel channels of the inner mitochondrial membrane. *Biochim Biophys Acta* 2009; 1787(5): 351-63.

Zoratti M, Szabó I. Electrophysiology of the inner mitochondrial membrane. *J Bioenerg Biomembr* 1994; 26(5): 543-53.

Zorov DB, Juhaszova M, Sollott SJ. Mitochondrial reactive oxygen species (ROS) and ROS-induced ROS release. *Physiol Rev* 2014; 94(3): 909-50.

Appendix

Appendix 1

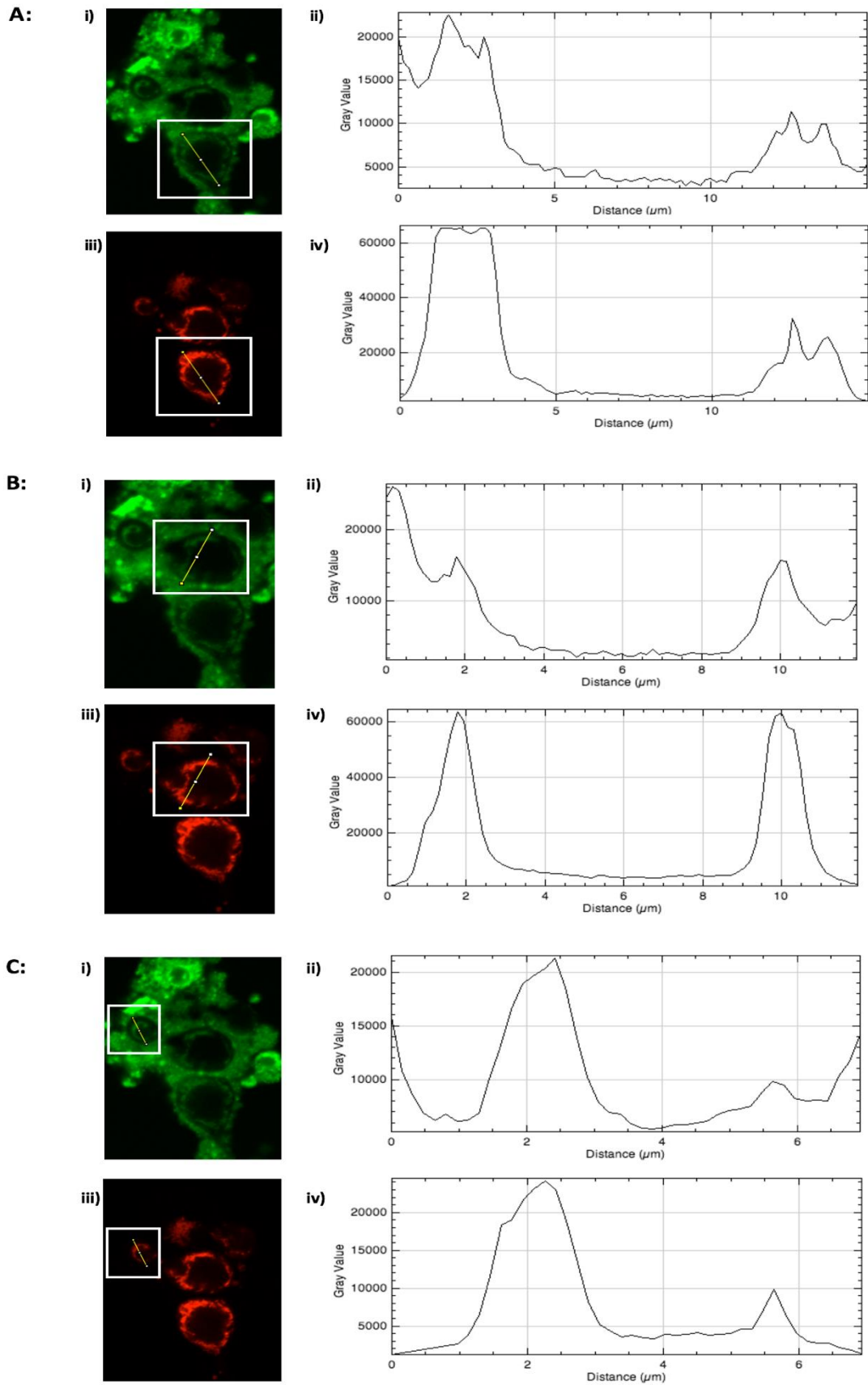


Figure A1 (previous page): Fluorescein-tagged quinolinium co-localised with mitochondria labelled with TMRM in DIV10 rat cortical neurons. A: Colocalization in Cell 1. i) Fluorescein-tagged quinolinium (488nm). Selected cell is highlighted in white box, yellow line represents line profile to be plotted. ii) Line profile plot of fluorescein-tagged quinolinium. iii) TMRM labelled mitochondria (555nm). Selected cell is highlighted in white box, yellow line represents line profile to be plotted. iv) Line profile plot of TMRM labelled mitochondria. B: Colocalization in Cell 2. i) Fluorescein-tagged quinolinium (488nm). Selected cell is highlighted in white box, yellow line represents line profile to be plotted. ii) Line profile plot of fluorescein-tagged quinolinium. iii) TMRM labelled mitochondria (555nm). Selected cell is highlighted in white box, yellow line represents line profile to be plotted. iv) Line profile plot of TMRM labelled mitochondria. C: Colocalization in Cell 3. i) Fluorescein-tagged quinolinium (488nm). Selected cell is highlighted in white box, yellow line represents line profile to be plotted. ii) Line profile plot of fluorescein-tagged quinolinium. iii) TMRM labelled mitochondria (555nm). Selected cell is highlighted in white box, yellow line represents line profile to be plotted. iv) Profile plot of TMRM labelled mitochondria. ImageJ was used to produce line profile intensity plots, using the command “Plot Profile.” In each panel, the intensity profile of the fluorescein tagged quinolinium matches the intensity profile of the TMRM labelled mitochondria.

Appendix 2

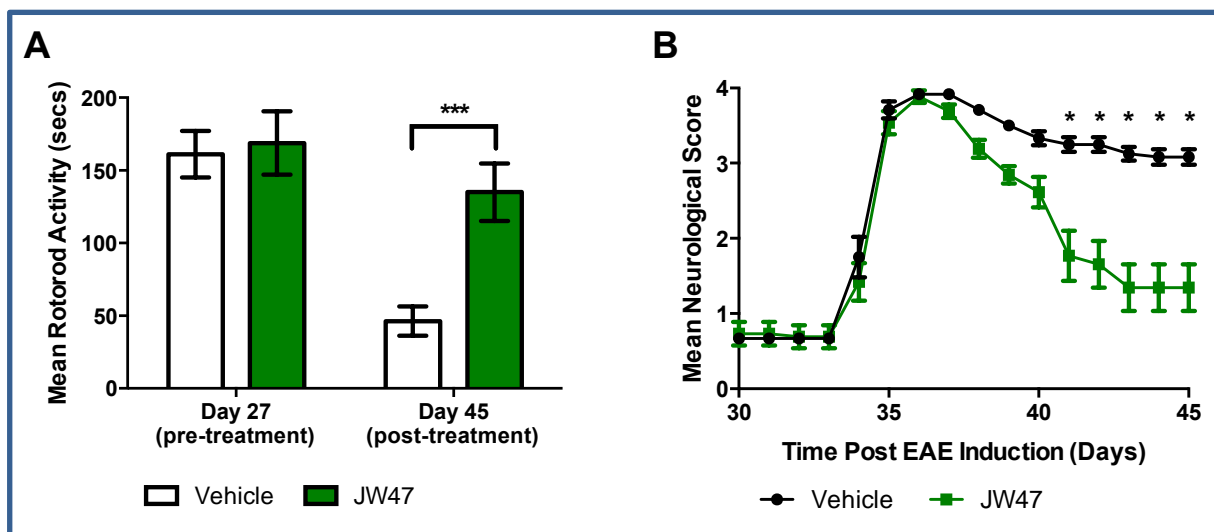


Figure A2: In an experimental autoimmune encephalomyelitis (EAE) mouse model, JW47 significantly prevented deterioration of motor skills and improved neurological clinical score.

A: In mice treated with JW47 (1mg/kg), rotarod performance (time before falling from a rotating bar) was significantly higher than in mice treated with vehicle only. N of 12 (vehicle) and 13 (compound).

B: Treatment with JW47 (1mg/kg) significantly reduced neurological scoring after a relapse (with higher numbers indicating increased severity) in comparison to vehicle treated mice. N of 12 (vehicle) and 13 (compound). *denotes significance, p value <0.001. Error bars are SEM.

Experiments done by, and data used with permission of Dr Gareth Pryce, Queen Mary University.

Appendix 3

Table A1: The NINDS-2 Compound Library

Compound	Plate	Position	Molecular Weight	Therapeutic Use
CARBINOXAMINE MALEATE	001	A02	406.87	anti-histaminic
AMIKACIN SULFATE	001	A03	781.77	anti-bacterial
CETYLPYRIDINIUM CHLORIDE	001	A04	340.00	anti-infective (topical)
AZATHIOPRINE	001	A05	277.27	immunosuppressant anti-neoplastic, anti-rheumatic
beta-CAROTENE	001	A06	536.89	provitamin A
CHLORTHALIDONE	001	A07	338.77	diuretic, anti-hypertensive
CEFOTAXIME SODIUM	001	A08	477.45	anti-bacterial
CHLOROTHIAZIDE	001	A09	295.72	diuretic, anti-hypertensive
CHLORZOXAZONE	001	A10	169.57	muscle relaxant (skeletal)
BETHANECHOL CHLORIDE	001	A11	196.68	cholinergic
ACETAZOLAMIDE	001	B02	222.25	carbonic anhydrase inhibitor, diuretic, anti-glaucoma
AMILORIDE HYDROCHLORIDE	001	B03	266.09	Na ⁺ channel inhibitor, diuretic
AMPHOTERICIN B	001	B04	924.10	antifungal
BACITRACIN	001	B05	1422.73	anti-bacterial
BETAMETHASONE	001	B06	392.47	glucocorticoid, anti-inflammatory
CARBACHOL	001	B07	182.65	cholinergic, miotic
CEPHALOTHIN SODIUM	001	B08	418.43	anti-bacterial
CHLOROXYLENOL	001	B09	156.61	anti-bacterial, topical and urinary antiseptic
CICLOPIROX OLAMINE	001	B10	268.36	antifungal
CLOXACILLIN SODIUM	001	B11	457.87	anti-bacterial
ACETOHYDROXAMIC ACID	001	C02	75.07	urease inhibitor, antiurolithic, anti-bacterial
POTASSIUM p-AMINO BENZOATE	001	C03	175.23	ultraviolet screen

AMPICILLIN SODIUM	001	C04	371.39	anti-bacterial
BACLOFEN	001	C05	213.67	muscle relaxant (skeletal)
CLONIDINE HYDROCHLORIDE	001	C06	266.56	anti-hypertensive
CARBAMAZEPINE	001	C07	236.28	analgesic, anticonvulsant
CEPHAPIRIN SODIUM	001	C08	445.45	anti-bacterial
CHLOROTRIANISENE	001	C09	380.88	estrogen
CINOXACIN	001	C10	262.22	anti-bacterial
CLOXYQUIN	001	C11	179.61	anti-bacterial, antifungal
AMOXICILLIN	001	D02	365.41	anti-bacterial
6-AMINOCAPROIC ACID	001	D03	131.18	hemostatic
AMPROLIUM	001	D04	315.25	coccidiostat
BENSERAZIDE HYDROCHLORIDE	001	D05	293.71	decarboxylase inhibitor
BISACODYL	001	D06	361.40	cathartic
CARBENICILLIN DISODIUM	001	D07	422.37	anti-bacterial
ACETYLCYSTEINE	001	D08	163.20	mucolytic
CHLORPHENIRAMINE (S) MALEATE	001	D09	390.87	anti-histaminic
CLEMASTINE	001	D10	459.97	anti-histaminic
COLCHICINE	001	D11	399.45	anti-mitotic, antigout agent
ADENOSINE	001	E02	267.25	anti-arrhythmic, cardiac depressant
AMINOGLUTETHIMIDE	001	E03	232.28	aromatase inhibitor, anti-neoplastic, testosterone suppressant
ACETAMINOPHEN	001	E04	151.17	analgesic, antipyretic
BENZETHONIUM CHLORIDE	001	E05	448.09	anti-infective (topical)
BITHIONOL	001	E06	400.02	anthelmintic, antiseptic
ANTHRALIN	001	E07	226.23	antipsoriatic
CHLORAMPHENICOL HEMISUCCINATE	001	E08	423.21	anti-bacterial, antirickettsial, inhibits protein synthesis
CHLORPROMAZINE	001	E09	318.87	antiemetic, anti-psychotic
CLIDINIUM BROMIDE	001	E10	432.36	anti-cholinergic

COLISTIMETHATE SODIUM	001	E11	1735.82	anti-bacterial
COTININE	001	F02	176.22	antidepressant
AMINOSALICYLATE SODIUM	001	F03	175.12	anti-bacterial, tuberculostatic
ANTIPYRINE	001	F04	188.23	analgesic
BENZOCAINE	001	F05	165.19	anesthetic (topical)
BUSULFAN	001	F06	246.30	anti-neoplastic, alkylating agent
CARISOPRODOL	001	F07	260.34	muscle relaxant (skeletal)
CHLORAMPHENICOL	001	F08	323.13	anti-bacterial, antirickettsial, inhibits protein synthesis
CHLORPROPAMIDE	001	F09	276.74	anti-diabetic
CLINDAMYCIN HYDROCHLORIDE	001	F10	461.45	anti-bacterial, inhibits protein synthesis
ALLOPURINOL	001	F11	136.11	antihyperuricemia, antigout, antiurolithic
ALVERINE CITRATE	001	G02	473.57	anti-cholinergic
AMITRIPTYLINE HYDROCHLORIDE	001	G03	313.87	antidepressant
APOMORPHINE HYDROCHLORIDE	001	G04	303.79	emetic
BENZTHIAZIDE	001	G05	431.94	diuretic, anti-hypertensive
CAFFEINE	001	G06	194.19	CNS stimulant
CEFADROXIL	001	G07	363.39	anti-bacterial
CHLOROCRESOL	001	G08	142.59	anti-infectant
CHLORTETRACYCLINE HYDROCHLORIDE	001	G09	515.35	anti-bacterial, antiamebic, Ca chelator, hepatotoxic; inhibits protein synthesis
CLOFIBRIC ACID	001	G10	214.65	anti-hyperlipoproteinemic
CORTISONE ACETATE	001	G11	402.49	glucocorticoid
AMANTADINE HYDROCHLORIDE	001	H02	187.71	anti-viral, anti-parkinsonian; treatment of drug-induced extrapyramidal reactions
AMODIAQUINE DIHYDROCHLORIDE	001	H03	428.79	anti-malarial
ATROPINE	001	H04	387.46	anti-cholinergic, mydriatic

BENZTROPINE	001	H05	405.52	anti-cholinergic
1R-CAMPHOR	001	H06	152.24	analgesic, anti-infective, antipruritic
CEFAZOLIN SODIUM	001	H07	476.49	anti-bacterial
CHLOROQUINE DIPHOSPHATE	001	H08	515.87	anti-malarial, antiamebic, anti-rheumatic, intercalating agent
CAPREOMYCIN SULFATE	001	H09	766.80	anti-bacterial, tuberculostatic
CLOMIPHENE CITRATE	001	H10	598.10	gonad stimulating principle
CRESOL	001	H11	108.14	anti-infectant
CROMOLYN SODIUM	002	A02	512.34	antiasthmatic, antiallergy
DEFEROXAMINE MESYLATE	002	A03	656.80	chelating agent (Fe & Al)
DIBUCAINE HYDROCHLORIDE	002	A04	379.93	anesthetic (local)
DIHYDROSTREPTOMYCIN SULFATE	002	A05	681.68	anti-bacterial, tuberculostatic
DISULFIRAM	002	A06	296.54	alcohol antagonist
ESTRADIOL	002	A07	272.39	estrogen
ETHOPROPAZINE HYDROCHLORIDE	002	A08	348.94	anti-parkinsonian, anti-cholinergic
FUSIDIC ACID	002	A09	516.72	anti-bacterial
GUANETHIDINE SULFATE	002	A10	296.39	anti-hypertensive, mitotic agent
HOMATROPINE METHYLBROMIDE	002	A11	370.29	anti-cholinergic (ophthalmic)
CYCLIZINE	002	B02	266.39	H1 antihistamine
SODIUM DEHYDROCHOLATE	002	B03	424.52	choleretic
DICLOFENAC SODIUM	002	B04	318.14	anti-inflammatory
DIMENHYDRINATE	002	B05	469.98	antiemetic
DOPAMINE HYDROCHLORIDE	002	B06	189.64	cardiotonic, anti-hypotensive
ESTRADIOL CYPIONATE	002	B07	396.58	estrogen
EUGENOL	002	B08	164.21	analgesic (topical), antiseptic, antifungal
GALLAMINE TRIETHIODIDE	002	B09	891.54	muscle relaxant (skeletal)
HALAZONE	002	B10	270.09	anti-infectant
HYDRALAZINE HYDROCHLORIDE	002	B11	196.64	anti-hypertensive

CYCLOPENTOLATE HYDROCHLORIDE	002	C02	327.85	mydriatic
DEMECLOCYCLINE HYDROCHLORIDE	002	C03	501.32	anti-bacterial
DICLOXACILLIN SODIUM	002	C04	492.32	anti-bacterial
DIOXYBENZONE	002	C05	244.25	ultraviolet screen
DYCLONINE HYDROCHLORIDE	002	C06	325.88	anesthetic (topical)
ESTRADIOL VALERATE	002	C07	356.51	estrogen
FLUDROCORTISONE ACETATE	002	C08	422.50	mineralocorticoid
GEMFIBROZIL	002	C09	250.34	anti-hyperlipoproteinemic
HALOPERIDOL	002	C10	375.87	antidyskinetic, anti-psychotic
HYDROCHLOROTHIAZIDE	002	C11	297.74	diuretic
CYCLOPHOSPHAMIDE HYDRATE	002	D02	279.10	anti-neoplastic, alkylating agent
DESIPRAMINE HYDROCHLORIDE	002	D03	302.85	antidepressant
DICUMAROL	002	D04	336.30	anti-coagulant
DIPHENHYDRAMINE HYDROCHLORIDE	002	D05	291.82	anti-histaminic
DYPHYLLINE	002	D06	254.25	bronchodilator
ESTRIOL	002	D07	288.39	estrogen
FLUOCINONIDE	002	D08	494.54	anti-inflammatory, glucocorticoid
GENTAMICIN SULFATE	002	D09	575.68	anti-bacterial
HETACILLIN POTASSIUM	002	D10	427.57	anti-bacterial
HYDROCORTISONE ACETATE	002	D11	404.51	glucocorticoid, anti-inflammatory
CYCLOSERINE	002	E02	102.09	anti-bacterial (tuberculostatic)
DEXAMETHASONE ACETATE	002	E03	434.51	glucocorticoid, anti-inflammatory
DIENESTROL	002	E04	266.34	estrogen
DIPHENYLPIRALINE HYDROCHLORIDE	002	E05	317.86	anti-histaminic
TRISODIUM ETHYLENEDIAMINE TETRACETATE	002	E06	361.22	chelating agent, antioxidant

ESTRONE	002	E07	270.37	estrogen
FLUOROURACIL	002	E08	130.08	anti-neoplastic, pyrimidine antimetabolite
GENTIAN VIOLET	002	E09	407.99	anti-bacterial, anthelmintic
HEXACHLOROPHENE	002	E10	406.91	anti-infective (topical)
HYDROFLUMETHIAZIDE	002	E11	331.29	anti-hypertensive, diuretic
CYTARABINE	002	F02	243.22	anti-neoplastic, anti-viral, antimetabolite
DEXAMETHASONE SODIUM PHOSPHATE	002	F03	516.42	glucocorticoid, anti-inflammatory
DIETHYLCARBAMAZINE CITRATE	002	F04	391.42	anthelmintic
DIPYRIDAMOLE	002	F05	504.64	coronary vasodilator
EMETINE	002	F06	553.58	inhibits RNA, DNA and protein synthesis
ETHAMBUTOL HYDROCHLORIDE	002	F07	277.24	anti-bacterial (tuberculostatic)
FLURBIPROFEN	002	F08	244.27	anti-inflammatory, analgesic
GLUCOSAMINE HYDROCHLORIDE	002	F09	215.64	antiarthritic
HEXYLRESORCINOL	002	F10	194.28	anthelmintic, topical antiseptic
HYDROXYPROGESTERONE CAPROATE	002	F11	428.62	progestogen
DANAZOL	002	G02	337.47	anterior pituitary suppressant
DEXTROMETHORPHAN HYDROBROMIDE	002	G03	352.32	antitussive
DIFLUNISAL	002	G04	250.20	analgesic, anti-inflammatory
PYRITHIONE ZINC	002	G05	319.70	anti-bacterial, antifungal, antiseborrheic
ADRENALINE BITARTRATE	002	G06	333.30	adrenergic agonist, bronchodilator, antiglaucoma agent
ETHINYL ESTRADIOL	002	G07	296.41	estrogen, plus progestogen as oral contraceptive
FURAZOLIDONE	002	G08	225.16	anti-bacterial
GUAIFENESIN	002	G09	198.22	expectorant
HISTAMINE	002	G10	184.07	H receptor agonist, induces edema in mammalian tissues; gastric secretion

DIHYDROCHLORIDE				stimulant
HYDROXYUREA	002	G11	76.06	anti-neoplastic, inhibits ribonucleoside diphosphate reductase
DAPSONE	002	H02	248.31	anti-bacterial, leprostatic, dermatitis herpetiformis suppressant
DIBENZOTHIOPHENE	002	H03	184.26	keratolytic
DIGOXIN	002	H04	780.96	cardiac stimulant
DISOPYRAMIDE PHOSPHATE	002	H05	437.48	anti-arrhythmic
ERGONOVINE MALEATE	002	H06	441.49	oxytocic, 5HT antagonist
ETHIONAMIDE	002	H07	166.25	anti-bacterial, tuberculostatic
FUROSEMIDE	002	H08	330.75	diuretic, anti-hypertensive
GUANABENZ ACETATE	002	H09	291.14	anti-hypertensive
HOMATROPINE BROMIDE	002	H10	356.26	anti-cholinergic (ophthalmic)
HYDROXYZINE PAMOATE	002	H11	763.29	anxiolytic, anti-histaminic
DIGITOXIN	003	A02	764.96	inotropic, cardiotoxic
ISONIAZID	003	A03	137.14	anti-bacterial, tuberculostatic
LEVONORDEFIN	003	A04	183.21	vasoconstrictor
MEDROXYPROGESTERONE ACETATE	003	A05	386.54	contraceptive
METHOCARBAMOL	003	A06	241.25	muscle relaxant (skeletal)
MICONAZOLE NITRATE	003	A07	479.15	antifungal (topical)
NEOSTIGMINE BROMIDE	003	A08	303.20	cholinergic
NORETHYNODREL	003	A09	298.43	progestogen, in combination with estrogen as oral contraceptive
ORPHENADRINE CITRATE	003	A10	461.52	muscle relaxant (skeletal), anti-histaminic
PENICILLAMINE	003	A11	149.21	chelating agent (Cu), anti-rheumatic
HYOSCYAMINE	003	B02	289.38	anti-cholinergic, analgesic
ISOPROPAMIDE IODIDE	003	B03	480.44	anti-cholinergic
LINCOMYCIN HYDROCHLORIDE	003	B04	443.01	anti-bacterial
MEDRYSONE	003	B05	344.50	glucocorticoid

METHOTREXATE	003	B06	454.45	anti-neoplastic, anti-rheumatic, folic acid antagonist
MINOXIDIL	003	B07	209.25	anti-hypertensive, antialopecia agent
NIACIN	003	B08	123.11	antihyperlipidemic, vitamin (enzyme cofactor)
NORFLOXACIN	003	B09	319.34	anti-bacterial
OXACILLIN SODIUM	003	B10	423.43	anti-bacterial
BENZYL PENICILLIN POTASSIUM	003	B11	372.49	anti-bacterial
IBUPROFEN	003	C02	206.29	anti-inflammatory
ISOPROTERENOL HYDROCHLORIDE	003	C03	247.72	bronchodilator
MAFENIDE HYDROCHLORIDE	003	C04	222.69	anti-bacterial
MEGESTROL ACETATE	003	C05	384.52	progestogen, anti-neoplastic
METHOXSALEN	003	C06	216.20	antipsoriatic, pigmentation agent
MOXALACTAM DISODIUM	003	C07	564.44	anti-bacterial
NIFEDIPINE	003	C08	346.34	antianginal, anti-hypertensive
NORGESTREL	003	C09	312.46	progestogen
OXYBENZONE	003	C10	228.25	ultraviolet screen
PHENAZOPYRIDINE HYDROCHLORIDE	003	C11	249.70	analgesic
IMIPRAMINE HYDROCHLORIDE	003	D02	316.88	antidepressant
ISOSORBIDE DINITRATE	003	D03	236.14	antianginal
MAPROTILINE HYDROCHLORIDE	003	D04	313.87	antidepressant
MEPENZOLATE BROMIDE	003	D05	420.35	anti-cholinergic
METHSCOPOLAMINE BROMIDE	003	D06	398.30	anti-cholinergic
NAFCILLIN SODIUM	003	D07	436.47	anti-bacterial
NITROFURANTOIN	003	D08	238.16	anti-bacterial
NORTRIPTYLINE	003	D09	263.39	antidepressant
OXYMETAZOLINE	003	D10	296.84	adrenergic agonist, nasal decongestant

HYDROCHLORIDE				
PHENELZINE SULFATE	003	D11	234.28	antidepressant
INDAPAMIDE	003	E02	365.84	diuretic, anti-hypertensive
ISOXSUPRINE HYDROCHLORIDE	003	E03	337.85	vasodilator
MECAMYLAMINE HYDROCHLORIDE	003	E04	203.76	anti-hypertensive
MERCAPTOPYRINE	003	E05	152.18	anti-neoplastic, purine antimetabolite
METHYLDOPA	003	E06	211.22	anti-hypertensive
NALOXONE HYDROCHLORIDE	003	E07	363.84	narcotic antagonist
NITROFURAZONE	003	E08	198.14	anti-infective (topical)
NOSCAPINE HYDROCHLORIDE	003	E09	449.89	antitussive
OXYQUINOLINE HEMISULFATE	003	E10	243.24	anti-infectant
PHENINDIONE	003	E11	222.25	anti-coagulant
INDOMETHACIN	003	F02	357.80	anti-inflammatory, antipyretic, analgesic
KANAMYCIN SULFATE	003	F03	582.59	anti-bacterial
MECHLORETHAMINE	003	F04	156.06	anti-neoplastic, alkylating agent
METAPROTERENOL	003	F05	211.26	bronchodilator
METOCLOPRAMIDE HYDROCHLORIDE	003	F06	336.26	antiemetic
NAPHAZOLINE HYDROCHLORIDE	003	F07	246.74	adrenergic agonist, nasal decongestant
NITROMIDE	003	F08	211.14	anti-bacterial, coccidiostat
NOVOBIOCIN SODIUM	003	F09	634.62	anti-bacterial
OXYTETRACYCLINE	003	F10	496.91	anti-bacterial
1S,2R- PHENYLPROPANOLAMINE HYDROCHLORIDE	003	F11	187.67	decongestant, anorexic
INDOPROFEN	003	G02	281.31	analgesic, anti-inflammatory
KETOCONAZOLE	003	G03	531.44	antifungal
MECLIZINE HYDROCHLORIDE	003	G04	463.88	antiemetic
METHENAMINE	003	G05	140.19	anti-bacterial (urinary)

METOPROLOL TARTRATE	003	G06	417.46	anti-hypertensive, antianginal
NAPROXEN(+)	003	G07	230.27	anti-inflammatory, analgesic, antipyretic
NOREPINEPHRINE	003	G08	169.18	adrenergic agonist, anti-hypotensive
NYLIDRIN HYDROCHLORIDE	003	G09	335.88	vasodilator (peripheral)
PAPAVERINE HYDROCHLORIDE	003	G10	375.86	muscle relaxant (smooth), cerebral vasodilator
PHENYTOIN SODIUM	003	G11	274.26	anticonvulsant, antiepileptic
IDOQUINOL	003	H02	396.96	antiamebic
LEUCOVORIN CALCIUM	003	H03	511.51	antianemic, antidote to folic acid antagonists
MECLOFENAMATE SODIUM	003	H04	318.14	anti-inflammatory, antipyretic
METHIMAZOLE	003	H05	114.17	antihyperthyroid
METRONIDAZOLE	003	H06	171.16	anti-protozoal
NEOMYCIN SULFATE	003	H07	712.73	anti-bacterial
NORETHINDRONE ACETATE	003	H08	340.47	Oral contraceptive (in combination with estrogen)
NYSTATIN	003	H09	926.12	antifungal, binds to membrane sterols
PARACHLOROPHENOL	003	H10	128.56	topical anti-bacterial (topical)
PHYSOSTIGMINE SALICYLATE	003	H11	413.48	cholinergic, anticholinesterase, miotic
PILOCARPINE NITRATE	004	A02	271.28	antiglaucoma agent, miotic
DEXPROPRANOLOL HYDROCHLORIDE	004	A03	295.81	anti-hypertensive, antianginal, anti- arrhythmic
RIFAMPIN	004	A04	822.96	anti-bacterial (tuberculostatic)
STREPTOZOSIN	004	A05	265.22	anti-neoplastic, alkylating agent
SULFATHIAZOLE	004	A06	255.32	anti-bacterial
TOLBUTAMIDE	004	A07	270.35	anti-diabetic
TRIFLUOPERAZINE HYDROCHLORIDE	004	A08	480.43	anti-psychotic
TRYPTOPHAN	004	A09	204.23	antidepressant, nutrient; LD50(rat) 1634 mg/kg ip
ACRIFLAVINIUM HYDROCHLORIDE	004	A10	259.74	anti-infective, intercalating agent
PENTAMIDINE ISETHIONATE	004	A11	592.69	anti-protozoal, inhibits nucleic acid &

				protein synthesis
PIPERAZINE	004	B02	86.14	anthelmintic
PSEUDOEPHEDRINE HYDROCHLORIDE	004	B03	201.70	decongestant
ROXARSONE	004	B04	263.04	anti-bacterial
SULFACETAMIDE	004	B05	214.24	anti-bacterial
SULINDAC	004	B06	356.42	anti-inflammatory
TOLNAFTATE	004	B07	307.42	antifungal
TRIHXYPHENIDYL HYDROCHLORIDE	004	B08	337.94	anti-cholinergic, anti-parkinsonian
TUAMINOHEPTANE SULFATE	004	B09	213.30	adrenergic agonist
BROXYQUINOLINE	004	B10	302.95	anti-infectant, disinfectant
PHENACETIN	004	B11	179.22	analgesic, antipyretic
PRAZIQUANTEL	004	C02	312.42	anthelmintic
PYRANTEL PAMOATE	004	C03	594.69	anthelmintic
SALICYL ALCOHOL	004	C04	124.14	anesthetic (local), anti-inflammatory
SULFADIAZINE	004	C05	250.28	anti-bacterial
TETRACYCLINE HYDROCHLORIDE	004	C06	480.91	anti-bacterial, antiamebic, antirickettsial
TRANLYCYPROMINE SULFATE	004	C07	231.27	antidepressant
TRIMEPRAZINE TARTRATE	004	C08	448.54	antipruritic
TYROTHRIN	004	C09	1272.48	topical anti-bacterial (topical)
CARNITINE HYDROCHLORIDE	004	C10	197.66	anti-hyperlipoproteinemic, gastric/ pancreatic secretion stimulant
PHENYLMERCURIC ACETATE	004	C11	336.74	antifungal
PRIMAQUINE DIPHOSPHATE	004	D02	455.34	anti-malarial
PYRIMETHAMINE	004	D03	248.72	anti-malarial
SCOPOLAMINE HYDROBROMIDE	004	D04	384.27	anti-cholinergic, treatment of motion sickness
SULFAMERAZINE	004	D05	264.31	anti-bacterial
THEOPHYLLINE	004	D06	180.17	bronchodilator
TRIACETIN	004	D07	218.21	antifungal (topical)

TRIMETHOBENZAMIDE HYDROCHLORIDE	004	D08	424.93	antiemetic
URSODIOL	004	D09	392.58	anticholelithogenic; LD50(rat) 890 mg/kg ip
HEXESTROL	004	D10	270.37	estrogen, anti-neoplastic (hormonal)
PREGNENOLONE	004	D11	316.49	glucocorticoid, anti-inflammatory
PROCHLORPERAZINE EDISYLATE	004	E02	564.15	antiemetic, anti-psychotic, treatment of vertigo
QUINACRINE HYDROCHLORIDE	004	E03	472.89	anthelmintic, anti-malarial, intercalating agent
SISOMICIN SULFATE	004	E04	545.61	anti-bacterial, binds to ribosomes
SULFAMETHAZINE	004	E05	278.33	anti-bacterial
THIABENDAZOLE	004	E06	201.25	anthelmintic
TRIAMCINOLONE ACETONIDE	004	E07	434.51	anti-inflammatory
TRIMETHOPRIM	004	E08	290.32	anti-bacterial
VANCOMYCIN HYDROCHLORIDE	004	E09	1484.76	anti-bacterial
HEXETIDINE	004	E10	339.61	antifungal
AZELAIC ACID	004	E11	188.23	antiacne, antiproliferative agent
PROMAZINE HYDROCHLORIDE	004	F02	320.89	anti-psychotic
QUINIDINE GLUCONATE	004	F03	520.58	anti-arrhythmic, anti-malarial
SPECTINOMYCIN HYDROCHLORIDE	004	F04	405.28	anti-bacterial
SULFAMETHOXAZOLE	004	F05	253.28	anti-bacterial, antipneumocystis
THIMEROSAL	004	F06	404.81	anti-infective, preservative
TRIAMCINOLONE DIACETATE	004	F07	478.52	anti-inflammatory
TRIOXSALEN	004	F08	228.25	melanizing agent, antipsoriatic
VIDARABINE	004	F09	267.25	anti-viral
IPRONIAZID SULFATE	004	F10	277.30	monoamine oxidase inhibitor, antidepressant
THEOBROMINE	004	F11	180.17	diuretic, bronchodilator, cardiotonic
PROMETHAZINE	004	G02	320.89	anti-histaminic

HYDROCHLORIDE				
QUININE SULFATE	004	G03	422.50	anti-malarial, skeletal muscle relaxant
SPIRONOLACTONE	004	G04	416.58	diuretic
SULFAPYRIDINE	004	G05	249.29	anti-bacterial
THIOGUANINE	004	G06	167.19	anti-neoplastic, purine antimetabolite
TRIAMTERENE	004	G07	253.27	diuretic
TRIPROLIDINE HYDROCHLORIDE	004	G08	314.86	anti-histaminic
XYLOMETAZOLINE HYDROCHLORIDE	004	G09	280.84	adrenergic agonist, nasal decongestant
MERBROMIN	004	G10	750.66	anti-bacterial
AJMALINE	004	G11	326.44	anti-arrhythmic (Class Ia): inhibits glucose uptake by mitochondria, & PAF blocker
PROPANTHELINE BROMIDE	004	H02	448.40	anti-cholinergic
RESORCINOL	004	H03	110.11	keratolytic, antiseborheic
STREPTOMYCIN SULFATE	004	H04	679.66	anti-bacterial (tuberculostatic)
SULFASALAZINE	004	H05	398.40	anticolitis and Crohn's disease
TIMOLOL MALEATE	004	H06	432.50	betaadrenergic blocker
TRICHLORMETHIAZIDE	004	H07	380.66	diuretic, anti-hypertensive
TROPICAMIDE	004	H08	284.36	anti-cholinergic (ophthalmic)
ZOMEPIRAC SODIUM	004	H09	291.74	analgesic, anti-inflammatory
OCTOPAMINE HYDROCHLORIDE	004	H10	189.64	adrenergic agonist
HYDROQUINIDINE	004	H11	326.44	anti-arrhythmic, anti-malarial
KETOTIFEN FUMARATE	005	A02	425.51	antiasthmatic
MYCOPHENOLIC ACID	005	A03	320.35	anti-neoplastic
KYNURENIC ACID	005	A04	189.17	nutritient in vitamin B deficiency diseases
NEOHESPERIDIN DIHYDROCHALCONE	005	A05	612.59	sweetener
KINETIN	005	A06	215.22	auxin, plant growth regulator, plant cell division promotor

ALTHIAZIDE	005	A07	383.90	diuretic
PALMATINE CHLORIDE	005	A08	387.87	anti-bacterial, uterine contractant
DROPROPIZINE	005	A09	236.32	antitussive
BERBAMINE HYDROCHLORIDE	005	A10	681.66	anti-hypertensive, skeletal muscle relaxant
PROTOPORPHYRIN IX	005	A11	562.67	hepatoprotectant
YOHIMBINE HYDROCHLORIDE	005	B02	390.91	alpha adrenergic blocker, mydriatic, antidepressant
OLEANDOMYCIN PHOSPHATE	005	B03	785.87	anti-bacterial
LIDOCAINE HYDROCHLORIDE	005	B04	270.81	anesthetic (local), anti-arrhythmic
QUERCITRIN	005	B05	448.39	anti-hemorrhagic
NARINGIN	005	B06	580.55	anti-hemorrhagic, anti-inflammatory
BERBERINE CHLORIDE	005	B07	371.82	anti-arrhythmic, alpha2 agonist, cholinesterase, anticonvulsant, anti- inflammatory, anti-bacterial, antifungal, antitrypanosomal, anti-neoplastic, immunostimulant; LD50(mouse) 329 mg/kg po
PIPERINE	005	B08	285.35	analeptic, anti-bacterial
ETODOLAC	005	B09	287.36	anti-inflammatory
FENDILINE HYDROCHLORIDE	005	B10	351.92	coronary vasodilator
NALBUPHINE HYDROCHLORIDE	005	B11	393.91	analgesic, narcotic antagonist
BENFLUOREX HYDROCHLORIDE	005	C02	387.83	anti-hyperlipoproteinemic
OUABAIN	005	C03	584.67	anti-arrhythmic, cardiotonic, hypertensive, Na/K ATPase inhibitor
ACETYL TYROSINE ETHYL ESTER	005	C04	251.28	chymotrypsin substrate
ESERINE	005	C05	275.35	anticholinesterase, miotic, antiglaucoma, cognition activator
BUTAMBEN	005	C06	193.25	anesthetic (local)
CANRENOIC ACID, POTASSIUM SALT	005	C07	396.58	aldosterone antagonist, diuretic
AESCULIN	005	C08	340.29	anti-inflammatory

FENOTEROL HYDROBROMIDE	005	C09	384.27	betaadrenergic agonist
METHACYCLINE HYDROCHLORIDE	005	C10	478.89	anti-bacterial
MEBHYDROLIN NAPHTHALENESULFONATE	005	C11	564.68	H1 antihistamine
SULFANILAMIDE	005	D02	172.21	anti-bacterial
AMINOPTERIN	005	D03	440.42	anti-neoplastic, anti-rheumatic, folic acid antagonist
ACETYLTRYPTOPHANAMIDE	005	D04	245.28	antidepressant, nutrient
XANTHURENIC ACID	005	D05	205.17	caspase activator, guanylyl cyclase stimulant
CEFACLOR	005	D06	367.81	anti-bacterial
HARMALOL HYDROCHLORIDE	005	D07	236.70	anthelmintic, narcotic agent
PROTOVERATRINE B	005	D08	809.96	anti-hypertensive, emetic; LD50(mouse) 0.21 mg/kg sc
FENBUFEN	005	D09	254.29	anti-inflammatory
PUROMYCIN HYDROCHLORIDE	005	D10	544.44	anti-neoplastic, anti-protozoal
MEBEVERINE HYDROCHLORIDE	005	D11	466.02	muscle relaxant (smooth)
STRYCHNINE	005	E02	334.42	central stimulant
ARECOLINE HYDROBROMIDE	005	E03	236.11	anthelmintic (Cestodes), hypotensive, cathartic
N-ACETYLPROLINE	005	E04	157.17	anti-rheumatic
LOBELINE HYDROCHLORIDE	005	E05	373.93	antiasthmatic, respiratory stimulant
IODIPAMIDE	005	E06	627.95	radioopaque agent
HARMALINE	005	E07	214.27	CNS stimulant, anti-parkinsonian agent
18alpha-GLYCYRRHETINIC ACID	005	E08	470.70	anti-inflammatory
1R,9S-HYDRASTINE	005	E09	383.40	uterine hemostatic, antiseptic
PICROTOXININ	005	E10	292.29	convulsant, GABA receptor antagonist, ichthyotoxin
MECLOCYCLINE SULFOSALICYLATE	005	E11	695.06	anti-bacterial

QUERCETIN	005	F02	302.24	capillary protectant, antioxidant. anti-neoplastic, anti-HIV; LD50(mouse) 159 mg/kg po
CAPTOPRIL	005	F03	217.29	anti-hypertensive
CITROPTEN	005	F04	206.20	photosensitizing agent
HECOGENIN	005	F05	430.63	anti-inflammatory
THYROXINE	005	F06	776.88	antihypercholesterimic, thymomimetic
HARMINE	005	F07	212.25	anti-parkinsonian, CNS stimulant
FLUMEQUINE	005	F08	261.26	anti-bacterial
FENOFIBRATE	005	F09	360.84	antihyperlipidemic
MEFEXAMIDE	005	F10	316.83	stimulant (central)
PROGLUMIDE	005	F11	334.42	anti-cholinergic
VALPROATE SODIUM	005	G02	166.20	anticonvulsant
CIMETIDINE	005	G03	252.34	anti-ulcerative
CHRYSIN	005	G04	254.24	diuretic
CALCEIN	005	G05	622.55	chelating agent (Ca, Mg)
ALLOXAN	005	G06	142.07	specific cytotoxin (pancreatic islet betacell)
MIMOSINE	005	G07	198.18	depilatory agent
FLUPHENAZINE HYDROCHLORIDE	005	G08	510.45	H1 antihistamine
FENOPROFEN	005	G09	242.28	anti-inflammatory
PROBUCOL	005	G10	516.86	antihyperlipidemic
MINAPRINE HYDROCHLORIDE	005	G11	371.31	psychotropic
MOLSIDOMINE	005	H02	242.24	antianginal
CLOZAPINE	005	H03	326.83	anti-psychotic
NARINGENIN	005	H04	272.26	anti-ulcer, gibberellin antagonist
GUANIDINE CARBONATE	005	H05	121.10	striated muscle stimulant
ALLANTOIN	005	H06	158.12	wound healing agent
NORHARMAN	005	H07	168.20	plant growth inhibitor; mutagen
FAMOTIDINE	005	H08	337.45	H2 antihistamine

FENBENDAZOLE	005	H09	299.35	anthelmintic
MEBENDAZOLE	005	H10	295.30	anthelmintic
MEMANTINE HYDROCHLORIDE	005	H11	215.77	muscle relaxant (skeletal)
3- AMINOPROPANESULPHONIC ACID	006	A02	139.17	anti-bacterial; GABA agonist
NEFOPAM	006	A03	253.35	analgesic
SUXIBUZONE	006	A04	438.48	analgesic, antipyretic, anti-inflammatory
ESTRADIOL METHYL ETHER	006	A05	286.42	estrogen
RETINOL	006	A06	286.46	vitamin A
FOSFOSAL	006	A07	218.10	analgesic, anti-inflammatory
CEFUROXIME SODIUM	006	A08	446.37	anti-bacterial
BEZAFIBRATE	006	A09	361.83	antihyperlipidemic
CYCLOCREATINE	006	A10	143.15	regulator of creatine biosynthesis
1,2-DIMETHYLHYDRAZINE HYDROCHLORIDE	006	A11	133.02	anti-neoplastic
5-AMINOPENTANOIC ACID HYDROCHLORIDE	006	B02	153.61	GABA _B antagonist
PIRENZEPINE HYDROCHLORIDE	006	B03	424.33	anti-ulcerative
SUPROFEN	006	B04	260.31	anti-inflammatory
ESTRADIOL ACETATE	006	B05	314.43	estrogen
LAPACHOL	006	B06	242.28	anti-neoplastic, antifungal
MESNA	006	B07	164.18	mucolytic
METAMPICILLIN SODIUM	006	B08	383.40	anti-bacterial
LIOTHYRONINE SODIUM	006	B09	672.96	thyroid hormone
alpha-CYANO-3- HYDROXYCINNAMIC ACID	006	B10	189.17	inhibit mitochondrial pyruvate transport
ATRACTYLOSIDE POTASSIUM	006	B11	803.01	oxidative phosphorylation inhibitor
ATENOLOL	006	C02	266.34	beta adrenergic blocker
PRAMOXINE HYDROCHLORIDE	006	C03	329.87	anesthetic (topical)

ACETAMINOSALOL	006	C04	271.28	analgesic, antipyretic
5-FLUORO-5'-DEOXYURIDINE	006	C05	246.20	anti-neoplastic, pyrimidine antimetabolite
KETOPROFEN	006	C06	254.29	anti-inflammatory
TRETINON	006	C07	300.44	keratolytic
LOMEFLOXACIN HYDROCHLORIDE	006	C08	387.82	anti-bacterial
CEPHALORIDINE	006	C09	415.49	anti-bacterial
PERILLIC ACID (-)	006	C10	166.22	inhibits posttranslational cys isoprenylation, blocks G-protein
GUVACINE HYDROCHLORIDE	006	C11	163.61	muscarinic agonist, GABA uptake inhibitor
CARBETAPENTANE CITRATE	006	D02	525.60	antitussive
MEPHENESIN	006	D03	182.22	muscle relaxant (skeletal)
ACETANILIDE	006	D04	135.17	analgesic, antipyretic
ESTRIOL BENZYL ETHER	006	D05	378.52	estrogen
LISINAPRIL	006	D06	405.50	ACE inhibitor
BRETYLIUM TOSYLATE	006	D07	414.36	inhibitor of norepinephrine release
FOSFOMYCIN	006	D08	176.12	anti-bacterial
5-CHLOROINDOLE-2-CARBOXYLIC ACID	006	D09	195.61	NMDA receptor antagonist (gly)
QUINOLINIC ACID	006	D10	167.12	differentiates between cerebral and forebrain NMDA receptors
TINIDAZOLE	006	D11	247.27	anti-protozoal
AMINOPYRIDINE	006	E02	94.12	K channel blocker
SULFAPHENAZOLE	006	E03	314.37	anti-bacterial
TODRALAZINE HYDROCHLORIDE	006	E04	268.70	anti-hypertensive, peripheral vasodilator
ESTRADIOL-3-SULFATE, SODIUM SALT	006	E05	374.43	estrogen
ACETYL-L-LEUCINE	006	E06	173.21	anti-vertigo
FOSCARNET SODIUM	006	E07	191.95	anti-viral
CEFAMANDOLE NAFATE	006	E08	512.50	anti-bacterial

7-CHLOROKYNURENIC ACID	006	E09	223.62	NMDA receptor antagonist (gly)
ANTHRAQUINONE	006	E10	208.22	irritant
CYCLOLEUCINE	006	E11	129.16	NMDA receptor antagonist (gly)
NEROL	006	F02	154.25	weak estrogen receptor blocker
RANITIDINE	006	F03	314.41	H2 antihistamine
ESTRIOL METHYL ETHER	006	F04	302.42	estrogen
TOLFENAMIC ACID	006	F05	261.71	anti-inflammatory, analgesia
BUMETANIDE	006	F06	364.42	diuretic
FOLIC ACID	006	F07	441.41	hematopoietic vitamin
PRALIDOXIME MESYLATE	006	F08	232.26	cholinesterase reactivator
4-NAPHTHALIMIDOBUTYRIC ACID	006	F09	283.29	aldose reductase inhibitor
CARBOPLATIN	006	F10	371.26	anti-neoplastic, convulsant
AMINOCYCLOPROPANECARB OXYLIC ACID	006	F11	101.11	NMDA partial agonist (gly)
NICERGOLINE	006	G02	484.40	vasodilator
SULOCTIDIL	006	G03	337.57	peripheral vasodilator
ESTRADIOL PROPIONATE	006	G04	328.46	estrogen
ZAPRINAST	006	G05	271.28	cGMP phosphodiesterase inhibitor
CARBENOXOLONE SODIUM	006	G06	614.74	anti-inflammatory, antisecretory, anti-ulcer
TRANEXAMIC ACID	006	G07	157.21	hemostatic
OFLOXACIN	006	G08	361.38	anti-bacterial
INDOLE-2-CARBOXYLIC ACID	006	G09	161.16	NMDA receptor antagonist (gly)
AZACITIDINE	006	G10	244.21	anti-neoplastic, pyrimidine antimetabolite
5-NITRO-2-PHENYLPROPYLAMINOBENZOIC ACID [NPPB]	006	G11	300.32	chloride channel blocker
PIMOZIDE	006	H02	461.56	anti-psychotic
RONIDAZOLE	006	H03	200.16	anti-protozoal
ESTRONE ACETATE	006	H04	312.41	estrogen

GALANTHAMINE HYDROBROMIDE	006	H05	368.27	anticholinesterase, analgesic, antiAlzheimer
CARPROFEN	006	H06	273.72	anti-inflammatory, analgesic
CEFOXITIN SODIUM	006	H07	449.44	anti-bacterial
PIROMIDIC ACID	006	H08	288.31	anti-bacterial
N- (9- FLUORENYLMETHOXYCARBO NYL)-L-LEUCINE	006	H09	353.42	anti-inflammatory
AZASERINE	006	H10	173.13	anti-neoplastic, amino acid antagonist
N-FORMYLMETHIONYL- LEUCYLPHENYLALANINE	006	H11	437.56	chemotactic peptide
N- FORMYLMETHIONYLPHENYLA LANINE	007	A02	324.40	chemotactic peptide
ANISINDIONE	007	A03	252.27	anti-coagulant
LYSYLPHENYLALANYLTYSOSIN E	007	A04	456.55	TAN inhibitor
ABRINE (L)	007	A05	218.26	insecticide, anti-inflammatory, antiophthalmic
MONENSIN SODIUM (monensin A is shown)	007	A06	690.90	anti-bacterial
ACEXAMIC ACID	007	A07	173.21	wound healing agent
AMBROXOL HYDROCHLORIDE	007	A08	414.57	expectorant
DEQUALINIUM CHLORIDE	007	A09	527.59	anti-infectant
PYRIDOSTIGMINE BROMIDE	007	A10	261.12	cholinergic
BETA-PROPIOLACTONE	007	A11	72.06	anti-infective
METHIONYL- LEUCYLPHENYLALANINE ACETATE	007	B02	469.60	chemotactic peptide
CYCLOSPORINE	007	B03	1202.64	immunosuppressant
S-METHYL-L-THIOCITRULLINE ACETATE	007	B04	205.28	nitro oxide synthase inhibitor
HARMOL HYDROCHLORIDE	007	B05	234.69	MAO inhibitor
MORIN	007	B06	302.24	P450 and ATPase inhibitor
FLOXURIDINE	007	B07	246.20	anti-neoplastic, antimetabolite

GLUCONOLACTONE	007	B08	178.14	chelating agent
MENTHOL(-)	007	B09	156.27	analgesic (topical), antipruritic agent
ISOXICAM	007	B10	335.34	anti-inflammatory
PAROMOMYCIN SULFATE	007	B11	713.72	anti-bacterial, antiamebic
LEUCINE ENKEPHALIN	007	C02	555.64	opioid neuromodulator
TROLEANDOMYCIN	007	C03	813.99	anti-bacterial
S-(1,2-DICARBOXYETHYL)GLUTATHIONE	007	C04	437.43	anti-inflammatory, antiallergy, mast cell degranulation inhibitor
VINBURNINE	007	C05	294.40	cerebral vasodilator, muscle stimulant
BENZYL ISOTHIOCYANATE	007	C06	149.22	anti-neoplastic, anti-bacterial, antifungal
ALTRETAMINE	007	C07	210.28	anti-neoplastic
TIOXOLONE	007	C08	168.17	antiseborrheic
THIAMPHENICOL	007	C09	356.23	anti-bacterial
LABETALOL HYDROCHLORIDE	007	C10	364.88	adrenergic blocker
LEVAMISOLE HYDROCHLORIDE	007	C11	240.76	immunomodulator
LYSYL-TYROSYL-LYSINE ACETATE	007	D02	497.60	Induces nicks at apurinic and apyrimidinic sites in circular DNA
L-LEUCYL-L-ALANINE	007	D03	202.26	ubiquitin blocker, neurite growth inhibitor
N-HISTIDYL-2-AMINONAPHTHALENE (betaNA)	007	D04	280.33	beta-glucosidase inhibitor
RHAPONTIN	007	D05	420.42	antifungal, antioxidant
BIOTIN	007	D06	244.31	vitamin B complex
AMINOHIPURIC ACID	007	D07	194.19	renal function diagnosis
BACAMPICILLIN HYDROCHLORIDE	007	D08	501.99	anti-bacterial
TENOXCAM	007	D09	337.38	anti-inflammatory
NIFENAZONE	007	D10	308.34	analgesic, anti-inflammatory
6alpha-METHYLPREDNISOLONE	007	D11	416.52	glucocorticoid

ACETATE				
SPAGLUMIC ACID	007	E02	304.26	neurotransmitter; mGluR3 receptors
Tfa-VAL-TYR-VAL-OH	007	E03	475.47	elastase (human) inhibitor
1-BENZYLOXYCARBONYLAMINO PHENETHYL CHLOROMETHYL KETONE	007	E04	331.80	peptidase inhibitor, esterase inhibitor
ELLAGIC ACID	007	E05	302.20	hemostatic, anti-neoplastic, antimutagenic
DINITOLMIDE	007	E06	225.16	anti-protozoal
MEFLOQUINE	007	E07	378.32	anti-malarial
BEPRIDIL HYDROCHLORIDE	007	E08	403.01	anti-arrhythmic
CETRIMONIUM BROMIDE	007	E09	364.46	anti-infectant
HALCINONIDE	007	E10	454.97	glucocorticoid, anti-inflammatory
HYDROCORTISONE BUTYRATE	007	E11	432.56	glucocorticoid, anti-inflammatory
Ng-METHYL-L-ARGININE ACETATE	007	F02	248.28	NO synthesis inhibitor
PHENETHYL CAFFEATE (CAPE)	007	F03	284.31	anti-neoplastic, anti-inflammatory, immunomodulator, NFkB blocker
PHENYLALANYLTYSOSINE	007	F04	328.37	TAN inhibitor
GLUTATHIONE	007	F05	307.33	antioxidant
NICOTINYL TARTRATE	007	F06	259.22	vasodilator
ADIPHENINE HYDROCHLORIDE	007	F07	347.89	muscle relaxant (smooth)
CARMUSTINE	007	F08	214.05	anti-neoplastic, alkylating agent
CHLOROXINE	007	F09	214.05	chelating agent
HYCANTHONE	007	F10	356.49	anthelmintic, hepatotoxic
MITOXANTHRONE HYDROCHLORIDE	007	F11	517.41	anti-neoplastic
PIRACETAM	007	G02	142.16	antinauseant
VALYLTRYPTOPHAN	007	G03	303.36	ACE inhibitor
RESVERATROL	007	G04	228.25	antifungal, anti-bacterial
MONOCROTALINE	007	G05	325.36	anti-neoplastic, insect sterilant

AMINOHYDROXYBUTYRIC ACID	007	G06	119.12	antiepileptic
ALEXIDINE HYDROCHLORIDE	007	G07	581.73	anti-bacterial
CEFTRIAXONE SODIUM	007	G08	598.55	anti-bacterial
CLOFOCTOL	007	G09	365.35	anti-bacterial
NIMESULIDE	007	G10	308.31	anti-inflammatory
URETHANE	007	G11	89.09	anti-neoplastic, cytotoxic
PIPERIDOLATE HYDROCHLORIDE	007	H02	359.90	antispasmodic
GLYCYLLEUCYLPHENYLALANINE	007	H03	335.41	immunostimulant
CAMPTOTHECIN	007	H04	348.36	anti-neoplastic
SALICIN	007	H05	286.28	analgesic, antipyretic
ARTEMISININ	007	H06	282.34	anti-malarial
QUINAPRIL HYDROCHLORIDE	007	H07	474.99	anti-hypertensive, ACE inhibitor
TRAZODONE HYDROCHLORIDE	007	H08	408.33	antidepressant
LASALOCID SODIUM	007	H09	612.79	anti-bacterial
MEPHENTERMINE SULFATE	007	H10	261.34	vasoconstrictor
THIOTEPA	007	H11	189.22	anti-neoplastic, alkylating agent
CHLOROACETOXYQUINOLINE	008	A02	221.64	antifungal
NIMODIPINE	008	A03	418.45	vasodilator
3,5-DINITROCATÉCHOL (OR-486)	008	A04	200.11	catechol O-methyltransferase inhibitor
ESTRONE HEMISUCCINATE	008	A05	370.45	estrogen
SODIUM beta-NICOTINAMIDE ADENINE DINUCLEOTIDE PHOSPHATE	008	A06	765.40	cofactor in aryl & steroidal hydroxylation
PROPAFENONE HYDROCHLORIDE	008	A07	377.92	anti-arrhythmic
CONVALLATOXIN	008	A08	550.65	cardiotonic
PHYSCION	008	A09	284.27	anti-bacterial, cathartic
GLICLAZIDE	008	A10	323.42	anti-diabetic

PRISTIMERIN	008	A11	464.65	anti-neoplastic, anti-inflammatory
EXALAMIDE	008	B02	221.30	antifungal
SALINOMYCIN, SODIUM	008	B03	773.00	anti-bacterial
N- (3-TRIFLUOROMETHYLPHENYL)PIPERAZINE HYDROCHLORIDE (TFMPP)	008	B04	266.70	5HT agonist
AZITHROMYCIN	008	B05	749.00	anti-bacterial
PACLITAXEL	008	B06	853.93	anti-neoplastic
PERICIAZINE	008	B07	365.50	anti-psychotic
BAICALEIN	008	B08	270.24	anti-viral (HIV)
SENNOSIDE A	008	B09	862.76	cathartic
TRIMEDLURE	008	B10	232.75	arthropod pheromone
TETRANDRINE	008	B11	622.77	analgesic, anti-neoplastic, anti-hypertensive, lymphotoxin
ETANIDAZOLE	008	C02	214.18	anti-neoplastic, hypoxic cell radiosensitizer
ACYCLOVIR	008	C03	225.21	anti-viral
3-METHYL-1-PHENYL-2-PYRAZOLIN-5-ONE (MCI-186)	008	C04	174.20	antioxidant, lipoxigenase inhibitor
AZADIRACTIN	008	C05	720.73	anti-feedant, insecticide
BUTACAINE	008	C06	306.45	anesthetic (local)
SPERMIDINE TRIHYDROCHLORIDE	008	C07	254.63	ornithine decarboxylase inhibitor
GOSSYPOL	008	C08	518.57	anti-spermatogenic, anti-neoplastic, anti-HIV
PHENOTHRIN	008	C09	350.46	ectoparasiticide
MELOXICAM	008	C10	351.41	anti-inflammatory
ISOLIQURITIGENIN	008	C11	256.26	aldose reductase inhibitor, anti-neoplastic, anti-inflammatory
MIZORIBINE	008	D02	259.22	immunosuppressant
NITRENDIPINE	008	D03	360.37	anti-hypertensive
METHIOTHEPIN MALEATE	008	D04	472.63	5HT1&2 receptor antagonist

CEVADINE	008	D05	591.75	anti-hypertensive
TRYPTAMINE	008	D06	160.22	psychotropic
LOVASTATIN	008	D07	404.55	antihyperlipidemic, HMGCoA reductase inhibitor
LUPININE	008	D08	169.27	anti-feedant, anti-inflammatory, oxytoxic
SILDENAFIL	008	D09	474.59	impotency therapy
NIMUSTINE	008	D10	272.70	anti-neoplastic
DELTALINE	008	D11	451.56	anti-arrhythmic
NAFRONYL OXALATE	008	E02	473.57	vasodilator
CIPROFLOXACIN	008	E03	331.35	anti-bacterial, fungicide
RAUWOLSCINE HYDROCHLORIDE	008	E04	390.91	alpha2 adrenergic antagonist
CLOPIDOGREL SULFATE	008	E05	419.91	platelet aggregation inhibitor
IOPANIC ACID	008	E06	570.94	radioopaque agent
METHOXYAMINE HYDROCHLORIDE	008	E07	83.52	hydroxymethyltransferase inhibitor
SALSOLINE	008	E08	193.25	anti-hypertensive, antihistamine
TETRACHLOROISOPHTHALON ITRILE	008	E09	265.91	antifungal
PINOCEMBRIN	008	E10	256.26	anti-inflammatory
BOVINOCIDIN (3- nitropropionic acid)	008	E11	119.08	anti-neoplastic
SEMUSTINE	008	F02	247.73	anti-neoplastic
SAFROLE	008	F03	162.19	anesthetic (topical) and antiseptic, pediculicide
1-PHENYLBIGUANIDE HYDROCHLORIDE	008	F04	213.67	5HT3 receptor agonist
LORATADINE	008	F05	382.89	H1 antihistamine
LANSOPRAZOLE	008	F06	369.37	anti-ulcerative
AGMATINE SULFATE	008	F07	228.27	NMDA blocker, alpha-2 adrenergic agonist; NO synthase inhibitor
CYTISINE	008	F08	190.25	anti-inflammatory, respiratory stimulant

DIHYDROJASMONIC ACID	008	F09	212.29	plant growth regulator
VENLAFAXINE	008	F10	277.41	antidepressant
ATOVAQUONE	008	F11	366.85	antipneumocystic, anti-malarial
SPIRAMYCIN	008	G02	843.07	anti-bacterial
OXOTREMORINE SESQUIFUMARATE	008	G03	322.36	muscarinic agonist
VERATRIDINE	008	G04	703.83	anti-hypertensive
SELAMECTIN	008	G05	769.98	antiparasitic, antimitic
OXYPHENCYCLIMINE HYDROCHLORIDE	008	G06	380.92	anti-cholinergic
2-THIOURACIL	008	G07	128.15	thyroid depressant
EMODIC ACID	008	G08	300.23	cathartic, purgative
TANNIC ACID	008	G09	1701.23	nonspecific enzyme/receptor blocker
BUPROPION	008	G10	276.21	antidepressant
CHLOROGUANIDE HYDROCHLORIDE	008	G11	290.20	anti-malarial
RESORCINOL MONOACETATE	008	H02	152.15	antiseborrheic, antipruritic
N-AMINOHEXYL-5-CHLORO- 1- NAPHTHALENESULFONAMIDE HYDROCHLORIDE	008	H03	377.34	calmodulin antagonist, PDE and kinase inhibitor
CELECOXIB	008	H04	381.38	antiarthritic, cyclooxygenase2 inhibitor
ATORVASTATIN CALCIUM	008	H05	582.71	antihyperlipidemic, HMGCoA reductase inhibitor
PENTOLINIUM TARTRATE	008	H06	538.60	anti-hypertensive, ganglionic blocker
CLEBOPRIDE MALEATE	008	H07	489.96	antiemetic, antispasmodic
BETULINIC ACID	008	H08	442.69	anti-neoplastic
FORMESTANE	008	H09	300.44	anti-neoplastic, aromatase inhibitor
TETRAHYDROPALMATINE	008	H10	355.44	analgesic, hypnotic, papaverine-like
CHLORANIL	008	H11	245.88	antipsoriatic
N-ACETYLASPARTIC ACID	009	A02	175.14	analeptic, neurostimulant
2,3-DIHYDROXY-6,7- DICHLOROQUINOXALINE	009	A03	231.04	NMDA receptor antagonist (gly)

LEVOFLOXACIN	009	A04	361.38	anti-bacterial
MOXIFLOXACIN HYDROCHLORIDE	009	A05	465.96	anti-bacterial
ALMOTRIPTAN	009	A06	335.47	5HT 1B/2D receptor agonist
ROSUVASTATIN	009	A07	481.55	antihyperlipidemic
TROXERUTIN	009	A08	742.69	vasoprotectant
HUPERZINE A	009	A09	242.32	anticholinesterase, cognition enhancer
CROTAMITON	009	A10	203.29	antipruritic, scabicide
AMITRAZ	009	A11	293.42	pesticide, carcinogen
N,N- HEXAMETHYLENEAMILORIDE	009	B02	311.78	Na/H+ antiporter inhibitor, diuretic
ROFECOXIB	009	B03	314.36	COX2 inhibitor, anti-inflammatory, antiarthritic
CANDESARTAN CILEXIL	009	B04	610.68	angiotensin 1 receptor antagonist
PIOGLITAZONE HYDROCHLORIDE	009	B05	392.91	anti-diabetic
OLMESARTAN MEDOXOMIL	009	B06	558.60	Angiotensin II inhibitor prodrug, anti- hypertensive
TEGASEROD MALEATE	009	B07	417.47	5HT4 receptor agonist, peristaltic stimulant
GINKGOLIC ACID	009	B08	346.51	cytotoxic, apoptosis inducer, antitubercular
SILIBININ	009	B09	482.45	hepatoprotective agent, antioxidant
BENZANTHRONE	009	B10	230.27	hepatotoxic, P450 suppressant
PURPURIN	009	B11	256.22	xanthin oxidase inhibitor, irritant
ZOXAZOLAMINE	009	C02	168.58	muscle relaxant, antirrhematic
HYDROQUINONE	009	C03	110.11	antioxidant
ROSIGLITAZONE	009	C04	357.43	anti-diabetic
PICROPODOPHYLLOTOXIN	009	C05	414.42	anti-neoplastic; 10% cytotoxicity of podophyllotoxin
CEFTIBUTEN	009	C06	410.43	anti-bacterial
DERACOXIB	009	C07	397.38	anti-inflammatory, antiarthritic, COX-2 inhibitor

CANRENONE	009	C08	340.47	aldosterone antagonist; antifibrogenic
ICARIIN	009	C09	676.68	hepatoprotective
ZOLMITRIPTAN	009	C10	287.36	antimigraine, 5HT[1B/1D] agonist
GENETICIN	009	C11	692.72	anti-bacterial
ACRISORCIN	009	D02	388.51	antifungal
OXCARBAZEPINE	009	D03	252.28	anti-psychotic
LOSARTAN	009	D04	422.92	anti-hypertensive, AT1 angiotensin II antagonist
DIHYDROJASMONIC ACID, METHYL ESTER	009	D05	226.32	plant growth regulator
CEFDINIR	009	D06	395.42	anti-bacterial
CILOSTAZOL	009	D07	369.47	phosphodiesterase inhibitor
APRAMYCIN	009	D08	539.59	anti-bacterial; LD50(iv) 280mg/kg(mouse)
SERTRALINE HYDROCHLORIDE	009	D09	342.70	antidepressant, 5HT uptake inhibitor
DIALLYL SULFIDE	009	D10	114.21	antibacterial, antifungal, anti-neoplastic, antihypercholesterolaemic, hepatoprotectant
SECNIDAZOLE	009	D11	185.18	antiameobic, antitrichomonas
PHENYLBUTYRATE SODIUM	009	E02	186.19	antihyperlipidemic
BETAMIPRON	009	E03	193.20	sweetener
GATIFLOXACIN	009	E04	375.40	anti-bacterial
BENZAEPRIIL HYDROCHLORIDE	009	E05	460.96	ACE inhibitor, anti-hypertensive
VALSARTAN	009	E06	435.53	Angiotensin II inhibitor, anti-hypertensive
AVOCADYNE	009	E07	284.44	anti-bacterial, antifungal
MADECASSIC ACID	009	E08	504.71	wound healing
ALFLUZOCIN	009	E09	389.46	alpha(1)-adrenergic blocker
CARBADOX	009	E10	262.23	anti-bacterial
PEFLOXACINE MESYLATE	009	E11	429.47	anti-bacterial, antiproliferative
CRUSTECDYSONE	009	F02	480.65	insect molting hormone

CARVEDILOL TARTRATE	009	F03	556.57	betaadrenergic blocker
MIGLITOL	009	F04	207.23	alpha-glucosidase inhibitor, anti-diabetic
FAMCICLOVIR	009	F05	321.34	anti-viral
SIBUTRAMINE HYDROCHLORIDE	009	F06	316.32	anorexic, antidepressant, uptake inhibitor (5HT, norepinephrine, dopamine)
AVOCADYNONE ACETATE	009	F07	324.46	anti-bacterial, antifungal
IMIDACLOPRID	009	F08	254.68	nicotinyl AChR agonist; antiparasitic
TRANDOLAPRIL	009	F09	430.55	anti-hypertensive, ACE inhibitor
OXFENDAZOLE	009	F10	315.35	anthelmintic
ASPARTAME	009	F11	294.31	sweetener
METAXALONE	009	G02	221.26	muscle relaxant (skeletal)
NATEGLINIDE	009	G03	317.43	anti-diabetic
ORLISTAT	009	G04	495.75	reversible lipase inhibitor, antiobesity
AMLODIPINE BESYLATE	009	G05	567.06	Ca channel blocker
TORSEMIDE	009	G06	348.43	diuretic, inhibits Na/K/2Cl carrier system
SPARTEINE HYDROIODIDE	009	G07	362.30	oxytocic
PALMATINE	009	G08	368.41	uterine contractant, anti-bacterial, anti-arrhythmic, inotropic, adrenocorticotropic, anticholinesterase, analgesic
TELITHROMYCIN	009	G09	824.04	anti-bacterial
PERILLYL ALCOHOL	009	G10	152.24	anti-neoplastic, apoptosis inducer; skin irritant, LD50(rat) 2100 mg/kg po
TRIADIMEFON	009	G11	293.76	antifungal, P450 inhibitor
CLARITHROMYCIN	009	H02	747.97	anti-bacterial
IRBESARTAN	009	H03	428.54	angiotensin 2 receptor antagonist
VALDECOXIB	009	H04	314.37	anti-inflammatory, COX-2 inhibitor
EZETIMIBE	009	H05	409.44	sterol absorption inhibitor
PERINDOPRIL ERBUMINE	009	H06	441.62	anti-hypertensive, ACE inhibitor
CITICOLINE	009	H07	488.33	cognition enhancer, phosphocholine cytidyltransferase activator

SINOMENINE	009	H08	329.40	weak abortifacient, immunosuppressant, analgesic, anti-inflammatory; LD50 (po) 580 mg/kg; (ip) 285 mg/kg(mouse)
OXAPROZIN	009	H09	293.33	anti-inflammatory
3-ISOBUTYL-1-METHYLXANTHINE (IBMX)	009	H10	222.25	phosphodiesterase inhibitor
CHLOROPHYLLIDE Cu COMPLEX Na SALT	009	H11	682.15	anti-neoplastic
BIFONAZOLE	010	A02	310.40	antifungal, calmodulin antagonist
INDOLE-3-CARBINOL	010	A03	147.18	anti-neoplastic
3,3'-DIINDOLYMETHANE	010	A04	246.31	apoptosis inducer
7-NITROINDAZOLE	010	A05	163.14	NO synthetase inhibitor
PRAVASTATIN SODIUM	010	A06	446.52	antihyperlipidemic, HMGCoA reductase inhibitor
CAPSANTHIN	010	A07	584.89	anti-neoplastic
ASTEMIZOLE	010	A08	458.58	H1 antihistamine (nonsedating)
GLYBURIDE	010	A09	494.01	antihyperglycemic
JUGLONE	010	A10	174.16	anti-neoplastic, antifungal
ACETOSYRINGONE	010	A11	196.20	insect attractant, plant hormone
DIBENZOYLMETHANE	010	B02	224.26	anti-neoplastic
RIFAXIMIN	010	B03	785.90	anti-bacterial, RNA synthesis inhibitor
AZAPERONE	010	B04	327.41	tranquilizer, neuroleptic, alpha adrenergic blocker
RIBOFLAVIN	010	B05	376.37	Vitamin B2; Vitamin cofactor; LD50(rat) 560 mg/kg ip
PEONIFLORIN	010	B06	482.49	anti-inflammatory, antispasmodic, anti-hypertensive, antidiuretic
COLCHICEINE	010	B07	385.42	anti-mitotic
N-ACETYLNEURAMIC ACID	010	B08	309.28	immunomodulator, adjuvant
NICOTINE DITARTRATE	010	B09	462.41	nicotinyl acetylcholine receptor agonist, ectoparasiticide
ANISODAMINE	010	B10	305.38	anti-cholinergic, antispasmodic
POMIFERIN	010	B11	420.47	antioxidant

TYLOSIN TARTRATE	010	C02	916.12	anti-bacterial
CEPHARANTHINE	010	C03	606.73	anti-neoplastic, hepatoprotectant, radioprotective
TRANILAST	010	C04	327.34	antiallergic, mast cell degranulation inhibitor, angiogenesis blocker
CURCUMIN	010	C05	368.39	antiedemic, anti-inflammatory, bile stimulant; anti-bacterial, antifungal, lipo/cyclooxygenase inhibitor
N-CHLOROETHYL-N-ETHYL-2'-METHYLBENZYLAMINE HYDROCHLORIDE	010	C06	248.20	inhibits dopamine & norepinephrine accumulation in brain
KOJIC ACID	010	C07	142.11	chelator, anti-bacterial, skin whitening agent
VESAMICOL HYDROCHLORIDE	010	C08	295.86	acetylcholine transport blocker (vesicular)
1-METHYLXANTHINE	010	C09	166.14	diuretic, adenosine antagonist
VULPINIC ACID	010	C10	322.32	anti-inflammatory, anti-bacterial, plant growth inhibitor
CELASTROL	010	C11	450.62	anti-neoplastic, antiinflammatory, NO synthesis inhibitor, chaperone stimulant
SARAFLOXACIN HYDROCHLORIDE	010	D02	421.83	anti-bacterial
CARBIMAZOLE	010	D03	186.23	antithyroid
SECURININE	010	D04	217.27	GABAA receptor blocker, CNS stimulant
RILUZOLE	010	D05	234.20	anticonvulsant, glutamate release inhibitor
PREGABALIN	010	D06	159.23	anticonvulsant
ISOBUTYLMETHYLXANTHINE	010	D07	222.25	phosphodiesterase inhibitor
MEXAMINE	010	D08	226.71	5HT agonist
NIPECOTIC ACID	010	D09	129.16	GABA uptake inhibitor
USNIC ACID	010	D10	344.32	anti-bacterial
DEGUELIN(-)	010	D11	394.43	anti-neoplastic, anti-viral, insecticide
6-AMINONICOTINAMIDE	010	E02	137.14	anti-neoplastic, apoptosis inducer
CHLORMADINONE ACETATE	010	E03	404.94	progestin, antiandrogen
VALERYL SALICYLATE	010	E04	222.24	COX-1 inhibitor

CEFDITORIN PIVOXIL	010	E05	620.73	anti-bacterial
2,6-DI-t-BUTYL-4-METHYLPHENOL	010	E06	220.36	antioxidant
DESMETHYLDIHYDROCAPSAIN	010	E07	293.41	analgesic (topical), depletes Substance P
HYDROXYTACRINE MALEATE	010	E08	330.34	cholinesterase inhibitor, anti-parkinsonian
PENTETRAZOL	010	E09	138.17	analeptic, circulation stimulant
PHLORIDZIN	010	E10	436.42	induces experimental glucosuria, anti-feedant
RUTILANTINONE	010	E11	428.40	coccidiostat
PROTHIONAMIDE	010	F02	180.27	anti-bacterial
4'-DEMETHYLEPIPODOPHYLLOXIN	010	F03	400.39	anti-neoplastic
ELAIDYLPHOSPHOCHOLINE	010	F04	433.62	anti-neoplastic
MODAFINIL	010	F05	273.36	analeptic
CHAULMOSULFONE	010	F06	777.22	antilepreptic
KAINIC ACID	010	F07	213.24	glutamate receptor agonist, anthelmintic
9-AMINO-1,2,3,4-TETRAHYDROACRIDINE HYDROCHLORIDE	010	F08	234.73	anticholinesterase, K channel blocker
1-(2-METHOXYPHENYL)PIRAZINE HYDROCHLORIDE	010	F09	228.72	5HT1 receptor agonist
SPARTEINE SULFATE	010	F10	332.47	oxytocic
ROTENONE	010	F11	394.43	acaricide, ectoparasiticide, anti-neoplastic, mitochondrial poison
CARMOFUR	010	G02	257.27	anti-neoplastic
MILTEFOSINE	010	G03	407.58	anti-neoplastic
L-PHENYLALANINOL	010	G04	151.21	anti-ulcer
TOPIRAMATE	010	G05	339.37	anticonvulsant, antimigraine, GABA-A agonist, AMP/kinate glutamate receptor antagonist, carbonic anhydrase inhibitor

CREATININE	010	G06	113.12	metabolic enhancer
PODOFILOX	010	G07	414.42	anti-neoplastic, inhibits microtubule assembly, and human DNA topoisomerase II; anti-mitotic agent
N-HYDROXYMETHYLNICOTINAMIDE	010	G08	152.15	cholagogue
HYDROCORTISONE	010	G09	362.47	glucocorticoid, anti-inflammatory
ISORESERPINE	010	G10	608.69	anti-hypertensive
GAMBOGIC ACID	010	G11	628.77	anti-inflammatory, cytotoxic, inhibits HeLa cells in vitro; LD50(rat) 88 mg/kg ip
CLOPIDOL	010	H02	192.05	coccidiostat, antiplatelet
OXICONAZOLE NITRATE	010	H03	492.15	antifungal
AZELASTINE HYDROCHLORIDE	010	H04	418.37	H1 antihistamine (nonsedating); leucotriene synthesis blocker
GEMIFLOXACIN MESYLATE	010	H05	485.49	anti-bacterial
PAEONOL	010	H06	166.18	anti-bacterial
EDROPHONIUM CHLORIDE	010	H07	201.70	acetylcholinesterase inhibitor
LEVODOPA	010	H08	197.19	anti-parkinsonian
PIMPINELLIN	010	H09	246.22	GABA receptor antagonist, phototoxin
BERGAPTEN	010	H10	216.20	antipsoriatic, anti-inflammatory
AKLAVINE HYDROCHLORIDE	010	H11	606.08	anti-bacterial, anti-neoplastic
TETRACAINE HYDROCHLORIDE	011	A02	300.83	anesthetic (local)
METHYLTHIOURACIL	011	A03	142.18	antithyroid agent
SULFAMETHIZOLE	011	A04	270.33	anti-bacterial
ROSOLIC ACID	011	A05	290.32	diagnostic aid
NICARDIPINE HYDROCHLORIDE	011	A06	516.00	vasodilator
AZOBENZENE	011	A07	182.23	acaricide
TETRAHYDROZOLINE HYDROCHLORIDE	011	A08	236.75	adrenergic agonist, nasal decongestant
OXYPHENBUTAZONE	011	A09	324.38	anti-inflammatory

SULFINPYRAZONE	011	A10	404.49	uricosuric
ACEBUTOLOL HYDROCHLORIDE	011	A11	372.90	anti-hypertensive, antianginal, anti-arrhythmic
FLUNARIZINE HYDROCHLORIDE	011	B02	477.43	vasodilator
SULCONAZOLE NITRATE	011	B03	460.77	antifungal
FLURANDRENOLIDE	011	B04	436.53	anti-inflammatory
ENALAPRIL MALEATE	011	B05	492.53	ACE inhibitor, anti-hypertensive
THIORIDAZINE HYDROCHLORIDE	011	B06	407.04	anti-psychotic
PROPYLTHIOURACIL	011	B07	170.23	antihyperthyroid
SULFISOXAZOLE	011	B08	267.31	anti-bacterial
MELATONIN	011	B09	232.28	sleep induction, modifies circadian rhythm
FLUTAMIDE	011	B10	276.22	antiandrogen
RITODRINE HYDROCHLORIDE	011	B11	323.82	muscle relaxant (smooth)
ESTRADIOL DIACETATE	011	C02	356.47	estrogen
CEFMETAZOLE SODIUM	011	C03	493.52	anti-bacterial
THIOTHIXENE	011	C04	443.63	anti-psychotic
PYRAZINAMIDE	011	C05	123.12	anti-bacterial, tuberculostatic
AMINOPHENAZONE	011	C06	203.25	antipyretic, analgesic
ACETYLTRYPTOPHAN	011	C07	246.27	antidepressant
SUPROFEN METHYL ESTER	011	C08	274.34	anti-inflammatory
GLAFENINE	011	C09	372.81	analgesic
SULPIRIDE	011	C10	341.43	dopamine receptor antagonist, anti-psychotic
ECONAZOLE NITRATE	011	C11	444.70	antifungal
CEFOPERAZONE SODIUM	011	D02	667.66	anti-bacterial
TOLAZOLINE HYDROCHLORIDE	011	D03	196.68	adrenergic blocker
PYRVINIUM PAMOATE	011	D04	769.91	anthelmintic
VINCAMINE	011	D05	354.45	vasodilator

ACETYLGUTAMIC ACID	011	D06	189.17	excitatory aminoacid
AMINACRINE	011	D07	194.24	local antiseptic
ETHAVERINE HYDROCHLORIDE	011	D08	431.96	antispasmodic
SPIPERONE	011	D09	395.48	anti-psychotic
FLUNISOLIDE	011	D10	434.51	anti-inflammatory
NARASIN	011	D11	765.05	anti-bacterial, anti-viral
TOLMETIN SODIUM	011	E02	279.27	anti-inflammatory
SALICYLAMIDE	011	E03	137.14	analgesic
gamma-AMINO BUTYRIC ACID	011	E04	103.12	anti-hypertensive
ACETYLGUCOSAMINE	011	E05	221.21	antiarthritic
DROPERIDOL	011	E06	379.44	neuroleptic
SULFAMETER	011	E07	280.31	anti-bacterial
EBSELEN	011	E08	274.18	antioxidant, lipoxygenase inhibitor, inhibits oxidation of LDL
SNAP (S-NITROSO-N- ACETYLPENICILLAMINE)	011	E09	220.25	muscle relaxant (smooth)
TRIAMCINOLONE	011	E10	394.44	glucocorticoid
SULFABENZAMIDE	011	E11	276.32	anti-bacterial
QUINALIZARIN	011	F02	272.22	anti-viral, HIV-1 integrase inhibitor
BUDESONIDE	011	F03	430.55	anti-inflammatory
FLUFENAMIC ACID	011	F04	281.24	anti-inflammatory, analgesic
SULFAMETHOXYPIRIDAZINE	011	F05	280.31	anti-bacterial
FUREGRELATE SODIUM	011	F06	275.24	thromboxane synthetase inhibitor
6,7-DICHLORO-3-HYDROXY-2- QUINOXALINECARBOXYLIC ACID	011	F07	259.05	NMDA and kainate receptor antagonist
CINEOLE	011	F08	154.25	anthelmintic, antiseptic, expectorant
DOXYCYCLINE HYDROCHLORIDE	011	F09	480.91	anti-bacterial
ACONITINE	011	F10	645.75	anesthetic (gastric), antipyretic, and cardiotoxin
CORALYNE CHLORIDE	011	F11	399.88	cytostatic, intercalating agent

PATULIN	011	G02	154.12	anti-bacterial
SACCHARIN	011	G03	183.19	sweetener
XYLAZINE	011	G04	220.34	analgesic
ACETYLCARNITINE	011	G05	225.67	cholinergic
5-FLUOROINDOLE-2-CARBOXYLIC ACID	011	G06	179.15	NMDA receptor antagonist (gly)
TARGININE HYDROCHLORIDE	011	G07	224.69	NO synthase inhibitor
TIAPRIDE HYDROCHLORIDE	011	G08	364.89	neuroleptic
CITIOLONE	011	G09	159.21	hepatoprotectant
METHAZOLAMIDE	011	G10	236.27	carbonic anhydrase inhibitor
HEXAMETHONIUM BROMIDE	011	G11	362.19	anti-hypertensive, ganglionic blocker
RAMIFENAZONE	011	H02	281.79	analgesic, antipyretic, anti-inflammatory
PERPHENAZINE	011	H03	403.98	anti-psychotic
ETHYLNOREPINEPHRINE HYDROCHLORIDE	011	H04	233.70	bronchodilator
ROSMARINIC ACID	011	H05	360.32	anti-inflammatory, antithrombotic, antiplatelet, cytostatic, anti-viral
AMYGDALIN	011	H06	457.44	anti-inflammatory, experimental anti-neoplastic
AZLOCILLIN SODIUM	011	H07	483.48	anti-bacterial
CYCLOBENZAPRINE HYDROCHLORIDE	011	H08	311.86	muscle relaxant (skeletal)
METHYLBENZETHONIUM CHLORIDE	011	H09	462.12	anti-infectant
DIPYRONE	011	H10	333.34	analgesic, antipyretic
2- (2,6-DIMETHOXYPHENOXYETHYL) AMINOMETHYL-1,4-BENZODIOXANE HYDROCHLORIDE (WB 4101)	011	H11	381.86	alpha1a adrenergic blocker
NIGERICIN SODIUM	012	A02	746.96	anti-bacterial
THIOCTIC ACID	012	A03	206.33	hepatoprotectant
TENIPOSIDE	012	A04	656.67	anti-neoplastic
CISPLATIN	012	A05	300.06	anti-neoplastic, convulsant

BENDROFUMETHIAZIDE	012	A06	421.42	diuretic
ENOXACIN	012	A07	320.33	anti-bacterial
MIDODRINE HYDROCHLORIDE	012	A08	290.75	anti-hypertensive, vasoconstrictor
NABUMETONE	012	A09	228.29	anti-inflammatory
CLOBETASOL PROPIONATE	012	A10	466.98	glucocorticoid, anti-inflammatory
CACODYLIC ACID	012	A11	138.00	antieczema, dermatologic, herbicide
DIRITHROMYCIN	012	B02	835.09	anti-bacterial
ZIDOVUDINE [AZT]	012	B03	267.25	RT transferase inhibitor, anti-viral
AKLOMIDE	012	B04	200.58	anti-protozoal, coccidiostat
BROMHEXINE HYDROCHLORIDE	012	B05	412.60	expectorant
ETHISTERONE	012	B06	312.46	progestogen
NADOLOL	012	B07	309.41	betaadrenergic blocker
D-PHENYLALANINE	012	B08	165.19	antidepressant
ANDROSTERONE SODIUM SULFATE	012	B09	392.49	menstrual regulation
CLOPERASTINE HYDROCHLORIDE	012	B10	366.33	antitussive
TULOButEROL	012	B11	264.20	bronchodilator, beta adrenergic agonist
MEPIVACAINE HYDROCHLORIDE	012	C02	282.82	anesthetic (local)
N (g)-NITRO-L-ARGININE	012	C03	219.20	NO synthase inhibitor
BUCLADESINE	012	C04	469.39	vasodilator
BROMOPRIDE	012	C05	344.25	antiemetic
FIPEXIDE HYDROCHLORIDE	012	C06	425.32	psychostimulant
NALTREXONE HYDROCHLORIDE	012	C07	341.41	morphine antagonist
RETINYL PALMITATE	012	C08	524.88	provitamin, antixerophthalmic
NAPROXOL	012	C09	216.28	antiflammatory, analgesic, antipyretic
CYPROTERONE	012	C10	374.91	antiandrogen
HYDROXYCHLOROQUINE SULFATE	012	C11	433.96	anti-malarial, lupus suppressant

NILUTAMIDE	012	D02	317.23	antiandrogen
p-CHLOROPHENYLALANINE	012	D03	199.64	Irreversible inhibitor of tryptophan hydroxylase
PRIDINOL METHANESULFONATE	012	D04	391.53	anti-cholinergic
VINPOCETINE	012	D05	350.46	cerebral vasodilator, antimotion
PERHEXILINE MALEATE	012	D06	393.57	coronary vasodilator
NOMIFENSINE MALEATE	012	D07	354.41	antidepressant, dopamine uptake inhibitor
BENZALKONIUM CHLORIDE	012	D08	354.02	anti-infective (topical)
AMCINONIDE	012	D09	502.59	glucocorticoid, anti-inflammatory
KETOROLAC TROMETHAMINE	012	D10	376.41	anti-inflammatory
BROMPHENIRAMINE MALEATE	012	D11	435.32	H1 antihistamine
d[-Arg-2]KYOTORPHAN ACETATE	012	E02	397.43	analgesic
AMIPRILOSE	012	E03	341.84	immunomodulator, anti-inflammatory
TRIMIPRAMINE MALEATE	012	E04	410.52	antidepressant
METHAPYRILENE HYDROCHLORIDE	012	E05	297.85	H1 antihistamine
NORCANTHARIDIN	012	E06	168.15	anti-neoplastic, protein phosphatase inhibitor
PRILOCAINE HYDROCHLORIDE	012	E07	256.78	anesthetic (local)
PENTOXIFYLLINE	012	E08	278.31	vasodilator
BUPIVACAINE HYDROCHLORIDE	012	E09	324.90	anesthetic (local)
LEFUNOMIDE	012	E10	270.21	anti-neoplastic, PDGF receptor blocker
ETHOSUXIMIDE	012	E11	141.17	anticonvulsant
PYRITHYLDIONE	012	F02	167.21	hypnotic, sedative
CINNARAZINE	012	F03	368.53	H1 antihistamine
METARAMINOL BITARTRATE	012	F04	317.30	anti-hypotensive
ROXITHROMYCIN	012	F05	837.07	anti-bacterial

PRONETALOL HYDROCHLORIDE	012	F06	265.79	beta adrenergic agonist, anti-arrhythmic
CYSTAMINE DIHYDROCHLORIDE	012	F07	225.20	hepatoprotectant, radioprotectant
MORANTEL CITRATE	012	F08	412.47	anthelmintic
AVOBENZONE	012	F09	310.40	sunscreen
CYCLOHEXIMIDE	012	F10	281.35	protein synthesis inhibitor
METOLAZONE	012	F11	365.84	diuretic, anti-hypertensive
CLOMIPRAMINE HYDROCHLORIDE	012	G02	351.32	antidepressant
DIPLOSALSALATE	012	G03	300.27	analgesic, antipyretic
ACIVICIN	012	G04	178.58	anti-neoplastic
ERYTHROMYCIN ESTOLATE	012	G05	1056.41	anti-bacterial
1R,2S-PHENYLPROPYLAMINE	012	G06	151.21	decongestant
CHLORMEZANONE	012	G07	273.74	anxiolytic, muscle relaxant
FENBUTYRAMIDE	012	G08	163.22	antihyperlipidemic
ANISOMYCIN	012	G09	265.31	anti-protozoal, antifungal, protein synthesis inhibitor
SULFADIMETHOXINE	012	G10	310.33	anti-bacterial
DILTIAZEM HYDROCHLORIDE	012	G11	450.99	Ca channel blocker, coronary vasodilator
1,3-DIPROPYL-8- CYCLOPENTYLXANTHINE [DPCPX]	012	H02	304.40	A1 adenosine antagonist
FLUOXETINE	012	H03	345.80	antidepressant
2- MERCAPTOBENZOTHAZOLE	012	H04	167.25	antifungal
PYRILAMINE MALEATE	012	H05	401.47	anti-histaminic
SULFAGUANIDINE	012	H06	214.25	anti-bacterial
PARAXANTHINE	012	H07	180.17	adenosine receptor agonist
ETHYL 1-BENZYL-3-HYDROXY- 2-OXO[5H]PYRROLE-4- CARBOXYLATE	012	H08	261.28	aldose reductase inhibitor
MERCAPTAMINE	012	H09	113.61	depigmentation, radiation protectant

HYDROCHLORIDE				
LOXAPINE SUCCINATE	012	H10	445.91	anti-psychotic
CEPHALEXIN	012	H11	347.40	anti-bacterial
DIAZOXIDE	013	A02	230.67	anti-hypertensive, diuretic, activates K channels and AMPA receptors
METERGOLINE	013	A03	403.53	analgesic, antipyretic
3-METHYLXANTHINE	013	A04	166.14	phosphodiesterase inhibitor
beta-PELTATIN	013	A05	414.42	anti-neoplastic, cytotoxic
LOPERAMIDE HYDROCHLORIDE	013	A06	513.51	Ca channel blocker
8- CYCLOPENTYLTHEOPHYLLINE	013	A07	248.29	A1 adenosine agonist
AMOXAPINE	013	A08	313.79	antidepressant, inhibits norepinephrine uptake
AMINOLEVULINIC ACID HYDROCHLORIDE	013	A09	167.59	anti-neoplastic
CHRYSANTHEMIC ACID	013	A10	168.24	esters as insecticide
GEDUNIN	013	A11	482.58	anti-feedant
MEFENAMIC ACID	013	B02	241.29	anti-inflammatory, analgesic
VERAPAMIL HYDROCHLORIDE	013	B03	491.08	adrenergic blocker, Ca channel blocker, coronary vasodilator, anti-arrhythmic
AMIODARONE HYDROCHLORIDE	013	B04	681.78	adrenergic agonist, coronary vasodilator, Ca channel blocker
DIETHYLTOLUAMIDE	013	B05	191.28	insect repellent
TELENZEPINE HYDROCHLORIDE	013	B06	406.94	anti-ulcer, M1 muscarinic antagonist
PROPRANOLOL HYDROCHLORIDE (+/-)	013	B07	295.81	anti-hypertensive, antianginal, anti-arrhythmic
TOLAZAMIDE	013	B08	311.41	anti-diabetic
SULFACHLORPYRIDAZINE	013	B09	284.73	anti-bacterial
PHENOXYBENZAMINE HYDROCHLORIDE	013	B10	340.30	alpha adrenergic blocker
COLFORSIN	013	B11	410.51	adenylate cyclase activator, antiglaucoma, hypotensive, vasodilator

METHACHOLINE CHLORIDE	013	C02	195.69	cholinergic, diagnostic aid
PHENYLEPHRINE HYDROCHLORIDE	013	C03	203.67	mydriatic, decongestant
PRIMIDONE	013	C04	218.26	anticonvulsant
ACETYLCHOLINE	013	C05	181.66	anti-arrhythmic, miotic, vasodilator (peripheral)
EPHEDRINE (1R,2S) HYDROCHLORIDE	013	C06	201.70	bronchodilator, cardiac stimulant
METHICILLIN SODIUM	013	C07	402.40	anti-bacterial
PINDOLOL	013	C08	248.33	anti-hypertensive, antianginal, anti- arrhythmic, antiglaucoma agent
PROBENECID	013	C09	285.36	uricosuric
QUASSIN	013	C10	388.46	insecticide, antiamoebic
PROADIFEN HYDROCHLORIDE	013	C11	389.97	cytochrome P450 inhibitor, Ca antagonist
ERGOCALCIFEROL	013	D02	396.66	antirachitic vitamin; LD50 (rat) 56 mg/kg po
METHOXAMINE HYDROCHLORIDE	013	D03	247.72	alpha1 adrenoreceptor agonist, vasoconstrictor
PIPERACILLIN SODIUM	013	D04	539.55	anti-bacterial
PROCAINAMIDE HYDROCHLORIDE	013	D05	271.79	anti-arrhythmic
ASPIRIN	013	D06	180.16	analgesic, antipyretic, anti-inflammatory
FLUMETHAZONE PIVALATE	013	D07	494.58	glucocorticoid, anti-inflammatory
METHYLERGONOVINE MALEATE	013	D08	455.52	oxytocic
PIROXICAM	013	D09	331.35	anti-inflammatory
PROCYCLIDINE HYDROCHLORIDE	013	D10	323.91	anti-cholinergic
CITRININ	013	D11	250.25	anti-bacterial
alpha-TOCHOPHERYL ACETATE	013	E02	472.76	vitamin E
CEPHRADINE	013	E03	349.41	anti-bacterial
FLUOROMETHOLONE	013	E04	376.47	glucocorticoid, anti-inflammatory

METHYLPREDNISOLONE	013	E05	374.48	glucocorticoid
OXIDOPAMINE HYDROCHLORIDE	013	E06	205.64	adrenergic agonist (ophthalmic)
PROGESTERONE	013	E07	314.47	progestogen
DIETHYLSTILBESTROL	013	E08	268.36	estrogen
HYDROCORTISONE HEMISUCCINATE	013	E09	462.54	glucocorticoid
PREDNISOLONE	013	E10	360.45	glucocorticoid
APIGENIN	013	E11	270.24	antispasmodic, anti-neoplastic, topoisomerase I inhibitor
FENSPIRIDE HYDROCHLORIDE	013	F02	296.80	anti-inflammatory, bronchodilator
DIMETHADIONE	013	F03	129.12	anticonvulsant
IPRATROPIUM BROMIDE	013	F04	412.37	bronchodilator, anti-arrhythmic
PENICILLIN V POTASSIUM	013	F05	388.49	anti-bacterial
PREDNISOLONE ACETATE	013	F06	402.49	glucocorticoid
TAMOXIFEN CITRATE	013	F07	563.65	estrogen antagonist, anti-neoplastic
VERATRINE SULFATE	013	F08	689.83	anti-hypertensive
DOXEPIN HYDROCHLORIDE	013	F09	315.85	antidepressant
LACTULOSE	013	F10	342.30	laxative
GRISEOFULVIN	013	F11	352.77	antifungal, inhibits mitosis in metaphase
PREDNISON	013	G02	358.44	glucocorticoid
TERBUTALINE HEMISULFATE	013	G03	323.37	betaadrenergic agonist, bronchodilator
PHENIRAMINE MALEATE	013	G04	356.43	anti-histaminic
RACEPHEDRINE HYDROCHLORIDE	013	G05	201.70	bronchodilator, decongestant
DESOXYCORTICOSTERONE ACETATE	013	G06	372.51	mineralocorticoid
ANTAZOLINE PHOSPHATE	013	G07	363.36	anti-histaminic
DOXYLAMINE SUCCINATE	013	G08	388.47	anti-histaminic, hypnotic
PERUVOSIDE	013	G09	548.68	cardiotonic
PARAROSANILINE PAMOATE	013	G10	675.75	anthelmintic, antischistosomal
MENADIONE	013	G11	172.19	prothrombogenic agent

AMINOTHIAZOLE	013	H02	100.14	antithyroid agent
NALIDIXIC ACID	013	H03	232.24	anti-bacterial
GABOXADOL HYDROCHLORIDE	013	H04	176.60	GABA _A agonist, GABA _C antagonist
DEXAMETHASONE	013	H05	392.47	glucocorticoid
CLOTRIMAZOLE	013	H06	344.85	antifungal
TOMATINE	013	H07	994.15	antifungal, anti-bacterial, anti-inflammatory agent
RETINYL ACETATE	013	H08	328.50	vitamin precursor
EUCATROPINE HYDROCHLORIDE	013	H09	327.85	anti-cholinergic (ophthalmic)
PINACIDIL	013	H10	245.33	K channel agonist, anti-hypertensive
ALAPROCLATE	013	H11	255.75	antidepressant

Appendix 4

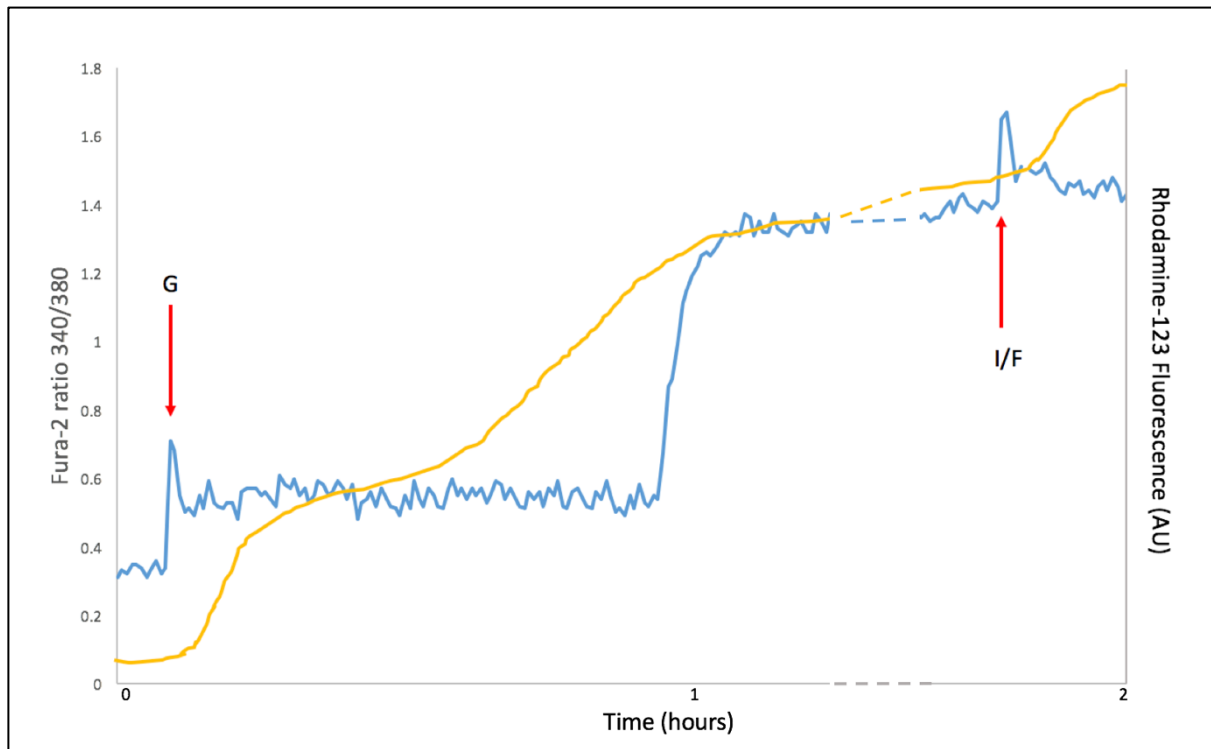


Figure A3: Delayed calcium deregulation is characterised by an initial small Ca^{2+} rise in response to glutamate, followed up to two hours after initial glutamate exposure by a secondary, larger Ca^{2+} rise, simultaneous to a collapse of $\Delta\Psi\text{m}$.

To carry out DCD experiments, DIV14 neurons on 22mm glass coverslips were loaded for 30 minutes at 37°C with either Fura-2 AM (2 μM), or Rhodamine-123 (10 $\mu\text{g}/\text{ml}$) in recording buffer (see page 68), after which the buffer was removed, cells were gently rinsed, and recording buffer^{DCD} (NaCl (150mM), KCl (4.25mM), NaH_2PO_4 (1.25mM), NaHCO_3 (4mM), CaCl_2 (1.2mM), HEPES (10mM), glucose (10mM), glycine (10 μM)) was replaced. Cells were imaged using an Olympus TH4-200 microscope, at 20X objective. For Fura-2 AM, cells were excited at 340nm and 380nm (emission 510nm), and for Rhodamine-123 at 488nm (emission 510nm). A baseline was measured for 5 minutes, prior to the addition of glutamate (G) (100 μM). Cells were then imaged every 30 seconds for another 1 hour and 45 minutes, at which point either ionomycin (I) (2 μM , in the Fura-2 AM experiments), or FCCP (F) (2 μM , in the Rhodamine-123 experiments) was added. Cells were imaged for a further 10 minutes. Images were taken every 60 seconds, and were analysed using MetaFluor software: the background was subtracted, and ROIs were drawn. The fluorescence intensity was then calculated, and for Fura-2 AM, a ratio was made of 340/380. The blue line represents Fura-2 ratio 340/380, the yellow line represents Rhodamine-123 Fluorescence.